U.PORTO

PROGRAMA DOUTORAL EM BIOLOGIA MOLECULAR E CELULAR

Phosphoregulation of the *Drosophila* tumor suppressor Lgl during the cell-cycle

Sofia Raquel Moreira

D
2019

U.PORTO

Sofia Raquel Moreira. Phosphoregulation of the *Drosophila* tumor suppressor Lgl during the cell-cycle

Phosphoregulation of the *Drosophila* tumor suppressor Lgl during the cell-cycle
Sofia Raquel Moreira

D.ICBAS **2019**

SEDE ADMINISTRATIVA
INSTITUTO DE CIÊNCIAS BIOMÉDICAS ABEL SALAZAR
FACULDADE DE CIÊNCIAS

SOFIA RAQUEL ROCHA MOREIRA

PHOSPHOREGULATION OF THE *DROSOPHILA* TUMOR SUPPRESSOR LGL DURING THE CELL – CYCLE

Tese de Candidatura ao grau de Doutor em Biologia Molecular e Celular;
Programa Doutoral da Universidade do Porto (Instituto de Ciências Biomédicas de Abel Salazar e Faculdade de Ciências)

Orientador – Doutor Eurico Morais de Sá
Categoria – Investigador Principal
Afiliação – Instituto de Investigação e Inovação em Saúde (i3S), IBMC, Universidade do Porto

Co-orientador – Professor Doutor Claudio Sunkel
Categoria – Professor Catedrático
Afiliação – Instituto de Ciências Biomédicas Abel Salazar da Universidade do Porto e Instituto de Investigação e Inovação em Saúde (i3S), IBMC, Universidade do Porto

It is good to have an end to journey toward;
but it is the journey that matters, in the end.

Ursula K. Le Guin (1929-2018)
in The Left Hand of Darkness

Preface

This thesis gathers the work performed in Epithelial Polarity and Cell Division group at i3S (Institute for Research and Innovation in Health), under the supervision of Dr Eurico Morais de Sá and co-supervision of Dr Claudio Sunkel, and it is presented to Instituto de Ciências Biomédicas Abel Salazar (ICBAS, Porto) for the degree of Doctor of Philosophy in Molecular and Cell Biology. All the described results were the outcome of my own work, except when clearly stated in the figure legends.

This research was supported by national funds of Fundação para a Ciência e a Tecnologia (FCT, FEDER funding) under the project PTDC/BEX-BCM/0432/2014 and from the project Norte-01-0145-FEDER-000029, supported by Norte Portugal Regional Operational Program (NORTE 2020). During my PhD, I was in receipt of a PhD fellowship from FCT (SFRH/BD/99898/2014).

FCT Fundação para a Ciência e a Tecnologia

MINISTÉRIO DA CIÊNCIA, TECNOLOGIA E ENSINO SUPERIOR

O NOVO NORTE
PROGRAMA OPERACIONAL REGIONAL DO NORTE

QUADRO DE REFERÊNCIA ESTRATÉGICO NACIONAL
PORTUGAL 2007.2013

UNIÃO EUROPEIA
Fundo Europeu de Desenvolvimento Regional

Original Publications[1]

This thesis contains results from the following original publications:

Moreira, S., Osswald, M., Ventura, G., Gonçalves, M., Sunkel, C.E., and Morais-de-Sá, E. (2019). PP1-Mediated Dephosphorylation of Lgl Controls Apical-basal Polarity. Cell Rep. *26*, 293-301.e7. DOI:10.1016/j.celrep.2018.12.060

Moreira, S., and Morais-de-Sá, E. (2016). Spatiotemporal phosphoregulation of Lgl: Finding meaning in multiple on/off buttons. BioArchitecture *6*, 29–38.
DOI: 10.1080/19490992.2016.1149290

[1] The original publications can be found in Appendix B

Agradecimentos

- But it doesn't take a thousand men to open a door, my lord.
- It might to keep it open.

Ursula K. Le Guin, in The Left Hand of Darkness

Em nenhuma outra língua, senão nesta que respiro, poderia expressar a minha imensa gratidão para com todos os que me acompanharam, guiaram e me seguraram ao longo destes quatro anos. Aos que me abriram a porta a este "happy lab" em 2014, onde a ciência se vive com muita paixão, alegria e entreajuda, e aos que me ajudaram a manter essa porta aberta contra os ventos contrários, porque nunca teria chegado ao fim desta jornada sem os mil (a)braços de aconchego. Foram muitas as pessoas que não me deixaram cair nos momentos menos bons, muitas com quem partilhei alegrias e tristezas, e que ficarão para sempre *aqui,* no papel ou na memória. Não sei o que virá a seguir, nem o que me falta viver, mas por tudo o que senti nestes quatro anos que passaram, por todos os momentos de palpitação e curiosidade que moveram as experiências que fiz, por todas as pessoas boas que conheci, algumas que por limitação de espaço ficarão apenas pelas entrelinhas (e no meu coração) – posso por fim dizer que estes foram talvez os quatro anos mais felizes da minha vida.

Gostaria de agradecer, em primeiro lugar, ao meu orientador, Eurico – e não chegam palavras para te dizer o quão grata e privilegiada me sinto por ter feito parte do teu grupo. Obrigada por teres sido um *orientador,* no sentido literal do termo, por me teres guiado e ensinado a encontrar o caminho. Por toda a tua paciência, apenas ela capaz de lidar com os meus devaneios e teimosias, e por estares sempre, sempre *lá* quando precisei. Acima de tudo, Eurico, quero agradecer-te por me teres dado tudo o que tinhas e me podias dar: o teu conhecimento, o teu exemplo de dedicação e paixão pela ciência, o teu exemplo de bondade e humildade e o teu optimismo, leveza e clareza de ver o mundo. Como diz Bill Callahan na música "One Fine Morning" , "I am a part of the road/The hardest part", e muitas vezes sei que lutei contra mim mesma, mas tu estiveste sempre lá quando dentro de mim era muitas vezes desalento e labirinto. Por isso, obrigada, também, por teres sido um ombro amigo quando mais precisei. Não tenho palavras para descrever toda a tua paciência e apoio quando estive doente, e por nunca teres deixado de acreditar que eu seria capaz de recuperar, quando durante dias de escuridão eu mostrava acreditar no

contrário. Obrigada por teres dado lugar a essa mão de amigo, quando a de chefe poderia ter pesado mais. Obrigada pelo teu enorme coração, “chefinho”.

Em segundo lugar, gostaria muito de agradecer ao Professor Claudio por me ter dado esta oportunidade única de pertencer a este grupo sem igual e por ter aceitado co-orientar o meu trabalho de doutoramento. Foi um privilégio para mim ter sentido na pele o que muitos diziam ser o laboratório do Professor Claudio: uma escola única de aprendizagem e paixão pela ciência. Muito obrigada, Claudio, por todos os seus conselhos e partilhas, por muitas vezes ter acrescentado o seu olhar criativo e inovador à interpretação dos meus resultados, obrigando-me tantas vezes a olhar o meu trabalho de diferentes prismas e a enquadrá-lo num *todo*. Foram valiosos os conhecimentos que me transmitiu e que procurarei preservar no meu trajecto futuro.

Ao meu grupo do coração, o recente Epithelial Polarity and Cell Division group, agradeço por todas as partilhas, aprendizagens, sorrisos e por serem simplesmente o grupo ideal, ao qual qualquer cientista gostaria de pertencer. Quero muito agradecer à Mariana por toda a ajuda durante todo este tempo, pela tua generosidade e pelo teu *coração de ouro*. Obrigada por teres estado sempre lá quando precisei, pelas tuas macros mágicas, pelos teus conselhos valiosos e pelo conhecimento que tens e que sempre partilhas connosco. Ao meu camarada Gui, que apesar de já não estar neste grupo, ainda pertence. Obrigada por todo o teu conhecimento de Bioquímica que partilhaste comigo e que foi crucial quando me vi sozinha no laboratório a fazer ensaios de cínase, fosfatase, e outras coisas tais que teriam sido impossíveis terem sido sucedidas sem a tua ajuda, Gui. Obrigada por todo o teu apoio, todas as experiências divertidas que planeamos e fizemos juntos, por todo o conhecimento que partilhaste comigo. À Magui, por toda a ajuda que deste em experiências importantes para o nosso artigo, e por seres sempre aquela amiga e companheira com quem podemos desabafar e partilhar o que nos vai cá dentro. Obrigada por teres estado comigo naqueles momentos mesmo difíceis e por me teres ajudado, tantas vezes, a levantar a cabeça. Obrigada à Mafalda, o nosso presentinho inesperado - receber-te e poder conviver contigo todos os dias foi uma dádiva. Obrigada pela tua boa energia e pela tua força, és e serás sempre uma lutadora exemplar para mim. À Cátia, pelo teu carinho e por teres sido sempre um ombro amigo. Apesar de não teres estado no grupo durante tanto tempo quanto todos nós gostaríamos, deixaste uma marca para sempre pela tua bondade, pela tua dedicação e pela tua humildade. Para todas as restantes pessoas do nosso pequeno grupo, que tenho vindo orgulhosamente ver crescer com pessoas fantásticas e profissionalmente incríveis: à Filipa (a minha companheira de poesia e alienações literárias), ao André e à Ana Maria. E à minha Ritinha, que apesar de não ser oficialmente

do grupo de polaridade, é como se fosse. Obrigada pelo teu carinho e pelas tuas palavras de conforto, sempre prontas, sempre tão assertivas, tão fáceis de absorver, e que fazem tão bem.

A todas as pessoas do Cell Division and Genomic Stability group, com quem partilhamos muito mais do que o mesmo espaço. Obrigada a todos, um a um, por tudo o que me ensinaram e por todo o apoio que me deram – ao Pedro, pela amizade e pelos comentários valiosos a esta tese; à Ana, Carlos, João, Margarida e Nelso (o Carlos estará orgulhoso de mim de certeza). Em especial, gostaria de agradecer à minha Sofs, com quem partilhei tantos e bons momentos como colega de laboratório e como *housemate* – e nem assim fiquei cansada de estar contigo! És uma pessoa incrível, ímpar, e uma cientista exemplar. Obrigada por tudo o que me ensinaste e por todo o apoio que me deste quando o trabalho e problemas pessoais se tendiam a misturar. Obrigada por me teres ajudado a separar as águas. Obrigada também à minha antiga *housemate* Joaninha, por tantas vezes me ter feito rir com a sua maneira de ser única e por ter sido uma grande aliada em fases menos boas. Queria muito, por fim agradecer a uma pessoa muito especial, à Augusta, que é muito mais do que uma simples lab manager - a pessoa que está ali nos bastidores a garantir que está tudo bem e que nós estamos bem. Ela é a pessoa que se preocupa genuinamente com cada um de nós e é o nosso porto seguro. Obrigada, Augusta, por teres estado comigo na fase mais difícil desta jornada, porque sem a tua ajuda, compreensão e os teus conselhos valiosos tudo teria sido mais difícil.

Às minhas amigas de todo o sempre, à minha Nádia, Marta, Marina, Dani, Clara...obrigada por todo o vosso apoio, incondicional.

Por fim, embora não os últimos: aos meus pais. Obrigada por sempre terem acreditado em mim e por me terem oferecido a maravilhosa oportunidade que é estudar e poder chegar até aqui. Sem a vossa motivação e carinho, todos os dias, mesmo à distância, nada disto teria sido possível. Ao meu irmão, por ser sempre, sempre, o meu maior exemplo de ser humano. À minha cunhadinha Inês, obrigada por fazeres parte na minha (nossa) vida! És também um grande exemplo para mim. Obrigada por teres sempre acreditado em mim e me apoiado em tudo o que precisei.

Pour Étienne – le bonheur de tous les jours. J'aime bien ce mot en français, "bonheur", et je n'ai jamais songé l'écrire dans ma thèse, mais la vie est drôle …Et, en fait, ce mot est parfait pour décrire tout ce que tu représentes dans ma vie: la bonne heure. Merci pour toute ta tendresse.

Acknowledgments

- But it doesn't take a thousand men to open a door, my lord.
- It might to keep it open.

Ursula K. Le Guin, in The Left Hand of Darkness

I would like to express my immense gratitude to all those who accompanied me, guided and held me over these four years. To those who opened the door to this "Happy Lab" in 2014, where people live science with a lot of passion, joy and mutual help, and those who helped me to keep this door open against the opposite winds, because I would never have come to the end of this journey without the help of thousand arms. There were many people who did not let me fall in the hardest moments, many with whom I shared joys and sorrows, and who will stay forever *here*, on paper or memory. I do not know what will come next, nor what I lack to live, but for everything that I have felt in these four years, for all the intense moments and for all the good people I've known, some of them that by space limitation will only be between these lines (and in my heart) - I can finally say that these were perhaps the happiest four years of my life.

I would like to thank first of all to my supervisor, Eurico – there are no words to tell you how grateful and privileged I feel to have been part of your group. Thank you for being a mentor, for guiding and teaching me to find the way. For all your patience and for always being there when I needed to. Above all, Eurico, I want to thank you for giving me everything you had and you could ever give me: your knowledge, your example of dedication and passion for science, your example of goodness and humility and your optimism, lightness and clarity of seeing the world. As Bill Callahan says in “One Fine Morning” song, "I am a part of the road/The hardest part", and I know that I often fought against myself, but you were always there when I was feeling discouraged. So thank you, too, for being a friendly shoulder when I needed it the most. I have no words to describe all your patience and support when I was sick, and for always believing that I would be able to recover, when during these days of darkness I showed to believe otherwise. Thank you for choosing your friend’s hand when so many times the chief one could have weighed more. Thank you for your enormous heart, “Chefinho”.

Secondly, I would like to thank Professor Claudio for giving me this unique opportunity to belong to this group and for having accepted co-supervise my PhD work. It was a privilege for me to belong to the laboratory of Professor Claudio: a unique school of learning and passion for science. Thank you very much, Claudio, for all your advice and sharing, for your creative interpretations of my results and for teaching me so many times to look at my work through a different prism and to frame it as a whole.

To my group, the recent Epithelial Polarity and Cell Division Group, I thank you for all the shared experiments, knowledge, smiles and for being the ideal group to which any scientist would like to belong. I really want to thank Mariana for all her help all this time, for your generosity and your *heart of gold*. Thank you for always being there when I needed you, for your magical macros, for your valuable advice and for all the knowledge you always share with us. To my comrade Gui who, although not in this group anymore, still belongs to it. Thank you for all your knowledge of biochemistry, which was crucial when I was alone in the lab doing kinase and phosphatase assays, and other such things that would have been impossible to succeed without your help. Thank you for all your support, all the fun experiences we've planned and done together, for all the knowledge you've shared with me. To Magui, for all the help you have given in important experiments for our article, and for always being the friend with whom we can share our problems. Thank you for being with me in those really hard times and for helping me to raise above them. Thank you to Mafalda, our unexpected gift - receiving you and living with you every day was a bless. Thank you for your good energy and your strength. You are, and you will always be, an exemplar fighter for me. To Cátia, for your affection and for always being a *shoulder friend*. Though you have not been in the group for as long as we all would like, you have left a mark forever for your kindness, for your dedication and your humility. For all the other people of our little group, that I have been proudly seeing growing up so fantastic and professionally amazing people: to Filipa (my mate of poetry and literary alienations), to André and to Ana Maria. And to my Ritinha, thank you for your affection and your words of comfort, always ready, always so assertive, so easy to absorb.

To all the people of the Cell Division and Genomic Stability Group, with whom we share much more than the same space. Thank you all, one by one, for all that you have taught me and for all the support you have given me – Pedro, Ana, Carlos, João, Margarida and Nelso (Carlos will be proud of me for sure). In particular, I would like to thank my Sofs, with whom I have shared so many and good times as a lab colleague and housemate. You're an amazing, singular person, and an exceptional scientist. Thank you for everything you've taught me and for all the support you gave me when work and personal problems tended

to mix up. Thank you for everything. Thank you also to my old housemate Joaninha, for so many times have made me laugh with your unique personality and for having been a great supporter in less good moments. Finally, I want to thank a very special person, to Augusta, which is much more than a simple lab manager – she is the person who's backstage to make sure everything is okay and that we are okay. She is the person who genuinely cares about each and every one of us. Thank you, Augusta, for having been with me in the hardest phase of this journey, because without your help, understanding and your valuable advice all would have been more difficult.

To my friends of all time, to my Nádia, Marta, Marina, Dani, Clara...Thank you for all your unconditional support.

Lastly, although not the last: to my parents. Thank you for always believing in me and for offering me the wonderful opportunity that is to study and be able to get here. Without your motivation and affection, every day, even at a distance, none of this would have been possible. To my brother, for always being my greatest example of human being. To my sister in law, Inês, thank you for being a part of my (our) life! You are also a great example for me. Thank you for always believing in me and supporting me in everything I needed.

Pour Étienne – le bonheur de tous les jours. J'aime bien ce mot en français, "bonheur", et je n'ai jamais songé l'écrire dans ma thèse, mais la vie est drôle …Et, en fait, ce mot est parfait pour décrire tout ce que tu représentes dans ma vie: la bonne heure. Merci pour toute ta tendresse.

Abstract

Apical-basal cell polarity, or the asymmetric distribution of cellular components along an apical-basal axis, underlies the organization and function of most epithelial tissues. Several studies have focused on the antagonistic interactions established between different proteins that regulate polarity through the formation of distinct subcellular domains with specialized functions. However, some epithelial tissues are constantly dividing during development to ensure proper tissue homeostasis and function, imposing a challenge to the equilibrium established between polarity regulators during interphase. Recent advances have provided a better understanding on how epithelial tissues coordinate interphase cell polarity with the dramatic changes associated with cell division, ultimately ensuring the maintenance of correct tissue architecture during proliferation. Temporal analyses of the subcellular localization of polarity proteins revealed that epithelial cell polarity is remodeled during mitosis, with a dramatic change in the subcellular localization of the tumor suppressor and basolateral determinant Lethal giant larvae (Lgl). During mitosis, Lgl is released from the cortex to the cytoplasm by a mechanism that relies on Aurora A phosphorylation in two residues redundantly phosphorylated by aPKC. However, how Lgl cortical localization is restored to polarize the cortex of the new daughter cells is still completely unknown.

In my PhD thesis, I addressed how epithelial cells coordinate mitotic exit with the recovery of cortical Lgl localization in the new daughter cells to preserve the tissue polarity and integrity during proliferation. Combining live imaging in the *Drosophila* follicular epithelium with photoconversion experiments in S2 cells, we have shown that Lgl is fully reloaded from the cytoplasm to the cortex at mitotic exit in a cell-cycle dependent manner. Importantly, we found that cortical reloading depends on the protein phosphatase 1, PP1, that directly dephosphorylates Lgl on serines phosphorylated by aPKC and Aurora A kinases and uses its regulatory subunit Sds22 to boost Lgl dephosphorylation. Additionally, we identified a PP1-interacting RVxF motif on Lgl, which is essential for Lgl cortical localization. Thus, we highlight the importance of PP1 as a phosphatase that balances the activity of aPKC during interphase and the activity of Aurora A during mitosis to promote the localization of Lgl in the basolateral cortex.

During interphase, Lgl acts together with other two cortical proteins, Dlg and Scribble, to specify the basolateral domain by antagonizing the activity of apical polarity proteins. However, which cooperative or individual functions are performed by these proteins to

preserve the identity of the basolateral domain remains to be understood. Some studies suggest that Lgl and Dlg may form a complex, but this hypothesis is mainly based on *in vitro* studies. In the last chapter of results, we report the use of Fluorescence Recovery After Photobleaching (FRAP) in intact follicle epithelial tissue to understand Lgl dynamics and interaction with its cortical partners, in particular with Dlg. We found that the dynamics of the three basolateral proteins is strikingly different and that the presence of Dlg and Scribble slows down Lgl dynamics. In light of our results, we favour a model where Dlg and Scribble affect Lgl dynamics through the repression of aPKC extension in the basolateral domain and not by anchoring Lgl in the basolateral domain through direct interactions.

Altogether, our work sheds light on how cell-cycle-dependent regulation of kinase and phosphatase activities controls the localization of a key apico-basal polarity determinant, Lgl, ensuring the maintenance or *de novo* polarization of epithelial cells in a proliferative tissue.

Key-words: Apical-basal polarity; cell-cycle; mitotic-exit; Lethal giant larvae (Lgl); phosphoregulation; Protein phosphatase 1; atypical Protein Kinase C; Aurora A; FRAP

Resumo

A polaridade apical-basal, designação pela qual se conhece a distribuição assimétrica de componentes celulares ao longo de um eixo apico-basal, está na base da função e organização da maioria dos tecidos epiteliais. Ao longo dos anos tem sido amplamente explorado o carácter antagónico das interações estabelecidas entre os complexos de polaridade para a formação de domínios funcionais distintos. No entanto, alguns tecidos epiteliais estão em constante processo de divisão e remodelação durante o desenvolvimento para assegurar a homeostasia e função do epitélio, impondo um desafio ao equilíbrio apico-basal estabelecido pelos reguladores de polaridade nas células epiteliais durante interfase. Deste modo, estudos recentes têm incidido na compreensão de como a polaridade celular é coordenada com as alterações associadas ao processo de divisão para assegurar a manutenção da arquitetura dos tecidos em proliferação. Análises temporais da localização subcelular de proteínas de polaridade revelaram que a polaridade apical-basal é altamente remodelada durante mitose, observando-se uma perda da localização basolateral da proteína Lethal giant larvae (Lgl). Durante mitose, observou-se que a proteína Lgl é excluída do córtex celular para o citoplasma através da fosforilação pela Aurora A em dois resíduos também fosforiláveis por aPKC. No entanto, permanecem ainda por esclarecer os mecanismos que governam o restabelecimento da localização cortical de Lgl para a polarização apico-basal das células-filhas.

Durante o meu doutoramento, investiguei de que forma as células epiteliais coordenam a saída de mitose com a recuperação da localização cortical de Lgl a fim de preservar a manutenção da polaridade e integridade do epitélio durante proliferação. Combinando a análise temporal da divisão celular no epitélio folicular de *Drosophila* com experiências de fotoconversão em células S2, percebemos que a proteína de polaridade Lgl é totalmente relocalizada do citoplasma para o córtex à saída de mitose por mecanismos moleculares coordenados com o ciclo-celular. O processo de recuperação de Lgl no córtex implica a ação de uma fosfatase, PP1, que desfosforila diretamente Lgl nos resíduos fosforilados pelas cínases aPKC e Aurora A, conjuntamente com uma subunidade reguladora, Sds22. Adicionalmente, identificámos um motivo RVxF no Lgl que medeia a interação com a PP1 e que é essencial para a localização cortical de Lgl. Desta forma, a fosfatase PP1 contrabalança a atividade de aPKC durante interface e de Aurora A durante mitose para promover a localização de Lgl no córtex basolateral.

Em interfase, Lgl interage com mais duas proteínas de polaridade basolaterais, Dlg e Scribble, para especificar o domínio basolateral através da antagonização de proteínas apicais. No entanto, estão ainda por identificar que funções conjuntas ou individuais são desempenhadas por destas proteínas para preservar a identidade do domínio basolateral. Alguns estudos têm sugerido que Lgl e Dlg formam um complexo, apesar de se basearem maioritariamente em experiências *in vitro*. No último capítulo de resultados, reportamos o uso da técnica de microscopia confocal FRAP para perceber, num tecido epitelial intacto, a dinâmica e interação de Lgl com parceiros corticais, particularmente com Dlg. Neste trabalho, observámos que a dinâmica das três proteínas basolaterais é significativamente diferente no epitélio folicular e que a presença de Dlg e Scribble interferem negativamente com a dinâmica de Lgl. À luz dos nossos resultados, favorecemos a hipótese de que Dlg e Scribble afetam a dinâmica de Lgl reprimindo a extensão de aPKC no domínio basolateral e não através da ancoragem direta de Lgl ao córtex. Esta questão é extremamente relevante para perceber como estas proteínas de polaridade cooperam para assegurar a manutenção da polaridade dos tecidos epiteliais, uma questão que permanece ainda sem uma resposta sólida.

Por fim, o nosso trabalho esclarece de que forma a regulação das atividades de cínase e fosfatase dependentes do ciclo celular controla a localização de uma proteína essencial para a polaridade apico-basal, Lgl, garantindo a manutenção ou a polarização *de novo* das células epiteliais num tecido proliferativo.

Palavras-chave: polaridade apical-basal; ciclo celular; saída de mitose; Lethal giant larvae (Lgl); fosforegulação; PP1; aPKC; Aurora A; FRAP

Table of Contents

Preface **1**

Original Publications **3**

Agradecimentos **5-7**

Acknowledgments **9-11**

Abstract **13,14**

Resumo **15,16**

Table of contents **17-20**

Figure Index **21-25**

Table Index **27**

Abbreviations **29,30**

Chapter 1: General Introduction

1. Asymmetries in (cell) life: an overview on cell polarity 33-35
2. Apical-basal polarity in epithelial tissues 35,36
   - 2.1. An overview on the main apical-basal polarity proteins 37-49
     - 2.1.1. The apical Crumbs and aPKC/Par complexes 37,38
     - 2.1.2. The basolateral Lgl/Dlg/Scribble module 39-42
     - A) Scribble module on the regulation of intracellular signaling pathways 42-44
     - B) Scribble module proteins on the regulation of vesicle trafficking 44,45
     - 2.1.3. Mutual antagonism between apical complexes and the Scribble module 45-48
3. The importance of aPKC and Aurora A kinases in cell polarity 49-57
   - 3.1. aPKC: “the kinase that phosphorylates cell polarity” 49,51
   - 3.2. Aurora A: the kinase that links cell-cycle regulation with cell polarity... 52-53

3.3. Spatiotemporal phosphoregulation of Lgl by aPKC and AurA in epithelial cells 54-57
4. The protein phosphatases in cell polarity 58-64
4.1. PP1 and PP2A: roles and regulation during the cell-cycle 58-62
4.2. Implications of PP1 and PP2A in cell polarity and cancer 63,64

5. Cell polarity disruption and cancer 65,66
6. *Drosophila melanogaster* as a model system 67-71
6.1. The *Drosophila* follicular epithelium 68-71
7. Aims of the work 71-73

Chapter 2: Experimental Procedures

2.1. *Drosophila* husbandry and genetics 77-101

2.1.1. The GAL4-UAS *expression system* 77,78
2.1.2. Generation of mosaic tissues 79-81
A) The Flp-FRT system 79,80
B) Flp-out technique 81

2.2. *Drosophila* S2 cells cultures and RNAi interference 101

2.3. Immunofluorescence of ovaries and salivary glands 102

2.4. Imaging of *Drosophila* ovarioles, embryos and S2 cells 102, 103

2.5. Photoconversion experiments in S2 cells 107

2.6. Fluorescence recovery after photobleaching (FRAP) of *Drosophila* egg chambers 107-109
A) FRAP imaging 107,108
B) FRAP protocols 108
C) Processing FRAP raw data and data analyses 109

2.7. Drug treatments 110

2.8. Molecular biology techniques and experiments 110-114

2.8.1. Cloning of Lgl variants 110,111

2.8.2. Preparation of protein extracts from ovaries and S2 cells 111
2.8.3. Western blotting (WB) 111, 112
2.8.4. *In vitro* protein expression and purification 112
2.8.5. Immunoprecipitations (IPs) 112,113

2.8.6. *In vitro* dephosphorylation assays.....113,114
2.8.7. RT-PCR..... 114

2.9. Data analyses and quantifications 114-117

2.9.1. Lgl cytoplasmic decay..... 115

2.9.2. Lgl accumulation in daughter-daughter interface 115
2.9.3. Lgl-Dendra2 intensity upon photoconversion 115,116
2.9.4. Interphase cortical/ cytoplasm intensity ratio of Lgl in S2 cells 116
2.9.5. aPKC accumulation in the apical interface formed between daughter cells at mitotic exit..... 116
2.9.6. Quantification of the band intensity in WB and RT-PCR 116,117

2.10. Multiple sequences analyses..... 117
2.11. Statistical analysis 117,118

Chapter 3: The role of phosphatases in Lgl phosphoregulation and cortical localization

3.1. Introduction 121,122

3.2. Identification of a phosphatase that controls Lgl cortical localization 123-131

3.3. Pp1-87B is the only PP1 isoform essential to control Lgl localization in the follicular epithelium 131-134
3.4. PP1 dephosphorylates Lgl in aPKC/Aurora A phosphorylation sites..... 134-143
3.5. Lgl contains an evolutionarily conserved PP1 docking site..... 143-151
3.6. $Lgl^{KA,FA}$-GFP is unable to maintain epithelial organization..... 152-155
3.7. Discussion..... 156-160

Chapter 4: Molecular mechanisms controlling the recovery of cortical Lgl at mitotic exit

4.1. Introduction 163,164
4.2. Lgl is reloaded from the cytoplasm to the cortex at mitotic exit..... 165-167
4.3. The impact of Aurora A and aPKC kinases in Lgl cortical reloading 167-173
4.3.1. Aurora A degradation is not the timer for Lgl cortical reloading..... 167-171
4.3.2. aPKC does not repress Lgl cortical reloading at mitotic exit in the follicular epithelia..... 171-174
4.4. PP1/Sds22 is involved in Lgl cortical reloading at mitotic exit 174-179

4.5. Lgl cortical localization at mitosis is important for correct polarization of daughter cells 179-184
4.6. Discussion 185-190

Chapter 5: Exploring the potential interaction of Lgl with Dlg *in vivo* using FRAP
5.1. Introduction 193-195
5.2. Characterization of basolateral polarity protein dynamics using FRAP 196-202
5.3. Loss of Dlg accelerates Lgl recovery due to increased aPKC phosphorylation and not by disruption of Dlg-Lgl complexes 202-208
5.4. Dlg and Scribble could act as competitors of Lgl for aPKC phosphorylation 208-213
5.5. Discussion 214-220

Chapter 6: General discussion 221-226

References 229-259

Appendix A: Movie Legends
Appendix B: Original publications

Figure Index

Chapter 1: General Introduction

Figure 1.1: Different types of cell polarity in multicellular organisms

Figure 1.2: Comparative representation of the apical-basal epithelial cell polarity in *Drosophila* and vertebrates

Figure 1.3: Structural representation of Lgl, Dlg and Scrib

Figure 1.4: Apical and basolateral polarity proteins are fundamental for the maintenance of epithelial tissue architecture

Figure 1.5: Aurora A and aPKC phosphorylate Lgl to control its localization and interaction with cortical binding partners

Figure 1.6: Lgl phosphorylation by Aurora A and cortical release during mitosis promotes planar mitotic spindle orientation

Figure 1.7: Phosphorylation of Lgl and basolateral restriction by aPKC is important for epithelial cell polarity

Figure 1.8: Regulation of PP1 and PP2A phosphatases during the cell-cycle

Figure 1.9: Schematic representation of *Drosophila* ovaries and the basic units of ovaries, the ovarioles

Figure 1.10: Graphical illustration of the main objectives of this work

Chapter 2: Experimental Procedures

Figure 2.1: Schematic representation of the GAL4/UAS system for expression of transgenes in a cell-type or tissue specific manner

Figure 2.2: Schematic representation of Flp-FRT system for generation of homozygous mutant clones and Flp-FRT system combined with expression of Gal80 for clonal tissue-specific expression of a gene of interest or RNAi

Figure 2.3. Schematic representation of a cross designed to generate Flp-out clones

Chapter 3: The role of phosphatases in Lgl phosphoregulation and cortical localization

Figure 3.1: Schematic representation of the hypothesis on how Lgl phosphoregulation controls its localization at the cortex

Figure 3.2: Flowchart of a targeted RNAi screen to search for phosphatases and phosphatase regulatory subunits controlling Lgl cortical localization in the follicular epithelium

Figure 3.3: Pp1-87B depletion induces a strong mislocalization of Lgl-GFP to the cytoplasm in follicle cells

Figure 3.4: Pp1-87B and Sds22 are required for proper Lgl cortical localization in the follicular epithelium

Figure 3.5: PP1 regulates Lgl cortical localization in S2 cells

Figure 3.6: Localization pattern of PP1 catalytic isoforms in follicle cells

Figure 3.7: Pp1-87B is the only PP1 isoform that is essential for Lgl cortical localization in the follicular epithelium

Figure 3.8: General PP1 activity regulates Lgl cortical localization

Figure 3.9: α-spectrin remains cortical upon depletion of Pp1-87B

Figure 3.10: PP1 is partially required for the cortical localization of Dlg

Figure 3.11: PP1 activity balances aPKC function in the follicular epithelium

Figure 3.12: PP1 controls Lgl cortical localization by antagonizing phosphorylation on aPKC/AurA phosphorylation sites

Figure 3.13: PP1 antagonizes aPKC/AurA phosphorylation by dephosphorylating Lgl

Figure 3.14: *Drosophila melanogaster* has two putative RVxF docking site motifs conserved in *Drosophila*, one of which is evolutionarily conserved in Metazoa

Figure 3.15: Disruption of the conserved PP1 docking leads to cytoplasmic accumulation of Lgl

Figure 3.16: $Lgl^{KA,FA}$-GFP is hyperphosphorylated in *Drosophila* ovaries

Figure 3.17: PP1 interaction with Lgl is not dependent on the docking site motif

Figure 3.18: $Lgl^{KA,FA}$-GFP is maintained in the cytoplasm when aPKC is depleted in the follicular epithelium

Figure 3.19: Depletion of aPKC promotes cortical localization of $Lgl^{KA,FA}$-GFP in salivary gland epithelium

Figure 3.20: $Lgl^{KA,FA}$-GFP does not support epithelial cell polarity and tissue architecture

Figure 3.21: Proposed model for PP1 regulation of Lgl cortical localization during interphase and antagonization of apical aPKC for maintenance of epithelial polarity

Chapter 4: Molecular mechanisms controlling the recovery of cortical Lgl at mitotic exit

Figure 4.1: Understanding Lgl re-establishment in the cortex of daughter cells at mitotic exit

Figure 4.2: Characterization of Lgl-GFP localization and dynamics at mitotic exit in epithelial cells

Figure 4.3: Cytoplasmic Lgl returns to the cortex at mitotic exit in S2 cells

Figure 4.4: Stabilization of AurA at mitotic exit does not affect Lgl reloading

Figure 4.5: Overexpression of a stabilized version of AurA, $AurA^{\Delta Ab\text{-}GFP}$, or depletion of AurA does not change the kinetics of Lgl cortical reloading

Figure 4.6: aPKC inactivation does not affect Lgl cortical reloading at mitotic exit in the follicular epithelium

Figure 4.7: PP1/Sds22 regulates Lgl cortical reloading at mitotic exit in follicle cells

Figure 4.8: Depletion of PP1 and Sds22 delays Lgl reloading in S2 cells

Figure 4.9: $Lgl^{KA,FA}$ -GFP is delayed in reloading to the cortex in epithelia

Figure 4.10: The role of cytokinesis in Lgl cortical reloading

Figure 4.11: Lgl reloading to the cortex precedes aPKC accumulation in the new daughter-daughter interface

Figure 4.12: Lgl cortical reloading represses the lateral localization of aPKC in the new daughter-daughter interface

Figure 4.13: Model for how PP1/Sds22 controls Lgl cortical reloading at mitotic exit in epithelial cells

Chapter 5: Exploring the potential interaction of Lgl with Dlg using FRAP

Figure 5.1: Implementation of a FRAP (Fluorescence Recovery After Photobleaching) protocol to study Lgl-Dlg interaction *ex vivo*

Figure 5.2: Characterization of the dynamics of Dlg, Lgl and Scribble using FRAP

Figure 5.3: FRAP protocol used to analyze the biological relevance of the immobile fraction of Lgl

Figure 5.4: Lgl and Dlg dynamics are coupled to lateral membrane diffusion

Figure 5.5: Exploring the lateral-diffusion properties of Lgl

Figure 5.6: Unphosphorylatable forms of Lgl display similar dynamics to the wild-type form in the basolateral domain

Figure 5.7: Mutation of the aPKC phosphorylation sites prevents Lgl cytoplasmic localization in *dlg* mutants

Figure 5.8: The rate of Lgl recovery after photobleaching increases in *dlgA* mutants in a similar extent to depletion of PIP_2

Figure 5.9: Increase in Lgl dynamics is not related with PIP_2 levels in *dlg* mutant clones

Figure 5.10: Acute inhibition of aPKC activity does not rescue Lgl cortical localization in *dlgA* epithelia mutants.

Figure 5.11: Exploring Dlg and Scribble as competitors/ inhibitors of Lgl phosphorylation by aPKC

Figure 5.12: Lgl-GFP recovery dynamics is strongly increased in mutants for *scrib*.

Chapter 6: General discussion

Figure 6: Graphic illustration of the main results of this thesis

Table Index

Chapter 2: Experimental procedures

Table 2.1: *Drosophila melanogaster* genotypes used in this thesis

Table 2.2: Genotypes used in each figure of the presented work

Table 2.3: List of primers used in this study

Table 2.4: List of the antibodies used in this study

Chapter 3: The role of phosphatases in Lgl phosphoregulation and cortical localization

Table 3.1: Summary of the Lgl endogenous localization in RNAi experiments

Table 3.2: Quantification of epithelial architecture and Lgl localization upon genetic inactivation of protein phosphatase function

Abbreviations

A-B	Apical-Basal
A-P	Anterior-Posterior
AJ	Adheres Junctions
APC	Adenomatous Polyposis Coli
APC/C	Anaphase Promoting Complex/Cyclosome
aPKC	Atypical Protein Kinase C
Arm	Armadillo
Baz	Bazooka
BH domain	Basic and Hydrophobic domain
CDK1	Cyclin-Dependent Kinase 1
Cora	Coracle
Crb	Crumbs
diAP1	*Drosophila Inhibitor of APoptosis 1*
Dlg	Discs large
Ecad	E-Cadherin
FERM domain	band **4**.1/**E**zrin/**R**adixin/**M**oesin domain
FRAP	Fluorescence Recovery After Photobleaching
Friz	Frizzled
FSC	Follicle Stem Cells
GSC	Germline Stem Cells
GUK	Guanylate Kinase-like
GUKH	Guk Holder
HPV	Human Papilloma Viruses
HS	Heat-Shock
IP	Immunoprecipitation
JNK	Jun N-terminal kinase
LAP domain	Leucin-rich repeats and PDZ domain
Lgl	Lethal giant larvae
LLGL1	Lethal(2) giant larvae protein homolog 1
LLGL2	Lethal(2) giant larvae protein homolog 2
LRR	Leucin-rich repeats
MAPK	Mitogen-activated protein kinase
mts	Microtubule star
NEBD	Nuclear envelope breakdown
NiPP1	Nuclear inhibitor of protein phosphatase 1
NMII	Non-muscle myosin II
Nrx IV	Neurexin IV
OA	Okadaic Acid
PB domain	Polybasic domain
PCP	Planar cell polarity
PDZ domain	PSD-95/Dlg/Zho1 domain
PI(4)P	Phosphatidylinositol-4-phosphate
PIP_2	Phosphatidylinositol 4,5-biphosphate
PIP_s	Phosphoinositides
PM	Plasma membrane

PP1	Protein phosphatase 1
PP2A	Protein phosphatase 2 A
RNAi	RNA interference
ROI	Region of interest
Scrib	Scribble
SH3	Src homology 3
SJ	Septate junctions
SOP	Sensory Organ Precursor
TJ	Tight Junctions
UAS	Upstream activation sequence
Yrt	Yurt
Zip	Zipper

Chapter 1

General Introduction

1. Asymmetries in (cell) life: an overview on cell polarity

Harmony and perfection, both in the universe and art, have always been associated with symmetries. According to the Online Etymology Dictionary[2], the word “symmetry” is derived from Greek (*syn* - “together” + *metron*- “measure”) and Latin (*symmetria*) words meaning ”measure together” and also “harmonic arrangement of parts”. When thinking about symmetry, my mind suggests the drawing of the human body inside a circle in the Leonardo da Vinci’s “Vitruvian Man” (ca.1487). The symmetry and perfection inherent in this drawing are also shared across nature, composing the perfect mirror-symmetry of an oak leaf, the radial symmetry of a starfish or the hexagonal symmetry of a simple crystal snowflake. However, behind the symmetric patterns of the universe, there is an asymmetric world without which life would be untenable. Inside the apparent symmetry of the human body, there is a left lung that is smaller than its right counterpart to accommodate the heart, or billions of cells that share a microscopic asymmetric composition, making asymmetries part of the harmonic symphony of life.

It is this last type of asymmetry, the asymmetry of cells, that I will discuss in this thesis. In biology, this asymmetry is referred as cell polarity, one of the most important features of cells due to its involvement in the regulation of several basic processes both in unicellular (such as the yeast *Saccharomyces cerevisae*) and multicellular organisms. The spatial asymmetry of vesicle trafficking and distribution of proteins, lipids and organelles, allows the organization of a cell into discrete domains with specialized functions. This intracellular asymmetry can be classified according to the organization of the polarity machinery in a defined axis inside the cell. Here, I highlight four essential types of cell polarity and processes in which they are involved: the apical-basal polarity, commonly found in epithelial monolayers and also in *Drosophila* neuroblasts during asymmetric cell division; the anterior-posterior polarity, found in the *Drosophila* oocyte or neuronal polarity; the front-rear polarity, involved in cell migration; and the planar polarity, found in the *Drosophila* wing cells that give rise to bristles (Figure 1.1). The localization of two key proteins governing cell polarity in many different cell types, aPKC and Lgl, are also represented as they will be the main focus of this thesis.

[2] https://www.etymonline.com/

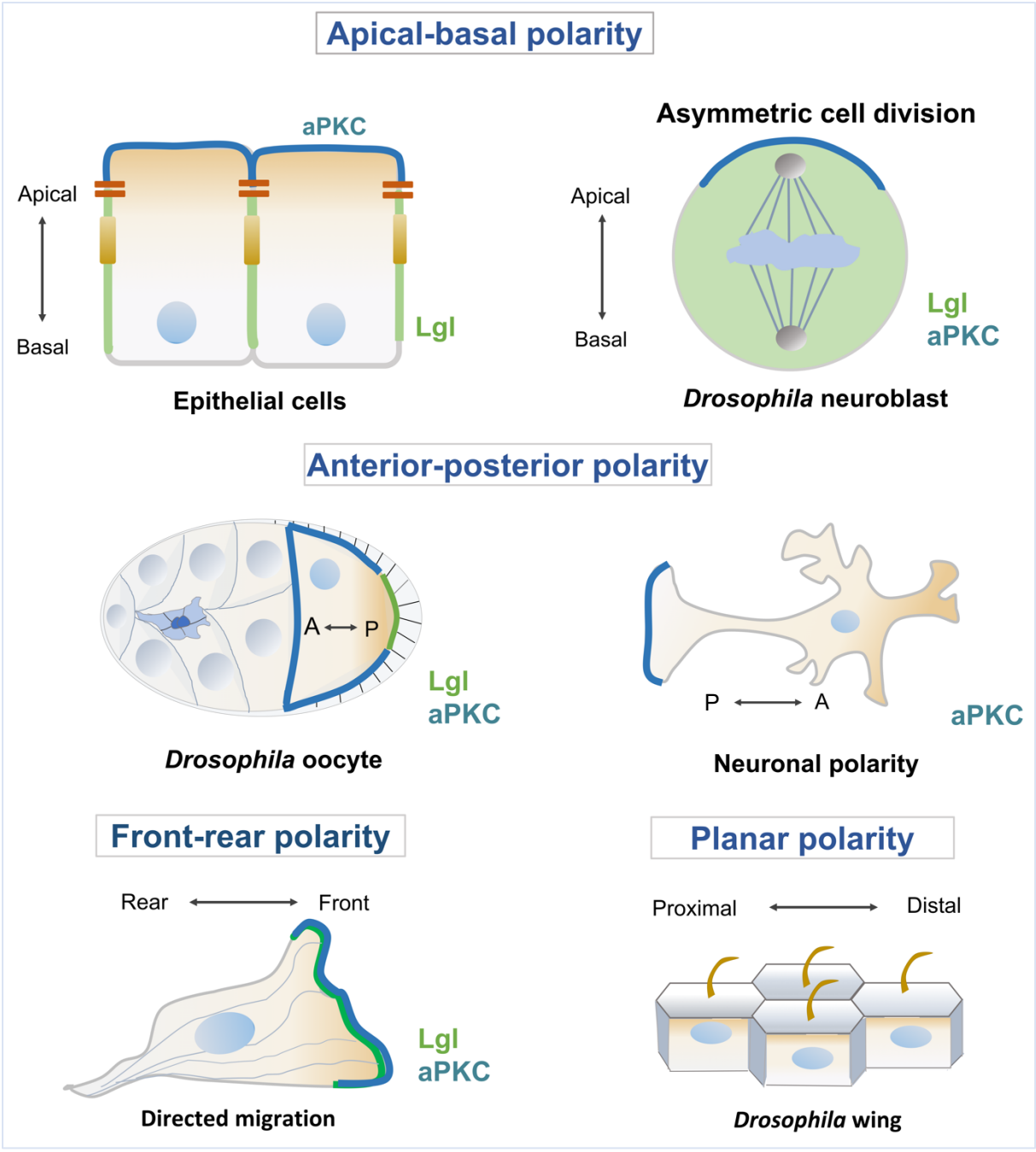

Figure 1.1: Different types of cell polarity in multicellular organisms. Schematic representation of apical-basal polarity (in epithelial cells and neuroblasts), anterior-posterior polarity (found in the *Drosophila* oocyte or in neuronal polarity), front-rear polarity (typically found in migrating cells) and planar cell polarity (involved, for instance, in the orientation of bristles in *Drosophila* wing). The localization of Lgl (green) and aPKC (blue) proteins is also represented. A – anterior; P – posterior

Since the generation of an asymmetric organization is essential in a wide array of biological processes, it is extremely important to understand how these molecular asymmetries are established in order to understand the development of human diseases. In this work, we focused on a particular type of cell polarity, the apical-basal cell polarity found in epithelial cells and whose disruption is a first hallmark of epithelial cancers (Wodarz and Näthke, 2007).

2. Apical-basal polarity in epithelial tissues

Epithelia consist of sheets of polarized cells that are held together through an adhesive belt of adheres junctions (AJ). This particular type of cell polarity is known as apical-basal polarity, defined by an axis where the apical membrane faces the outside or lumen of the organ and the basal surface contacts the extracellular matrix. Epithelial cell polarity relies on the asymmetric intracellular distribution of evolutionary conserved polarity complexes along the apical-basal axis, together positioning the AJ (conserved within mammals and invertebrates) and sealing junctions (tight junctions in mammals and septate junctions in invertebrates). Sealing junctions are crucial as selective barriers between internal and external environments (Rodriguez-Boulan and Macara, 2014) and are positioned above AJ in mammals and below AJ in most epithelial cells of *Drosophila* (St Johnston and Ahringer, 2010) (Figure 1.2). This type of organization is essential for epithelial function, including the directional transport of molecules and the compartmentalization of multicellular organisms, and was an important evolutionarily step towards the separation of the outside from the inside environment in Metazoa.

Apical-basal polarity depends on antagonistic interactions between polarity proteins that define distinct cortical domains (St Johnston and Ahringer, 2010) (Figure 1.2 and Figure 1.4). Three core polarity complexes were found to be evolutionarily conserved among worms, flies and mammals (Tepass *et al*., 2001) and play an essential role in the establishment and maintenance of apical-basal cell polarity. In the apical domain, the aPKC/Par (Par3-Par6-aPKC) and Crumbs (Crumbs-PatJ-Stardust) complexes promote apical membrane identity (Margolis and Borg, 2005; Suzuki, 2006) (Figure 1.2). In turn, the apical determinants are antagonized by the basolateral module, Scribble (Scrib), Lethal giant larvae (Lgl) and Discs large (Dlg), which together specify the basolateral domain (Bilder, 2004) (Figure 1.2). Although these complexes depend on each other for their correct localization and function, for simplicity, I will proceed with their individual description.

An additional group of lateral proteins, formed by Yurt (Yrt), Coracle (Cora) and the membrane proteins Neurexin IV (Nrx IV) and α subunit of Na^+/K^+-ATPase, was also recently shown to be important for basolateral membrane identity by antagonizing apical determinants (Laprise *et al*., 2006; Laprise *et al*., 2009), as will be latter discussed.

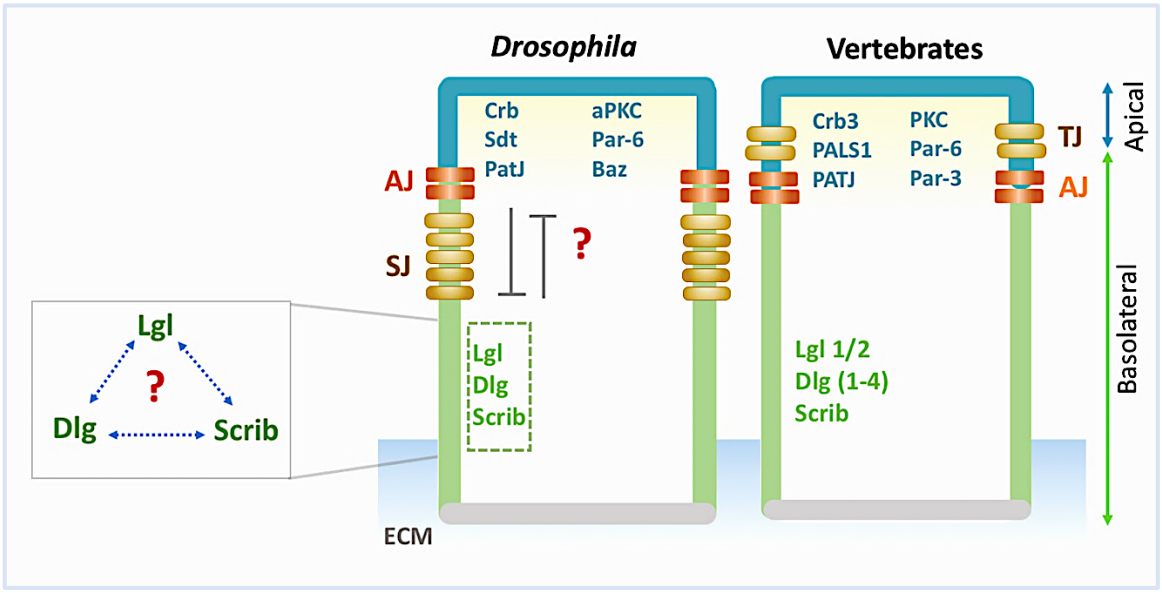

Figure 1.2: Comparative representation of the apical-basal epithelial cell polarity in *Drosophila* and vertebrates. Epithelial cell polarity is organized in discrete domains: the apical domain, defined by the main apical polarity complexes (in *Drosophila*: Crb/Std/Patj and aPKC/Par-6/Baz; in vertebrates: Crb3/PALS1/PATJ and PKC/Par-6/Par-3) and the basolateral module specified by Lgl, Dlg and Scrib (in vertebrates: Lgl1 or Lgl2/ Dlg1 to Dlg4/ Scrib). The adherens junctions (AJ) are also represented, being positioned above septate junctions (SJ) in *Drosophila* and below tight junctions (TJ) in vertebrates. Apical and basolateral proteins antagonize each other to maintain the position of these junctions and define the boundaries of each domain. However, how the basolateral domain antagonizes the apical domain is not well understood. Another unanswered question is whether there are direct interactions between the three basolateral polarity proteins, Lgl, Dlg and Scrib.

2.1. An overview on the main apical-basal polarity proteins

2.1.1. The apical Crumbs and aPKC/Par complexes

Crumbs (Crb, Crb1-3 in vertebrates) is a transmembrane protein localized apically to adherens junctions (AJ), according to immunoelectron microscopy data (Tepass, 1996). In the *Drosophila* embryonic epithelia, loss of Crb leads to disruption of apical membrane identity, whereas overexpression of Crb causes an extension of the apical membrane (Wodarz *et al*., 1993; Wodarz *et al*., 1995), suggesting a critical role for Crb in the establishment of apical-basal polarity in this tissue. However, Crb is not expressed in all *Drosophila* epithelial types and it is dispensable for the maintenance of epithelial polarity in some epithelia (Tepass, 2012). In the *Drosophila* follicular epithelium, Crb is required for the formation and maintenance of tissue integrity (Tanentzapf *et al*., 2000). Crb has been proposed to interact with two adaptors, Sdt (Pals1 in mammals) and Patj, in an obligatory manner (Bulgakova and Knust, 2009). This is further supported by the observation that loss of Sdt and Patj induces epithelial defects which closely resemble Crb loss (Bulgakova and Knust, 2009; Tepass and Knust, 1993; Bachmann *et al*., 2008). However, subsequent analyses of null Patj mutants of *Drosophila* suggest that Patj is dispensable for apical-basal polarity in some tissues, such as embryonic ectoderm (Sen *et al*., 2012; Pénalva and Mirouse, 2012), although it has important functions in supporting apical-basal polarity of follicular epithelium (Pénalva and Mirouse, 2012; Zhou and Hong, 2012) and early pupal photoreceptors (Zhou and Hong, 2012).

In the sub-apical region of *Drosophila* epithelial cells lies a complex composed by the atypical Protein Kinase C, a serine/threonine kinase (aPKCγ/ι and aPKCζ homologues in mammals), and two aPKC scaffold proteins, Bazooka (Baz) (Par-3 in mammal) and Par-6 (whose mammalian homologues are Par-6 α, β and γ), containing PDZ domains and protein interaction motifs. Par-6, aPKC and Baz bind to form the Par complex (Goldstein and Macara, 2007; Suzuki, 2006). aPKC kinase is self-inhibited due to binding between its N-terminal pseudosubstrate domain and the kinase domain (Zhang *et al*., 2014). Contrasting with other PKC families, aPKC activity is regulated by protein-protein interactions and not by calcium or other restricting molecules (Hong, 2018). Accordingly, Par-6 was shown to be important for aPKC inhibition until active (GTP-loaded) Cdc42 recruits Par-6 and prevents this inhibitory interaction (Yamanaka *et al*., 2001; Hutterer *et al*., 2004). There are also studies suggesting that, instead of inhibiting aPKC, Par-6 might activate the kinase by

displacing the auto-inhibitory pseudosubstrate from the kinase domain (Graybill *et al*., 2012), leading to conflicting interpretations regarding the function in the regulation of aPKC activity. Since aPKC does not have well-defined plasma membrane domains, it has been assumed that its subcellular localization depends only on protein-protein interactions (Rosse *et al*., 2010). However, it was recently suggested that the pseudosubstrate region of aPKC is sufficient to target this kinase to the plasma membrane by electrostatic interactions and that Par-6 could induce a conformational change that exposes this membrane binding domain (Dong *et al*., 2019).

Bazooka (Baz), the third element of this complex, is a peculiar aPKC substrate, proposed to act both as an activator of aPKC activity towards some substrates (Wirtz-Peitz *et al*., 2008), or as an inhibitor of aPKC by binding to its kinase domain (Soriano *et al*., 2016). In follicular epithelial cells, Baz seems to be required for the recruitment of Par-6 and aPKC to form a complex, but its localization was shown to be independent of aPKC and Par-6 (Franz and Riechmann, 2010; Morais de Sá *et al*, 2010). Depending on the cell-type, Baz can localize to the apical cortex or to the AJs. In most *Drosophila* epithelial cells, the interaction between aPKC/Par-6 and Baz seems to be short lived; aPKC phosphorylation of Baz weakens the interaction with aPKC and, additionally, Crb enhances the recruitment of aPKC/Par6 to the apical domain through Par-6 interaction, outcompeting the Par-6/Baz interaction and positioning Baz to the adherens junctions (Morais-de-Sá *et al*., 2010; Walther and Pichaud, 2010). aPKC and Par-1 phosphorylation of Bazooka in *Drosophila* were found to restrict Bazooka to the subapical region, where it was found to be important for the assembly of adherens junctions, recruiting E-Cadherin into spot adherens (Harris and Peifer, 2004; McGill *et al*., 2009). Finally, there is increasing evidence that the Crb and aPKC/Par complexes act as interdependent apical protein networks. These complexes cooperate semi-redundantly with each other to define the apical domain of an epithelial cell, since the mutual removal of these complexes is necessary for a complete loss of the apical domain in *Drosophila* embryonic epithelia (McGill *et al*., 2009). Their components were found to either interact or co-localize. In fact, Par-6/aPKC colocalize with Crb, Sdt and Patj (St Johnston and Ahringer, 2010), aPKC/Par complex was described to phosphorylate Crb (Sotillos *et al*., 2004) and Par-6/aPKC co-immunoprecipitate with the Crb complex in mammals and *Drosophila* epithelia (Assémat *et al*., 2008). Interestingly, a recent study suggests that the interaction between Crb and Par-6 prevents the Par-6 inhibition of aPKC activity (Dong *et al*., 2019).

2.1.3. The basolateral Lgl/Dlg/Scrib module

In 1967, Elizabeth Gateff and Howard Schneiderman described a mutation in *Drosophila* that acts in a recessive fashion, inducing cells to "grow rapidly and invasively and kill their hosts" and to behave "like a malignant tumour" (Gateff and Schneiderman, 1967). Scientists have thus provided the first example of a tumour-suppressor gene. Its name, *lethal giant larvae* (lgl), came from the observation that loss of this gene causes neuroblast overproliferation in the brain and overgrowth of imaginal discs, resulting in "giant larvae" that die in a pre-pupa developmental stage (Gateff and Schneiderman, 1974). After *lgl*, a genetic screen in imaginal discs identified a mutation with a similar phenotype, *discs-large* (*dlg*; Stewart *et al*, 1972) and twenty-eight years later, Scribble (*scrib*) was isolated, and shown to display very similar phenotypes to *lgl* and *dlg* (Bilder and Perrimon, 2000). In addition to overproliferation, these mutations cause a dramatic loss of cell polarity with consequent disorganization of cell tissue cellular architecture, one of the primary features of carcinomas (malignant tumours of epithelial origin) (Bilder, 2004). In the absence of one of these three proteins, the balance between distinct domains is disrupted, and apical components extend to the basolateral membrane (Bilder and Perrimon, 2000) (Figure 1.4). Curiously, the *Drosophila* midgut epithelium is an exception to this rule, as in this tissue none of these basolateral proteins or even other canonical polarity proteins, such as aPKC, are required for apical-basal polarity (Chen *et al*., 2018).

The common localization of Lgl, Dlg and Scrib in the basolateral domain of epithelial cells, as well as the genetic interactions observed between these three genes, place them in a common pathway that controls apical-basal polarity (Bilder, 2004; Bilder and Perrimon, 2000; Tanentzapf and Tepass, 2003). In fact, the idea that Lgl, Dlg and Scrib form a tripartite complex came from the observation that these proteins have interdependent localizations and that individual mutations for these genes give rise to very similar phenotypes (Bilder and Perrimon, 2000). Recently, analysis of the interdependence for their localization at septate junctions of the midgut revealed that Scrib is required to localize Dlg, which in turn is required to localize Lgl (Chen *et al*., 2018). However, *in vivo* evidence for a direct physical interaction between the three proteins in the basolateral domain has not yet been reported. Thus, the term *complex* has been often replaced by the term *module* to highlight the possibility that these three proteins might not form an *in vivo* tripartite complex, but might instead be highly dynamic entities (Figure 1.2). Moreover, it is not well understood how the three proteins cooperate to antagonize apical determinants and maintain cell polarity. In *Drosophila* synapses, Dlg and Scrib were found to interact indirectly through an adapting protein called Guk holder (Mathew *et al*., 2002). Scrib was also found to

coimmunoprecipitate with Lgl2 in mammalian cells (Kallay *et al*., 2006), but domains of Lgl required for this interaction are unknown. Lastly, in mammalian cells, Dlg4 and Lgl2 were found to interact in a phosphorylation dependent manner through the evolutionarily conserved serine residues of Lgl targeted by aPKC and the GUK domain of Dlg (Zhu *et al*., 2014). However, the major conclusions of this work rely on *in vitro* and crystallography analyses, remaining to be confirmed *in vivo*.

Structurally, Lgl, Dlg and Scrib proteins are rich in protein-protein interaction domains (Figure 1.3). Scribble, encoded by a single gene in *Drosophila* and vertebrates, is a protein with about 210 kDa (Bilder and Perrimon, 2000) that belongs to the LAP (Leucin-rich repeats and PDZ domain) family, containing four PDZ domains at the C-terminus and sixteen LRR (Leucin-rich repeats) in the N-terminus (Bonello and Peifer, 2019) (Figure 1.3). Dlg, which has 4 orthologues in vertebrates, is a member of the MAGUK family of proteins with about 102 KDa (Woods and Bryant, 1991) containing three PDZ domains, a Src homology 3 (SH3) and a guanylate kinase-like (GUK) domain (Humbert *et al*., 2015) (Figure 1.3). The GUK domain of MAGUK proteins does not have an ATP-binding site, being therefore inactive (Funke *et al*., 2005). However, it regulates protein interactions, as well as the SH3 domain, which can enhance the assembly of multiprotein complexes (Humbert *et al*., 2015). In *Drosophila* embryonic epithelial cells, Scrib and Dlg are co-localized basally to the adherens junctions and were both found to be required for the proper formation of septate junctions and zonula adherens (Bilder and Perrimon, 2000; Woods *et al*., 1996). Finally, Lgl, encoded by two Lgl orthologues in mammalians, Lgl-1 and Lgl-2 (Hugl-1 and Hugl-2 in humans), is a protein with about 130 kDa (Klämbt and Schmidt, 1986) containing fourteen WD40 repeats predicted to fold into two β-propellers, which mediate the coordination of multiprotein complexes assemblies (Cao *et al*., 2015). Moreover, Lgl contains a Basic and Hydrophobic (BH) domain, also known as polybasic domain (PB), which is within a loop between the 10^{th} and 11^{th} WD40 repeats in the C-terminal β – propeller, according to the structure of the Lgl yeast orthologue, Sro7 (Hattendorf *et al*., 2007; Dong *et al*., 2015). This BH domain mediates Lgl binding to the plasma membrane and contains the three evolutionarily conserved serines that were found to be the phosphorylation sites for aPKC and Aurora A (S656, S660 and S664) (Bailey and Prehoda, 2015; Dong *et al*., 2015) (Figure 1.5). This BH domain interacts electrostatically with phosphatidylinositol phosphates (PIPs), mainly phosphatidylinositol 4,5-biphosphate (PIP_2), of the plasma membrane (Dong *et al*., 2015; Bailey and Prehoda, 2015) (Figure 1.5). Beyond binding to the plasma membrane, Lgl is partially localized in the cytoplasm and is highly associated with the actomyosin cytoskeleton in the cortex (Strand, 1994; Betschinger *et al*., 2003).

Biochemical assays revealed a physical interaction between Lgl and non-muscle myosin II (NMII) heavy chain [encoded by zipper (zip) gene in *Drosophila*] (Betschinger *et al*., 2005). However, depletion of PIPs from the plasma membrane by hypoxia fully induces Lgl cortical release without interfering with the localization of other cortical components (Dong *et al*., 2015), suggesting that cortical interactions may require Lgl concentration near the plasma membrane (Moreira and Morais-de-Sá, 2016).

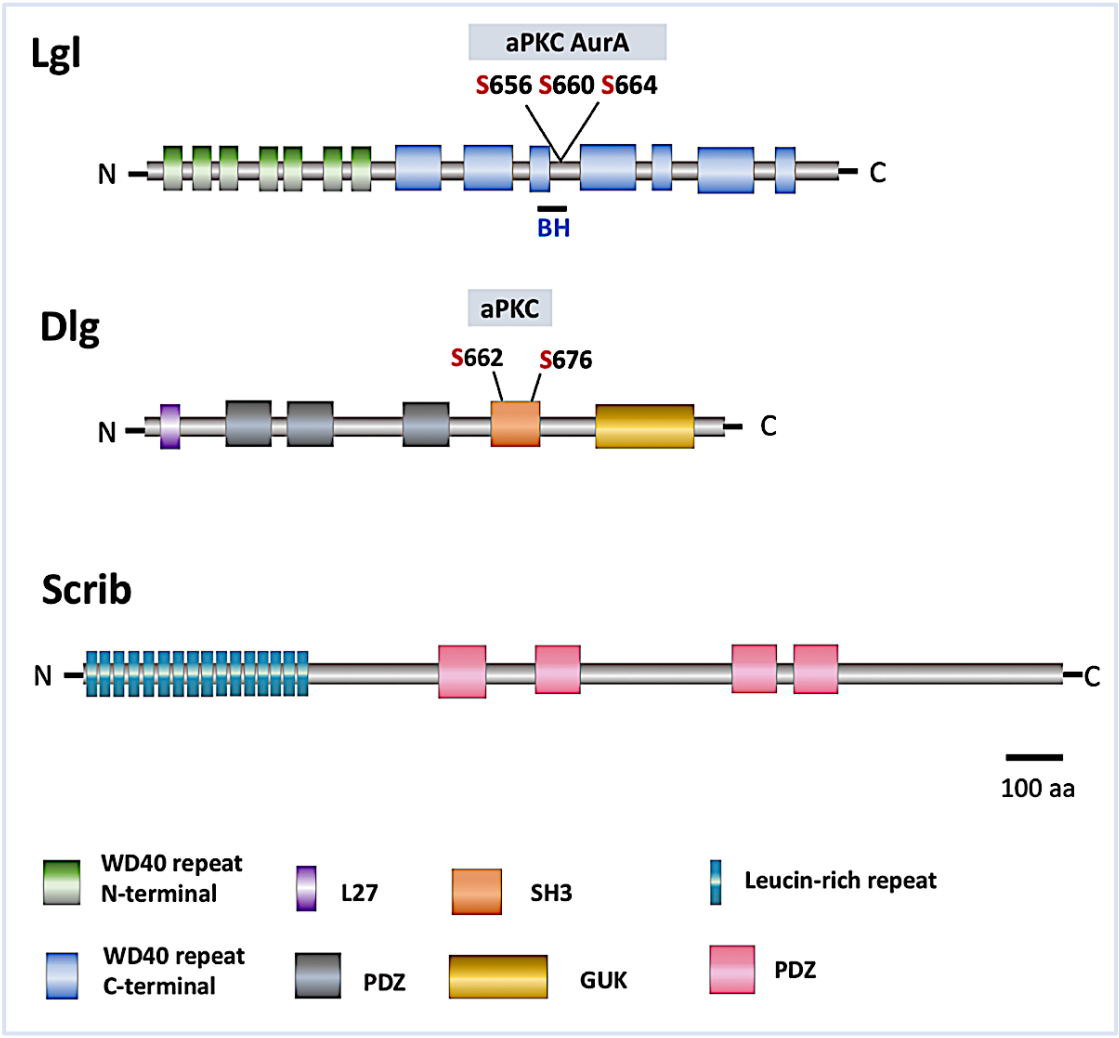

Figure 1.3: Structural representation of Lgl, Dlg and Scrib. Lgl contains fourteen WD40 repeats predicted to fold into two β-propellers. The localization of the Basic and Hydrophobic (BH) domain is shown, containing the three evolutionarily conserved serines found to be the phosphorylation sites for aPKC and Aurora A (S656, S660 and S664). Dlg is a member of the MAGUK family of proteins containing three PDZ domains, a Src homology 3 (SH3) and a guanylate kinase-like (GUK) domains for the assembly of multiprotein complexes. The aPKC-phosphorylated serines in the SH3 domain of Dlg are also represented. Scribble is a protein that belongs to the LAP (Leucin-rich repeats and PDZ domain) family, containing four PDZ domains at the C-terminus and sixteen LRR (Leucin-rich repeats) in the N-terminus. This scheme was based on Flores-Benitez and Knust, 2016.

Moreover, Lgl cortical localization was shown to be partially independent of myosin II (Betschinger *et al*., 2005). In fact, beyond myosin II, other proteins localized at the cortex have been described to form alternative complexes with Lgl, namely the apical polarity proteins aPKC, Par6 and potentially the basolateral proteins Dlg or Scrib (Betschinger *et al*., 2003; Plant *et al*., 2003; Kallay *et al*., 2006; Yamanaka *et al*., 2003; Zhu *et al*., 2014).

Despite the initial scepticism associated with the identification of single gene mutations able to induce a dramatic overproliferation, the role of basolateral polarity proteins has been confirmed in human carcinoma, highlighting the importance of *Drosophila* for our current understanding of human diseases (Bilder, 2004; Mathew *et al*., 2002; Zhan *et al*., 2008). Additionally, there are several evidences for a functional conservation between these proteins, since expression of human orthologues of Lgl-1, Dlg and Scrib rescues *Drosophila lgl* (Grifoni *et al*., 2004), *dlg* (Thomas *et al*., 1997) and *scrib* (Dow *et al*., 2003) mutants, respectively.

A) Scribble module on the regulation of intracellular signaling pathways

Beyond their important role in cell polarity, proteins of the basolateral Scribble module have been implicated in the regulation of several signaling pathways in a wide range of cellular contexts and organisms, acting as signalling scaffolds to control tissue growth, differentiation and proliferation. Briefly, I will provide an overview of four of these signaling pathways, which have been strongly linked to cancer development: Wingless/Wnt, Notch, JNK and Salvador-Warts-Hippo pathway.

The Wingless/Wnt pathway relies on a large number of proteins from the Wnt protein family, Wnt receptors from the Frizzled (Fzd) family and mediators of the signaling, such as Dishevelled (Dvl) (Cao *et al*., 2015). Upon Wnt receptor activation, this signaling pathway is involved in a noncanonical planar cell polarity (PCP) pathway or in the canonical Wnt/β-catenin cascade, shown to regulate the stability of β-catenin, a component of adherens junctions, by inhibiting adenomatous polyposis coli (APC)-mediated degradation (Humbert *et al*., 2015). Disruption of this pathway has been implicated in colorectal cancer and other human tumours (Clevers, 2006). The three members of the basolateral module have been described to interact with components of this pathway. Dlg was the first protein implicated in the Wnt signaling by interacting with the negative regulator of Wnt, the APC tumour suppressor (Matsumine *et al*., 1996), which is important for the effects of Dlg in polarized

cell migration (Etienne-Manneville *et al*., 2005). Dlg was also found to bind the Wnt receptor Frizzled (Fzd). Lgl has also been linked to this pathway since it has been shown that Dvl is important for the maintenance of Lgl localization in the cortex in *Xenopus* ectoderm and *Drosophila* follicular epithelium and that expression of one of the Fzd receptors disrupts the membrane localization of Lgl in *Xenopus* embryos (Dollar *et al*., 2005). Last, Scrib has been also been linked to the non-canonical Wnt pathway in controlling PCP (Humbert *et al*., 2008).

The evolutionarily conserved Notch signaling pathway has been strongly implicated in the maintenance of stem cell self-renewal, proliferation, cell fate or determination and apoptosis, and is therefore related with several diseases (Bi and Kuang, 2015). Lgl affects Notch signaling by controlling the localization of an inhibitor of Notch signaling, Numb, which upon cell division concentrates in the daughter cell inhibiting Notch signaling and enabling neural differentiation (Ohshiro *et al*., 2000). Lgl was found to block aPKC activity to control the asymmetric localization of Numb. When Lgl is released from aPKC, this kinase binds Par-3 (Bazooka) and can phosphorylate Numb, excluding it from the apical cortex to the basal side of the cell (Wirtz-Peitz *et al*., 2008). Loss of *lgl* was reported to upregulate notch signaling in *Drosophila* eye tissue (Parsons *et al*., 2014), in neural tubes of *lgl* mutant mice (Klezovitch *et al*., 2004) and zebrafish retinal neuroepithelial cells, which has been associated with the failure to segregate Numb and inhibit Notch signaling in daughter cells. Additionally, it was proposed that Lgl regulates Notch signaling pathway by controlling the endosomal trafficking of Notch (Clark *et al*., 2012).

Salvador-Warts-Hippo and JNK signaling pathways have emerged as important regulators of cell proliferation. The first evidence that Dlg, Lgl and Scrib could participate in signaling pathways controlling proliferation came from a screen for suppressors of a mutation of *cyclin E*, a key regulator of the cell cycle (Brumby *et al*., 2004). When the Salvador-Warts-Hippo pathway is active, the kinase Warts (Wts) induces the phosphorylation of Yki, a transcriptional co-activator, which results in cytoplasmic retention; on the other hand, when Wts is inactive, Yki is able to enter the nucleus and activate the transcription of genes involved in cell growth, proliferation and resistance to apoptosis, such as *cycE* and *diAP1* (***D****rosophila* ***I****nhibitor of* ***AP****optosis* ***1***) (Humbert *et al*., 2015; Halder and Johnson, 2011). The members of the Scrib polarity module were shown to be involved in regulation of Hippo pathway in both *Drosophila* and mammals (Humbert *et al*., 2015). Lgl regulates the localization of the kinase Hippo, and loss of Lgl or upregulation of aPKC in *Drosophila* (which completely releases Lgl from the membranes, phenocopying *lgl* mutants) leads to

downregulation of the Hippo pathway, increasing proliferation and cell survival (Grzeschik *et al*., 2010).

The c-Jun N-terminal kinase (JNK) pathway is an evolutionarily conserved stress-induced mitogen-activated protein kinase (MAPK) with roles in proliferation, tumour development and apoptosis, and which has been described to have both tumour-suppressing and tumour-promoting functions (Bubici and Papa, 2014). Mutations in *lgl*, *dlg* and *scrib* lead to an activation of this pathway, which downregulates E-cadherin/beta-catenin adhesion complex and, in combination with activated Ras^{v12}, induced tumours in *Drosophila* eye (Pagliarini, 2003). However, when *scrib* mutant cells are surrounded by wild-type cells, a JNK-mediated apoptotic pathway directed by wild-type cells induces apoptosis, supressing tumour development in *Drosophila* eye (Brumby and Richardson, 2003). Similarly, *lgl* mutant cells also undergo apoptotic cell death mediated by JNK signaling in mutant clones, except when overgrowth potential is re-established by promoting c-Myc-induced cell competition (Froldi *et al*., 2010). These examples underline the importance to consider the surrounding tumour microenvironment in tumour survival and progression.

B) Scribble module proteins on the regulation of vesicle trafficking

Scribble polarity proteins have also been linked to the regulation of vesicle trafficking, which is shown to be fundamental for the regulation of signaling pathways. One example was already mentioned, where Lgl controls the endosomal trafficking of a negative regulator of the Notch pathway (Parsons *et al*., 2014). In fact, several studies report the interaction of Lgl with components of the vesicle trafficking pathways, such as the basolateral exocyst machinery (Müsch *et al*., 2002). Early studies in yeast also show that the Lgl orthologues, Sro7 and Sro77, interact with the exocyst machinery (Zhang *et al*., 2005), and secretion defects observed in mutants for these yeast homologues can be rescued by mammalian Lgl through a mechanism that depends on binding of Lgl to the vesicle docking t-SNARE protein, Sec9 (Gangar *et al*., 2005). Lgl might therefore regulate exocytosis, controlling the polarized transport of proteins and lipids to the cell surface through interaction with exocyst components, or regulating pathways which mediate the fusion of post-Golgi transport vesicles to membranes (Cao *et al*., 2015). Moreover, a role for Scribble in the regulation of the proper recycling of a thyroid-stimulating hormone receptor was also found (Lahuna *et al*., 2005), as well as for vesicle recycling dynamics (Roche *et al*., 2002). In mammalian cells, Scrib was described to stabilize Ecad-p120 interaction and prevent retromer sorting of Ecad destined to lysosomes (Lohia *et al*., 2012). However, analyses of Ecad localization

and trafficking mutant cells for members of the Scrib module suggest that a different mechanism might act in *Drosophila* (de Vreede *et al*., 2014).

Interestingly, basolateral determinants play an important role in the exocyst-mediated transport of Crumbs to the apical membrane (Blankenship *et al*., 2007). Recently, a mechanism related with Scrib module involvement in retrograde transport (a traffic mechanism that allows the recycling of plasma membrane proteins to the trans-Golgi network or from the Golgi to the endoplasmic reticulum) has been suggested. The Scrib module protein was described to be required for proper retromer localization to endosomes, promoting cargo sorting into the retromer pathway and regulating epithelial cell polarity by their impact on endocytic pathways that transport Crumbs and other cargo (de Vreede *et al*., 2014).

2.1.3. Mutual antagonism between apical and basolateral proteins

Several studies have suggested that the apical protein complexes and the basolateral module establish antagonistic interactions, balancing their activities to define the boundaries and sizes of their complementary cortical domains, as well as the position of the cellular junctions (Bilder and Perrimon, 2000; Tanentzapf and Tepass, 2003). The aPKC/Par apical complex was found to be essential to restrict Lgl localization at the basolateral membrane (Hutterer *et al*., 2004). Conversely, Lgl (together with Dlg and Scribble) specify the basolateral domain by excluding apical proteins (Hutterer *et al*., 2004). Accordingly, loss of Scrib members induce an extension of apical determinants aPKC and Crb, together with cell junction proteins, along the cortex (Bilder and Perrimon, 2000) (Figure 1.4). This mutual antagonism between apical and basolateral polarity networks has been suggested by several genetic interaction experiments, one of them showing that reduction of aPKC levels suppresses cell proliferation and polarity defects observed in *lgl* mutants (Rolls *et al*., 2003). On the other hand, Crb overexpression mimics the loss of Scribble module, resulting in an expansion of the apical domain and reduction of the basolateral one (Wodarz *et al*., 1995; Tanentzapf and Tepass, 2003). Additionally, reduction of Scrib module proteins suppress mutations of Crb complex elements (Bilder *et al*., 2003).

The best described mechanism for apical antagonism of basolateral determinants is centered on aPKC's ability to phosphorylate Lgl on the three evolutionarily conserved serines in the apical domain, which restricts Lgl to the basolateral domain (Figure 1.6)

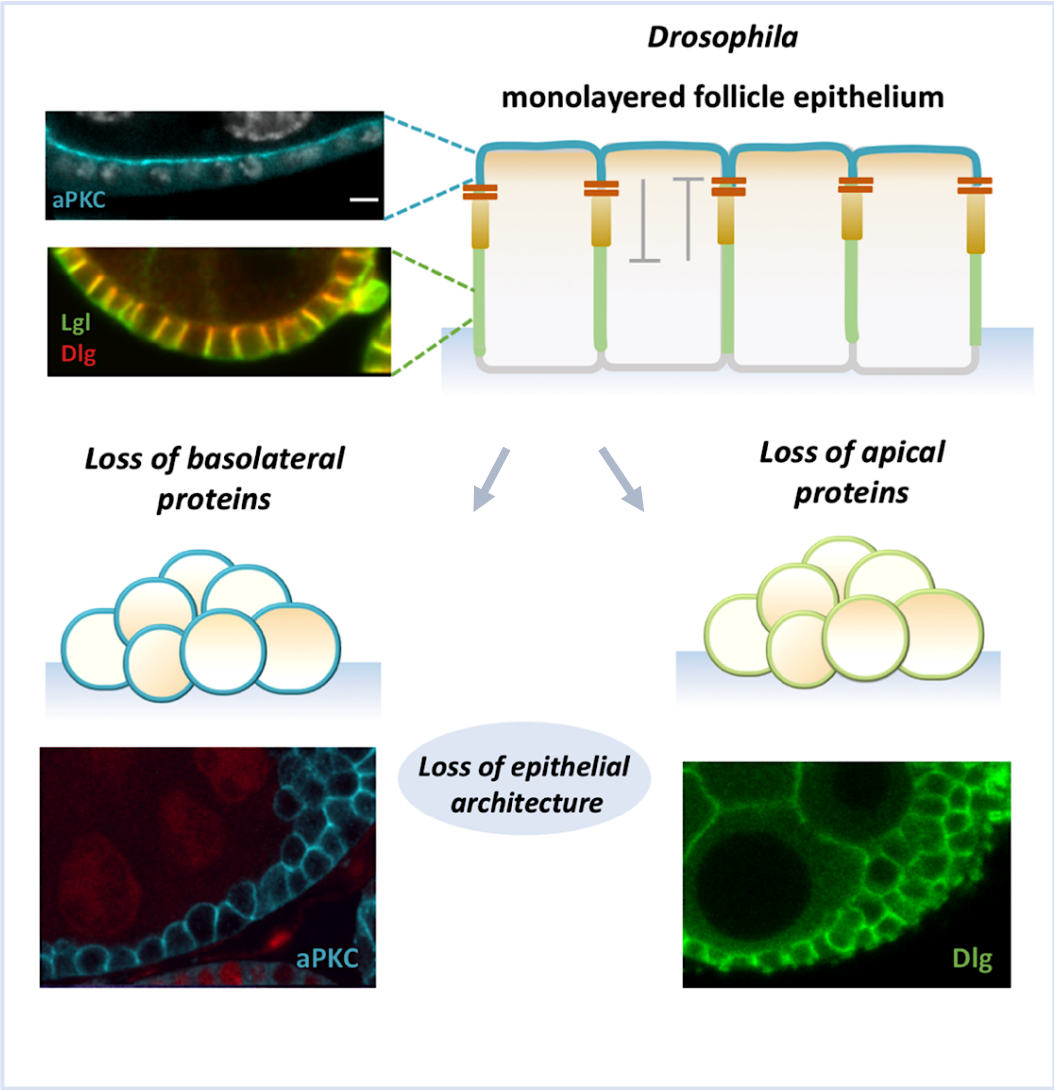

Figure 1.4: Apical and basolateral polarity proteins are fundamental for the maintenance of epithelial tissue architecture. Confocal microscopy images of the *Drosophila* follicular epithelium are shown. When an equilibrium between apical and basolateral activities is established, epithelial cells are organized in a single monolayer, with apical proteins and basolateral proteins properly localized. When cell polarity is disrupted, both by interfering with expression or localization of basolateral or apical proteins, epithelial cells lose their polarity and the highly organized architecture of the tissue is disrupted. Loss of apical restriction provided by basolateral proteins induces a mislocalization of apical proteins, such as aPKC. On the other hand, when apical proteins are perturbed, basolateral proteins are no longer under the antagonistic positioning control of the apical domain and lose their proper localization.

(Betschinger *et al*., 2003; Betschinger *et al*., 2005; Dong *et al*., 2015). Similarly, aPKC targets mammalian Lgl (mLgl) on conserved serine residues, which is important for the restriction of Lgl to the basolateral domain (Plant *et al*., 2003). Other possible mechanisms contributing to the involvement of Lgl in defining the basolateral identity may rely on its role in vesicle trafficking and secretion of basolateral proteins (Müsch *et al*., 2002), and on its interaction with Myosin II in the basolateral cortex (Betschinger *et al*., 2005). Much less understood is how the apical complex restricts the localization of Dlg and Scribble to the basolateral domain. None of the apical complexes exclude Dlg from the apical membrane domain in the follicular epithelia, since it was shown that loss of *baz*, *par-6*, *apkc* and *crb* does not affect Dlg localization (Franz and Riechmann, 2010). Instead, a role for armadillo (Arm) and AJs in preventing the apical localization of Dlg was proposed (Franz and Riechmann, 2010).

The molecular mechanisms involved in the inhibition of aPKC in the basolateral domain are still largely unknown, but several hypothesis have been proposed. One suggests that Lgl, Par-6 and aPKC are able to interact in the basolateral cortex and prevent Par-3 association with this complex, thus inhibiting the formation of the apical complex in the basolateral side of mammalian cells (Yamanaka *et al*., 2003; Yamanaka, 2006). In fact, Lgl was reported to tightly associate with aPKC in the Par protein complex (Betschinger *et al*., 2003). A role for Lgl in inhibiting the basolateral localization of Par-6 and Patj was also demonstrated in *Drosophila* (Hutterer *et al*., 2004). A computational model of apical-basal polarity predicts that the ectopic spreading of apical determinants in the basolateral domain, induced by reducing the rate by which apical determinants are endocytosed, can be counteracted by 5-fold increasing of basolateral determinants (Fletcher *et al*., 2012). In fact, when Lgl-GFP is overexpressed, it was shown to be sufficient to restore the normal polarity in follicle epithelia where endocytosis pathway is compromised and when Crb is overexpressed, thus suggesting that Lgl is able to promote endocytic removable of apical determinants in the basolateral membrane (Fletcher *et al*., 2012). Another hypothesis relies on Scrib's ability to assembly a physical barrier that separates apical and basolateral domains, similarly to the barrier function proposed for the tight junctions in vertebrates (Bilder and Perrimon, 2000; Tsukita *et al*., 2001). The existence of a barrier has been proposed to control lipid lateral diffusion in the plasma membrane and thus in maintaining lipid composition of apical and basolateral membranes (Dragsten *et al*., 1981; van Meer and Simons, 1986). Finally, it was proposed that Scrib can control the polarized targeting of transport proteins carrying apical proteins (Bilder and Perrimon, 2000) and that the Scribble module regulates cell polarity by controlling the delivery of Crumbs to the apical domain (de Vreede *et al*., 2014).

Other basolateral proteins beyond the Scrib module proteins were found to act in parallel to restrict the localization of apical complex. For instance, it was shown that Par1 phosphorylation of Bazooka creates new sites for binding to 14-3-3 proteins, thus impairing the association of Bazooka with aPKC-Par6 and restricting the aPKC-Par6-Bazooka complex to the apical side (Benton and St Johnston, 2003). A second group of basolateral proteins, the Yurt/Cora group, composed by the FERM (band **4**.1/**E**zrin/**R**adixin/**M**oesin domain) proteins Yurt (Yrt), Coracle (Cora), the membrane proteins Neurexin IV (Nrx-IV) and the α subunit of Na^+/K^+-ATPase, were also shown to antagonize the activity of the apical determinants independently on the Scrib module (Laprise *et al*., 2006, Laprise *et al*., 2009). This group of epithelial polarity proteins promotes basolateral membrane identity by antagonizing the activity of the Crb complex during mid-embryonegesis in *Drosophila*, with mutants for Yrt displaying extended apical membranes and epithelial polarity defects (Laprise *et al*., 2006; Laprise *et al*., 2009). In contrast to *dlg*, *lgl* and *scrib*, *yurt* mutants can only suppress *crb* mutant phenotype in the presence of some Crb activity, but not in the total absence of Crb, suggesting a direct role of Yurt on Crb. In fact, the antagonistic interaction between Yurt and Crb mainly relies on direct binding of the Crb cytoplasmic tail with the FERM domain of Yrt, leading to the apical recruitment of Yrt by Crb, which subsequently negatively regulates the activity of Crb during late embryogenesis (Laprise *et al*., 2009). However, Yurt only becomes part of the Crb complex in later stages of epithelial differentiation (Laprise *et al*., 2009), being localized in the basolateral membrane by aPKC phosphorylation in early stages to regulate epithelial polarity together with Nrx-IV and α subunit of Na^+/K^+-ATPase (Gamblin *et al*., 2014; Laprise *et al*., 2006; Laprise *et al*., 2009). However, unidentified mechanisms exist in late embryos that ensure polarization of epithelia independently of Yrt/Cora and Lgl-group proteins (Laprise *et al*., 2009).

3. The importance of aPKC and Aurora A kinases in cell polarity

Kinases are essential proteins controlling a broad range of processes, including the subcellular localization of polarity proteins. Here we will focus on two important serine/threonine protein kinases for cell polarity, aPKC and Aurora A, which will be frequently mentioned due to their role in Lgl regulation. First, I will focus on aPKC, which was recently considered the "kinase that phosphorylates cell polarity" (Hong, 2018), due to its role in phosphorylating a wide number of proteins in different types of cell polarity. After, I will focus on Aurora A, a key kinase that is usually associated with key mitotic processes, such as the assembly of a bipolar spindle and maturation of centrosomes (Kollareddy *et al*., 2008; Nikonova *et al*., 2013) and which also has important non-mitotic roles in microtubule dynamics (Lorenzo *et al*., 2009; Yamada *et al*., 2010), cell migration and, most importantly for this work, cell polarity.

3.1. aPKC: "the kinase that phosphorylates cell polarity"

aPKC phosphorylates several polarity proteins to regulate their localization, generally promoting their exclusion to opposite domains of the plasma membrane/cortex (Betschinger *et al*., 2003; Hannaford *et al*., 2018). Recently, a mechanism was proposed by which phosphorylation by aPKC changes the affinity of polarity proteins like Lgl, Numb and Mira to the plasma membrane, allowing their reallocation (Dong *et al*., 2015; Bailey and Prehoda, 2015). As previously mentioned, aPKC-phosphorylation sites are often localized in polybasic (PB) domains highly rich in positively charged residues, such as Arg and Lys, which mediate electrostatic binding to negatively charged phosphoinositides of the plasma membrane (McLaughlin and Murray, 2005). Recently, it was shown that phosphorylation of these serines by aPKC disrupts binding to the plasma membrane by weakening the electrostatic interactions with phospholipids (Graybill and Prehoda, 2014; Dong *et al*., 2015; Bailey and Prehoda, 2015) (Figure 1.5). Moreover, *in vitro* studies also proposed that the positively charged domain of Lgl1 containing the aPKC phosphorylation sites binds to a negatively charged domain in NMII. Consequently, phosphorylation decreases the positive charge of the Lgl1 interacting domain, dissociating Lgl from the actomyosin cytoskeleton (Dahan *et al*., 2014). A similar mechanism might regulate Lgl binding to NMII in *Drosophila*, which was found to interact with NMII through the C-terminal domain, composed by highly positively charged amino acids (Figure 1.5) (Betschinger *et al*., 2005). aPKC phosphorylation might also induce conformational changes that prevent the polybasic

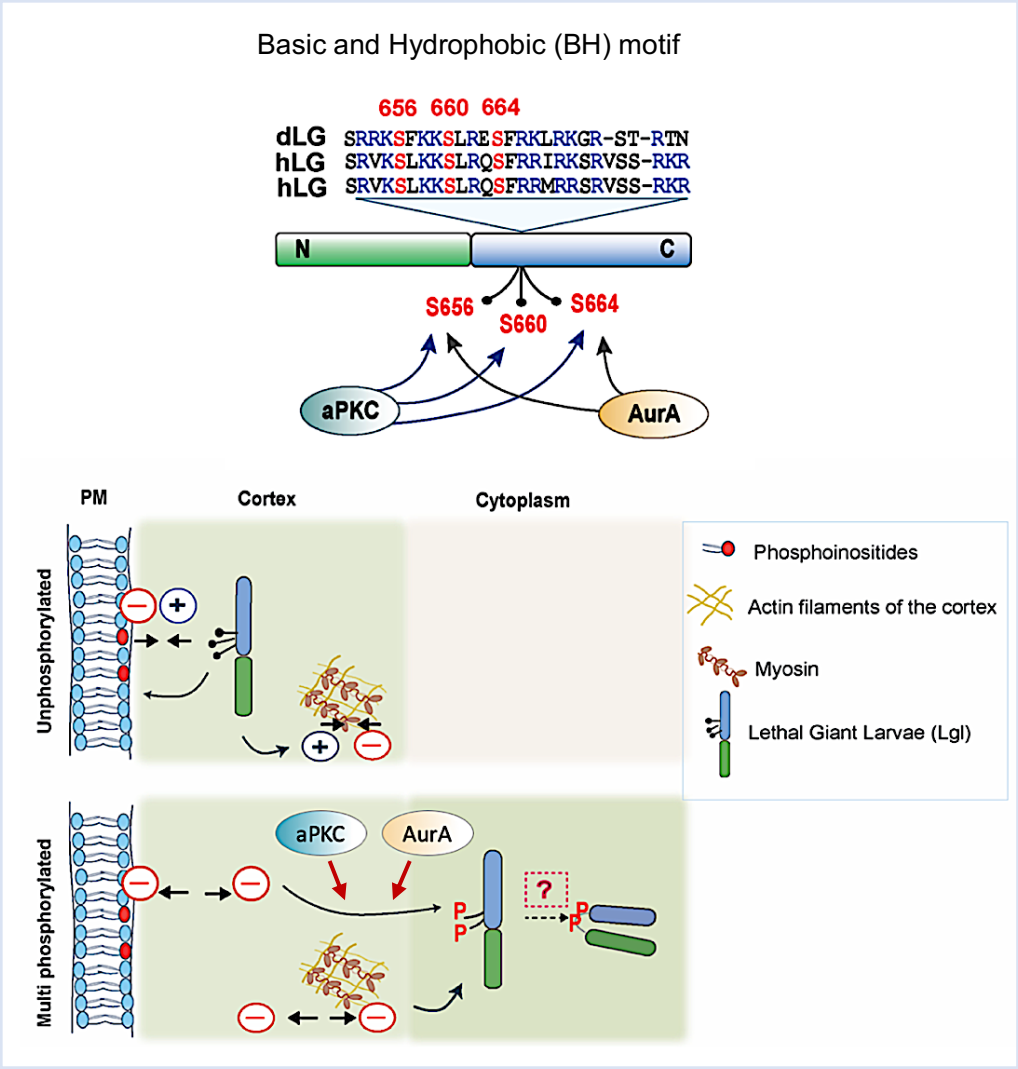

Figure 1.5: Aurora A and aPKC phosphorylate Lgl to control its localization and interaction with cortical binding partners. aPKC phosphorylates Lgl on three evolutionarily conserved serines and restricts its localization to the basolateral domain in epithelial interphase. Aurora A activation phosphorylates Lgl during mitosis on two of the serines also targeted by aPKC, providing temporal control for Lgl phosphorylation during mitosis. Recent studies suggest that Lgl binds to the plasma membrane through electrostatic interactions with phospholipids. Phosphorylation of Lgl disrupts the electrostatic binding of the BH domain with the plasma membrane. The same mechanism is expected to impair Lgl binding to cortical myosin upon phosphorylation. Whether phosphorylation induces additional conformational change in Lgl is still unclear. Adapted from Moreira and Morais-de-Sá, 2016.

domain to bind the plasma membrane. Consistent with this, early studies propose a conformational change model for Lgl release and “inactivation” from the cortex/plasma membrane after aPKC phosphorylation (Betschinger *et al*., 2005). This model is based on *in vitro* experiments and analysis of deletion mutants in *Drosophila* neuroblasts, and proposes that phosphorylation of serine residues induces an intramolecular association between the C- and N-terminus of Lgl, closing the protein and masking the domains that mediate cortical and plasma localization of Lgl (Betschinger *et al*., 2005) (Figure 1.5). However, structural evidences able to support a conformational change of phosphorylated Lgl are still lacking. Moreover, recent crystal structure analyses of human Lgl2 in aPKC-phosphorylated state contradict the model of a phosphorylation-dependent conformational change of Lgl2 (Almagor *et al*., 2019).

aPKC phosphorylation was also recently reported to induce a conformational change of Dlg, an important step for its role in orienting the spindle in *Drosophila* neuroblasts (Golub *et al*., 2017). Phosphorylation by aPKC in serines localized in the SH3 domain of Dlg disrupts the inhibitory interaction between SH3 and GUK domains and renders Dlg in an open conformation, so that it can bind other proteins that mediate mitotic spindle orientation, such as GuKH (Golub *et al*., 2017). Another interesting mechanism where aPKC-mediated phosphorylation controls spindle orientation by changing protein conformation was reported in epithelial MDCK cells (Hao *et al*., 2010). In this case, aPKC phosphorylates Pins/LGN, a protein that links the cell cortex with the astral microtubules of the mitotic spindle, and hinders Pins/LGN binding to heterotrimeric G-protein in the apical cortex, thus restricting Pins ability to orient the spindle in the basolateral cortex which, otherwise, would be randomly oriented (Hao *et al*., 2010). A role for aPKC in orienting the spindle was reported in the wing disk epithelium, where aPKC controls the apical exclusion of Pins during mitosis (Guilgur *et al*., 2012). However, recent live imaging analyses of spindle orientation in the *Drosophila* wing disk reported that Pins is dispensable for orientation of spindle, since a Pins-independent mechanism that involves Mud can act redundantly for proper spindle orientation (Bergstralh *et al*., 2016). Thus, the role of aPKC in orienting the spindle is not universal, since in *Drosophila* follicular epithelium aPKC was also shown to be dispensable for planar spindle orientation, as well as in the chick neuroepithelium (Bergstralh et al., 2013, 2017; Peyre et al., 2011).

3.2. Aurora A: the kinase that links cell-cycle regulation with cell polarity

Several studies have suggested that Aurora A is activated at mitotic entry by interacting with some proteins including TPX2, Ajuba, Bora, or by autophosphorylation of its kinase activation loop (Nikonova *et al*., 2013). The best known mechanism by which AurA is activated relies on TPX2 binding and induction of a conformational change that activates Aurora A autophosphorylation and inhibits the access of PP1 to the phosphorylated residue, which would inactivate the kinase (Xu *et al*., 2010).

Aurora A expression and activity have to be temporally and spatially controlled for a proper mitotic progression, centrosome maturation, formation of the bipolar spindle and cytokinesis (Nikonova *et al*., 2013). High levels of this protein have been found in many types of solid tumours and are associated with centrosome amplification, defective mitotic spindles and aneuploidy (Zhou *et al*., 1998; Bischoff *et al*., 1998; Tanaka *et al*., 1999; Goepfert *et al*., 2002). In *Drosophila*, *aurora* mutants induce a mitotic arrest characterized by formation of monopolar spindles, inducing pupal lethality, and defects in chromosome separation, segregation, among others (Nikonova *et al*., 2013). Spatiotemporal regulation of Aurora A activity relies in ubiquitin-mediated proteolysis (Lindon *et al*., 2016). Aurora A undergoes targeted proteolysis by the proteasome upon ubiquitination mediated by the anaphase promoting complex/cyclosome (APC/C) and its co-activator Fzr/Cdh1 (Castro *et al*., 2002) after anaphase onset. Aurora A contains two recognition domains which are necessary for APC/Cdh1-mediated degradation, the N-terminal A-box and the C-terminal D-box (Littlepage and Ruderman, 2002). Mutated versions of Aurora A-GFP in D-box or A-box strongly delay Aurora A-degradation (Lindon *et al*., 2016). However, while the D-box mutant also disrupts the localization of AurA-GFP at centrosomes, the A-box mutant version maintains the normal localization of AurA-GFP (Lindon *et al*., 2016).

Aurora A was found to have an important role in cell polarity during asymmetric cell division. Early work performed in *Drosophila* sensory organ precursor (SOP) cells shows that activation of Aurora A at the onset of mitosis is important for the asymmetric segregation of Numb, a repressor of Notch signaling required for the establishment of the correct cell fate (Berdnik and Knoblich, 2002). In fact, the authors observed that in *aur* mutants, Numb fails to localize asymmetrically into one of the two daughter cells (Berdnik and Knoblich, 2002). Later on, a direct link between Aurora A and phosphorylation of a polarity protein was found to regulate Numb localization in *Drosophila* neural precursor cells. In these cells, it has been proposed that Lgl binds aPKC in the cell cortex during interphase, acting as a "molecular buffer" or inhibitor for the activity of aPKC over the cell fate determinants (Wirtz-

Peitz *et al*., 2008). During mitosis, Aurora A activates aPKC by phosphorylating Par-6, which promotes Lgl phosphorylation and consequently exclusion to the cytoplasm (Wirtz-Peitz *et al*., 2008). Release of Lgl allows Bazooka to enter the Par-6/aPKC complex, so that it works as a specificity factor to induce phosphorylation and consequent asymmetric segregation of the cell fate determinants (Wirtz-Peitz *et al*., 2008). This was the first example that cell polarity can be directly coupled with processes regulated by the cell-cycle. Later on, Bell and colleagues postulate a revised model for Lgl regulation during asymmetric cell division by suggesting that Aurora A, beyond its role in activating aPKC, also phosphorylates Lgl directly in neuroblasts (Bell *et al*., 2015).

Aurora A is also an important link between cell-cycle regulation and cell polarity during symmetric cell division. In the *Drosophila* follicular epithelia and wing disk, Aurora A triggers Lgl phosphorylation during prophase and induces its release from the cortex to the cytoplasm (Bell *et al*., 2015; Carvalho *et al*., 2015). This mechanism was found to be important for proper orientation of the spindle, as will be explored in more detail in the next subheading of this introduction. Finally, two recent studies reported additional roles for Aurora-A kinase, revealing an essential role for this kinase in breaking cell symmetry for the polarisation of the *Caenorhabditis elegans* embryo (Klinkert *et al*., 2019; Zhao *et al*., 2019). While in early cell cycle, Aurora A prevents symmetry breaking, Aurora A accumulated in centrosomes is sufficient to induce symmetry breaking thereafter (Klinkert *et al*., 2019; Zhao *et al*., 2019). One possible model by which Aurora A promotes asymmetry breaking relies on Aurora A disassembly of actomyosin around the centrosomes to promote cortical flows (Zhao *et al*., 2019).

3.3. Spatiotemporal phosphoregulation of Lgl by aPKC and AurA in epithelial cells

Phosphorylation of Lgl by aPKC and Aurora A provides spatiotemporal control for Lgl interaction with cortical partners and the plasma membrane, therefore affecting its localization and function during the cell-cycle. In interphase, aPKC phosphorylation restricts Lgl localization to the basolateral side of epithelial cells by preventing its association with the apical cortex/membrane (Betschinger *et al*., 2003; Hutterer *et al*., 2004; Plant *et al*., 2003; Yamanaka *et al*., 2003) (Figure 1.5 and Figure 1.6). As previously mentioned, phosphorylation of Lgl on aPKC/Aurora A phosphorylation sites disrupts the electrostatic binding of Lgl to PIPs in the plasma membrane (Dong *et al*., 2015). Consistent with the importance of Lgl phosphorylation by aPKC for its exclusion from the apical domain and function in supporting cell polarity, an unphosphorylatable form of Lgl, Lgl^{3A}, in which the three phosphorylatable serines were mutated to alanines, extends to the apical domain of epithelial cells (Carvalho et al., 2015; Hutterer et al., 2004) and also of MDCK mammalian cells (Zhu *et al*., 2014), but is unable to interfere with aPKC polarisation or rescue the multilayering phenotype induced by loss of *lgl* (Carvalho *et al*., 2015) (Figure 1.7). This suggests that Lgl^{3A} is unable to support cell polarity.

Lgl is excluded from the cortex to the cytoplasm during symmetric cell division in epithelial cells (Figure 1.6) (Bell *et al*., 2015; Carvalho *et al*., 2015), while the other basolateral proteins, Dlg and Scrib, remain associated with the cortex during mitosis. In contrast to neural precursor cells, Lgl mitotic relocation is mostly independent of aPKC in epithelial cells. One big difference between epithelial cells and neural precursor cells lies on the localization and temporal activation of aPKC. In epithelial cells aPKC is specifically active at the apical side during interphase. Importantly, Lgl starts to be excluded at prophase in epithelial cells, when most aPKC is still localized in the apical side and physically separated from the basolateral Lgl (Carvalho *et al*., 2015). Thus, it would be unlikely that aPKC phosphorylation *per se* would induce a fast and efficient exclusion of all cortical Lgl. Consistently, Lgl is still released from the cortex to the cytoplasm during mitosis in *apkc* mutant epithelial cells (Bell *et al*., 2015; Carvalho *et al*., 2015).

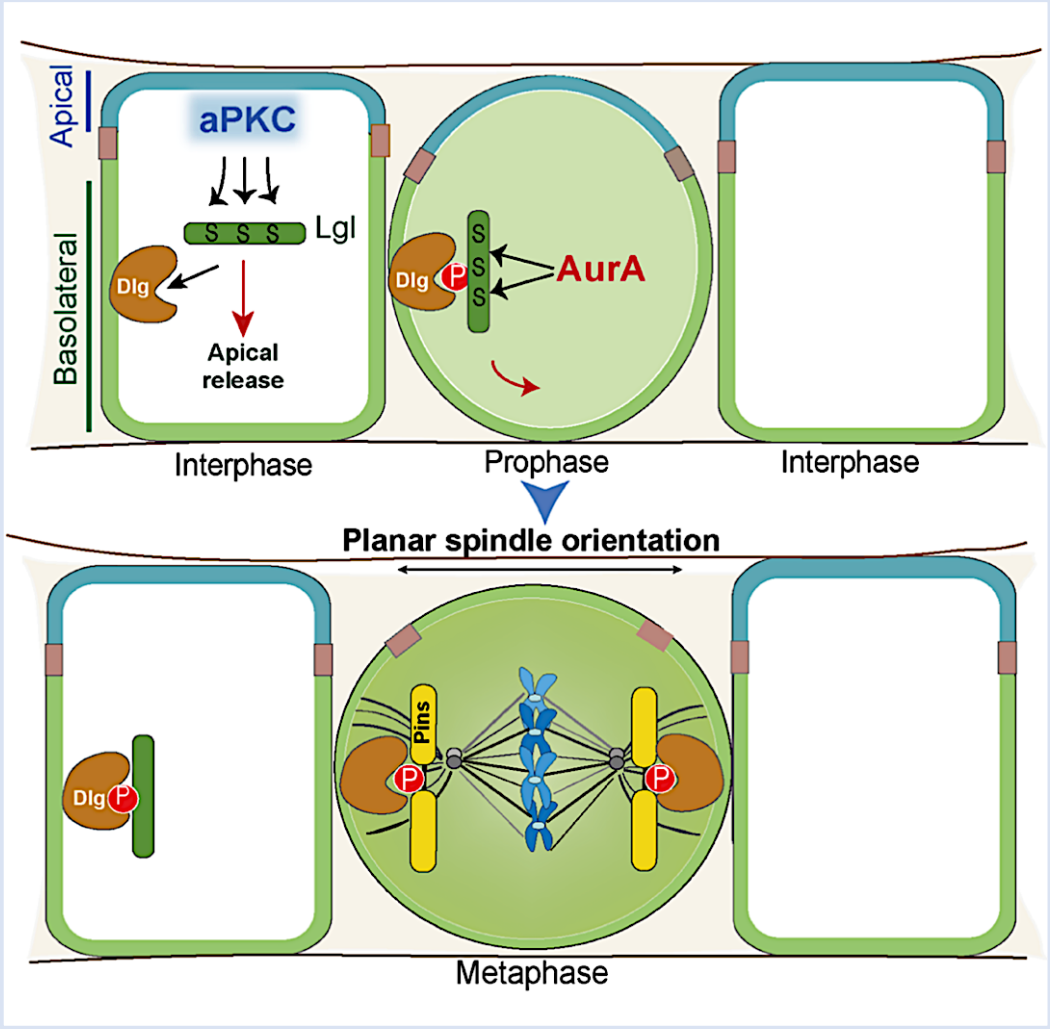

Figure 1.6: Lgl phosphorylation by Aurora A and cortical release during mitosis promotes planar mitotic spindle orientation. Schematic representation of a model for how Lgl phosphorylation during mitosis converts the Dlg/Lgl complex into a Dlg/Pins complex that can anchor the spindle at the lateral cortex. aPKC phosphorylates Lgl during interphase, inducing the apical release of the protein. Moreover, according to *in vitro* results (Zhu *et al*, 2014), one phosphorylated serine of Lgl allows interactions with the GUK domain of Dlg. When Aurora A is activated at prophase, further phosphorylation of Lgl induces its release from the basolateral cortex. This mechanism excludes Lgl from Dlg and allows another protein, Pins, which is also phosphorylated by Aurora A, to bind Dlg to orient the spindle in the plane of the epithelium. Adapted from Carvalho *et al*., 2015.

Aurora A has a major role in Lgl phosphorylation and release from the basolateral cortex to the cytoplasm during mitosis in follicular and wing disc epithelia (Bell *et al*., 2015; Carvalho *et al*., 2015). Our studies uncovered the direct phosphorylation of Lgl by Aurora A *in vitro* and a mechanism by which Aurora A phosphorylation of serines 656 and 664 induce Lgl cortical exclusion during mitosis (Figure 1.6). Consistent with the significance of AurA, and in contrast to *apkc* mutants, Lgl cortical release is strongly delayed in *aurA* mutant clones (Bell *et al*., 2015; Carvalho *et al*., 2015).

The functional significance of Lgl cytoplasmic reallocation during mitosis is not related with a role of Lgl in the cytoplasm (Carvalho *et al*., 2015) as was previously suggested in mammalian cells where Lgl was found to have a role in chromosome segregation (Yasumi *et al*., 2005). Instead, Lgl cortical release was shown to be important for planar spindle orientation, which is disrupted by retention of Lgl in the cortex using mutants in two aPKC/AurA-phosphorylatable serines (Carvalho *et al*., 2015). Lgl was found to bind and inhibit the assembly of myosin II filaments, impacting Myosin II contractility (Dahan *et al*., 2012, 2014; De Lorenzo *et al*., 1999; Strand, 1998). One possibility would be that cortical Lgl could influence cell rounding by interfering with changes in cortical actomyosin contractility, which could indirectly disrupt planar spindle orientation (Luxenburg *et al*., 2011). However, Lgl^{3A}, which is unphosphorylatable by aPKC, does not affect spindle orientation despite its ability to bind cortical myosin during mitosis and possibly inhibit actomyosin contractility (Carvalho *et al*., 2015). Therefore, defects in spindle orientation observed in double mutant forms of Lgl should not derive from effects on cortical myosin. One main difference between Lgl^{3A} and the double mutants forms relies on their ability to bind the GUK domain of Dlg. *In vitro*, phosphorylation in at least one single serine was shown to be important for binding to the GUK domain of Dlg (Zhu *et al*., 2014) and, therefore, Lgl^{3A} should be unable to bind Dlg in this domain. Dlg mediates planar spindle orientation in epithelia by recruiting the protein that connects astral microtubules with the lateral cortex, Pins (LGN in vertebrates) (Bergstralh *et al*., 2013; Nakajima *et al*., 2013; Saadaoui *et al*., 2014). After phosphorylation by Aurora A, Pins binds Dlg through the same binding region used to bind Lgl, according to crystallographic studies (Johnston *et al*., 2009, 2012; Zhu *et al*., 2011, 2014). Thus, it is expected that maintenance of Lgl/Dlg complex should impair Pins binding to Dlg for spindle orientation (Carvalho *et al*., 2015). We therefore proposed a model where Lgl phosphorylation by Aurora A rapidly reduces the amount of Lgl available to interact with the GUK domain of Dlg, thus enabling the interaction of the Dlg GUK domain with Pins. Aurora A would therefore mediate the conversion of the

Lgl/Dlg polarity complex into the Pins/Dlg complex to control spindle orientation during mitosis (Bell *et al*., 2015; Carvalho *et al*., 2015).

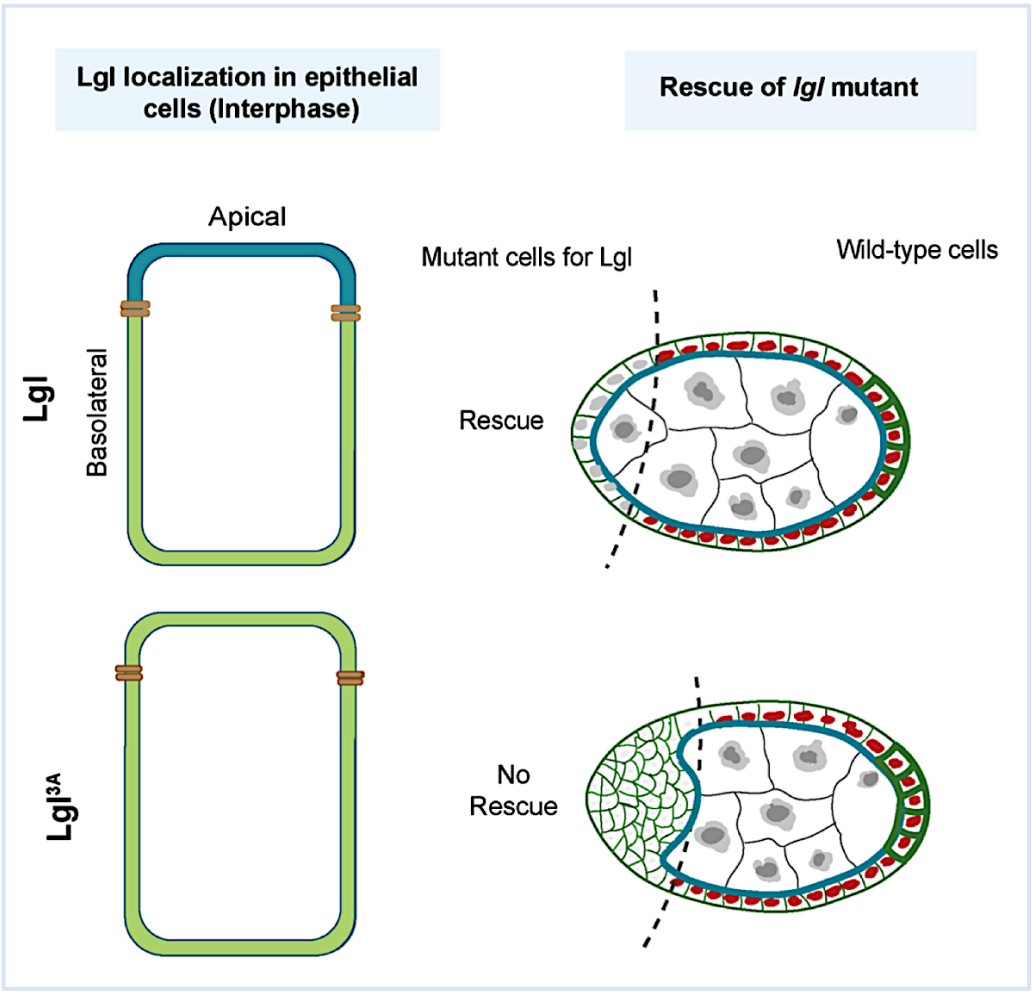

Figure 1.7: Phosphorylation of Lgl and basolateral restriction by aPKC is important for epithelial cell polarity. Schematic representation of the localization of Lgl and the unphosphorylatable version, Lgl^{3A}, and its ability to support epithelial polarity in *lgl* mutant clones. While Lgl is restricted in the basolateral side by aPKC phosphorylation, Lgl^{3A}, which is not phosphorylated by aPKC, extends to the apical domain. Lgl phosphorylation and apical exclusion by aPKC is an important mechanism for cell polarity. Lgl-GFP is able to rescue the polarity and multilayering phenotype of *lgl* mutant clones while Lgl^{3A}-GFP is unable to maintain a monolayered organization. aPKC – Blue; Lgl – Green

4. Protein phosphatases in cell polarity

Phosphorylation is an extremely important post-translational modification in cell polarity, influencing the localization, function and assembly of polarity complexes. However, phosphorylation must be reversed to ensure a dynamic and versatile responsiveness of cell polarity to physiological and cellular stimuli. This fine-tuned regulation of the phosphorylation status of polarity proteins is ensured by protein phosphatases, which can be typically classified according to the substrate specificity as serine/threonine phosphatases, tyrosine phosphatases or dual-specific phosphatases (Moura and Conde, 2019). Here, we will focus on two members of the phosphoprotein phosphatase family (PPP), protein phosphatase 1 (PP1) and protein phosphatase 2 (PP2A), which are the most prevalent serine/threonine phosphatases in eukaryotic cells with important functions in the regulation of cell-cycle processes and cell polarity.

4.1. PP1 and PP2A: roles and regulation during the cell-cycle

The activities of PP1 and PP2A have to be tightly controlled to ensure that these phosphatases are only active in a specific time-window and subcellular localization, and are selective for certain substrates. Since phosphatases, unlike most kinases, are not able to recognize a consensus sequence to target the phosphorylated residues, this specificity is achieved by association of the catalytic subunits with one or more scaffold proteins and/or regulatory subunits, forming a large number of multimeric holoenzyme complexes (Moura and Conde, 2019; Nilsson, 2019).

PP2A acts predominantly through heterotrimers, composed by a catalytic subunit (C) which binds to a scaffold subunit (A), and together recruit variable regulatory subunits (B) that provide substrate specificity (Moura and Conde, 2019) (Figure 1.8A). *Drosophila* has a single catalytic subunit, Microtubule star (Mts) (Snaith *et al*, 1996), only one scaffolding A subunit, PP2A-29B (Mayer-Jaekel *et al*., 1992) and three regulatory B-subunits, Twins (tws), Widerborst (Wdb) and PP2-B' (Hannus *et al*., 2002; Shiomi *et al*., 1994; Uemura *et al*., 1993). In humans, the diversity of core subunits is higher, being described 2 catalytic subunit isoforms, 2 scaffolding subunits and 16 regulatory subunits (Moura and Conde, 2019). In *Drosophila*, mutants for PP2Ac die during embryogenesis, showing several mitotic defects, including overcondensed chromatin and blocked mitosis (Janssens and Goris, 2001). The name, microtubule star (Mts), results from the phenotype observed in embryos

deficient for PP2Ac, which exhibit multiple centrosomes radiating disorganized and elongated arrays of microtubules, resembling a star (Snaith *et al*., 1996). This effect is due to a defective attachment of microtubules to chromosomal DNA at kinetochores, impairing mitotic progression (Snaith *et al*., 1996).

Similarly to PP2A, PP1 does not act as an individual catalytic subunit, but in association with regulatory subunits. In *Drosophila*, four PP1 catalytic isoforms (PP1c) were identified and named according to the chromosome localization and subtype: *PP1α87B (or Pp1-87B)*, *PP1α96A (or Pp1-96A), PP1β9C* (or *Flapwing*) and *PP1α13C (or PP1-13C*) (Bennett *et al*., 2006). Mammals also have four PP1c isoforms: PP1α, PP1β and PP1γ (subdivided into PP1γ1 and PP1γ2, the last being an alternative splicing variant specifically expressed in testis) (Moura and Conde, 2019). According to phylogenetic analysis, *PP1α87B, PP1α96A* and *PP1α13C* are equally related to mammalian PP1α and PP1γ, while *PP1β9C* is more related with PP1β (Bennett *et al*., 2006). Additionally, there is a high functional conservation across the evolutionary scale, since one *PP1c* gene of one species can be functionally replaced by another *PP1c* of the other species (Brautigan and Shenolikar, 2018).

The major PP1c in *Drosophila* is *PP1α87B*, accounting for about 80% of the PP1 activity in larvae extracts and with essential functions specially during mitosis (Dombrádi *et al*., 1990). First studies in *Schizosaccharomyces pombe* showed that mutations of PP1 (Dis2) cause defects in chromosome segregation (Kinoshita *et al*., 1990). In *Drosophila,* mutants for *PP1α87B* result in lethality at the larvae-pupa boundary (Axton *et al*., 1990), abnormal mitosis progression, with cells displaying chromosome hypercondensation and defective spindle organization (Axton *et al*., 1990; Dombrádi and Cohen, 1992; Dombrádi *et al*., 1990). Other phenotypes associated with loss of *PP1α87B* can be masked by the overlapping function of the other isoforms. Together, the two other isoforms, *PP1α96A* and *PP1β9C,* contribute to the remaining 20% of the total PP1 activity (Bennett and Alphey, 2006; Bennett *et al*., 2006), since *PP1α13C* was shown to have reduced expression levels in very few cells, having thereby a negligible activity (Dombrádi *et al*., 1993). In fact, *PP1α96A* and *PP1α13C* are not required for viability, in contrast to *PP1α87B* and *PP1β9C* (Clyne *et al*., 1999). Hypomorphic mutations in *PP1β9C* (flapwing) result in flightless flies with defects in indirect flight muscles (Raghavan *et al*., 2000), which is associated with a specific role for *flapwing* in the dephosphorylation of non-muscle myosin MRLC (spaghetti squash) (Vereshchagina *et al*., 2004).

Despite having redundant roles and indistinguishable *in vitro* substrate specificity, PP1c specificity *in vivo* is provided through interaction with regulatory subunits (Bennett and Alphey, 2006). Some regulatory subunits can localize PP1c to specific places and/or alter substrate specificity (Figure 1.8A). An example is the non-muscle target regulatory subunit, MYPT-75D, found to specifically bind to the *PP1β9C* (Flapwing) isoform and to stimulate its activity towards non-muscle myosin, as previously mentioned (Vereshchagina *et al*., 2004). Other regulatory subunits can act as inhibitors of PP1c, such as the nuclear inhibitor of protein phosphatase 1 (NIPP1), phosphatase nuclear targeting subunit (PNUTS), Inhibitor-1 (I-1) and Inhibitor-2 (Bennett *et al*., 2003; Parker *et al*., 2002; Udho *et al*., 2002). Another conserved regulatory subunit of PP1c is Sds22, a leucin-rich repeat protein required for completion of mitosis in yeast (Ohkura and Yanagida, 1991). However, the exact function of Sds22 in the PP1 holoenzyme remains controversial (Moura and Conde, 2019; Nilsson, 2019). In certain contexts, Sds22 seems to act as a positive modulator of PP1 activity. In *S.pombe*, Sds22 (named Sds22+) was found to enhance PP1-dependent dephosphorylation activity in mitosis (Ohkura and Yanagida, 1991). Later on, Sds22 was described to act together with PP1 to regulate the levels of aurora B activity and the correction rate of wrong kinetochore-microtubule interactions for faithful chromosome segregation (Posch *et al*., 2010; Wurzenberger *et al*., 2012). Also, the PP1/Sds22 holoenzyme was found to have an important role in dephosphorylating proteins at the cell poles, ezrin/radixin/moesin, for cortical softening and anaphase elongation (Rodrigues *et al*., 2015). On the other hand, accumulation of Sds22 at kinetochores and binding to Sds22 impairs PP1 dephosphorylation of kinetochore substrates (Eiteneuer *et al*., 2014) and, together with I3, maintains newly-synthetized PP1 in an inactive state (Weith *et al*., 2018).

The binding of PP1c with its interacting partners (both regulatory subunits or substrates) is mainly mediated by short linear motifs (SLiMs) generally located in unstructured regions that bind to surface grooves of PP1, thereafter called PP1 docking site motifs (Brautigan and Shenolikar, 2018; Heroes *et al*., 2013). There is a diversity of PP1 docking motifs, but the most common is the RVxF-type motif, better described as [KR] $[X]_{0-1}$[VI]{P} [FW] (where X denotes any residue and {P} any residue except Pro) (Wakula *et al*., 2003). This type of docking motif is present in nearly 90% of the PP1 binding proteins (Bollen *et al*., 2010) and binds to an hydrophobic pocket in PP1 without changing the conformation of the PP1 catalytic subunit (Bollen *et al*., 2010; Nilsson, 2019). Instead, binding of this motif to PP1 increases the local concentration of the interactor and therefore promotes secondary interactions that contribute to the activity and specificity of the holoenzyme (Bollen *et al*., 2010; Heroes *et al*., 2013). Due to the functional advantage of these docking site motifs, they are highly conserved among eukaryotes (Heroes *et al*., 2013). However, the presence

of SLiMs is not necessary for binding to PP1 holoenzymes, as well as the presence of *in silico* predicted SLiMs is not sufficient to indicate that a protein is a substrate or a PP1-interacting protein. Some PP1-interacting proteins do not have any obvious SLiMs, such as Sds22, which associates with PP1c via structured domains such as helical leucine (Leu) repeats (Ceulemans *et al*., 2002)

In order to control the half-time of substrate phosphorylation and ensure accurate mitotic progression, the activities of PP1 and PP2A have to be tightly controlled in a spatiotemporal manner. Mitotic entry is triggered by high levels of cyclin-dependent kinase 1 (CDK1) and its activator Cyclin B, which are assembled in a CDK1-Cyclin B complex before mitotic entry (Ma *et al*., 2016; Moura and Conde, 2019). However, along with increased levels of CDK1-Cyclin B, the activity of PP2A-B55 and PP1 holoenzyme has to be repressed to prevent premature dephosphorylation of CDK1-Cyclin B targeted substrates (Figure 1.8B). Inactivation of PP2A-B55 holoenzyme is promoted at G2/M transition by the Ser/Thr kinase Greatwall (Gwl), which is activated by CDK1-Cyclin B-mediated phosphorylation (Castilho *et al*., 2009). PP1 activity is repressed during mitosis by a dual mechanism involving CDK1 inhibitory phosphorylation on the C-terminus (Kwon *et al*., 1997) and binding to the inhibitory regulatory protein I-2 (Wu *et al*., 2009).

Mitotic exit events are not only regulated by inactivation of CDK1 triggered by APC^{cdc20} - proteasome-dependent degradation of Cyclin B and inhibition of Gwl kinases, but also by PP2A-B55 and PP1 phosphatase reactivation and dephosphorylation of a broad range of substrates (Wurzenberger and Gerlich, 2011). Upon transition into anaphase, degradation of cyclin B and a decrease in CDK1-Cyclin B activity initiates the process of reactivation of PP1, which partially inactivates Gwl, thus allowing the PP2A-B55 to dephosphorylate CDK1-phosphorylated substrates (Heim *et al*., 2015; Ma *et al*., 2016). In turn, PP2A-B55 dephosphorylates Gwl and fully inactivates this kinase, maintaining the levels of PP2A-B55 high and promoting a successful mitotic exit (Ma *et al*., 2016). As cells transit from metaphase to anaphase, PP1 induces its self-dephosphorylation, increasing its activity to the levels necessary to dephosphorylate numerous mitotic phosphoproteins, which leads to mitotic exit (Brautigan and Shenolikar, 2018).

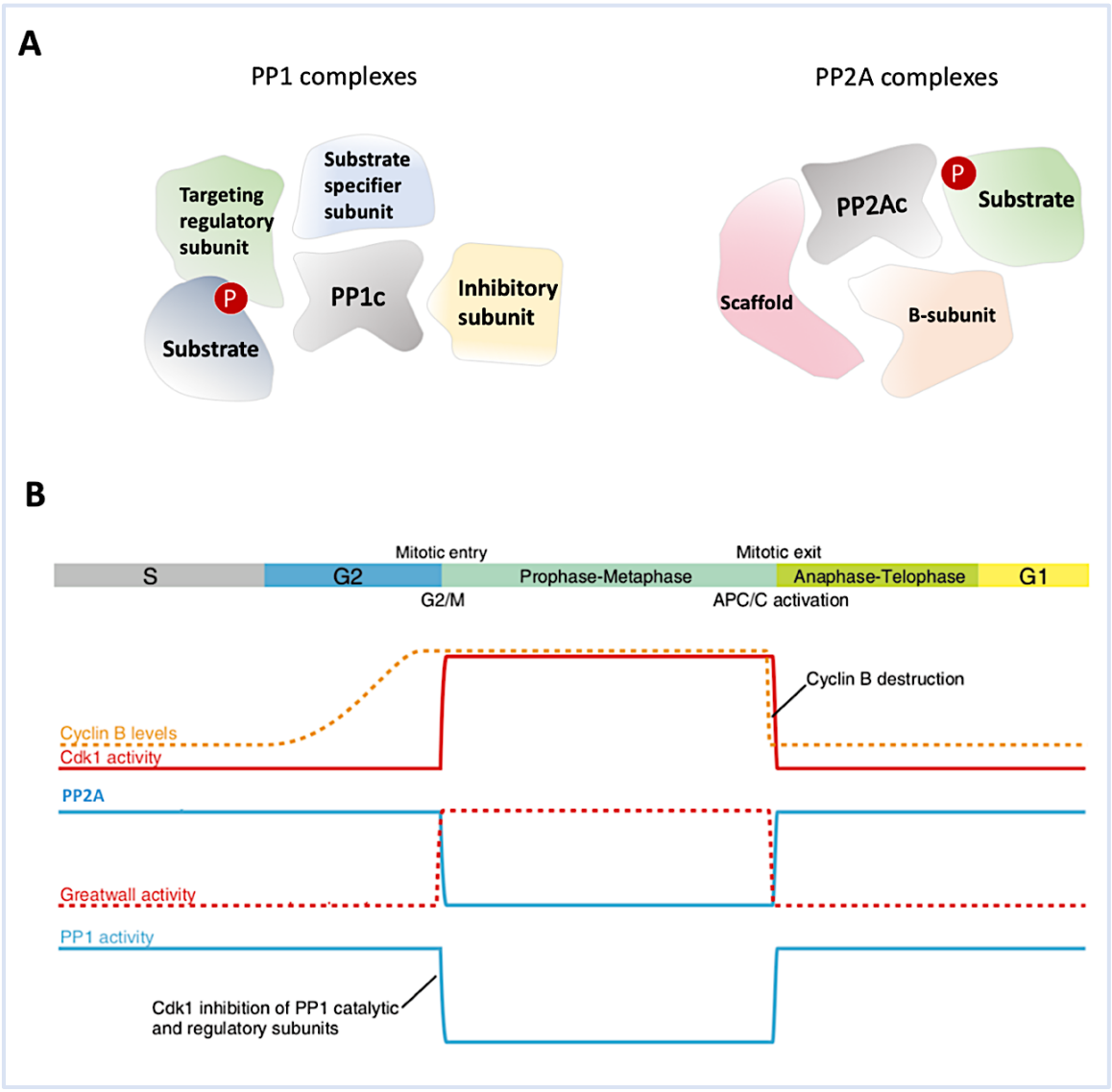

Figure 1.8: Regulation of PP1 and PP2A phosphatases during the cell-cycle. A) Schematic representation of the subunit structure of PP1 and PP2A holoenzymes. Adapted from Bollen *et al*, 2009; B) Temporal regulation of PP1 and PP2A during the cell cycle. The activity levels of PP1 and PP2A, as well as the kinases that regulate their function, Cdk1 and Gratewall, are also shown, together with the variation of Cyclin B levels throughout the cell cycle. Adapted from Barr *et al*., 2011.

4.2. Implications of PP1 and PP2A in cell polarity and cancer

Previous studies performed in mammalian cells and *Drosophila melanogaster* have described the role of PP2A and PP1 in the regulation of the cell polarity machinery. PP2A was demonstrated to have an important function in the assembly of E-cadherin/β-catenin complexes for proper AJ formation, co-localizing with these components in several epithelial cell lines (Schuhmacher *et al*., 2019). Additionally, PP2A was also found to play a role in the biogenesis and stability of the tight junctions (TJ) by the dephosphorylation of TJ proteins, including occludin, ZO-1 and claudin-1 (Dunagan *et al*., 2012; Nunbhakdi-Craig *et al*., 2002; Seth *et al*., 2007). In mammalian cells, PP2A was also found to modulate the Par complex by dephosphorylation of aPKC, regulating its distribution in the apical membrane, thus influencing the biogenesis of junctions which is promoted by aPKC phosphorylation of TJ proteins (Nunbhakdi-Craig *et al*., 2002). An interaction between PP2A and aPKC was also confirmed in *Drosophila* during asymmetric cell division. In neuroblasts, Twins (a B-type regulatory subunit of PP2Ac) and the catalytic subunit of PP2A (Mts) form a multi-protein complex with aPKC, negatively regulating this kinase and restricting its localization to the apical cortex for the maintenance of neuroblast polarity and self-renewal (Chabu and Doe, 2009). PP2A also plays a role in the dephosphorylation of Bazooka/Par-3 at the Par-1 phosphorylation sites, which promotes its apical localization in photoreceptor epithelial cells (Nam *et al*., 2007) and controls the polarisation of dividing *Drosophila* neuroblasts (Krahn *et al*., 2009). Curiously, PP2A was also described to dephosphorylate Par-6, thus promoting its interaction with aPKC and inhibiting aPKC signaling in neuroblasts during asymmetric cell division (Ogawa *et al*., 2009), constituting an additional mechanism for maintenance of restricted aPKC function in the apical side of neuroblasts.

Several PP1 substrates associated with cell polarity have been described. In human cells, Dlg2 and Dlg3 were found to bind the catalytic subunit of the PP1 phosphatase in pull down and co-immunoprecipitation assays (Hendrickx *et al*., 2009). PP1γ also binds and dephosphorylates another basolateral protein, Scrib, through a docking site motif of the hScrib in human cells (Nagasaka *et al*., 2013). In MDCKII cells, PP1α dephosphorylates Par-3 to regulate binding of 14-3-3 proteins and aPKCζ, thereby promoting the formation of functional TJs (Traweger *et al*., 2008). Curiously, in a genetic screen performed in the *Drosophila* embryo, the regulatory subunit of PP1c, Sds22, was found to interact genetically with Par-3/Bazooka to regulate epithelial structure of the embryos, namely the formation of adherens junctions (Shao *et al*., 2010). Sds22 was also linked with the regulation of

epithelial cell polarity and cell shape in *Drosophila* follicular epithelium and imaginal discs (Grusche *et al*., 2009). This subunit binds to all isoforms of PP1 and is important for PP1 dephosphorylation of Moesin and Sqh/MRLC, regulating the phosphorylation status of these proteins in the apical membrane and maintaining the integrity and columnar shape of the epithelia (Grusche *et al*., 2009). Loss of cell polarity is also a predominant phenotype observed in mutant follicle cells for Sds22, but cell polarity proteins were not described as direct targets for Sds22 (Grusche *et al*., 2009). The impact of Sds22 in the maintenance of cell polarity was also confirmed in *Drosophila* imaginal discs (Jiang *et al*., 2011). In this study, the authors found that Sds22 acts as a positive regulator of PP1 to restrict myosin II phosphorylation and the activity of Jun N-terminal kinase (JNK) to prevent overproliferation and metastasis (Jiang *et al*., 2011).

Sds22 is a potential tumour suppressor in *Drosophila,* since cells that loose Sds22 become invasive and tumorigenic when combined with Ras overexpression by inducing metalloproteinase 1 (MMP1) secretion downstream of JNK signaling (Jiang *et al*., 2011). Curiously, *Sds22* (*PP1R7* in humans) was shown to be downregulated in several carcinomas and deleted in six cancer subtypes (Jiang *et al*., 2011). PP1 was also found to interact with BRCA1, a breast cancer susceptibility protein (Winter *et al*., 2007), suggesting that Sds22/PP1 inactivation might be associated with tumour progression and metastasis in human cancers. Curiously, there is a compelling relationship between PP2A dysfunction and human carcinomas, which is consistent with an important function of PP2A in regulating cell-cell junctions and in maintaining cell polarity (Schuhmacher *et al*., 2019). For instance, some PP2A holoenzymes are downregulated in prostate cancer (Cheng *et al*., 2011; Singh *et al*., 2008) and the A scaffolding subunit was found to be downregulated in breast and lung cancer (Calin *et al*., 2000). Moreover, reduced levels of the a scaffold subunit of PP2A is associated with E-cadherin internalization in breast cancer lines (Suzuki, 2006).

5. Cell polarity disruption and cancer

Loss of epithelial cell polarity has been strongly linked to both pre-invasive stages and the progression of epithelial-derived tumours, a major source of human cancers (Halaoui and McCaffrey, 2015; Macara Ian G. and McCaffrey Luke, 2013). In fact, disruption of tissue disorganization is one of the hallmarks of cancer, used by pathologists to diagnose neoplasia and to evaluate the tumour grade (Lee and Vasioukhin, 2008;Saito *et al*., 2018).

The three basolateral polarity proteins, Lgl, Dlg and Scrib, are generally expressed at low levels in many primary human tumours as consequence of multiple events, including gene deletion and epigenetic or transcriptional regulation (Halaoui and McCaffrey, 2015). Loss of human DLG1 was shown recently to be associated with endometrial cancer and considered as a potential molecular biomarker for poor prognosis (Sugihara *et al*., 2016). Also another Dlg homologue, DLG3, was detected in low expression levels in colorectal cancer as a consequence of promotor hypermethylation (Feng *et al*., 2012). Downregulation of Scrib is also associated with loss of tissue architecture during tumour progression, including in colorectal cancer (Gardiol *et al*., 2006), mammary tumorigenesis (Zhan *et al*., 2008), endometrial cancer (Ouyang *et al*., 2010), among others. Several lines of evidences have suggested that in 90% of cervical cancers, Scrib and Dlg are targeted for degradation by human papilloma viruses (HPV) (Nakagawa and Huibregtse, 2000;Gardiol *et al*., 1999). Lgl expression was also shown to be strongly reduced in a wide variety of human malignancies, including gastric, breast and lung cancers (Halaoui and McCaffrey, 2015). Loss of Lgl1 was shown to induce dysplastic growth in the brain of mice, consitent with the tumour suppressor function described in *Drosophila* (Klezovitch *et al*., 2004). Human Lgl1 is also strongly reduced in malignant melanoma (Kuphal *et al*., 2006) and lymph node metastasis in endometrial cancer (Tsuruga *et al*., 2007), and loss or mislocalization of Lgl2 was shown to be strongly associated with gastric dysplasia (Lisovsky *et al*., 2009; Lisovsky *et al*., 2010). Curiously, expression of Dlg and Lgl in tumour-cell lines leads to an attenuation of neoplastic phenotypes, further supporting the role of these proteins as tumour suppressors in human cells (Massimi *et al*., 2004; Kuphal *et al*., 2006).

Polarity proteins are not always deleted or downregulated in cancer. Some isoforms of the apical polarity protein aPKC are overexpressed or amplified (Murray *et al*., 2011) including in ovarian and lung cancers (Eder *et al*., 2005; Regala *et al*., 2005) . Moreover, depending on the specific signaling pathways involved, different aPKC isoforms can promote or prevent tumorigenesis (Halaoui and McCaffrey, 2015). Similarly, Scrib and Par3 can have

a suppressive or protumorigenic activity, depending on tissue specific functions of each protein (Halaoui and McCaffrey, 2015). Importantly, tumour development is not only associated with changes in protein expression but also with mislocalization of polarity proteins. One example was reported for Lgl2 in human gastric cancer, where advanced stages of adenocarcinomas are associated with a diffused distribution of Lgl in the cytoplasm and loss of Lgl from the plasma membrane (Nam *et al*., 2014). Also mislocalization of Scrib and Par-6 from the membrane to the cytosol was observed in breast cancer cells (Feigin *et al*., 2014; Halaoui *et al*., 2017).

As previously described, many signaling pathways involved in cell growth/proliferation and tumour formation in mammalian cells have been originally described in *Drosophila*. *Drosophila* also provided the first examples of tumour-suppressor genes (*lgl*, *dlg* and *scrib*), whose single mutations were surprisingly sufficient to induce neoplastic overgrowth of the brain lobes or imaginal discs (Bilder and Perrimon, 2000; Gateff, 1978). Moreover, cells from these tumours show a metastatic capacity when implanted into the abdomen of adult hosts (Gateff, 1978; Woodhouse *et al*., 1998). Although individual mutants for these three basolateral polarity proteins exhibit most of the hallmarks of cancer when affecting the whole tissue or organism, clonal analyses of these genes highlight the importance of considering the tumour-microenvironment for tumour development. In fact, mutant cells for *scrib*, *lgl* and *dlg*, despite losing apical-basal polarity, fail to out-compete surrounding wild-type cells and are progressively eliminated by JNK-mediated apoptosis (Menéndez *et al*., 2010; Brumby and Richardson, 2003; Froldi *et al*., 2010). However, when combined with oncogenic Ras ($Rasv^{12}$) overexpression, *scrib*, *dlg* and *lgl* mutant clones resist cell death in *Drosophila* eye epithelium and acquire metastatic behavior (Brumby and Richardson, 2003; Doggett *et al*., 2011; Pagliarini, 2003). Noteworthy, overexpression of activated Ras alone fails to result in neoplastic tumour development, thus supporting the requirement of cooperating mutations in these basolateral polarity genes for tumorigenesis.

6. *Drosophila melanogaster* as a model system

As previously described, changes in expression or localization of polarity proteins have been strongly associated with development of several types of human cancer. However, these analyses are essentially based on correlative studies, therefore not supporting a causative contribution of loss of cell polarity in tumorigenesis. The direct implication of cell polarity disruption in cancer has been provided by work in *Drosophila melanogaster* since the discovery of the first tumour suppressor genes. This powerful and genetically amenable model organism displays an astonishing conservation of human disease-related processes and genes, despite over millions of years of the evolutionary distance (Miles *et al*., 2011;Brumby and Richardson, 2005). In fact, about 75% of genes related with human diseases have functional orthologues in *Drosophila melanogaster* (Yamaguchi and Yoshida, 2018). Not surprisingly, publications using *Drosophila* as a model organism for cancer have exponentially increased in the last 10 years (Mirzoyan *et al*., 2019).

Drosophila has been used for more than 100 years for the understanding of several questions in developmental biology and human diseases beyond cancer, including Alzheimer's and diabetes (Bellen *et al*., 2010). The *Drosophila* genome was the second to be sequenced among metazoans (Adams *et al*., 2000; Stefanatos and Vidal, 2011; Brumby and Richardson, 2005). It is estimated to contain 180 Mb distributed through four chromosome pairs and with much less redundancy compared with mammalian genomes, allowing detection of phenotypic effects resulting from single gene loss. Moreover, a large variety of features make the small fruit fly a unique model animal organism. These include its small size, the short life span compared with vertebrate models, such as mouse or zebrafish, and the large number of offspring produced in each generation (Jennings, 2011). Additionally, *Drosophila* provides a multiplicity of genetic tools and a plethora of mutants and transgenic lines which are available in several stock centers and accurately annotated in several freely-accessible databases. Some of these genetic tools were developed to specifically address the function of a gene of interest, including the establishment of diverse transgenic flies carrying inducible UAS-RNAi constructs against a protein, transposon P-element insertion mutants, genomic deficient mutants, among others. For instance, the GAL4-UAS gene expression system is routinely used to knock-down or express specific genes in a temporal and tissue-specific manner (Hales *et al*., 2015). The use of genome editing systems, such as CRISPR/Cas9, allows nowadays the complete loss-of-function of a gene and can also be used to insert specific reporters at precise localizations within a gene (Hales *et al*., 2015). In the case of mutations that induce lethality or infertility,

Drosophila provides a wide collection of “balancers”, engineered chromosomes displaying several inversions that prevent meiotic recombination and allow the maintenance of deleterious homozygous mutations which otherwise would be lost after few generations (Yamaguchi and Yoshida, 2018). When mutations induce lethality during development and prevent the analysis of the role of a gene, the best strategy is to perform clonal analysis, mosaics generated by mitotic recombination that have mutant patches of cells within an heterozygous background (Hales *et al*., 2015). This is in fact a great advantage of *Drosophila,* which displays many stocks for generating this mosaicism, allowing side-by-side comparison of mutant cells with controls.

Drosophila is also the source of several different cell lines that are commonly used to address specific questions, including cell-cycle dependent processes. One of the widely used line is the Schneider 2 (S2) cell line, a spontaneously immortalized line originally generated from mechanical dissociation of embryos, which is likely derived from a hematopoietic lineage (Hales *et al*., 2015; Schneider, 1972). *Drosophila* S2 cells are an amenable system to perform high-throughput RNAi approaches. In fact, plasmid transfection is very straightforward and efficient even for large targets, due to the ability of S2 cells to readily absorb dsRNA from the culture media (Hales *et al*., 2015).

6.1. The *Drosophila* follicular epithelium

Depending on the purpose of the study, *Drosophila* provides a plethora of tissues that can be used. In this study, we mostly used the *Drosophila* follicular epithelium to address our questions regarding cell polarity in a proliferative tissue. The basic unit of the *Drosophila* ovary is the ovariole, composed by different stem cell populations and by strings of egg chambers (the functional unit of oogenesis) in progressive stages of development (McLaughlin and Bratu, 2015) (Figure 1.9). The *Drosophila* female has two ovaries and in each single ovary the number of ovarioles can vary between 16 and 20. A single ovariole contains various stages of egg chamber development, from stem cells to mature eggs, being a valuable model to study many cellular processes, including cell specification, cell polarisation and epithelial morphogenesis (Bastock and St Johnston, 2008). The stem cell population of an ovariole is localized in the germarium, the most anterior structure localized in the tip of the ovariole. The germarium itself is composed by germline stem cells (GSC) that divide and differentiate giving rise to germline cysts, containing the nurse cells and the oocyte encapsulated by a somatic monolayer of epithelial cells. The nurse cells are polyploid due to several rounds of endocycles, providing them the capacity to support the

oocyte with nutrients, organelles, mRNAs and proteins during early embryonic development. The encapsulated germline cyst becomes an egg chamber that moves out of the germarium and progresses through 14 morphologically distinct stages, finally reaching the competent maturation stage for fertilization of the oocyte. The oocyte is arrested in prophase I of meiosis before exiting the germarium until roughly stage 13, where meiosis progresses until metaphase I (McLaughlin and Bratu, 2015). This arrest is maintained until the mechanical pressure of the oocyte during the passage in the oviduct triggers the completion of meiosis, which is independent on fertilization (McLaughlin and Bratu, 2015).

The follicle cells are derived from a different stem cell population of the germline cells, the follicle stem cells (FCS). During egg chamber development, distinct follicle cells are originated from the same follicle cell lineage: the polar cells, located at the anterior and posterior sides of an egg chamber and required for fate determination of adjacent cells (Grammont and Irvine, 2002); the stalk cells, which connect two adjacent egg chambers; and the epithelial follicle cells, that encase the germline. The first step of encapsulation of the germline cyst implicates a mesenchymal to epithelial transition of precursor follicle epithelial cells (Wu *et al*., 2008). The follicular epithelium develops in coordination with the oocyte, being important for its axis specification (Wu *et al*., 2008). Follicle epithelial cells have distinct apical and basal domains and divide until stage 6, consisting of a cuboidal epithelium, with distinct apical and basal domains. During stages 7-9, follicle cells complete three endoreplication cycles, becoming polyploid (Edgar and Orr-Weaver, 2001). At the beginning of stage 9, the 6-10 anterior-most follicle epithelial cells become the border cells, delaminating from the epithelium and migrating in-between the nurse cells until reaching the oocyte to form the micropyle (Wu *et al*., 2008). Collective migration of this small group of cells has been used as a model of cancer metastasis (Naora and Montell, 2005). Simultaneously with border cell migration, follicle epithelial cells migrate posteriorly to surround the oocyte and experience extensive cell shape changes and morphogenetic reorganization, giving rise to a secretory columnar epithelium. The polyploid somatic cells contain amplified genes which encode for chorion-related proteins, depositing vitelline membrane and eggshell to complete the maturation of the oocyte (Edgar and Orr-Weaver, 2001; Wu *et al*., 2008). The most anterior follicle cells became squamous and flatten over the nurse cells (Wu *et al*., 2008).

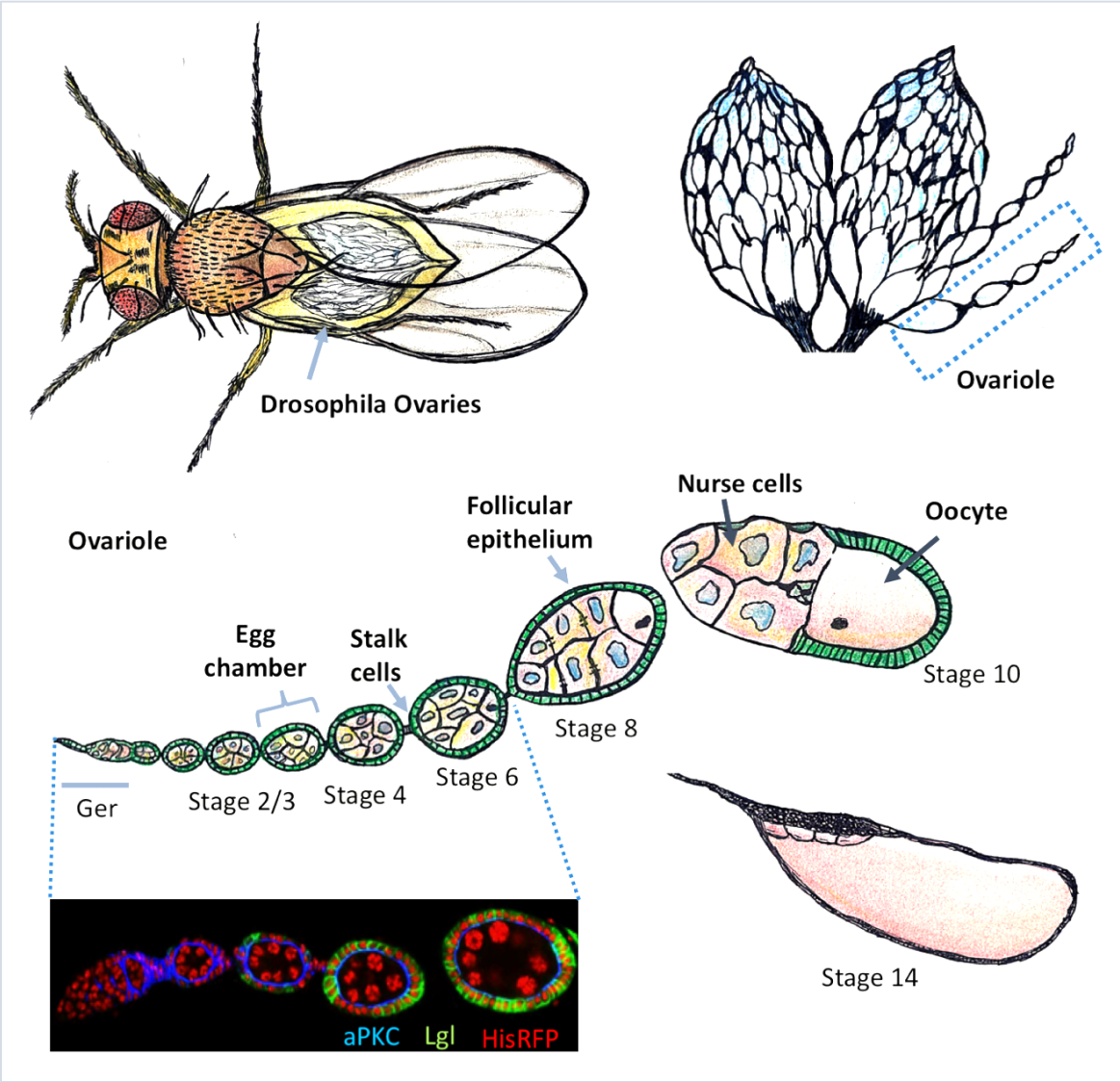

Figure 1.9: Schematic representation of *Drosophila* ovaries and its basic units, the ovarioles. Confocal microscopy image with corresponding egg chamber stages is shown, as well as the localization of the basolateral protein Lgl (green) and the apical protein aPKC (blue). The localization of the germarium (Ger), where the egg chambers are formed, is also indicated, as well as different developmental stages until stage 14.

The *Drosophila* follicular epithelium is a genetically tractable model to study several questions in biology. It has been optimized to generate mutant clones for mosaic analysis and for efficient depletion by RNAi. In the context of this project, the follicular epithelium is an extremely useful model due to well-defined apical and basal domains – an apical domain facing the germline and the basal domain in contact with the extracellular matrix in the opposite site. Moreover, *Drosophila* ovaries can be cultured *ex vivo* for at least 4 hours to perform live imaging of the follicular epithelium using already established conditions and protocols (Carvalho *et al.*, 2015; Morais-de-Sá and Sunkel, 2013; Prasad *et al.*, 2007).

Additionally, the follicular epithelium is highly proliferative until stage 6 of oogenesis, therefore allowing studies on the coordination of cell polarity during cell division (Carvalho *et al*., 2015; Morais-de-Sá and Sunkel, 2013).

7. Aims of the work

The main focus of this thesis is *Lethal giant larvae* (*Lgl*), the first identified and characterized tumour suppressor gene whose implication in several development processes and disease has been demonstrated across the years. Although Lgl has been extensively studied in all its strands, both as a tumour suppressor and as a cell polarity protein with signaling scaffold functions, half a century after its discovery in *Drosophila melanogaster* there is still a vast number of questions waiting to be answered.

Recent advances have shed light on how phosphorylation influences Lgl subcellular localization throughout the cell-cycle. However, the mechanisms that counteract this phosphorylation to ensure the correct localization of Lgl at the cortex are unknown. In Chapter 3, I will focus on the importance of phosphoregulation mechanisms that control Lgl localization and function in the cortex of epithelial cells (Figure 1.10). Since Lgl's role as a signaling scaffold and cell polarity regulator rely on its localization to the cortex, this question is extremely relevant for our understanding of how epithelial architecture and function is maintained.

Despite its apparent robust organization and steady order, the epithelia tissue is constantly remodeling and proliferating to maintain the physiology and homeostasis. Mitosis is in fact a demanding challenge for an epithelial cell that must coordinate the organization of its polarity complexes and cell-cell junctions with dramatic shape and cytoskeleton changes that are associated with cell division. At the same time, these two processes, mitosis and cell polarity, must be tightly synchronized to ensure that polarity is re-established in the new daughter cells at the exit of mitosis. Recent progress has been made in understanding how epithelia polarity complexes are remodeled during mitosis. Live imaging analyses of proliferative epithelial tissues revealed that the basolateral polarity complex is reorganized during mitosis, with Lgl being progressively released from the cortex to the cytoplasm (Bell *et al*., 2015; Carvalho *et al*., 2015). This dynamic behavior of Lgl is induced by activation of

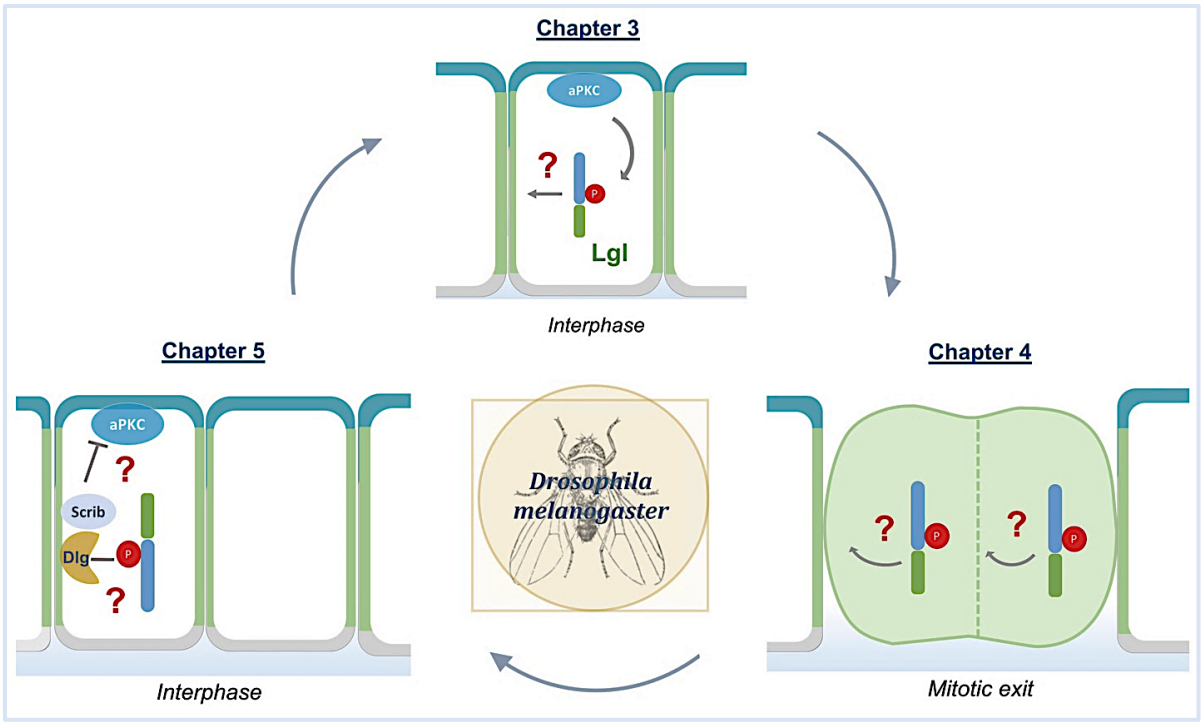

Figure 1.10. Graphical illustration of the main objectives of this work.

Aurora A, which phosphorylates Lgl to link cell-cycle progression with the temporal reorganization of cell polarity during mitosis. However, how epithelial cells coordinate cell mitosis exit with the recovery of Lgl to the cortex of daughter cells is still largely unknown. This is the focus of the Chapter 4, dedicated to understand how polarity of the daughter cells is re-established at mitotic exit, with an emphasis on the importance of restoring Lgl cortical localization (Figure 1.10). How epithelial cells propagate cell polarity during division is a crucial event for the maintenance of overall tissue polarity and tissue integrity during proliferation.

Finally, Lgl is localized in the cortex in interphase cells, where it collaborates with other partners, Dlg and Scrib, for the maintenance of epithelial cell polarity. However, how these three protein cooperate to antagonize the apical domain and ensure the integrity of epithelial polarity is still largely unknown. Some studies suggest that Lgl and Dlg might interact, but the assumption of a complex is mostly based on *in vitro* studies. In the last chapter of results, Chapter 5, we use Fluorescence Recovery After Photobleaching (FRAP) to test if modifications of Lgl's dynamic behaviour could provide evidence for interactions with its cortical partners, in particular with Dlg (Figure 1.10). This study is important to understand

how the three basolateral proteins cooperate and integrate themselves in the extensive polarity network.

I believe a deeper knowledge of the mechanisms underlying Lgl phosphoregulation and dynamic localization during the cell-cycle, as well as its interaction with other polarity proteins, will put together the “big puzzle” of how cell polarity is established and regulated. In the long term, I hope this knowledge could also pave the way to understand human diseases, such as cancer, which is associated with loss of cell polarity and epithelial disorganization.

Chapter 2

Experimental Procedures

In this chapter 2, I will detail the methods used to perform the experiments reported in the three chapters of results.

2.1. *Drosophila* husbandry and genetics

Drosophila melanogaster flies were cultured using cornmeal/agar/molasses/yeast media in chambers at 18ºC or 25ºC with controlled photoperiod and humidity. In experiments involving the expression of UAS-driven RNAi, crosses were maintained at 18ºC and eclosed flies incubated at 29ºC to boost the efficiency of RNAi depletion.

Most of the strains of *Drosophila melanogaster* used in this thesis are described in the FlyBase (https://flybase.org) and detailed in the Table 2.1. A large number of stocks were obtained from the Bloomington *Drosophila* Stock Center (https://bdsc.indiana.edu) and some RNAi lines are from Vienna *Drosophila* Resource Center (https://stockcenter.vdrc.at). Some stocks were generously provided by other labs or produced in the scope of this work. Genotypes resulting from crosses used in this thesis are detailed in the Table 2.2.

2.1.1. The GAL4-UAS expression system

Experiments involving temporal and spatial control of protein expression were performed using the two-part Gal4-UAS system, which takes advantage of the transcriptional activator derived from yeast, Gal4, to drive tissue specific expression in *Drosophila* (Brand and Perrimon, 1993). The method involves crossing two distinct transgenic lines, one line harbouring the targeting gene under the control of a Gal4-responsive upstream activation sequence (UAS) and the “driver” line providing the transcriptional activator Gal4, which is expressed under the control of a tissue-specific promotor or enhancer element (Figure 2.1). Therefore, the progeny will express a target gene in a tissue-specific pattern. In this work, we used this system to induce tissue-specific expression of RNAi or to express UAS-proteins. Our crosses were maintained at 18ºC to minimize GAL4 activity and then adult flies were raised at 29ºC, where Gal4 has maximal activity (Duffy, 2002), to potentiate the expression of the RNAi only in adult flies. The same approach was used to overexpress some proteins of interest in a particular tissue and adults were transferred for 29ºC or 25ºC to induce higher or milder expression, respectively, before dissection. Experiments involving expression of UAS-RNAi were performed at 29ºC for a variable number of days

(indicated in the figure legends), using the *tj-Gal4* driver. In this work, we used two different drivers to induce the expression of UAS transgenes in the follicular epithelium: *traffic jam (tj)-Gal4* and *GR1-Gal4*. *tj-Gal4* allows the expression of genes in all cells of the follicular epithelium, even in follicle stem cells (Olivieri *et al.*, 2010). The *GR1-Gal4* driver is more efficient in inducing expression at later stages of oogenesis (more pronounced from stage 5 onwards) (Gupta and Schüpbach, 2003). Moreover, we used *matα4-Gal4-VP16* to express proteins of interest in the embryo (Häcker and Perrimon, 1998a), *eyeless-Gal4* driver to induce the expression in salivary glands of 3rd instar larvae (Martins *et al.*, 2017) and *slbo-Gal4* driver to induce expression in border cells (Rørth, 1998).

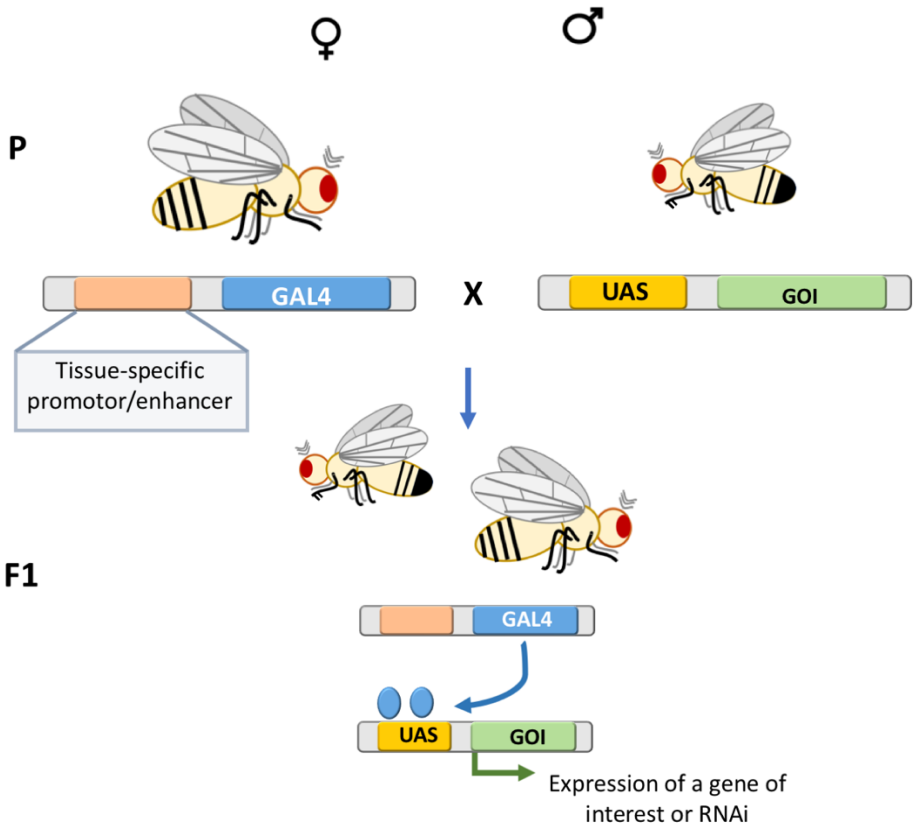

Figure 2.1. Schematic representation of the GAL4-UAS system for expression of transgenes in a cell - type or tissue specific manner. This involves crossing a fly carrying the gene encoding for the yeast GAL4 transcription factor under regulation of a tissue-specific promotor or enhancer and a fly carrying the gene of interest (GOI) under regulation of the upstream activating sequence (UAS), which is activated by GAL4 (P- parental flies). The progeny (F1) will express a gene or a hairpin RNA to knock down a gene in a particular tissue.

2.1.2. Generation of mosaic tissues

A) The Flp-FRT system

In this work, we used the Flp-FRT system to generate mutant clones in the follicular epithelium. This technique allows one to study the function of a gene without compromising the viability of the fly by generating patches of homozygous mutant cells in an heterozygous tissue (Xu and Rubin, 1993). The strategy was adapted from the site-specific recombination system of yeast, combining the FLPase (FLP) and its FRT target sites for recombination. To perform this technique, a fly has to carry, in the chromosome containing the FRT sites, a mutation of interest in *trans* with a homologous FRT chromosome containing markers, in our case nlsRFP or GFP (McLaughlin and Bratu, 2015) (Figure 2.2A). In a separate chromosome, the FLP gene is under control of a heat-shock (HS) promotor. The mitotic recombination will occur between the two FRT sites, generating homozygous clones for the mutation, which can be identified by lack of the visual marker. These clones will be surrounded by WT homozygous or heterozygous cells, resulting from the mitotic recombination specifically during G2 phase of the cell cycle (Figure 2.2A). Induction of Flp expression is achieved by placing pupae or adult flies at 37ºC for a variable number of hours and days.

To generate positive clones for expression of UAS-transgenes, we used a strategy which combines the Flp-FRT system with the suppressive ability of GAL80 over the GAL4-UAS system (Figure 2.2B). We used this strategy to generate positively marked clones expressing UAS-Pp1 RNAi, UAS-Lgl or UAS-AurAΔab. As for Flp-FRT system, it is based on the ability of the FLPase to recognize the FRT sites of homologous chromosomes and recombine during G2 phase of the cell cycle. A fly carrying the Gal80 under expression of a tubulin promotor inhibits the ability of Gal4 to bind the transcriptional activation domain UAS (Figure 2.2B). In the end, a tissue containing UAS-transgene expressing cells (Cell 1), WT cells (Cell 2) or heterozygous cells will be generated. Basically, daughter cells harbouring two copies of nlsRFP will not express Gal80 allowing GAL4 to drive the expression of the UAS-RNAi or other UAS-transgene. On the other hand, cells lacking the marker or heterozygous for nlsRFP will contain two or one copies of Gal80, respectively, thereby inhibiting totally or partially the expression of the transgene. Although some similarities can be found between this system and the MARCM (Germani *et al*., 2018), in this case the nlsRFP marker is not under control of a UAS activator and not associated with

the transgene. We choose the more intense nlsRFP labeled cells to ensure that the two copies of RNAi or the transgene are being expressed.

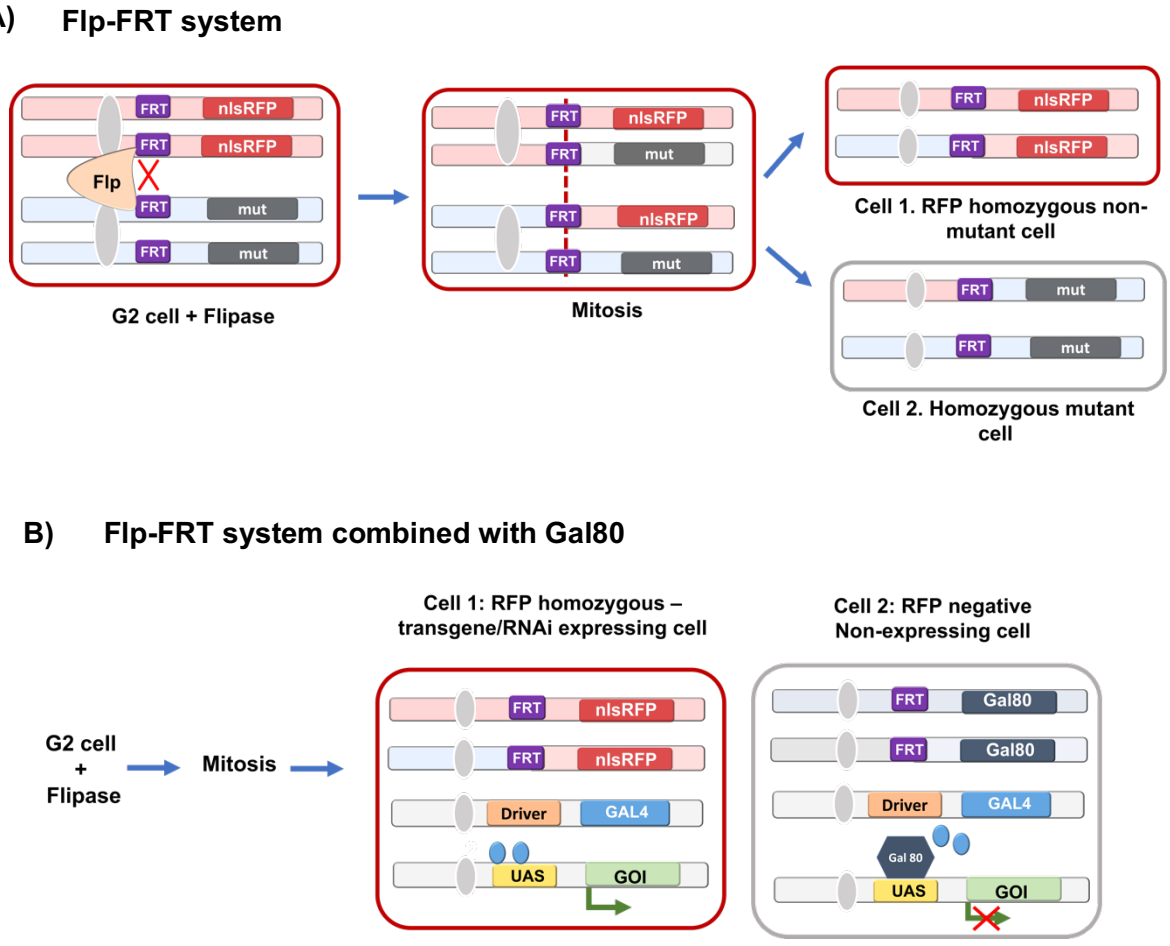

Figure 2.2. Schematic representation of Flp-FRT system for generation of homozygous mutant clones and Flp-FRT system combined with expression of Gal80 for clonal tissue-specific expression of a gene of interest or RNAi. A) Homozygous mutant clones are generated by expression of the Flp-recombinase in the G2 phase of the cell cycle, catalyzing the site-specific recombination between identical positioned FRT sites in homologous chromosomes. At mitosis, the segregation of homologous chromosomes will occur, and daughter cells can inherit two copies of the RFP under the control of a ubiquitin promotor (Cell 1, marked by strong red), two copies of the mutant chromosome arm (Cell 2, marked by the absence of RFP) or heterozygous (cell 3, not represented), inheriting one mutant and one RFP chromosome. B) The Flp-FRT system combined with Gal80 was used to generate clones positively marked for RFP. This technique relies on the constitutive expression of Gal80 (under the tubulin promoter), which inhibits GAL4 binding to the transcriptional domain. After recombination and cell division, cells expressing the RNAi or the gene of interest (GOI) will carry two copies of RFP and none of Gal80 (Cell 1), while a non-expressing cell will carry two copies of Gal80, therefore repressing the binding of GAL4 to the transcriptional site (Cell 2). Heterozygous cells are also generated, containing one copy of the RFP and one copy of the Gal80. These cells have a less strong red fluorescence than the homozygous ones and can still express RNAi or the transgene. In both schemes, A and B, the chromosome containing the Flp gene is not represented.

B) Flp-out technique

This technique also relies in the ability of the yeast site-specific recombinase, flipase (Flp), to recognize specific target sites (FRT) in the chromosomes of *Drosophila*, but without the requirement of cell cycle progression to generate clones (Germani *et al*., 2018). In this case, a gene is silenced by a transcriptional stop signal positioned between two FRT sites positioned in the same orientation on the same chromosome that can be removed by expression of Flp to activate the gene of interest (Rodríguez *et al*., 2011) (Figure 2.3). The Flp can catalyze the excision of a fragment between the two FRTs and join the resulting DNA ends (Germani *et al*., 2018). In our case, the Flp expression is under control of an HS promoter and allows the removal of the transcriptional stop sequence between the two FRTs (Figure 2.3). The constitutive actin promoter drives the expression of Gal4 which will induce the UAS-transgene expression in clones, as well as a UAS-RFP marking positively the clones.

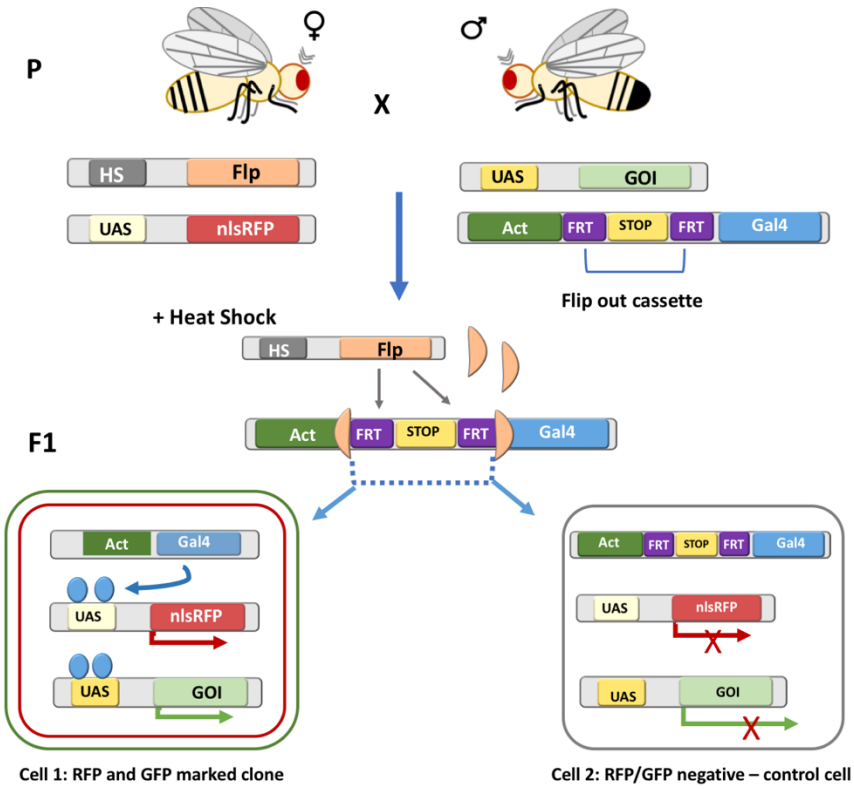

Figure 2.3. Schematic representation of a cross designed to generate Flp-out clones. This cross will generate offspring expressing the Flp under the HS promotor. After HS, Flp induces the recombination between FRT sequences and excision of a cassette containing a transcriptional stop sequence. This will allow cells to express Gal4 under the control of the actin promoter, which consequently binds to the UAS driving expression of the gene of interest and also the nlsRFP (Cell 1). This system will generate clones of cells expressing the gene of interest marked by nlsRFP and by cells lacking for RFP, not expressing the gene of interest (Cell 2).

Table 2.1: *Drosophila melanogaster* genotypes used in this thesis

	Genotypes	Source	Identifier	Notes
Gal4 driver	*tj>Gal4*	Pancratov *et al*., 2013	FlyBase ID: FBtp0089190	Used to drive expression in the follicular epithelium (Olivieri *et al*., 2010)
	GR1>Gal4	Goentoro *et al*., 2006	FlyBase ID: FBti0040373	Used to drive expression in the follicular epithelium (Olivieri *et al*,. 2010)
	ey-Gal4	Hazelett *et al*., 1998	FlyBase ID: FBtp0002646	Used to drive expression in salivary glands (Martins *et al*., 2016)
	slbo-Gal4	Bloomington *Drosophila* Stock Center	BDSC:#58435 FlyBase ID: FBst0058435	Used to drive expression in border cells (Rørth, 1998)
	matα4-Gal4-VP16	Bloomington *Drosophila* Stock Center	BDSC:#7063 FlyBase ID: FBst0007063	Used to drive expression of proteins in embryos (Häcker and Perrimon, 1998)
UAS-transgenes	*UAS-Lgl-GFP*	Gift from Knoblich, J.A. (Betschinger *et al*., 2003)	N/A	3rd chromosome
	UAS-Lgl-GFP	Grift from St Johnston, D.	N/A	2nd chromosome attP-VK18 insertion
	UAS-Lgl$^{K327A, F331A}$-GFP	This study	N/A	2nd chromosome attP-VK18 insertion

	Genotypes	Source	Identifier	Notes
UAS-transgenes	*UAS-Lgl-RFP*	Knoblich, J.A. (Betschinger *et al*., 2003)	N/A	2nd chromosome attP-VK18 insertion
	UAS-Lgl^{3A}-GFP	Gift from Knoblich, J.A. (Betschinger *et al*., 2003)	N/A	3rd chromosome
	UAS-Lgl^{3A}-GFP	Gift from St Johnston, D.	N/A	2nd chromosome attP-VK18 insertion
	UAS- Par-6 mCherry	Gift from St Johnston, D.	N/A	2nd chromosome
	UAS-Pp1-87B-HA	Bloomington *Drosophila* Stock Center	BDSC: #24098 FlyBase ID: FBti0078046	3rd chromosome
	UAS-Pp1α-96A-HA	Bloomington *Drosophila* Stock Center	BDSC: #23700 FlyBase ID: FBst0023700	3rd chromosome
	UAS-Flw-HA	Bloomington *Drosophila* Stock Center	BDSC: #23702 FlyBase ID: FBst0023702	3rd chromosome

	Genotypes	Source	Identifier	Notes
UAS-transgenes	*UAS-hPPP1cc*	Bloomington *Drosophila* Stock Center	BDSC: #64394 FlyBase ID: FBti0182016	2nd chromosome Expresses human PPP1CC under UAS control
	UAS-NiPp1-HA	Bloomington *Drosophila* Stock Center	BDSC: #23711 FlyBase ID: FBti0077905	3rd chromosome Expresses a nuclear inhibitor of PP1
	UAS-AurA-GFP	Gift from J. Knoblich (Berdnik and Knoblich, 2002)	N/A	3rd chromosome
	UAS-AurA$^{\Delta Ab}$-GFP	Gift from Kimata, Y. (Meghini *et al.*, 2016))	N/A	3rd chromosome
	UAS-Dlg-GFP	Gift from K.Prehoda (Golub *et al.*, 2017)	N/A	3rd chromosome
	UAS-Dlg^{S662D}-GFP	Gift from K.Prehoda (Golub *et al.*, 2017)	N/A	3rd chromosome
	UAS Myr-GFP	Bloomington *Drosophila* Stock Center	BDSC: #32197 FlyBase ID: FBti0131941	10X UAS sequences
	UAS-pmCIBN	Gift from S. de Renzis Guglielmi *et al*., 2015	N/A	For optogenetic depletion of PIP_2 in the plasma membrane

	Genotypes	Source	Identifier	Notes
UAS-transgenes	*UAS-CRY2-OCRL*	Gift from S. de Renzis Guglielmi *et al*., 2015	N/A	For optogenetic depletion of PIP_2 in the plasma membrane
	UAS-Twe RNAi	Vienna *Drosophila* Resource Center	*V*DRC:v104147 FlyBase ID: FBst0476005	2nd chromosome
	UAS-PTEN RNAi	Bloomington *Drosophila* Stock Center	BDSC: #33643 FlyBase FBst0033643	3rd chromosome
	UAS-PpV RNAi	Bloomington *Drosophila* Stock Center	BDSC: #57765 FlyBase ID:FBst0057765	2nd chromosome
	UAS-mts RNAi	Bloomington *Drosophila* Stock Center	BDSC: #38337 FlyBase ID: FBti0149551	3rd chromosome
	UAS-Pp1-87B RNAi	Bloomington *Drosophila* Stock Center	BDSC: #32414 FlyBase ID: FBti0132109	3rd chromosome
	UAS-Tws RNAi	Vienna *Drosophila* Resource Center	VDRC v104167 FlyBase ID: FBst0476025	2nd chromosome

	Genotypes	Source	Identifier	Notes
UAS-transgenes	UAS-Pp2A-29B RNAi	Vienna *Drosophila* Resource Center	*V*DRC: v49672 FlyBase ID: FBst0468588	3rd chromosome
	UAS- Pico RNAi	Vienna *Drosophila* Resource Center	*V*DRC:v16371 FlyBase ID:FBst0452269	3rd chromosome
	UAS-flw RNAi	Bloomington *Drosophila* Stock Center	BDSC: #57022 FlyBase ID: FBti0164842	2nd chromosome
	UAS-Sds22 RNAi	Vienna *Drosophila* Resource Center	VDRC: v42051 FlyBase ID: FBti0081237	2nd chromosome
	UAS- aPKC RNAi	Bloomington *Drosophila* Stock Center	*BDSC:#25946* *FlyBase ID: FBti0114676*	3rd chromosome
	UAS-PP1 RNAi	Vienna *Drosophila* Resource Center	VDRC:v27673 FlyBase ID: FBst0457078	targets: Pp1-96A Flapwing Pp1-87B
	UAS- Pavarotti RNAi	Bloomington *Drosophila* Stock Center	BDSC:#42573 FlyBase ID:FBti0151053	2nd chromosome

	Genotypes	Source	Identifier	Notes
Mutant of deficiency alleles	*FRT19 flw^{FP41}*	Bloomington *Drosophila* Stock Center	BDSC: #51338 FlyBase ID: FBal0267524	Loss-of-function mutation (Sun *et al*., 2011)
	Pp1-87B^{87Bg-3} e^{1} Pp1α-96A^{2}	Bloomington *Drosophila* Stock Center	BDSC:#23699 Flybase IDs: FBgn0004103 FBal0212815	Pp1-87B^{87Bg-3} Amorphic allele Pp1α-96A^{2} Loss of function allele
	FRT82 Pp1α-96A	This study	N/A	Stock obtained by recombination between FRT82B and Pp1α-96A2 from the *BDSC: #23699 stock*
	Df(3R)Exel7357	Bloomington *Drosophila* Stock Center	BDSC: #7948 FlyBase ID: FBab0038319	Chromosome deletion that disrupts the Pp1α-96A gene and some adjacent genes
	aPKC^{K06403}	Bloomington *Drosophila* Stock Center	BDSC: #10622 FlyBaseID: FBal0064438	Loss of function allele
	lgl^{4} FRT40A	Bloomington *Drosophila* Stock Center	BDSC: #36289 FlyBase ID: FBal0009225	Null allele
	lgl^{27S3} FRT40A	Bloomington *Drosophila* Stock Center	BDSC: #41561 FlyBase ID: FBal0175616	Null allele

	Genotypes	Source	Identifier	Notes
Mutant of deficiency alleles	*lgl^{ts3}*	Gift from Semeriva, M. (Manfruelli *et al*., 1996)	BDSC: #36288 FlyBaseID: FBal0051412	Heat sensitive hypomorphic allele
	fzr^{A} FRT19A	Bloomington *Drosophila* Stock Center	BDSC: #52384 FlyBaseID: FBst0052384	Nature of the allele unknown
	FRT42B sktl M5/Cyo GFP	Gift from A. Guichet	N/A	N/A
	FRT19A dlg^{1A}	Bloomington *Drosophila* Stock Center	BDSC: #57086 FlyBase ID: FBal0298896	dlg1^{A} encodes a stop codon on the third PDZ domain of Dlg. Allele behaves like a null (Yamamoto *et al*., 2014)
	aurA^{37}	Gift from J. Knoblich (Berdnik and Knoblich, 2002)	FlyBase ID: FBal0137332	Amino acid replacement in the catalytic domain
	aPKC^{ts}	Gift from R. Martinho (Guilgur *et al*., 2012)	FlyBase ID: FBal0277054	Heat sensitive hypomorphic allele
	FRT82B scrib^{2}/TM6	Gift from St Johnston D.	N/A	N/A

	Genotypes	Source	Identifier	Notes
Endogenous lines	Lgl-GFP	Gift from Hong, Y. (Dong *et al*., 2015)	N/A	2nd chromosome
	Dlg^{CC01936}-GFP	Buszczak *et al*., 2007	N/A	X chromosome
	Scrib^{CA07683}-GFP	Buszczak, M *et al*., 2007	N/A	3rd chromosome
	Lgl-mCherry	Gift from Hong, Y. (Dong *et al*., 2015)	N/A	2nd chromosome
	Lgl^{S5A}-GFP	Gift from Hong, Y. (Dong *et al*., 2015)	N/A	2nd chromosome
	aPKC-GFP	Gift from Schweisguth, F. (Besson *et al*., 2015)	N/A	X chromosome
	HisRFP	Bloomington *Drosophila* Stock Center	BDSC: #23651 FlyBase ID: FBst0023651	2nd chromosome

	Genotypes	Source	Identifier	Notes
Stocks for generation of mosaic clones	*hs-FLP tub-Gal80 FRT19*	Bloomington *Drosophila* Stock Center	BDSC: #5133 FlyBase ID: FBst0005133	N/A
	hs-FLP nls-RFP FRT19A	Bloomington *Drosophila* Stock Center	BDSC: #31418 FlyBase ID: FBst0031418	N/A
	actin-FRT-stop-FRT-GAL4, UAS-RFP/ CyO	Bloomington *Drosophila* Stock Center	N/A	N/A
	e22c-Gal4 UAS-FLP	Bloomington *Drosophila* Stock Center	BDSC: #5083 FlyBase ID: FBst0005083	2nd chromosome
Other Stocks	*pubiq RFP cnn*	Gift from Basto, R.	N/A	PCM marker centrosomin
	$Gal80^{ts}$	———	N/A	3rd chromosome
	ubi-PLCγ PH-mCherry (PH-ChFP)	Gift from Y.Bellaiche (Herszterg *et al*., 2013)	N/A	Used to label PIP2 (Szentpetery *et al*., 2009)
	w^{1118}	(Hazelrigg *et al*., 1984)	FlyBase ID: FBal0018186	Wild-type control Oregon R strain with a spontaneous deletion in the white (w) gene discovered by R. Levis

Table 2.2. Detailed genotypes resulted from the crosses performed in this work

Chapter	Figures	Genotypes
Chapter 3	Figure 3.3	*w; tj-Gal4*/+; *UAS-Lgl-GFP*/+ *w; tj-Gal4/ UAS-Twe RNAi*; *UAS-Lgl-GFP*/+ *w; tj-Gal4/ +*; *UAS-Lgl-GFP/ UAS-PTEN RNAi* *w*; *tj-Gal4/ UAS-PpV RNAi*; *UAS-Lgl-GFP/ +* *w*; *tj-Gal4*/+; *UAS-mts RNAi/ UAS-Lgl-GFP* *w; tj-Gal4/*+; *UAS-Pp1-87B RNAi/ UAS-Lgl-GFP* *w; tj-Gal4/UAS-tws RNAi*; *UAS-Lgl-GFP/+* *w; tj-Gal4/*+; *UAS-Lgl-GFP/UAS-Pp2A-29B RNAi* *w*; *tj-Gal4*/+*;UAS-Lgl-GFP/ UAS-Pico RNAi* *w*; *tj-Gal4*/*UAS-sds22 RNAi*; *UAS-Lgl-GFP/+*
	Figure 3.4	**A), B)** w^{1118} *w*; *tj-Gal4*/+; *UAS-mts RNAi*/+ *w; tj-Gal4/*+; *UAS-Pp1-87B RNAi/ +* *w*; *tj-Gal4*/*UAS-sds22 RNAi*; *+/+* **C)** *hs-FLP nls-RFP FRT19/hs-FLP tub-Gal80 FRT19*; *tj-GAL4*/+; *UAS-Pp1-87B RNAi*/+
	Figure 3.6	*w*; *tj-Gal4*/+; *UAS-Pp1-87B-HA*/+ *w*; *tj-Gal4*/+; *UAS-Pp1α-96A-HA/*+ *w*; *tj-Gal4*/+; *UAS-Flw-HA*/+

Chapter	Figures	Genotypes
Chapter 3	Figure 3.7	**A)** *w*^{1118} *w*; *tj-Gal4*/*UAS-flw RNAi*; +/+ *w*; ; *pp1-87B*$^{87Bg-3}$ *e pp1a-96A*^{2} / *Df(3R)Exel7357* **B)** *hs-FLP ubi-RFP-nls FRT19/flw*^{FP41} *FRT19*; ; +/+ *hs-FLP*/+;; *FRT82 ubi-RFP-nls/ FRT82 pp1*α*-96A*^{2} *hs-FLP*/+;; *FRT82 ubi-RFP-nls/ FRT82 pp1-87B*$^{87Bg-3}$ *e pp1*α*-96A*^{2}
	Figure 3.8	**A)** *w; tj-Gal4/+* *w; tj-Gal4/+*; *UAS-Pp1-87B RNAi/+* *w*; *tj-Gal4/UAS-hPpp1cc*; *UAS-Pp1-87B RNAi/+* **B)** *w; tj-Gal4; Lgl-GFP/+*; *UAS-NiPp1-HA/+*
	Figure 3.9	*w; tj-Gal4/+*; *UAS-Pp1-87B RNAi/+*
	Figure 3.10	*w; tj-Gal4/Lgl-GFP; UAS-Pp1-87B RNAi/+* *Dlg-GFP/+; tj-Gal4/+; UAS-Pp1-87B RNAi/+* *w; tj-Gal4/+; Scrib-GFP/ UAS-Pp1-87B RNAi*

Chapter	Figures	Genotypes
Chapter 3	Figure 3.11	**A)** *aPKC-GFP*/+; *CyO*/+; *UAS-Pp1-87B RNAi*/+ (Control) *aPKC-GFP*/+; *tj-Gal4*/+; *UAS-Pp1-87B RNAi*/+ (Pp1-87B RNAi) **B)** *w; tj-Gal4/CyO*; *UAS-Pp1-87B RNAi*/+ *w*; *tj-Gal4/ FRT82B aPKC*^{k06403}; *UAS-Pp1-87B RNAi* /+ aPKC-GFP/+; *tj-Gal4/* +; *UAS-Pp1-87B RNAi* /+ **C)** *w; tj-Gal4/UAS BH-GFP*; *UAS-Pp1-87B RNAi/Gal80*^{ts} *w; tj-Gal4/UAS Lgl-GFP*; *UAS-Pp1-87B RNAi/ Gal80*^{ts}
	Figure 3.12	**D), E), F)** *w;;tj-Gal4/UAS PP1 RNAi*; *UAS Myr-GFP/+* *w;tj-Gal4/UAS PP1 RNAi*; *UAS aPKC RNAi/+* **G)** *w*; *tj-Gal4/UAS-Lgl-RFP*; *UAS-Pp1-87B RNAi/UAS-Lgl*^{3A}*-GFP*
	Figure 3.13	w; *Lgl-GFP*
	Figure 3.15	*w*; *tj-Gal4*/*UAS-Lgl–GFP* *w*; *tj-Gal4*/*UAS-Lgl*^{K327A,F331A}*–GFP*

Chapter	Figures	Genotypes
Chapter 3	Figure 3.16	*w*; *tj-Gal4*/*UAS-Lgl^{3A}-GFP* *w*; *tj-Gal4*/*UAS-Lgl–GFP* *w*; *tj-Gal4*/*UAS-Lgl^{K327A,F331A}–GFP*
	Figure 3.17	**A)** *w*; *tj-Gal4*/*UAS-Lgl^{3A}-GFP; UAS-Pp1-87B-HA*/+ *w*; *tj-Gal4*/*UAS-Lgl–GFP; UAS-Pp1-87B-HA*/+ *w*; *tj-Gal4*/*UAS-Lgl^{K327A,F331A}–GFP; UAS-Pp1-87B-HA*/+ **B)** *w*; *tj-Gal4*/*UAS-Lgl–GFP; UAS-Pp1-87B-HA*/+
	Figure 3.18	*w*; *tj-Gal4*/*UAS-Lgl^{K327A,F331A}–GFP; +/+* *w*; *tj-Gal4*/*UAS-Lgl^{K327A,F331A}–GFP; UAS-aPKC RNAi/+*
	Figure 3.19	*ey-Gal4*/*UAS-Lgl–GFP; +/+* *ey-Gal4*/*UAS-Lgl–GFP; UAS-aPKC RNAi/+* *ey-Gal4*/*UAS-Lgl^{K327A,F331A}–GFP; UAS-aPKC RNAi/+*

Chapter	Figures	Genotypes
Chapter 3	**Figure 3.20**	**A)** *hs-FLP*/+; *lgl*^{27S3} *FRT40*/ *RFP FRT40* *hs-FLP*/+; *lgl*^{27S3} *FRT40 UAS-Lgl-GFP*/ *RFP FRT40*; *GR1-Gal4*/+ *hs-FLP*/+; *lgl*^{27S3} *FRT40 UAS-Lgl*^{K327A,F331A}*–GFP*/ *RFP FRT40*; *GR1-Gal4*/+ (*lgl* homozygous mutant cells are marked by absence of RFP in a tissue with the general expression of UAS-Lgl transgenes in the follicle epithelium) **B)** *hs-FLP*/+; *lgl*^{27S3} *FRT40 UAS-Lgl*^{K327A,F331A}*–GFP*/ *RFP FRT40*; *GR1-Gal4*/+ *hs-FLP*/+; *lgl*^{27S3} *FRT40 UAS-Lgl*^{K327A,F331A}*–GFP*/ *tub-Gal80 FRT40*; *GR1-Gal4*/+ (*lgl* homozygous mutant cells are the only ones expressing UAS-Lgl^{K327A,F331A}– GFP -Gal80 absence) **D)** *hs-FLP/+; actin-FRT-stop-FRT-Gal4, UAS-RFP/+; UAS-Lgl*^{K327A,F331A}*–GFP/+* *hs-FLP/+; actin-FRT-stop-FRT-Gal4, UAS-RFP/+; UAS-Lgl–GFP/+* **E)** *w; UAS-Lgl-GFP/+; slbo-Gal4/+* *w; UAS-Lgl*^{K327A,F331A}*–GFP /+; slbo-Gal4/+*

Chapter	Figures	Genotypes
Chapter 4	Figure 4.2	**A)** *hs-FLP nls-RFP FRT19/hs-FLP tub-Gal80 FRT19; tj-GAL4*/+; *UAS-Lgl-GFP*/+ (clonal expression to evaluate local Lgl-GFP signal specifically in dividing cell) **C)** *w*; *tj-Gal4*/+; *UAS-Lgl-GFP, HisRFP*/+ **D)** Embryos from females: *matα4-Gal4* crossed with males: *UAS-Lgl-GFP*
	Figure 4.4	**A)** *hs-FLP nls-RFP FRT19/rap^{A} FRT19* **B)** *w; tj-Gal4, ubi-RFP-cnn /+; UAS-AurA-GFP/+* *hs-FLP nls-RFP FRT19/ rap^{A} FRT19; tj-Gal4/+; UAS-AurA-GFP/+* **C)** *hs-FLP nls-RFP FRT19/ rap^{A} FRT19; tj-Gal4/+; UAS-Lgl-GFP*
	Figure 4.5	**A)** *w*; *UAS-Lgl-RFP/ tj-Gal4; UAS-AurA-GFP*/+ *w*; *UAS-Lgl-RFP/ tj-Gal4*; *UAS-AurAΔAb-GFP*/+ **B)** *hs-FLP nls-RFP FRT19/ hs-FLP tub-Gal80 FRT19 ; TJ/+; UAS-AurAΔAb-GFP /+* **D)** *w; e22c-Gal4 UAS-FLP/ UAS-Lgl-RFP; FRT82B aur^{37} / FRT82B nls-GFP*

Chapter	Figures	Genotypes
Chapter 4	**Figure 4.6**	*w ; +/+; UAS-Lgl-GFP/GR1-Gal4* (Control) *w ; FRT42B aPKC^{K06403}/FRT42B aPKC^{ts}; UAS-Lgl-GFP/GR1-Gal4* (restrictive temperature)
	Figure 4.7	**A)** *hs-FLP nls-RFP FRT19/hs-FLP tub-Gal80 FRT19; tj-Gal4/+; UAS-Lgl-GFP/+* *w; tj-Gal4/+; UAS-Pp1-87B RNAi/UAS-Lgl-GFP, HisRFP* *w; tj-Gal4/UAS-sds22 RNAi; UAS-Lgl-GFP, HisRFP/+* *w; tj-Gal4/+; UAS-Lgl-GFP, HisRFP/UAS-Pp1-87B-HA* **B)** *w; tj-Gal4/+; UAS-Lgl-GFP, HisRFP/+*
	Figure 4.9	**B)** *hs-FLP nls-RFP FRT19/hs-FLP tub-Gal80 FRT19; tj-Gal4/+; UAS-Lgl-GFP/+* *w; tj-Gal4/ UAS-Lgl–GFP* *w; tj-Gal4/ UAS-Lgl^{K327A,F331A}–GFP* *w; tj-Gal4/ UAS-Lgl^{K327A,F331A}–GFP,UAS-sds22 RNAi* **C)** Embryos from females: *matα4*-Gal4 crossed with males: *UAS-Lgl-GFP or UAS-Lgl^{K,AFA}-GFP*
	Figure 4.10	**B)** *hs-FLP nls-RFP FRT19/hs-FLP tub-Gal80 FRT19; tj-Gal4/+; UAS-Lgl-GFP/+* *w; tj-Gal4/+; UAS-Lgl-GFP, HisRFP/+* **C)** *hs-FLP nls-RFP FRT19/hs-FLP tub-Gal80 FRT19; tj-Gal4/+; UAS-Lgl-GFP/+* *w; tj-Gal4/UAS-Pav RNAi; UAS-Lgl-GFP/+*

Chapter	Figures	Genotypes
Chapter 4	Figure 4.11	**A),B),C)** *aPKC-GFP*; *Lgl-mCherry* **D)** *W;tj-Gal4/UAS- Par-6 mCherry; UAS-Lgl-GFP/+*
	Figure 4.12	**A)** *aPKC-GFP/+; tj-Gal4, Ph mCherry/+; UAS-Pp1-87B RNAi/ Gal80^{ts}* **C),D),E)** *aPKC-GFP*/+; *lgl^{4}* or ^{ts3}/ +; HisRFP/+ (control) *aPKC-GFP*/+; *lgl^{ts3}/lgl^{4}*; *HisRFP*/+ (*lgl* temperature sensitive)
Chapter 5	Figure 5.2	*w; Lgl-GFP/Lgl-GFP* *w;;Scrib-GFP/ Scrib-GFP* *Dlg-GFP/ Dlg-GFP*
	Figure 5.3	*w; Lgl-GFP/Lgl-GFP*
	Figure 5.4	*w; Lgl-GFP/Lgl-GFP* *w;; Scrib-GFP/ Scrib-GFP* *Dlg-GFP/ Dlg-GFP*
	Figure 5.5	*w; Lgl-GFP/Lgl-GFP*

Chapter	Figures	Genotypes
Chapter 5	Figure 5.6	**A)** *w;;Lgl-GFP/Lgl-GFP* *w;;Lgl^{5A}-GFP/ Lgl^{5A}-GFP* **B),C)** *w;;UAS-Lgl-GFP/ GR1-Gal4* *w;;UAS-Lgl^{3A}-GFP/GR1-Gal4*
	Figure 5.7	**A)** *dlg1^{A} FRT19A/hs-FLP nls-RFP FRT19A; Lgl-GFP/ Lgl-GFP* *dlg1^{A} FRT19A/hs-FLP nls-RFP FRT19A; Lgl^{S5A}-GFP FRT40A/ ubi-RFP-nls FRT40A* **B)** *dlg1^{A} FRT19A/hs-FLP nls-RFP FRT19A; tj-Gal4/UAS-Lgl-GFP*
	Figure 5.8	**A)** *w;tj-Gal4/UAS-Lgl-GFP* *dlg1^{A} FRT19A/hs-FLP nls-RFP FRT19A; tj-Gal4/UAS-Lgl-GFP* **B)** *w;; UAS-Lgl-GFP,GR1* *hs-FLP/+; FRT42B sktl / FRT42B RFP*; *UAS Lgl-GFP,GR1/+* **C)** *hs-FLP/+; FRT42B sktl/ FRT42B RFP*; *UAS Lgl-GFP,GR1/+* *hs-FLP/+; FRT42B sktl/ FRT42B GFP*; *ubi-PH mcherry*

Chapter	Figures	Genotypes
Chapter 5	Figure 5.9	**A)** *UAS-pmCIBN/UAS-CRY2-OCRL;tj-Gal4/+;UAS-Lgl^{3A}-GFP/ ubi-PH-mCherry* **B)** *w; tj-Gal4/+; UAS-Lgl^{3A}-GFP/+* *dlg1^{A} FRT19A/hs-FLP nls-RFP FRT19A; tj-Gal4/UAS-Lgl^{3A}-GFP* UAS-*pmCIBN/UAS-CRY2-OCRL;tj-Gal4/+;UAS-Lgl^{3A}-GFP/ ubi-PH-mCherry* *w; Lgl^{S5A} - GFP* *dlg1^{A} FRT19A/hs-FLP nls-RFP FRT19A; Lgl^{S5A}-GFP FRT40A/ ubi-RFP-nls FRT40A* UAS-*pmCIBN/UAS-CRY2-OCRL;tj-Gal4/Lgl^{S5A}-GFP; ubi-PH-mCherry/+*
	Figure 5.10	*dlg1^{A} FRT19A/hs-FLP nls-RFP FRT19A; Lgl-GFP/ Lgl-GFP*
	Figure 5.11	**C), D), E)** *w; ;GR1-Gal4/UAS-Dlg-GFP* *w;;GR1-Gal4/UAS-Dlg^{S662D}-GFP* *w;;GR1-Gal4/UAS-Scrib-GFP* **F)** *dlg1^{A} FRT19A/hs-FLP nls-RFP FRT19A; tj-Gal4/+; UAS-Dlg-GFP* *dlg1^{A} FRT19A/hs-FLP nls-RFP FRT19A; tj-Gal4+; UAS-Dlg ^{S662D}-GFP*

Chapter	Figures	Genotypes
Chapter 5	**Figure 5.12**	*w; tj-Gal4/UAS-Lgl-GFP* *dlg1^{A} FRT19A/hs-FLP nls-RFP FRT19A; tj-Gal4/UAS-Lgl-GFP* *w; e22c-Gal4 UAS-Flp/ UAS-Lgl-GFP; FRT82 Scrib^{2}* /FRT82, ubi-GFP-nls

2.2. *Drosophila* S2 cell culture and RNAi interference

Drosophila S2 cells (S2-DGRC) obtained from the *Drosophila* Genomics Resource Center, (Indiana University) (DGRC), were cultured at 25ºC in Schneider's *Drosophila* media supplemented with 10% FBS (fetal bovine serum). Stable S2 cell lines were generated using Cellfectin® II reagent [Life technology (Invitrogen)] or Effecten Transfection Reagent (Qiagen), according to the instructions provided by the manufacturers. The stable lines produced in this work are: 1) a line co-expressing Lgl-GFP and mCherry-Tubulin (Carvalho *et al*., 2015); 2) a line co-expressing Lgl^{3A}-RFP and Lgl-GFP (this study); 3) a line expressing Lgl-Dendra2 (this study). Stable lines were maintained by using a selection medium with 20 µg/ml of Blasticidin. Cells were incubated at 37 ºC for 1 hour to induce expression of Lgl under regulation of a heat-shock promoter (plasmids: pHW-Lgl-GFP and pHW-Lgl^{3A}-RFP). For double-strand RNAi production, primers containing a T7 RNA polymerase-binding site flanked by gene specific sequences were used to amplify genomic DNA (see Table 2.2). The length of sequences amplified was as follows: 362 bp of *aurA,* 311 bp of *aPKC*, 511 bp of *sds22* , 614 bp of *PP1,* 402 bp *Pp1-87B 5'UTR* and 600 bp *Mts.* Megascript® T7 kit (Ambion, Austin, TX, USA) was used to transcribe dsRNA from PCR-amplified sequences. For RNAi treatment, S2 cells in an exponential growth phase were incubated in Schneider's media without FBS at a concentration of 1x10^{6} cells/ml with 30 µg of each dsRNAi for 1 hour (except for *Pp1-87B,* where 15 µg was used). After 1 hour, 2 ml of Schneider supplemented with 10% of FBS was added and cells analysed after 96h or 120h.

2.3. Immunofluorescence of ovaries and salivary glands

For immunofluorescence, *Drosophila* ovaries were dissected in 0.05 % PBT [PBS with 0.05% TWEEN® *20* (Sigma-Aldrich)] and salivary glands of 3rd instar larvae were dissected in PBS (1x) on ice. Dissected material was immediately rinsed in a solution of 4% paraformaldehyde solution (PFA, Electron Microscopy Sciences) [in PBS, with additional 0.2% TWEEN® *20* (Sigma-Aldrich) for ovaries] for 20 min. Exceptionally for immunofluorescences using the pTAAC antibody, after the fixation step with PFA we performed a treatment of ovaries with cold methanol at 100% for 5 min at RT, followed by re-hydration steps with 75%, 50%, 25% and 5% of methanol solutions.

After three washing steps with 0.05 % PBT (PBS with 0.05% TWEEN® 20) and 1 hour of blocking with 10% bovine serum albumin (BSA, Sigma-Aldrich) in 0.2% PBT, ovarioles were incubated at room temperature with the primary antibodies listed in Table 2.3 and diluted in 0.05% PBT (supplemented with 1% BSA). After removing the antibody solution, washing steps with 0.05% PBT containing 1% BSA were performed and ovaries incubated 2 hours with the secondary antibody. After incubation with secondary antibodies, ovaries were washed with 0.05% PBT before mounting in Vectashield with DAPI (Vector Laboratories). In F-actin staining of ovaries, Phalloidin-TRITC (Sigma-Aldrich) at 1 mg/mL was added to the paraformaldehyde solution during the fixation. For salivary glands, a solution of 0.1% Triton X-100 in PBS was used to incubate with the primary and secondary antibodies and for the washing steps.

2.4. Imaging of *Drosophila* ovarioles, embryos and S2 cells

Immunostainings were analysed using a confocal microscope Leica TCS SP5 II (Leica Microsystems) with HC PL APO CS 40x/NA 1.10 objective or a HC PL APO CS 63x /1.30 Glycerine and using a LAS 2.6 software. Live imaging of *Drosophila* ovarioles, embryos and S2 cells was performed using a spinning disc confocal system (Andor Revolution XD) equipped with an electron multiplying charge-coupled device camera (iXonEM+; Andor) and a CSU-22 unit (Yokogawa) based on an inverted microscope (IX81; Olympus) with a PLAPON 60x/NA 1.42 objective using iQ software (Andor). Z-stacks were collected with serial optical sections separated by 0.5-1 µm. For live imaging of the *Drosophila* follicular epithelia, ovarioles were dissected in Schneider's medium (with 10% FBS) supplemented

with 200 µg/ml insulin solution from bovine pancreas (Sigma-Aldrich) imaging media, as previously described (Carvalho *et al*, 2015). *Drosophila* embryos (5 to 7 hours of development, corresponding to stage 10 to stage 11) were immobilized in glass bottom microwell dishes (MaTek) containing heptane glue and filmed in Halocarbon oil (700) (Sigma-Aldrich). When fluorescent proteins were expressed at low levels, we imaged egg chambers in 10S VOLTALEF® (VWR chemicals) to improve the low signal to noise ratio (for instance, endogenous lines or UAS Lgl-RFP). S2 cells were plated in poly-L-lysine-coated culture dishes for live imaging (MatTek). Live imaging experiments were performed at 25 ºC, except in experiments using the Lgl temperature sensitive mutants (*aPKC*^{ts} and *lgl*^{ts3}), which were filmed at 29ºC.

Table 2.3. List of primers used in this study

Purpose	Sense/Antisense (5'< >3')	
dsRNAi synthesis	*aurA*	**TAATACGACTCACTATAGGG**ACTACTTGCCACCCGAAATG
		TAATACGACTCACTATAGGGAATTAAATTACGCGGGGAGCA
	aPKC	**TAATACGACTCACTATAGGG**ACCCGTTCCTGGTCGGATTG
		TAATACGACTCACTATAGGGACCGCAGAATGTGGAGGTGGT
	sds22	**TAATACGACTCACTATAGGG**AGAACTTGTCCAGCCTGAA
		TAATACGACTCACTATAGGGTTCTTGGCCAAGTCGAGG
	PP1	**TAATACGACTCACTATAGGG**TCGGAAATTAAAGATTTCGAGG
		TAATACGACTCACTATAGGGAAGATCTTCTCGTCGACAATGG
	Pp1-87B 5'UTR	**TAATACGACTCACTATAGGG**GTCGGACTGCATTGTGGAC
		TAATACGACTCACTATAGGGGACCGACCAACCATTCACC
	Mts	**TAATACGACTCACTATAGGG**CAACCCAAAACTAAAAACCTCG
		TAATACGACTCACTATAGGGTGCTGCTTCATCGTTATCTTCC
RT-PCR	*α-tub*	CACACCACCCTGGAGCATTC
		CCAATCAGACGGTTCAGGTTG
	Pp1-87B	CGATCTGTTGCGTCTGTTC
		CTTGTGGATTTCGACTCGC
	Flw	CGGCAACCACGAGTGCGCCAG
		CCGAAGGTGAAGCTCACACCG

Purpose		Sense/Antisense (5'< >3')
RT-PCR	*Pp1α-96A*	CCAGCATCAATCGCATCTACG
		CAGGTCAAATTCGTGCTTCTG
Cloning of $Lgl^{KA,FA}$		CTTGACTTTACGTCTGCAGTGATTGACGCCTTTGTGAC
		AGACGTAAAGTCAAGACACACTTTGTGTCCATCGCTGG

Table 2.4. List of the antibodies used in this study

Antibody	Dilution	Source
Rabbit anti-Lgl (d-300)	1:100 (IF) 1:500 (WB)	Santa Cruz Biotech
Rabbit anti-aPKC (c-20)	1:100 (IF) 1:500 (WB)	Santa Cruz Biotech
Rabbit p-Lgl^{656}	1:500 (WB)	Carvalho *et al.*, 2015
Rabbit anti-GFP	1:1000 (WB)	i3S (Biochemical and Biophysical N/A Technologies)
Mouse anti-HA	1:200 (IF) 1:5000 (WB)	Invitrogen
anti α-spectrin	1:200 (IF)	Developmental Studies Hybridoma Bank (DSHB)
anti-pTAAC	1:100 (IF)	Gift from Raff, J. (Barros *et al.*, 2005)
anti-Dlg	1:1000 (WB)	Developmental Studies Hybridoma Bank (DSHB)
anti α–tub	1:10000 (WB)	DM1A, Sigma
anti-MBP-HRP conjugated	1:10000 (WB)	New England Biolabs (NEB)

2.5. Photoconversion experiments in S2 cells

For photoconversion experiments, Lgl-Dendra2 expression in S2 cells was induced adding 500 µm $CuSO_4$ to the medium for at least 12h before live imaging, and cells were plated in glass bottom microwell dishes (MaTek) coated with Poly-L-Lysine (Sigma-Aldrich). Using the previously mentioned confocal microscope system and HC PL APO CS 40x/NA 1.10 objective, photoconversion was performed using the 405 nm UV laser. Initial frames were taken using 488 nm and 561 nm lasers to validate photoconversion, but time-lapse imaging was only performed with 561 nm laser every 2 min, for at least 30 min after anaphase onset. Several stacks were performed every 2 min to cover whole dividing cells.

2.6. Fluorescence recovery after photobleaching (FRAP) of *Drosophila* egg chambers

A) FRAP imaging

To perform FRAP experiments, ovaries were dissected and individual ovarioles separated from the surrounding muscle sheath. Egg chambers in a developmental stage between 7 and 9 were chosen and live imaging performed using either Schneider medium supplemented with 10% FBS and insulin (200 µg/uL) (Carvalho *et al*, 2015) or 10S Voltalef® oil (VWR Chemicals) for endogenously tagged-GFP proteins. All FRAP experiments were performed using a 1.1 numerical aperture/40x water objective on a scanning laser confocal microscope Leica TCS SP5 II (Leica Microsystems) and using the FRAP Wizard application of the LAS Advance Fluorescence (AF) 2.6. Software. First, we focused on the best imaging plane of the lateral cortex of the follicular epithelium, since our FRAP experiments were performed for basolateral proteins. Afterwards, a region of interest (ROI) with a dimension of 3 µm x 1 µm or 1.5 µm x 1 µm cortical section of two neighbor cells was selected and bleaching was performed using a single pulse with the 405 laser line (50 mW) at maximum laser power using the Zoom In and Set the Background to Zero options of the FRAP Wizard. For live cell imaging process, a 488 nm laser with 20%-30% laser intensity was used and images acquired using a 256 x 256 format with 1000 Hz scanning speed and a 12x Zoom factor, minimizing the photobleaching induced during the acquisition process and optimizing the temporal resolution of the signal recovery after photobleaching. At least two

independent experiments for each condition were performed and using distinct biological replicates. The same ovariole was not used to perform more than 3 FRAP experiments.

B) FRAP protocols

For every FRAP experiment performed, a three-step protocol was developed: A) a pre-bleaching acquisition phase for the equilibration of the GFP; B) a photoperturbation step using a single pulse with 405 nm laser and C) three post-bleaching phases using 488nm laser. Pos-bleach acquisition time in the FRAP protocol was adjusted to accommodate different protein behaviors, ensuring the acquisition of sufficient data points for half-time measuring and the plateau recovery of proteins. The following protocols were applied:

Lgl-GFP

Pre-bleaching – 6 frames
Pos-Bleach 1 – 25 frames (1s/frame)
Pos-Bleach 2 – 25 frames (3s/frame)
Pos-Bleach 3 – 10 frames (10s/frame)

Dlg-GFP

Pre-bleaching – 6 frames
Pos-Bleach 1 – 50 frames (1s/frame)
Pos-Bleach 2 – 50 frames (3s/frame)
Pos-Bleach 3 – 30 frames (10s/frame)

Scrib-GFP

Pre-bleaching – 6 frames
Pos-Bleach 1 – 60 frames (1s/frame)
Pos-Bleach 2 – 60 frames (3s/frame)
Pos-Bleach 3 – 35 frames (10s/frame)

C) Processing FRAP raw data and data analyses

Image processing and analysis were performed using FIJI (Schindelin *et al*., 2012). Before measuring the FRAP recovery of proteins, the raw data was properly processed in three main steps: **1) Registration**: consists of the alignment of time-lapse images, correcting drifts in the plan of imaging that can influence quantification. This step was performed using the "Stack Reg" plugin (Rigid Body option) of ImageJ; **2) Measurement** of the pre-bleach and recovery mean grey intensity values for each time point using a ROI 3 µm x 1 µm in the photoperturbed region. Two cortical regions in non-adjacent regions to the photobleached region were also measured using a 3 µm x 1.5 µm ROI to correct for loss of fluorescence during the pos-bleaching process. A circular ROI with 2 µm diameter in the cell center was used for background subtraction as none of the proteins of interest is present in the nucleus; **3) Double normalization** (%F(t), equation 1): fluorescence intensity values were transferred from ImageJ to a Microsoft Excel file and background intensities subtracted. These values (BI) were normalized to the mean of the three pre-bleaching (pre) frames and corrected for the loss of fluorescence during the process of bleaching by using the mean of the background subtracted intensities of two non-bleached ROI (NB). The value of the first frame of the pos-bleach BI(t_0) is then set to zero to allow comparison of curves from different experiments with different bleach efficiencies. Finally, the fluorescence intensity values are set in percentage of recovery.

$$\%F(t) = \frac{Bl(t) - Bl(t_0)}{Bl(pre) - Bl(t_0)} * \frac{NB(pre)}{NB(t)} * 100 \quad (1)$$

The normalized data was represented in recovery plots of the mean fluorescence intensity for the total number of cells in each condition. Curve fitting was performed using a one phase association non-linear fit to compare the half-time values of each condition. Kymographs were obtained by drawing a line in a selected region and using the reslice tool (Image>Stack>Reslice) of ImageJ.

2.7. Drug treatments

To explore the role of PP1 and PP2A phosphatases in S2 cells, we added Okadaic Acid (OA) (Sigma-Aldrich) at a final concentration of 10 nM just before starting live imaging (Figure 3.5 A).

Ovaries expressing Lgl-GFP were incubated for 25 min at room temperature in Schneider's medium with 10% FBS and insulin (imaging media) containing Ionomycin (Sigma-Aldrich) before preparing the extracts for Immunoprecipitation (IP) in Figure 3.17.

Actin cytoskeleton disruption to induce failure in cytokinesis (Figure 4.10) was achieved by filming ovarioles with 5 ng/µL of Latranculin A (Sigma-Aldrich) diluted in imaging media.

aPKC inhibitor (CRT0103390) was added to the imaging media at a final concentration of 5 µM immediately before starting to film a choosed egg chamber. This concentration was shown to inhibit 80% of LLGL2 *in vitro* phosphorylation by aPKC (Rodriguez *et al*., 2017).

2.8. Molecular biology techniques and experiments

2.8.1. Cloning of Lgl variants

To generate mutations in the PP1 docking site of Lgl, we performed a site-directed mutagenesis protocol using the primers indicated in Table 2.3, which harbor the desired mutations. Using pENTR-Lgl as template (Carvalho *et al*, 2015), PCRs were performed with Phusion High Fidelity DNA polymerase (New England Biolabs, Ipswich, MA), followed by digestion of the template plasmid with DpnI restriction enzyme (New England Biolabs, Ipswich, MA) and transformation of competent bacteria.

The transference of the mutated transgene to a destination vector for injection of *Drosophila* embryos was achieved by using the Gateway Cloning System (Life Technologies). pEntr-Lgl^{K327A,F331A} was recombined using this system with a pUASt.attb.WG (Rugjee *et al*., 2013) plasmid to generate pUASt.attb.Lgl^{K327A,F331A}-GFP. The UAS- Lgl^{K327A,F331A}-GFP transgene was inserted into the attP-VK18 landing site (BDSC #9736) on chromosome II via PhiC31 site-specific transgenesis (BestGene Inc).

The Gateway Cloning System (Life Technologies) was also used to generate the following constructs: pMT-Lgl-Dendra2, upon recombination of pENTR-Lgl with pMT-W-Dendra2 [(Amine *et al*., 2013), gift of Gilles Hickson] and pHW-Lgl^{3A}-RFP resulted from recombination of pENTR-Lgl^{3A} with pHWR (Carvalho, 2015).

2.8.2. Preparation of ovaries and S2 cells protein extracts

For preparation of protein extracts, ovaries were dissected in Schneider's medium supplemented with 10% FBS and 200 µg/ml insulin (Sigma-Aldrich). Protein extracts were obtained by disrupting ovaries through sonication in Lysis Buffer (150 mM KCl, 75 mM HEPES, pH 7.5, 1.5 mM EGTA, 1.5 mM $MgCl_2$, 15% glycerol, 0.1% NP-40) after adding 1x protease inhibitors cocktail (Roche) and 1x phosphatase inhibitors cocktail 3 (Sigma-Aldrich). Afterwards, samples were centrifuged at 14000 rpm for 10 min at 4ºC and supernatant carefully removed to another tube and centrifuged again to remove the remaining lipids.

To prepare S2 cells extracts and analyze the depletion levels of proteins by Western blot, S2 cells were centrifuged at 5000 rpm for 10 min at 4ºC and washed twice with 2 ml of PBS (1x) supplemented with protease inhibitors cocktail (Roche). Lysis buffer was added and cells were disrupted by sonication. Samples were then centrifuged 10 min at 4ºC, 10 000 rpm, and supernatant removed, avoiding lipids.

Protein concentration was measured using a *NanoDrop 1000* Spectrophotometer (measuring the protein's absorbance at 280nm, which calculates the concentration in mg/ml).

2.8.3. Western blotting

For protein detection by western blot, protein samples were resolved by SDS-PAGE and transferred to nitrocellulose membranes using the iBlot Dry Blotting System (by Invitrogen) according to the manufacturer's instructions. After membrane blocking for 2 hours at room temperature with 5% dry milk in 0.05% PBS-Tween, membranes were incubated overnight at 4ºC with primary antibodies diluted in 0.05% PBS-Tween. After three washes of 10 min with 0.05% PBS-Tween for removal of the primary antibody, membranes were incubated

with Horseradish Peroxidase (HRP)-conjugated secondary antibodies (Amersham) diluted in 5% dry milk dissolved in 0.05% PBS-Tween. For protein detection, membranes were incubated for 5 min in Clarity ECL substrate (Bio-Rad) and proteins detected on X-ray film (Fuji Medical X-Ray Film).

2.8.4. *In vitro* protein expression and purification

MBP-Lgl$^{402-802}$ protein was expressed in BL21 Star *E.coli* and purified following the manufactures instructions using amylose magnetic beads (New England Biolabs). The plasmid pMal-Lgl$^{402-802}$ was provided by J. Knoblich.

For protein expression, bacteria were inoculated in 2 ml of standard LB (Luria-Bertani) media with antibiotic and incubated ON for 12-16h (at 37ºC with shaking). After, 1 ml of the pre-culture was used to inoculate 50 ml of LB with antibiotic and glucose (500 µl of a 0.1 g/ml solution) for 2.5h with shaking. A pre-induced sample was removed for posterior SDS-PAGE. The induction of expression of MBP-Lgl$^{402-802}$ was performed by adding 0.05 mM IPTG and incubation for additional 3 hours. An induced sample was also removed. After, the culture was centrifuged at 4000 rpm for 15 minutes, the pellet solubilized with 2.5 ml of PBS with 1mg/ml Lysozyme (Sigma Aldrich) and 10 Mm PMSF (Fisher Scientific), incubated on ice for 1 hour and frozen at -20ºC. Cells were after disrupted with sonifier until a fluid and clear mixture was obtained. After, 1% Triton X-10 was added followed by a step of centrifugation at 20000 G for 30 min at 4ºC. The pellet was dissolved in PBS 1x, a sample removed and resolved into a SDS-polyacrylamide gel electrophoresis (PAGE) together with the pre-induced, induced and supernatant (purified protein) samples. A Coomassie blue staining was then performed to evaluate the success and purity of the protein samples.

2.8.5. Immunoprecipitations (IP)

For co-immunoprecipitation (co-IP) assays, ovaries from 10-15 well-feed flies were dissected and protein samples prepared as previously described. Immunoprecipitation of GFP tagged Lgl was achieved by using the GFP-Trap_MA system (Chromotec GmbH, Planegg-Martinsried, Germany), whereas Dlg was immunoprecipitated using Protein G Magnetic Beads (NEB). Briefly, about 25 µl of washed bead slurry of GFP-Trap_MA system was added to final volume of 500 µl of extract (with a total protein range of 3-6 mg) and

incubated for 1 hour at 4ºC with slight shaking. At the end, the supernatant was removed, GFP-Trap beads washed three times with Lysis Buffer containing protease and phosphatase inhibitors (1x) were resuspended in 20 µl of 1x SDS Laemmli sample buffer (diluted in Lysis Buffer) and boiled for 5 min at 95ºC to dissociate the immunocomplex from the beads. Immunoprecipitation of Dlg using Protein G Magnetic Beads (NEB) requires an additional pre-clear step to avoid unspecific binding of proteins to the beads. Therefore, the extract was incubated with 20 µl of beads during 1 hour with shaking at 4ºC. After this step, the pre-cleared extract was incubated with about 20 µl of Dlg antibody ON. In the next day, 50 µl of beads was added to the extract for incubation during 2h30 with shaking at 4ºC. After washing steps with 500 µl of Lysis Buffer with inhibitors, beads were resuspended in 20 µl of sample buffer (2x) and heated for 5 min at 95ºC. To analyze the result, beads were magnetically separated from the supernatant and proteins resolved in an 8% SDS-PAGE followed by western blotting.

2.8.6. *In vitro* dephosphorylation assays

For *in vitro* dephosphorylation assays using Lgl from ovary extracts, Lgl-GFP was immunoprecipitated using the protocol previously described. After removal of the lysis buffer and a single wash with H_2O, we proceeded to an *in vitro* kinase assay, where Lgl bound to beads was incubated with the kinase reaction buffer with 200 ng of AurA (Millipore) in kinase reaction buffer (5 mM MOPS, pH 7.2, 2.5 mM β-glycerol-phosphate, 5 mM $MgCl_2$, 1 mM EGTA, 0.4 mM EDTA, 0.25 mM DTT, 0.2 mM ATP) during 30 min at 30 ºC to saturate Lgl phosphorylation. Then the kinase reaction mix was removed and the phosphatase reaction mix was added, containing 2 µM MLN8237 for inhibition of the AurA kinase, 1x PMP phosphatase buffer (New England Biolabs), 1x $MnCl_2$ and respective amounts of recombinant human GST PP1γ [MRC-PPU Reagents (University of Dundee)]. A sample was initially removed to access the phosphorylation status of the protein and dephosphorylation reactions were carried at 30ºC for 30 min. Then, the reaction was stopped by addition of SDS Laemmli sample buffer (4% SDS, 10% mercaptoetanol, 0.125 M Tris-HCl, 20% glycerol, 0.004% bromophenol blue) and heated for 5 min at 95°C. Samples were resolved in an 8% SDS-PAGE followed by western blot with p-Lgl656 antibody and another equivalent western blot with anti-GFP to control for the amount of Lgl-GFP used.

For *in vitro* dephosphorylation assays using recombinant MBP-Lgl, a kinase assay reaction was carried at 30ºC for 30 min, containing 0.5 µg of MBP-Lgl and recombinant Aurora A (Millipore) in ice-cold kinase assay buffer (5 mM MOPS, pH 7.2, 2.5 mM β-glycerol-phosphate, 5 mM $MgCl_2$, 1 mM EGTA, 0.4 mM EDTA, 0.25 mM DTT, 0.2 mM ATP). The dephosphorylation reaction was performed in a reaction solution containing 2 µM MLN8237, PMP phosphatase buffer (New England Biolabs), $MnCl_2$ and 1U of Protein Phosphatase 1 (New England Biolabs) or 1U Lambda PP (New England Biolabs). Dephosphorylation reactions were carried at 30 ºC for 30 min and stopped by addition of SDS Laemmli buffer. Samples were resolved by SDS-PAGE. p-Lgl656 antibody was used to detect phosphorylation in a western blot, whereas western blots with anti-GFP, anti-MBP-HRP conjugated or anti-GST were performed to control for the amount of Lgl substrate (the first two) or PP1-GST (the last one).

2.8.7. RT-PCR

This method was used to analyze, in a qualitative manner, the RNAi depletion in S2 cells. The first step was the isolation of the total RNA using the RNeasy Mini Kit and following the manufacturer's instructions. For each analysis, RNA samples from RNAi depleted and control S2 cells were extracted. To synthetize cDNA from the RNA samples, we used SuperScriptTM II Reverse Transcriptase and finally PCRs for the required genes were performed using DreamTaq DNA polymerase and the primers listed in the Table 2. PCR conditions were as follows: 1) 95ºC for 3 min (initial denaturation); 2) 95ºC for 30 sec (denaturation); 3) 58-63ºC for 30 sec (annealing); 4) 72ºC for 1 min (extension) (25 cycles from step 2 to step 4) and 72ºC for 15 min (final extension). The amplified fragments were resolved by 1% agarose gel electrophoresis.

2.9. Data analyses and quantifications

Most image processing and quantifications were performed using FIJI (Schindelin *et al*., 2012). Quantification of the intensity of Lgl-Dendra2 after photoconversion experiments was performed using ICY and statistical analysis and graphical representations were performed using GraphPad Prism 6 tools.

2.9.1. Lgl cytoplasmic decay

Lgl reloading at mitotic exit was quantified since anaphase in the follicular epithelium, embryonic epithelium and S2 cells. We measured the mean pixel intensity manually, using a circular ROI in the cytoplasm (12x12 in S2 cells, 8x8 in the follicular epithelium and 6x6 in the embryonic epithelia; 1 px = 0.13 mm) in sum intensity Z projections. We used a square in a region outside the cell to quantify the background, which was subtracted to mean intensity values of cytoplasmic Lgl in each time-point. The intensity values were normalized to the maximum intensity (the anaphase value) and presented as percentage. Since Lgl cytoplasmic intensity values are negligible at the end of mitosis in control cells or upon AurA overexpression/AurA RNAi, the average of cytoplasmic intensity at a minimum plateau was subtracted to represent cytoplasmic decay from 100% to 0%. However, in experiments involving RNAi depletion, cytoplasmic decay was not normalized to the minimum plateau since it is a useful parameter to allow comparison between experiments.

2.9.2. Lgl accumulation daughter- daughter interface

To quantify the intensity of Lgl in the new interface of follicular epithelia, we aligned the stack images using the "StackReg" plugin of FIJI (Plugin > Stacks > StackReg) and we drew a square in the new interface to track the mean intensity values over time since anaphase. To obtain the intensity accumulation in the new interface, the background subtracted mean intensity values of Lgl in the division cell equator and in the daughter-daughter interface were normalized to the background subtracted mean intensity in the cytoplasm. The anaphase value (average of the first three frames since anaphase) was set to 0% and the average intensities in the plateau of accumulation was set to 100%.

2.9.3. Lgl-Dendra2 intensity upon photoconversion

We used Icy (an open community platform for bioimage informatics, (http://icy.bioimageanalysis.org) to quantify the overall intensity of Lgl-Dendra2 at mitotic exit after photoconversion. After generating a Z sum-projection of all optical sections covering the cell, we used the Active Contour protocol of Icy to find the contour of cells in each time point and to quantify the overall intensity of Lgl in an automated manner. For each time-point, we subtracted the respective background value and calculated the integrated density (cell area x mean intensity value), which was normalized to the value at

anaphase onset (100%). Quantifications of the cytoplasmic decay were performed as described previously (for quantification of Lgl reloading in S2 cells).

2.9.4. Interphase cortical/ cytoplasm intensity ration of Lgl in S2 cells

In measurements of the cortical/cytoplasm mean intensity of Lgl in S2 cells during interphase, cortical intensity values were obtained using a macro on FIJI that segmented the image to find the cell contour (CC) and calculated the area between CC - 1 px and CC – 5 px (1 px = 0.13 mm). Cytoplasmic intensity was measured using a circular ROI in a homogeneous region of the cytoplasm. The value of the cortex/cytoplasm ratio was obtained after subtracting the background intensity for each value.

2.9.5. aPKC accumulation in the apical interface formed between daughter cells at mitotic exit

To quantify the accumulation of aPKC in the apical daughter-daughter interface, images were firstly processed using EpiTools (Heller *et al*., 2016) to generate the best plane projections of the apical area of the follicular epithelium. Signal of aPKC-GFP was then manually tracked in the equator of the dividing cell/ daughter-daughter interface using a 10 pixel width line, in the interface of four non-dividing/non-adjacent neighboring cells using a 10 pixel width line and three circular ROI with 8 pixels of diameter in the cytoplasm for background subtraction. A FIJI script developed by Mariana Osswald was then used to automatically measure the background subtracted mean intensities of aPKC-GFP at the new daughter-daughter interface and to normalize the signal of aPKC-GFP in the new daughter-daughter interface by the intensity values of the non-dividing interfaces.

2.9.6. Quantification of the band intensity in WB and RT-PCR

To quantify the intensity of DNA or protein bands in RT-PCR or WB experiments, a square adjusted to the size of the bands was used to determine the mean gray intensity for all conditions using the ROI manager tool of FIJI. A square outside was used to measure the background, which was then subtracted to the intensity of the bands. To determine the pLgl/Lgl ratio, each value was previously normalized to the respective intensity of α-tub and all values normalized by the WT levels (100%). The PP1/Lgl ratio in immunoprecipitations (IPs) were obtained by simply dividing the mean grey intensity values of PP1 by the

respective values of Lgl-GFP in each condition. Quantifications of RT-PCR bands were performed by normalizing each condition by the respective α-tub levels and values were normalized to the control levels of each gene.

2.10. Multiple sequences analyses

Multiple sequence alignment of Lgl proteins from several species of the metazoan phyla and Fungi (Ascomycota) was performed using CLUSTAL format by PROMALS3D (http://prodata.swmed.edu) and the aligned amino acid sequences were visualized using Jalview 2.10.5 (http://www.jalview.org). Protein sequences used were the following: *H. sapiens* L2GL1 (ID: Q15334); *H. sapiens* L2GL2 (ID: NP_001026973.1); *M. musculus* LGL1 (ID: NP_001152877.1); *M. musculus* LGL2 (ID: NP_663413.2); *D. rerio* LLGL1 (ID: XP_005164199.1); *S. purpuratus* (ID: XP_011678406.1); *D. melanogaster* (ID: NP_722584.1); *T. castaneum* (ID: NP_001280527.1); *C. teleta* (ID: ELT88587.1); *C. gigas* (ID: XP_011454121.1); *C. elegans* (ID: NP_508169.2); *N. vectensis* (ID: XP_001640099.1); *H. vulgaris* (ID: XP_002164128.2); *A.queenslandica* (ID: XP_019855603.1); *S. cerevisiae* SRO7 (ID: Q12038); *S. pombae* (ID: NP_593006.1); *K. lactis* (ID: XP_454237.1)

2.11. Statistical analysis

All the statistical analyses were performed using GraphPad Prism 6.

The data were first analysed to test for the assumptions of the One-way ANOVA and t tests: Gaussian distribution of the data and the homoscedasticity of the data. The Shapiro-Wilk test was used to test if the data were normally distributed. A p-value above 0.05 does not allow one to reject the null-hypothesis that the data are normally distributed. A p-value under 0.05 means that the test is significant, and that the data does not follow a normal distribution. Bartlett's test was used to test for the heteroscedasticity of the data. A p-value above 0.05 does not allow one to reject the null-hypothesis that the data are homoscedastic (i.e.: assumption of equal variances). A p-value under 0.05 means that the test is significant, and that the data are heteroscedastic.

When these assumptions were satisfied, we used the One-way ANOVA to test for a significant difference in the means of three or more groups, and the t-test to test for a significant difference in the means of two groups.

In case both the assumptions for normal distribution of the data and homoscedasticity were rejected, we used a non-parametric multiple comparison test, the Kruskal-Wallis test, to perform the statistical analysis or Mann-Whitney test to compare the distribution of two unmatched groups.

Chapter 3

The role of phosphatases in Lgl phosphoregulation and cortical localization

3.1. Introduction

In this chapter, we aim to understand how the cortex/plasma membrane (PM) localization of Lgl is maintained, a fundamental condition for its tumor suppression function and cell polarity regulation in epithelia. This has been suggested by several studies, including early findings showing that homozygous mutant females for a temperature sensitive mutation (*l(2)gl*^{ts3}), which is able to induce Lgl localization in the cytoplasm, display a severe loss of follicular cell polarity during oogenesis at a restrictive temperature (Manfruelli *et al*., 1996). Other studies report a strong association of human cancers with Hugl mislocalization in the cytoplasm, such as Hugl-1 in colorectal cancer (Schimanski *et al*., 2005) or Hugl-2 in gastric epithelial dysplasia and adenocarcinoma (Lisovsky *et al*., 2009; Nam *et al*., 2014).

However, until now, it is not fully understood how Lgl localization in the cortex/PM is regulated. It has been proposed that aPKC and AurA phosphorylation of Lgl excludes the protein to the cytoplasm by reducing its affinity to the PM and the underlying cortex (Bailey and Prehoda, 2015; Bell *et al*., 2015; Betschinger *et al*., 2003; Carvalho *et al*., 2015; Dong *et al*., 2015). Despite the important function of Lgl at the cortex/PM, its temporary cortical exclusion was shown to be involved in regulation of several biological processes, namely epithelial polarization of migrating fibroblasts (Plant *et al*., 2003) and asymmetric cell division (Betchinger *et al*, 2003). Additionally, the establishment of apical and basolateral domains in epithelial cells also relies on Lgl phosphorylation by aPKC on three main evolutionarily conserved serines and the consequent exclusion from the apical side (Hutterer *et al*., 2004; Yamanaka *et al*., 2003). While the impact of Lgl phosphorylation in inhibiting its cortical/PM localization has been widely studied, which molecular mechanisms restore Lgl's ability to bind to the cortex/PM remain to be understood. A possible scenario is that Lgl dephosphorylation would induce an increase in the affinity of Lgl to the cortex/PM.

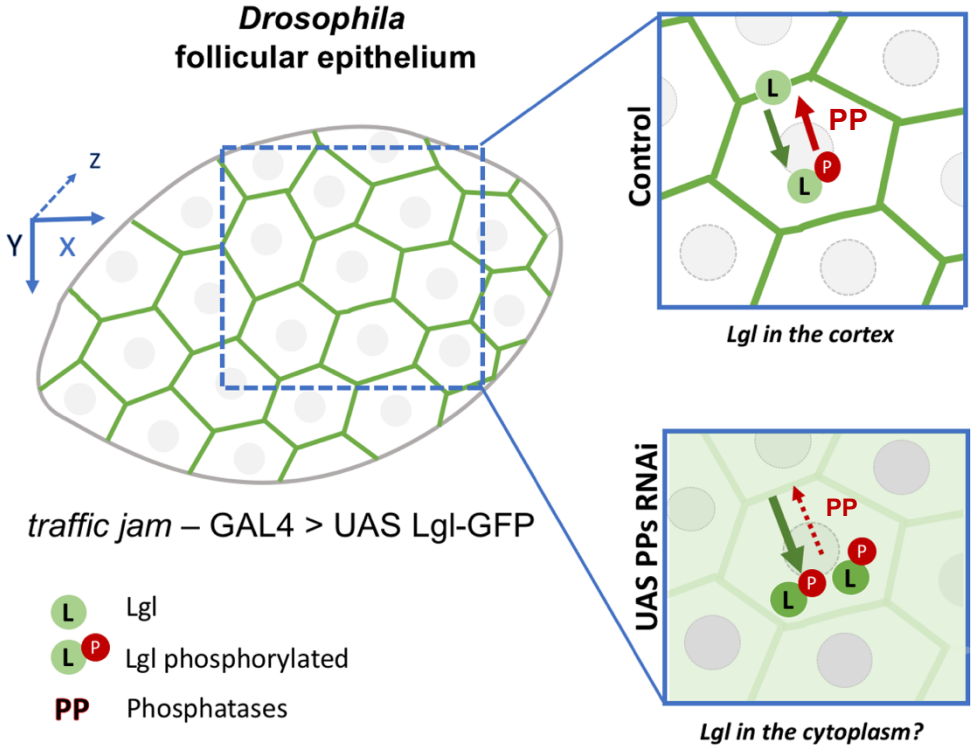

Figure 3.1: Schematic representation of the hypothesis on how Lgl phosphoregulation controls its localization at the cortex. Lgl phosphorylation could be counteracted by the action of phosphatases, which by dephosphorylating Lgl would maintain this basolateral protein in the cortex. To explore this hypothesis, we firstly performed an RNAi screen for phosphatases and phosphatase regulatory subunits in the follicular epithelium using a *traffic jam* > *Gal4* driver to express both the UAS-PP RNAi and UAS-Lgl-GFP. We would expect to see total or partial displacement of Lgl to the cytoplasm by interfering with the expression of important phosphatases or regulators involved in cortical Lgl localization.

Here, we address whether Lgl dephosphorylation is involved in Lgl cortical localization. I have started by a targeted RNA interference (RNAi) screening to identify phosphatases and associated regulatory subunits that regulate Lgl localization in the follicular epithelia of *Drosophila*. The rationale behind this approach is schematically illustrated in Figure 3.1: downregulation of a phosphatase directly involved in dephosphorylation and cortical maintenance of Lgl should unbalance the equilibrium towards a more phosphorylated and cytoplasmic pool of Lgl. From this screen, I found one serine/threonine phosphatase, protein phosphatase 1 (PP1), which dephosphorylates Lgl to regulate its localization and consequently preserve the overall architecture of the tissue.

3.2. Identification of a phosphatase that controls Lgl cortical localization

Driven by the hypothesis that opposing activities of kinases and phosphatases could regulate Lgl cortical/PM localization, we started an RNAi screen for catalytic and regulatory subunits of phosphatases using *traffic jam* > Gal4 driver to induce simultaneous over-expression of UAS-RNAi and UAS-Lgl-GFP simultaneous overexpression specifically in the follicular epithelium (Olivieri *et al*., 2010). In the flowchart of Figure 3.2, we describe the steps towards the selection of phosphatases/regulatory subunits included in this screen. According to the last reviewed data of FlyBase (2015-06-08), 90 members of protein phosphatases (PPases) were identified. Our screen was mainly focused on phosphoprotein phosphatases (PPP), a relatively small group of serine/threonine phosphatases (19 members) which could counteract the Lgl displacement from the cortex induced by aPKC/AurA phosphorylation. However, since not all PPP are expressed in the ovaries, we focused on those displaying a moderate to very high expression according to high-throughput RNA sequencing (RNA-seq) tissue expression data of the modENCODE project (www.modencode.org; www.genome.gov/modencode). From the seven highly expressed PPPs, we decided to focus on two major families, PP1 and PP2A, particularly on three phosphatases: PP1, PP2A/mts and PpV. PP1 and PP2A/mts are the most representative serine/threonine protein phosphatases in cells, together accounting for more than 90% of protein phosphatase activity in eukaryotes (Virshup and Shenolikar, 2009). Therefore, we decided to analyze Lgl localization by depleting the catalytic subunit of PP2A, microtubule star (Mts), and the most abundant isoform of PP1 in *Drosophila*, Pp1-87B (Kirchner *et al*., 2007). *Drosophila* protein phosphatase V (PpV) is an homologue of mammalian PP6 which belongs to the PP2A subfamily of serine/threonine phosphatases (Wang *et al*., 2012), being involved in Wnt pathway regulation (Swarup *et al*., 2015) and lipid homeostasis (Yin *et al*., 2014). We decided to include this phosphatase in our screen since PpV was found to interact with Lgl in a recent RNAi screen that identified novel genes interacting with polarity proteins (Parsons *et al*., 2017). PPPs phosphatases often work as holoenzymes, achieving substrate specificity and temporal activity through association of the catalytic subunit with regulatory proteins (Shi, 2009) and so we also tested a regulatory subunit of PP2A, Twins, (Shiomi *et al*., 1994), a scaffolding-A subunit, PP2A-29B (Mayer-Jaekel *et al*., 1992), and two regulatory subunits of PP1, Pico and Sds22, all of them highly expressed in the ovaries. Moreover, we extended our analyses to dual specific phosphatases (DSP), which could dephosphorylate both tyrosine and serine/threonine residues of Lgl. From the 23 members

of DSP, we selected only two of them, PTEN and Twin (Twe), whose depletion was found to induce egg chamber defects in an RNAi screen for genes controlling epithelial development (Berns *et al*., 2014).

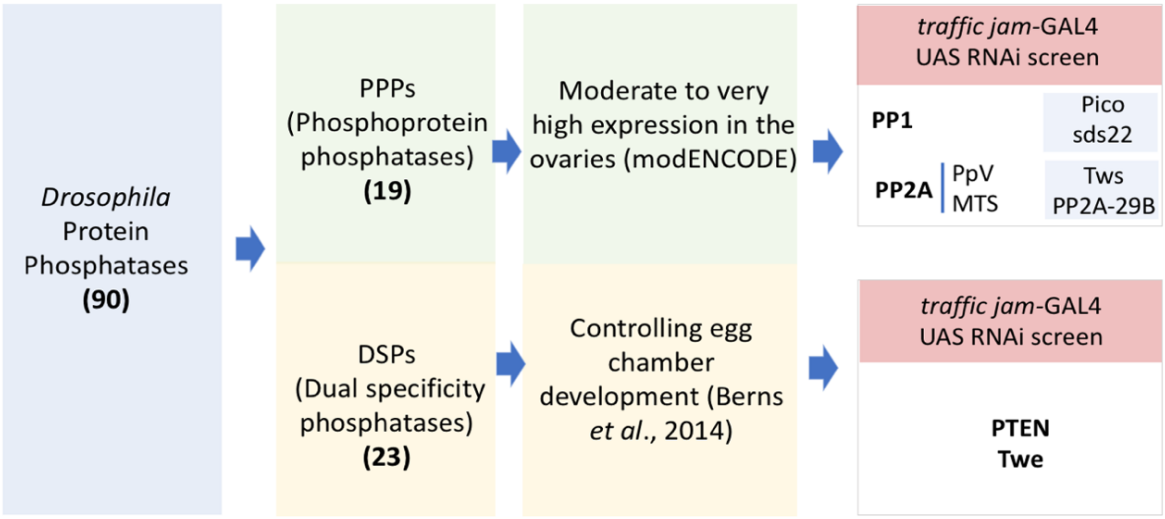

Figure 3.2: Flowchart of a targeted RNAi screen to search for phosphatases and phosphatase regulatory subunits controlling Lgl cortical localization in the follicular epithelia. This small screen was performed using a *traffic jam-Gal4 driver* to express both UAS-RNAi and UAS- Lgl-GFP. The numbers in bold represent the members found in the last reviewed data of FlyBase (from 2015-06-08) for the indicated protein families.

After inducing expression of different RNAis together with UAS-Lgl-GFP in the follicular epithelia (at 29ºC, for a variable number of days, indicated in figure legends), ovaries were dissected and fixed for posterior analyses of Lgl-GFP localization by confocal microscopy. Representative images for Lgl-GFP localization in each RNAi condition are shown in Figure 3.3. Comparing with the control situation, we observe normal localization of Lgl-GFP at the cortex when depleting different phosphatases, except for Pp1-87B (Figure 3.3). As indicated by the white arrow, Lgl-GFP is strongly mislocalized in the cytoplasm in follicle cells, rendering the nucleus shape visible. We also detected Lgl-GFP in the cytoplasm when depleting the regulatory subunit of PP1, sds22, although to a lesser extent than for Pp1-87B depletion (Figure 3.3, sds22 RNAi, white arrow). Moreover, depletion of the other regulatory subunits did not affect Lgl-GFP localization in the conditions tested.

Although depletion of Pp1-87B induces a change in Lgl-GFP localization, we considered the possible dilution effect of GAL4 caused by the co-expression of UAS Lgl-GFP, together

with the UAS-driven RNAi, interfering with RNAi expression. In fact, we consistently observed stronger cytoplasm accumulation of the endogenous Lgl than overexpressed Lgl-GFP when depleting Pp1-87B or Sds22 (Figure 3.4A). We quantified the percentage of egg chambers displaying wild-type localization of Lgl in different conditions. The results are summarized in Table 3.1: from 40 egg chambers depleted for Pp1-87B we found that all displayed aberrant cytoplasm accumulation of Lgl; a milder phenotype was observed when depleting Sds22, where 52% of the egg chambers analyzed displayed a wild-type localization of Lgl. However, we only observed minor changes in Lgl localization when depleting the catalytic subunit of PP2A, Mts (81% of the egg chambers displayed a wild-type localization of Lgl, as shown in Table 3.1). Quantifications of plasma membrane localization of Lgl (obtained by the cortex/cytoplasm ratio of Lgl signal intensity) confirmed a high and significant displacement of Lgl in Pp1-87B depleted cells when comparing with the control (Figure 3.4B). To confirm this phenotype, we performed a staining for Lgl in follicular epithelium upon clonal depletion of Pp1-87B by RNAi, combining the FRT/FLP technique with the Gal4/Gal80 system (see *Chapter 2: Material and methods* for details). This allowed a comparison in the same tissue of the localization of Lgl in wild-type and PP1 depleted cells, confirming that Pp1-87B is required for proper cortical localization of Lgl (Figure 3.4C).

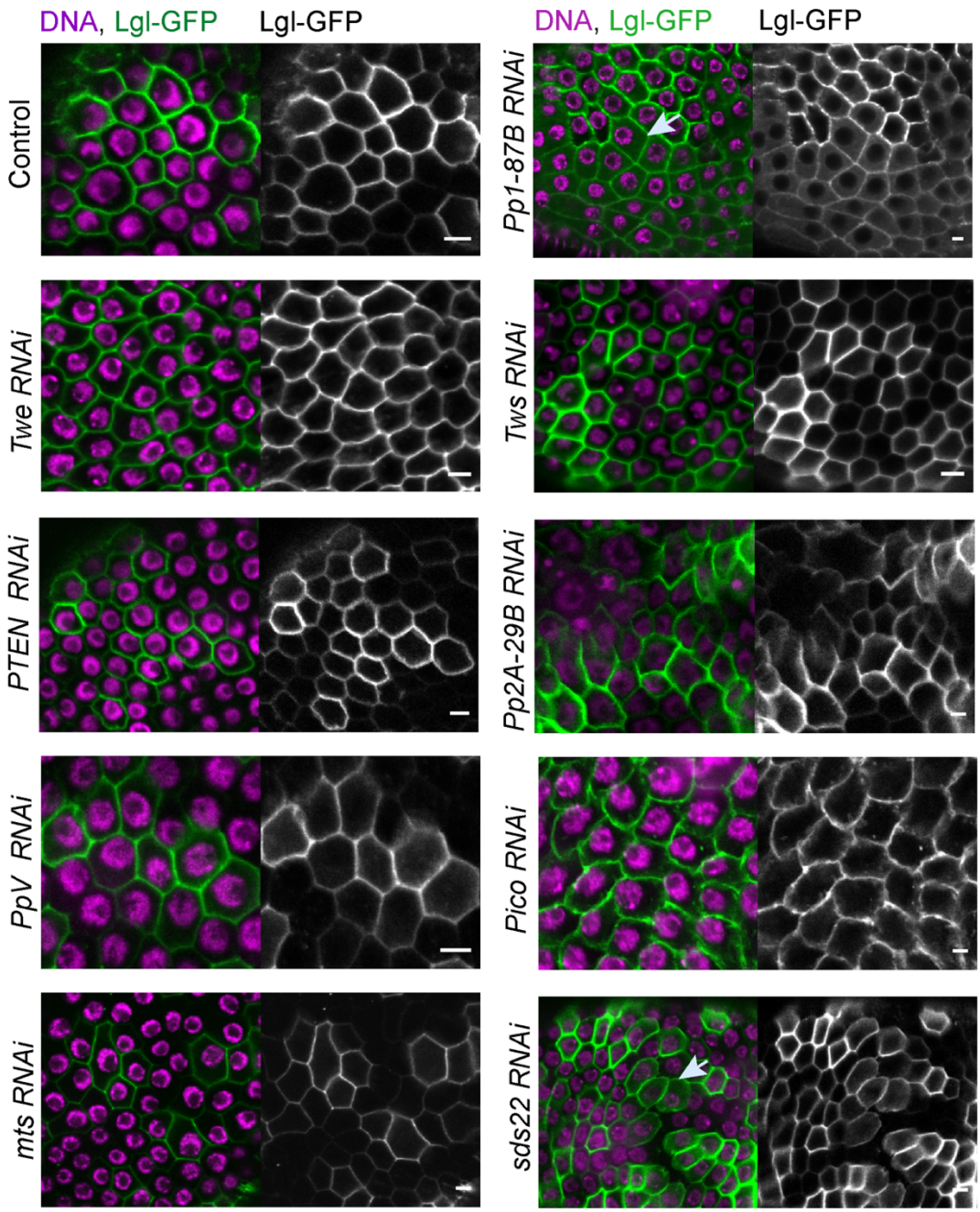

Figure 3.3: Pp1-87B depletion induces a strong mislocalization of Lgl-GFP to the cytoplasm in follicle cells. Representative images of Lgl-GFP localization for each RNAi condition is shown. Pp1-87B was the only one of the analysed phosphatases whose depletion lead to cytoplasmic reallocation of Lgl-GFP (white arrow). Depletion of the Sds22 regulatory subunit also induced a mild mislocalization of Lgl-GFP to the cytoplasm, as indicated by the white arrow in the sds22 RNAi image. No effect on Lgl-GFP localization was detected for the other regulatory subunits. The conditions used for depletion of each phosphatase/regulatory subunit were as follows: 29ºC for 2 days (*UAS-Twe RNAi*; *UAS-PTEN RNAi*; *UAS-PpV RNAi*; *UAS-mts RNAi*); 29ºC for 3 days (*UAS-Pp1-87B RNAi*; *UAS-Tws RNAi*); 29ºC for 1 day (*UAS-Sds22 RNAi*; *UAS Pp2A-29B RNAi*); 29ºC for 7 days (*UAS-Pico RNAi*). Scale bars: 5 μm.

Table 3.1: Summary of the Lgl endogenous localization in RNAi experiments. Depletion experiments were performed using the following conditions: *UAS-Pp1-87B:* 29ºC - 2 days *RNAi*; *UAS-Sds22 RNAi*:1 day at 29ºC*; UAS-Mts RNAi*: 2 days at 29ºC.

Genotype	Number of egg chambers	% Egg chambers with wild-type localization of Lgl	Number of independent experiments
TJ-GAL4/+; UAS – Pp1-87B RNAi/+	40	0	4
TJ-GAL4/UAS – Sds22 RNAi; +/+	91	52	2
TJ-GAL4/+;UAS – Mts RNAi/+	40	81	4

PP1 has been described to dephosphorylate other cell polarity proteins, such as Par-3 (Bazooka in *Drosophila*) (Traweger *et al* 2008). Moreover, there is a notable cell shape change upon Pp1-87B RNAi (Figure 3.4C).Therefore, we raised the possibility that Lgl cytoplasmic localization could result from an indirect effect of PP1 on apical-basal polarity. To address this question, we explored the role of this phosphatase in Lgl localization using an unpolarized system, *Drosophila* S2 cells, where Lgl is also associated with the cortex/PM during interphase. As a first approach, we used okadaic acid (OA) to inhibit PP1 and PP2A activities in S2 cells expressing Lgl-GFP. After adding 10 nM of OA to the cell culture, we observed progressive delocalization of Lgl from the cortex to the cytoplasm in interphase cells (Figure 3.5A, white arrows in the Lgl separate channel). The effect of the drug is confirmed by cortical deformations and bebblings (Figure 3.5A**,** green arrow), common features associated with phosphatase inhibition towards cortical components (Bøe *et al*., 1991; Kunda *et al*., 2012). Thus, this result indicates a potential role for PP1 and/or PP2A in Lgl cortical localization in S2 cells. However, we did not detect an effect on Lgl localization by depleting the catalytic subunit of PP2A, *mts* (Figure 3.5B and 3.5D). An increase in the mitotic timing of the depleted cells was observed [mean time of nuclear envelope breakdown (NEBD) to anaphase onset (AO): ~ 22 min in control; NEBD to AO in mts RNAi: ~ 90 min], which is consistent with an increase in mitotic index previously described after

mts depletion (Chen *et al*., 2007). On the other hand, we observed a strong mislocalization of Lgl to the cytoplasm when depleting PP1 (Figure 3.5B and 3.5D). Interestingly, the effect on Lgl mislocalization was stronger using a dsRNA that interferes with the expression of all the major PP1 isoforms (Pp1-87B, Pp1α-96A and Flapwing) when compared with a dsRNA specific for the 5'UTR region of Pp1-87B (RT-PCR in Figure 3.5C and quantifications in 3.5D). Although the specific depletion of Pp1-87B also induces a significant change in Lgl-GFP localization when compared with the control (Figure 3.5D), our results suggest that Lgl cortical localization could be synergistically regulated by PP1 isoforms. Another possibility could be related with a more efficient depletion Pp1-87B when using a dsRNA able to target all the PP1 isoforms. However, differences in the efficiency of mRNA depletion between the use of dsRNA for 5'UTR of Pp1-87B and dsRNA for all the PP1 isoforms were not detected by RT-PCR (Figure 3.5C).

Taken together, our results suggest a relevant role for Pp1-87B in Lgl cortical localization independently on the polarization status of the cell, acting redundantly and/or synergistically with other PP1 isoforms.

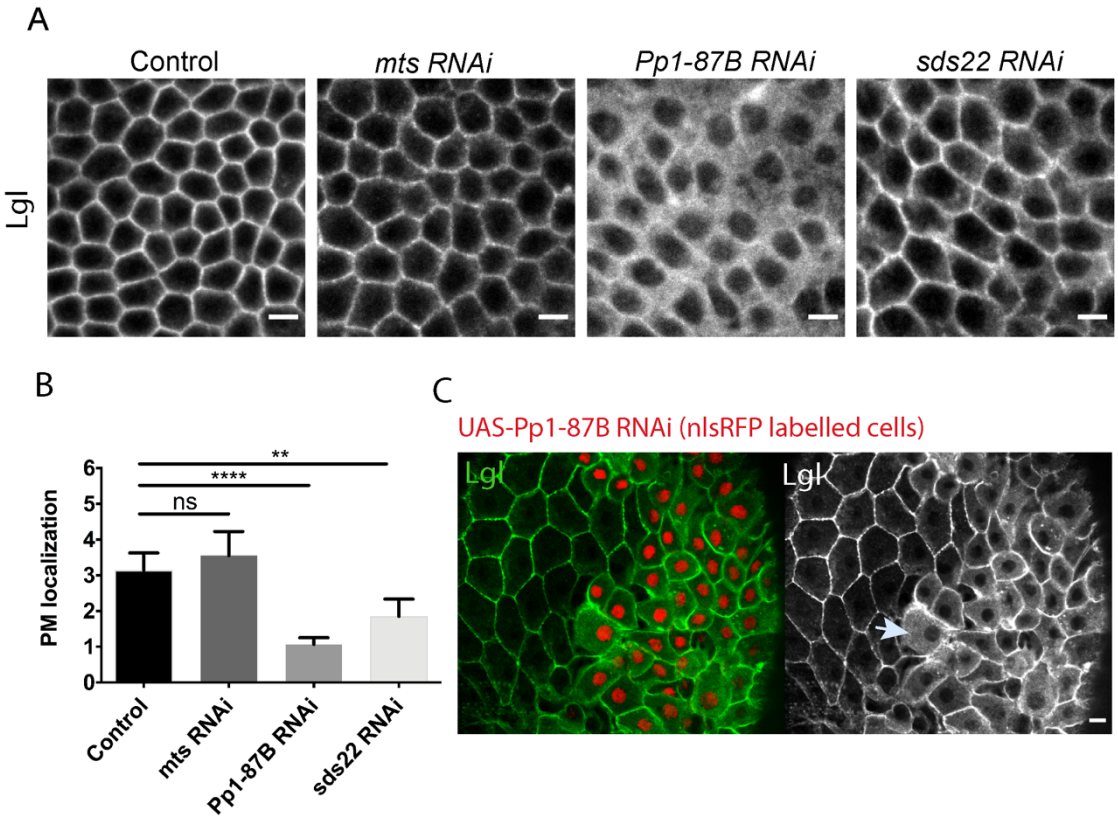

Figure 3.4: Pp1-87B and Sds22 are required for proper Lgl cortical localization in the follicular epithelium. A) Immunofluorescence images to detect endogenous Lgl show that Pp1-87B depletion induces Lgl mislocalization in the cytoplasm. Mild cytoplasmic localization of Lgl was also observed when Sds22 is depleted. Scale bars: 5 μm. B) Quantification of Lgl signal from the immunofluorescence in A) shows a significant reduction of plasma membrane (PM) localization (ratio cortical/cytoplasm) in cells depleted for Pp1-87B and Sds22 when compared with the control (cells non-expressing RNAi). Mean ± SD (n=5 cells randomly choosed from the same egg chamber). Statistical analysis was performed using ordinary one-way ANOVA (****p<0.0001; **p= 0.0033; ns-not significant), since data in each condition assume a Gaussian distribution and that SD for each group of data are identical (using the Bartlett's test). C) Clones generated using the Flp-FRT system combined with the Gal80 inhibitor over the GAL4-UAS system used for RNAi depletion of Pp1-87B. Cells labeled with nuclear localization of a red fluorescent protein (nlsRFP) are expressing Pp1-87B RNAi and induce a strong cytoplasmic accumulation of endogenous Lgl (light blue arrow). Scale bar: 10 μm.

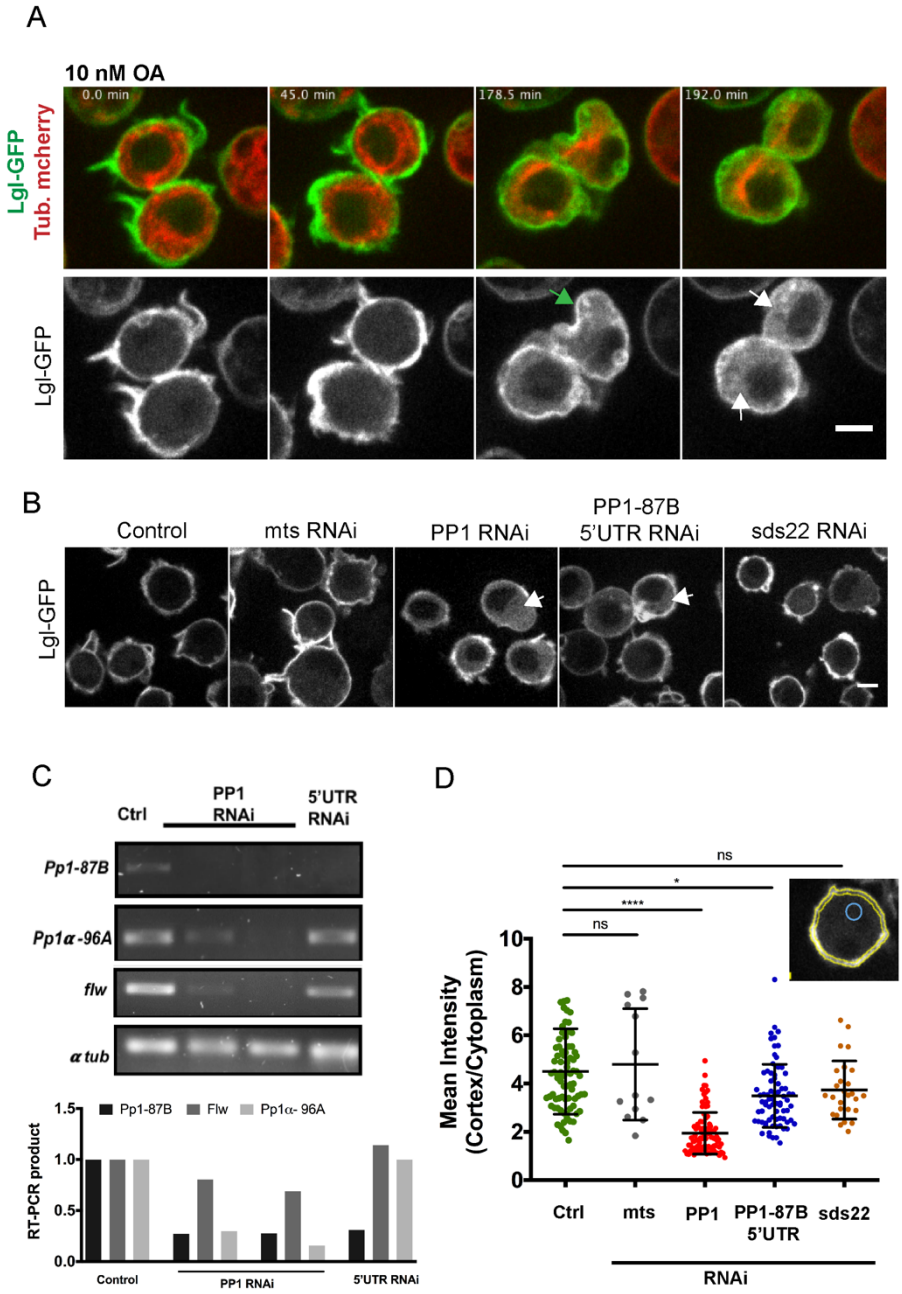

Figure 3.5: PP1 regulates Lgl cortical localization in S2 cells. A) S2 cells treated with 10 nM of OA, a drug that inhibits the activity of PP1/PP2A phosphatases, show a progressive mislocalization of Lgl-GFP to the cytoplasm (white arrows). The effect of the drug was confirmed by the presence of cortical deformations that are typical of PP1/PP2A inactivation (green arrow). B) Depletion of PP1 and Sds22, but not Mts, induces mislocalization of Lgl-GFP in the cytoplasm (white arrows). C) The RT-PCR confirms the depletion of Pp1-87B and reveals a partial depletion of flapwing and Pp1α-96A, showing that this dsRNA targets all three major PP1 isoforms. A dsRNA designed for the 5'UTR of Pp1-87B only affects the transcript levels of this isoform. Quantification of band intensity relative to α tub levels and normalized to the control is shown below. D) Quantification of the ratio of the mean fluorescence intensity in the cortex (yellow line in the cell periphery) vs cytoplasm (blue circle) shows that the dsRNA able to target the three main PP1 isoforms induces a stronger

mislocalization of Lgl-GFP in the cytoplasm than a dsRNA targeting specifically Pp1-87B. Depletion of Sds22 induces a mild mislocalization of Lgl in the cytoplasm. Mean ± SD (n=79 for control, n=14 for mts RNAi, n= 94 for PP1 RNAi, n=74 for Pp1-87B RNAi, n= 27 for sds22 RNAi). Statistical analysis was performed using the non-parametric Kruskal-Wallis test (*p=0.0246; ****p<0.0001; ns- not significant), since data from different conditions do not assume a normal distribution (according to Shapiro-Wilk normality test) and SD are different between conditions (using the Bartlett's test). Scale bars: 5 μm

3.3. Pp1-87B is the only PP1 isoform essential for proper Lgl localization in the follicular epithelium

From the last results, we conclude that Pp1-87B, the most abundant PP1 catalytic subunit (Bennett *et al*, 2006) could act redundantly with two other PP1 isoforms, namely flapwing, also known as PP1β9C, and Pp1α-96A. Thus, we addressed if Pp1-87B is the only isoform necessary for proper Lgl localization in the follicular epithelium, or if the other two isoforms could also play an important role. As a first approach, we analyzed the subcellular localization of the different isoforms in the follicular epithelium. Since there are no available *Drosophila* antibodies to detect specifically each PP1 isoform, we decided to induce the expression of different isoforms tagged with an N-terminal HA epitope that allows detection with an anti-HA antibody. Pp1-87B, Pp1α-96A and flapwing were detected in the cytoplasm of follicular epithelium cells from early egg chamber stages (Figure 3.6A). However, all the isoforms have a more cortical localization in latter stages of oogenesis than in early stages (Figure 3.6B), which could suggest specific roles in these stages or changes in cortical binding partners. Based on the localization pattern, all isoforms could play a role in Lgl cortical regulation: the cortical localization could reflect an interaction with Lgl with the cortex, whereas the localization in the cytoplasm could prevent Lgl localization in this compartment. However, the subcellular localization may not reflect the active pool that is effectively playing a biological role.

We then removed genetically the contribution of each isoform using RNAi depletion or mutant alleles. Immunofluorescence analysis of the endogenous Lgl localization upon RNAi-mediated depletion of flapwing show that it does not have a major impact on Lgl cortical localization (89% of the egg chambers show a normal cortical localization, as shown in Table 3.2 and Figure 3.7A). Moreover, we found that Lgl remains cortical in follicle cells transheterozyogous for deletion that removes the *pp1α-96A* loci (*Df(3R)Exel7357*) and a null *pp1α-96A*^{2} allele (Table 3.2 and Figure 3.7A).

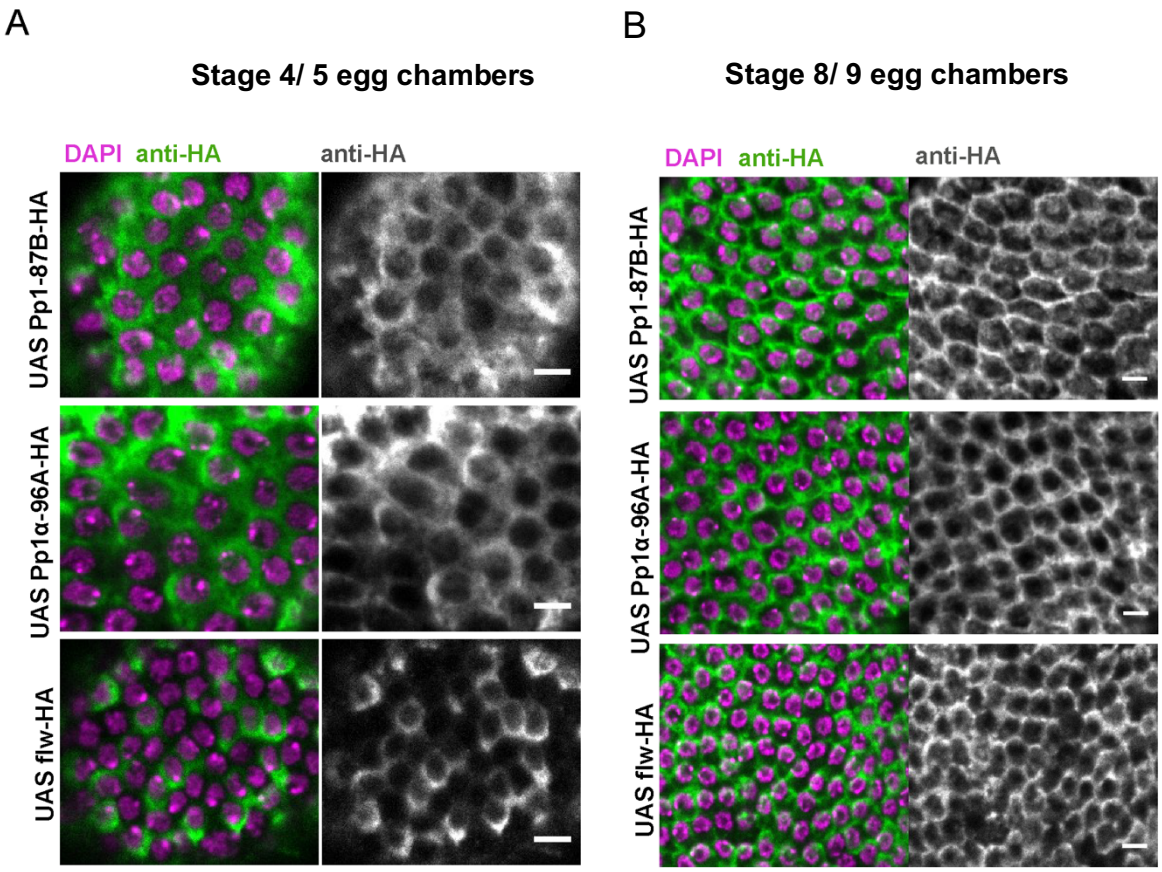

Figure 3.6: Localization pattern of PP1 catalytic isoforms in follicle cells. A, B) *tj* > *Gal4* – induced expression of PP1 isoforms fused to a HA tag was used to detect their localization with an anti-HA antibody. A) In early stages (stages 4/5 of oogenesis), Pp1- 87B-HA, Pp1α-96A-HA and flw-HA were mostly detected in the cytoplasm of follicle cells. B) In later stages (8/9), we found a strong association of all isoforms with the cortex. Scale bars: 5 μm

Additionally, we analyzed two RNAi lines targeting *Pp1α-96A* (#40906 and #42641), but we also did not detect abnormal Lgl-GFP localization (data not shown). To confirm these results, we generated mutant clones for these phosphatases, using null alleles for *flw* and for *Pp1α-96A*. As observed in Figure 3.7B, Lgl localization in these mutant cells is indistinguishable from its localization in wild-type cells, which confirms that these catalytic subunits are dispensable for proper Lgl localization. On the other hand, FRT/FLP-induced *pp1-87B, pp1α-96A* double mutant clones, generated using an amorphic allele for *pp1-87B* and a loss of function allele for *pp1α-96A,* consistently display cytoplasmic localization of endogenous Lgl (Figure 3.7B, white arrow). Our results therefore suggest that Pp1-87B is the only important phosphatase for Lgl cortical localization. The other isoforms could also play a role with Pp1-87B in localizing Lgl, but are not essential on their own.

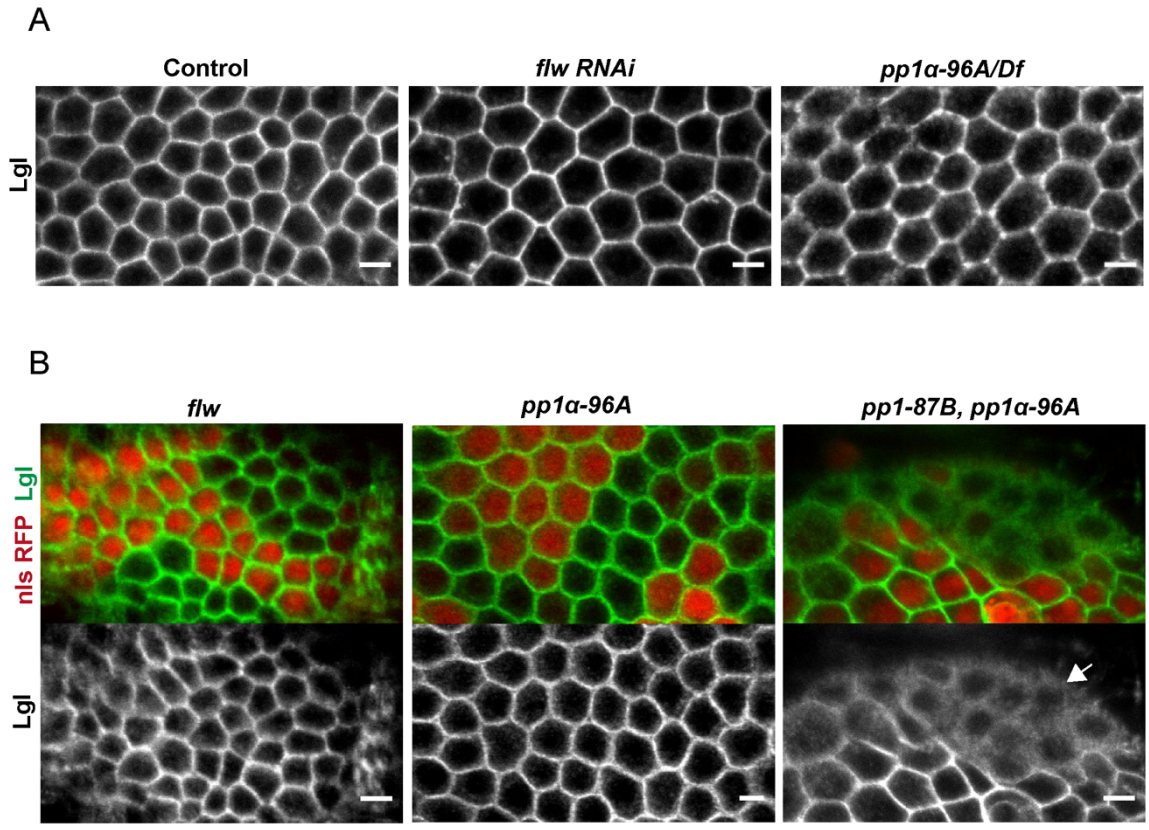

Figure 3.7: Pp1-87B is the only PP1 isoform that is essential for Lgl cortical localization in the follicular epithelium. A) The cortical localization of Lgl in cells depleted for flapwing by RNAi and completely lacking *Pp1α-96A* function is not affected. Loss of *Pp1α-96A* function was obtained in flies carrying *Df(3R)Exel7357* allele which removes the *Pp1α-96A loci* over the null allele for *Pp1α-96A*; B) Lgl staining in egg chambers containing mutant clones generated by Flp-FRT system shows that removing Pp1-87B is necessary for mislocalization of Lgl to the cytoplasm (white arrow). Mutant clones are marked by nlsRFP absence. The null mutant alleles used were flw^{FP41}, $pp1\text{-}87B^{87Bg\text{-}3}$ and $pp1\alpha\text{-}96A^{2}$. Scale bars: 5 μm.

Since PP1 isoforms often share their substrates, we asked why is Pp1-87B the only isoform necessary for proper Lgl cortical localization. Could this reflect a specific function for Pp1-87B or is it rather a consequence of being the most abundant PP1c isozyme? To address this issue, we analyzed the ability of human PPP1cc (catalytic subunit gamma) to rescue the Lgl cytoplasmic localization induced by Pp1-87B depletion. Disruption of Lgl localization due to Pp1-87B depletion (100% of egg chambers display cytoplasmic localization of Lgl, n=40) was significantly rescued by overexpressing PPP1cc (12% of egg chambers displaying cytoplasmic localization of Lgl, n= 34), whose closest orthologue is PP1-96A (based in BLAST: Basic Local Alignment Search Tool) (Figure 3.8A and Table 3.2). Beyond the rescue of Lgl cortical localization, overexpression of PPP1cc also induced a total rescue of the highly penetrant multilayering phenotype (Figure 3.8A, yellow arrow) associated with depletion of Pp1-87B (present in 98% of the egg chambers analyzed, as indicated in Table 3.2). These results therefore suggest that PP1 has global ability to promote Lgl cortical localization, since overexpression of a human orthologue of Pp1α-96A rescues the phenotype. To further confirm that Lgl cortical regulation depends on PP1 phosphatases, we expressed a global PP1 inhibitor, NiPp1 (Bennett *et al*., 2003). Consistent with previous results, overexpression of NiPp1 strongly disrupts Lgl cortical localization (Figure 3.8B) and induces multilayering of the follicular epithelium (Figure 3.8B, yellow arrow). Taken together, our results suggest that Lgl cortical localization is regulated by PP1 activity, and Pp1-87B is likely to be essential due to its major abundance compared with other isoforms. In fact, PP1 catalytic subunits have been shown to have highly overlapping roles (Kirchner *et al*., 2007).

3.4. PP1 dephosphorylates Lgl in aPKC/Aurora A phosphorylation sites

Our previous data suggest that PP1 promotes Lgl cortical localization, but it remains unknown whether this role is related to its ability to dephosphorylate Lgl or to another unrelated event. This question is particularly relevant in the follicular epithelia, where PP1 depletion could also affect other components of the polarity machinery and induce Lgl mislocalization. For instance, sds22 was reported to have an important role in the maintenance of epithelial architecture in *Drosophila* imaginal discs and follicular epithelia (Grusche *et al*., 2009) and was found to interact genetically with Bazooka to regulate epithelial structure in the embryo (Shao *et al*., 2010).

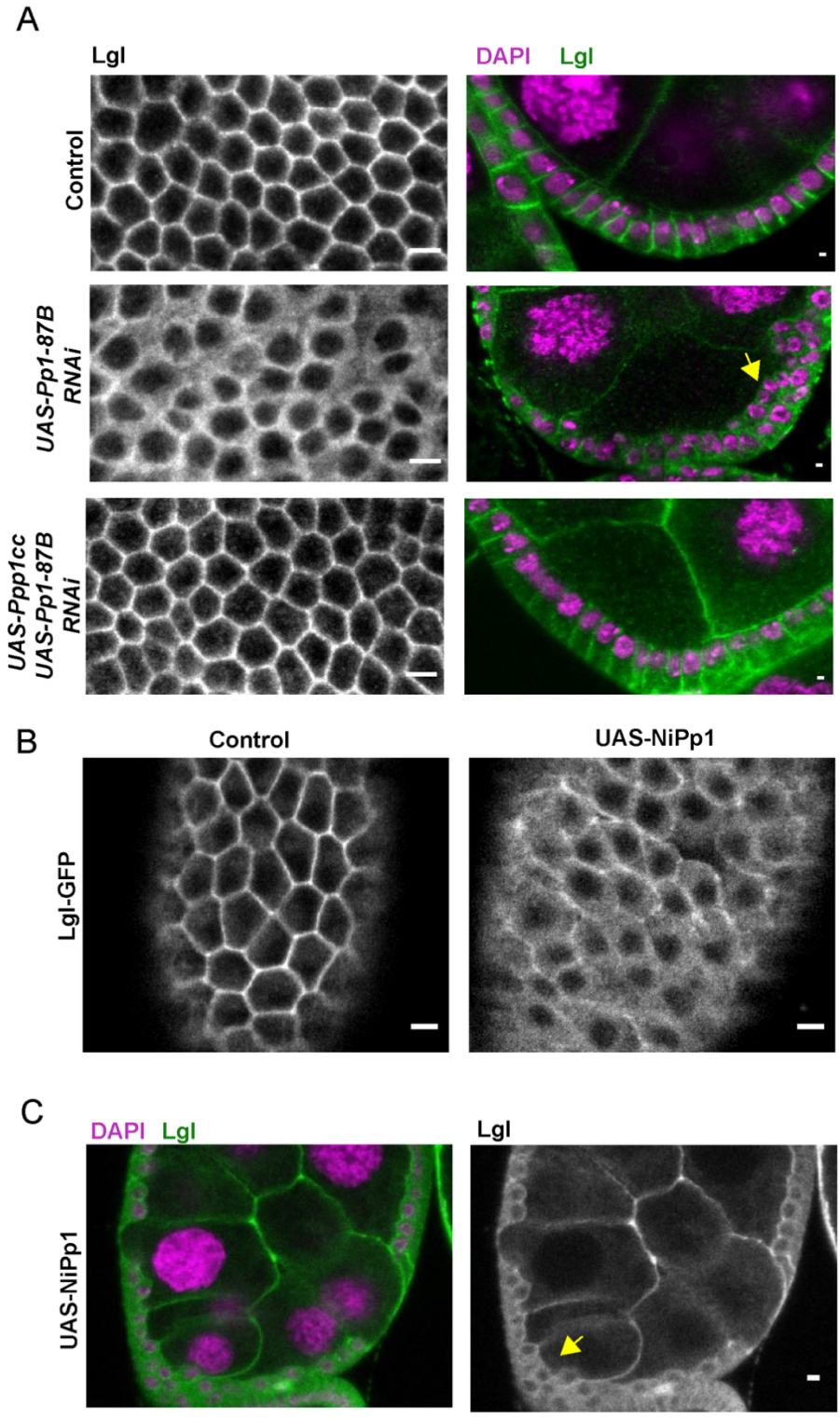

Figure 3.8: General PP1 activity regulates Lgl cortical localization. A) Overexpression of the human PPP1cc using *tj>Gal4* driver is able to rescue Lgl cytoplasmic localization and multilayering phenotypes (yellow arrow) associated with *Pp1-87B RNAi* depletion. B) Overexpression of the general inhibitor of PP1 function, NiPp1, using *tj>Gal4* driver (2 days at 29ºC) induces cytoplasmic localization of Lgl and C) multilayering (yellow arrow). Scale bars: 10 μm

Table 3.2: Quantification of epithelial architecture and Lgl localization upon genetic inactivation of protein phosphatase function. Depletion experiments were performed using the following conditions: *Mts RNAi* - 2 days at 29ºC; *Sds22 RNAi* – 1 day at 29ºC; *Flw RNAi* – 2 days at 29ºC. Rescue experiment (Figure 3.8A) was performed at 29º C for 1 day. Stages 4 to 9 were used for quantifications.

Figure	Genotype	Number of egg chambers	% Egg chambers with multilayering	% Egg chambers with WT localization of Lgl	N experiments
Fig. 3.4	*TJ-GAL4/+; UAS – Mts RNAi/+*	40	0	81	4
Fig. 3.4	*TJ-Gal4/UAS - Sds22 RNAi; +/+*	91	50	52	2
Fig. 3.7	*TJ-GAL4/+/+; UAS - Flw RNAi/+*	64	0	89	2
Fig. 3.7	+/+; *Df(3R)Exel7357/Pp1-87B^{87Bg-3} e^{1} Pp1α-96A^{2}*	70	1.4	97	2
Fig. 3.8	*TJ-GAL4/+;UAS - Pp1-87B RNAi/+*	40	98	0	4
Fig. 3.8	*TJ-GAL4/UAS - hPPP1CC.Z; UAS - Pp1-87B RNAi/+*	34	0	88	2

To better understand the role of PP1 in Lgl localization, we have further characterized the PP1 RNAi phenotype, focusing on the localization of some polarity-related proteins. We firstly analyzed the localization of α-spectrin, a cytoskeleton protein important for monolayer and cell shape maintenance in the follicular epithelium (Ng *et al*., 2016). In control cells, α-spectrin is co-localized in the basolateral cortex with Lgl (Figure 3.9), also extending into the subapical region (Figure 3.9**,** sagittal section). In a Pp1-87B depleted tissue, we observed an effect in Lgl cortical localization, as expected, but not in α-spectrin, which remains localized at the cortex (Figure 3.9).

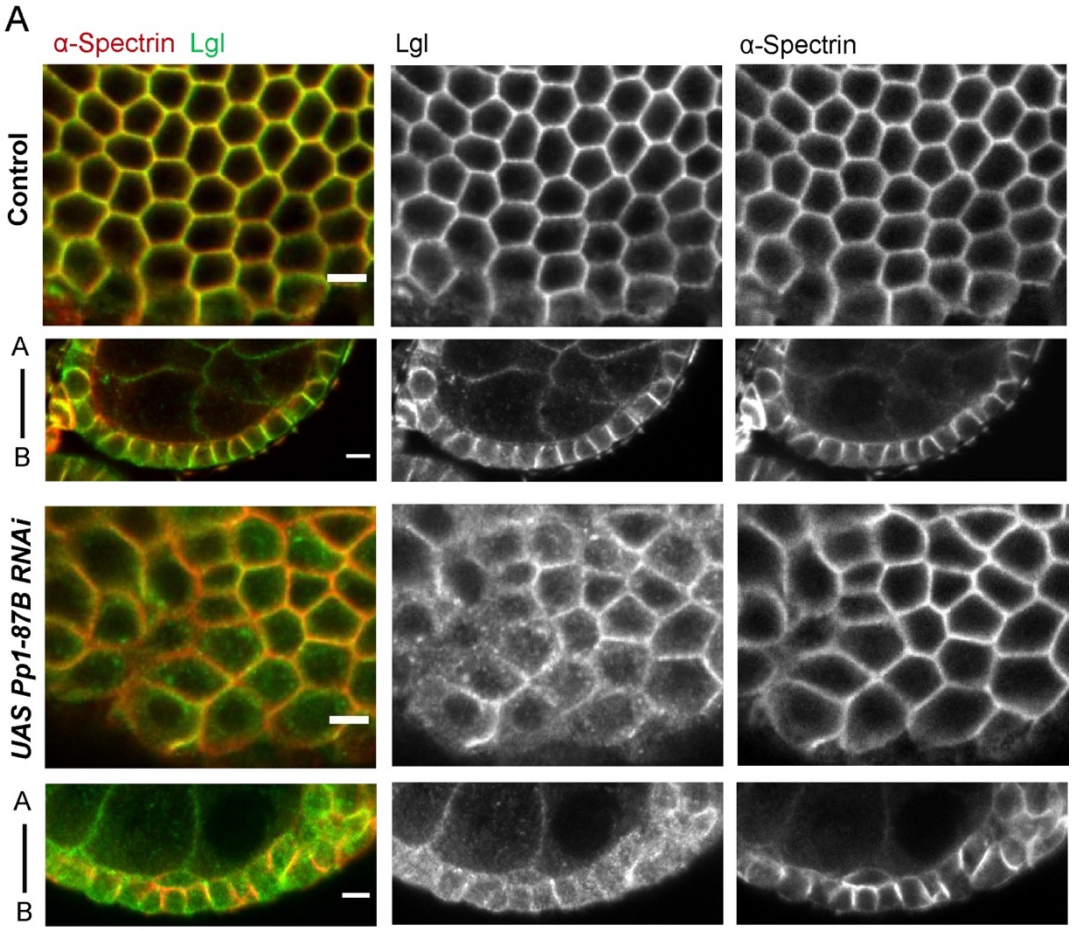

Figure 3.9: α-spectrin remains cortical upon depletion of Pp1-87B. Immunofluorescence of *Drosophila* ovaries showing the localization of endogenous α-spectrin and Lgl in a surface and midsagittal view (AB) in control and follicle cells expressing Pp1-87B RNAi. Scale bars: 5 μm

We also analyzed the effect of PP1 in the localization of the two other basolateral proteins, Dlg and Scrib, which act together with Lgl to regulate cell polarity (Bilder *et al*., 2000). Using endogenous lines tagged with GFP, we found that although a large pool of these proteins remains associated with the cortex, there is mislocalization of Dlg-GFP to the cytoplasm in Pp1-87B depleted cells (Figure 3.10A). The finding that Dlg is also mislocalized in the cytoplasm raised the possibility that Lgl mislocalization could result from the loss of Dlg binding in a context of PP1 depletion, since it was reported that Dlg and Lgl interact *in vitro* (Zhu *et al*., 2014). However, simultaneous analysis of Lgl and Dlg localization in Pp1-87B RNAi shows that all Lgl becomes cytoplasmic when there is only minor mislocalization of Dlg (Figure 3.10B). Due to the importance of Lgl in antagonizing apical determinants, we examined the localization of the apical protein aPKC when PP1 is downregulated. We found that Pp1-87B depletion, associated with multilayering and invasion of epithelial cells in

between the germline, also disrupts the apical localization of aPKC-GFP (Figure 3.11A, indicated by white arrows in the separated aPKC channel). This loss of wild-type localization of aPKC is not only observed in multilayered parts of the tissue but also in monolayered ones (Figure 3.11A, yellow arrow), suggesting that aPKC depolarization is not a secondary consequence of the multilayering. Moreover, the phenotype associated with PP1 depletion, such as multilayering and invasion, resembles the one found in loss of Lgl function (Bilder *et al*., 2000). Although we cannot exclude the hypothesis that this phenotype could result from the pleiotropic effects of PP1, we raised the possibility that aPKC mislocalization might reflect the loss of Lgl in the cortex, with a consequent loss of cell polarity and multilayering.

To further address if the phenotype of PP1 RNAi is related with its ability to balance the antagonistic interaction between Lgl and aPKC in the cortex, we manipulated the levels of aPKC by removing or adding a copy of this gene in flies. We found that loss of one copy of aPKC strongly rescues the multilayering phenotype associated with Pp1-87B RNAi (a rescue of about 58%). On the other hand, adding an extra copy of aPKC induces an even more penetrant and aggressive multilayering phenotype (100% of the egg chambers with multilayering, contrasting with 94% in RNAi for PP1) (Figure 3.11B**).** We also performed an additional experiment where we expressed Lgl-GFP in a Pp1-87B depleted background. We found that in this context Lgl-GFP was able to induce a rescue of the multilayering in about 20% of the egg chambers (Figure 3.11C). Our results therefore suggest that the multilayering phenotype of PP1 depletion is at least partially related with its ability to promote Lgl cortical localization, which is necessary to repress aPKC activity.

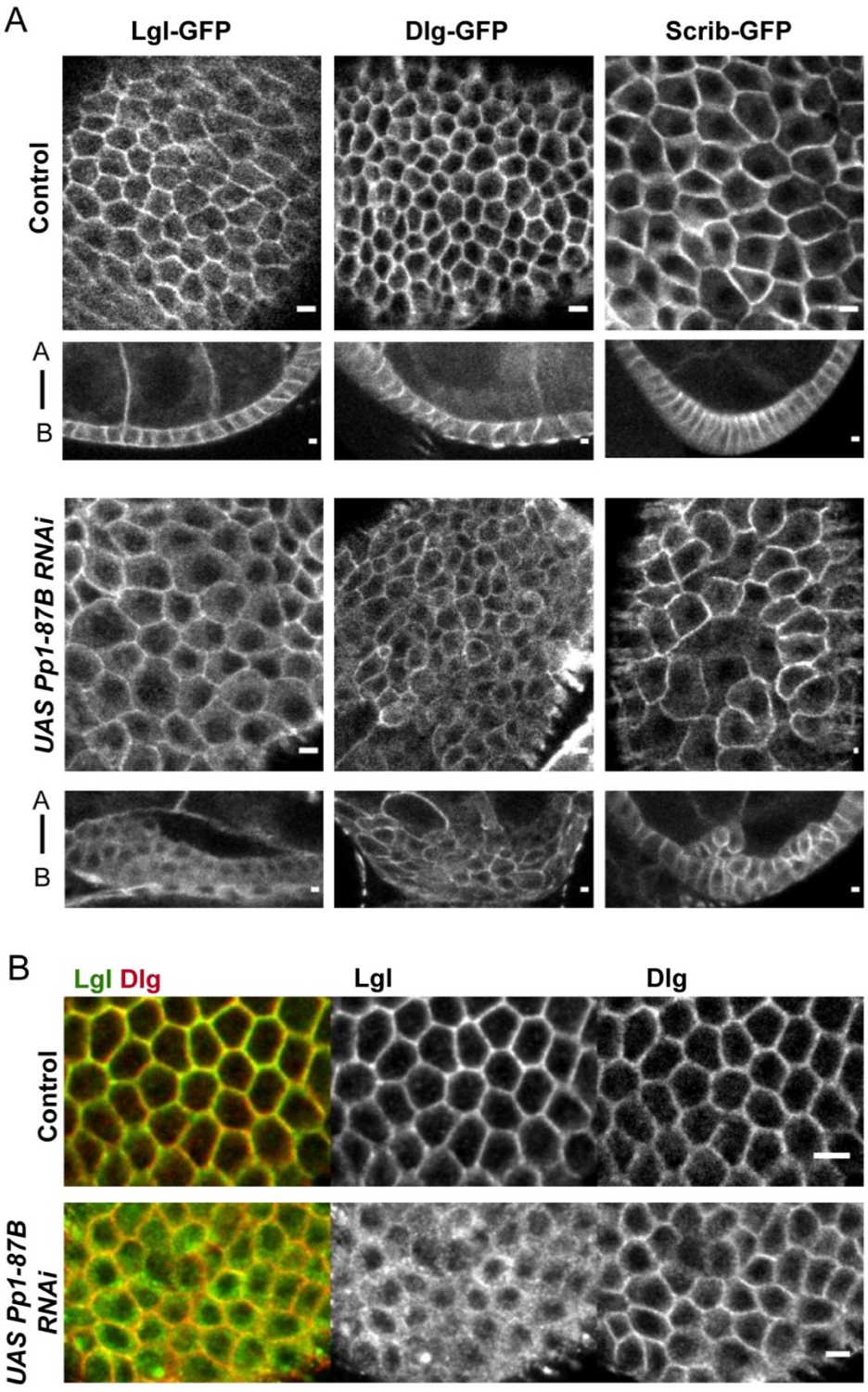

Figure 3.10: PP1 is partially required for the cortical localization of Dlg. A) Depletion of Pp1-87B by UAS-RNAi using *tj>Gal4* driver (for 3 days at 29ºC) induces partial displacement of Dlg-GFP (expressed at endogenous levels) to the cytoplasm; B) Follicular epithelia co-stained for Lgl (green) and Dlg (red) shows that Pp1-87B depletion affects more strongly Lgl than Dlg. Scale bars: 5 μm

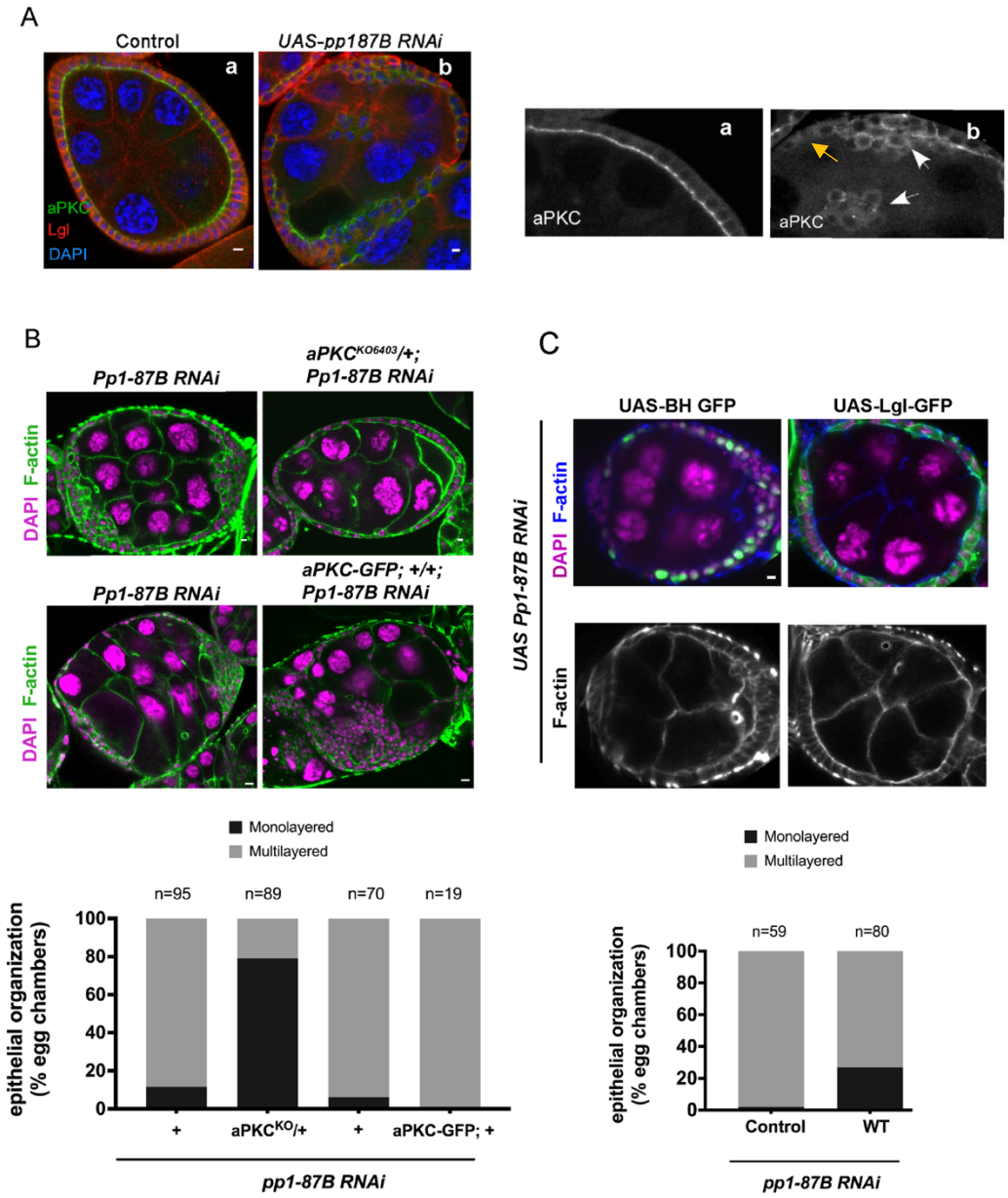

Figure 3.11: PP1 activity balances aPKC function in the follicular epithelium. A) Pp1-87B RNAi induces multilayering and invasion of epithelial cells in-between the germline (white arrows), resulting in aPKC depolarization even in cells that remain in a monolayered tissue (yellow arrow in the separate channel for aPKC). B) Heterozygosity for the *aPKC*^{K06403} null allele strongly suppresses the multilayering phenotype observed in Pp1-87B RNAi, whereas adding an extra copy of aPKC makes the multilayering phenotype of Pp1-87B RNAi even more severe. The plot below represents the percentage of egg chambers with multilayering epithelium (from stage 4 to stage 8). In *tj-Gal4/+; UAS Pp1-87B RNAi/+*, about 88% of egg chambers have multilayering, being reduced for about 30% when aPKC function is reduced by removing a copy of aPKC *in tj-Gal4/aPKC*^{k06403}*;UAS-Pp1-87B RNAi/+* (results obtained from 4 independent experiments, expression at 29ºC for 3 days). When adding an extra copy of aPKC we found that all the egg chambers analyzed displayed a more aggressive multilayering phenotype (from 5 independent experiments). C) Expression of the wild-type form of Lgl rescues the multilayering phenotype observed by Pp1-87B RNAi depletion in about 20%, as indicated in the graph (results from 1 experiment, 2 days at 29ºC, from stage 4 to stage 8). *tj-Gal4/UAS BH-GFP*; *UAS-Pp1-87B RNAi/+* was used as a control for *tj-Gal4/UAS Lgl-GFP*; *UAS-Pp1-87B RNAi/+*. Scale bars: 5 μm

As Lgl cortical localization is disrupted by phosphorylation, we tested whether Lgl cytoplasmic localization in PP1 depleted cells is due to accumulation of Lgl phosphorylated by aPKC. Since Lgl cytoplasmic localization is reproduced in Pp1-87B S2 cells, we co-depleted aPKC and PP1 by RNAi to test its impact on Lgl cortical localization. aPKC depletion was validated by western blot and the PP1 depletion by RT-PCR (Figure 3.12B). aPKC co-depletion rescues the cortical localization of Lgl, as observed in Figure 3.12A and C. We also performed a similar experiment in the follicular epithelium. Co-depletion of these two proteins was however highly harmful for follicular epithelial cells, as suggested by the severe loss of follicular epithelium (data not shown). Nevertheless, we found a relevant rescue of Lgl cortical localization (*tj-Gal4/RNAi PP1*; *UAS-MyrGFP*: about 88% of egg chambers with Lgl in the cytoplasm; *tj-Gal4/RNAi PP1*; *aPKC RNAi/+*: about 15% of egg chambers with Lgl in the cytoplasm) (Figure 3.12 D and F). Specific depletion of aPKC in the follicular epithelium was also confirmed by immunofluorescence, which shows that it is absent in the apical side of epithelial cells but visible in the oocyte (Figure 3.12E). To further confirm these results, we analyzed simultaneously how PP1 depletion affects the localization of Lgl and an unphosphorylatable form of Lgl, Lgl^{3A}, in which the three serine residues phosphorylated by aPKC and AurA were replaced by alanines (Betschinger *et al*., 2003; Carvalho *et al*., 2015; Bell *et al*., 2015). We found that PP1 depletion is able to delocalize Lgl but not Lgl^{3A}, both in follicular epithelia and in S2 cells (Figure 3.12G), suggesting that Lgl mislocalization in a PP1 depletion context is induced by hyperphosphorylation on the aPKC/Aurora A phosphorylation sites.

To confirm that PP1 acts in the aPKC/AurA phosphorylation sites of Lgl, we did an *in vitro* phosphatase assay using as substrate Lgl-GFP immunoprecipitated from ovaries and phosphorylated *in vitro* by Aurora A. Using a phosphospecific antibody for serine 656, we found that recombinant PP1 dephosphorylates Lgl *in vitro* in a concentration dependent manner (Figure 3.13A). Moreover, the activity of PP1 is specific towards Lgl, since λ phosphatase fails to dephosphorylate Lgl as efficiently as PP1 (Figure 3.13B) (Moreira *et al*., 2019). Thus, our results indicate that Lgl is dephosphorylated by PP1 in the same serines phosphorylated by aPKC/AurA, and so PP1 promotes Lgl localization in the cortex by reverting Lgl phosphorylation.

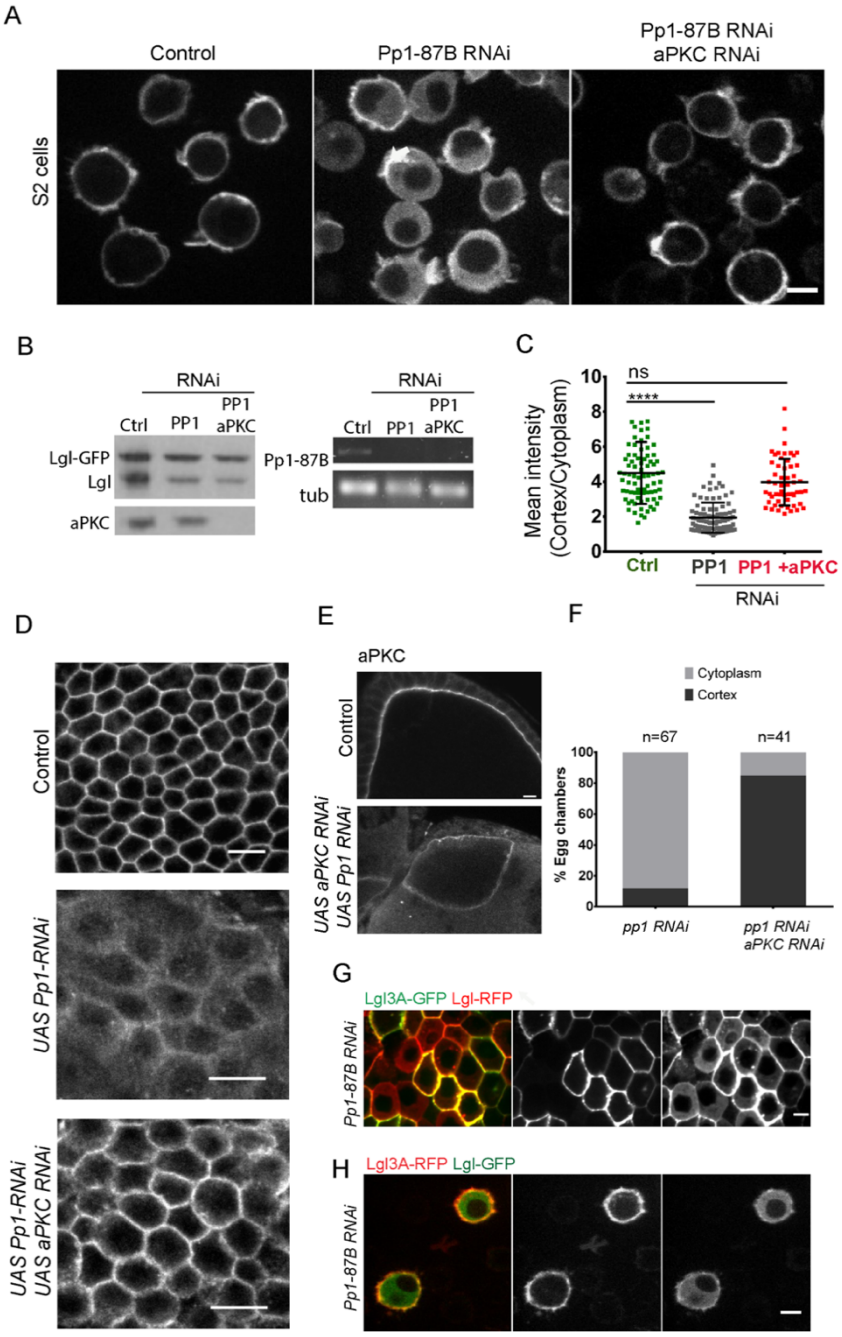

Figure 3.12: PP1 controls Lgl cortical localization by antagonizing phosphorylation on aPKC/AurA phosphorylation sites. A) Co-depletion of aPKC with PP1 rescues Lgl cortical localization; B) WB and RT-PCR showing the efficiency of aPKC (in the WB, left) and PP1 (in RT-PCR, right) depletion. C) Quantification of the cortex/cytoplasm intensity ratio for different conditions. Mean ± SD (control: n=79; PP1 RNAi: n=94; PP1 RNAi + aPKC RNAi: n=74) (Moreira *et al*., 2019). The p value was calculated with one-way ANOVA (****p < 0.0001). D), F) Co-depletion of aPKC rescues Lgl cortical localization in PP1 depleted follicle cells, as shown by images with Lgl staining and graph F) for quantifications of % of egg chambers with cortical Lgl in 3 independent experiments. Experiments were performed at 29ºC (for 2 days); E) Staining for aPKC to confirm protein depletion. G) H) Depletion of PP1, both in the follicular epithelium (G) and in S2 cells (H), induce a cytoplasmic localization of Lgl-GFP/Lgl-RFP but does not interfere with the localization of an aPKC unphosphorylatable Lgl version (Lgl^{3A}-GFP/Lgl^{3A}-RFP) (Moreira *et al*., 2019). Scale bars: 5 μm (A, G); 10 μm (D, E).

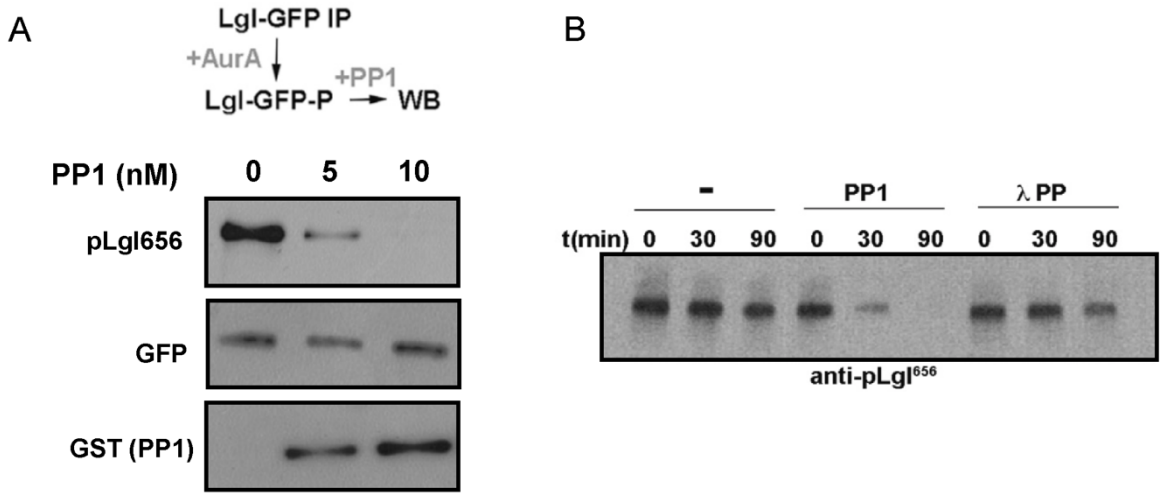

Figure 3.13: PP1 antagonizes aPKC/AurA phosphorylation by dephosphorylating Lgl. A) Western blot (WB) using a phosphospecific antibody for Ser656 shows that Lgl is dephosphorylated by PP1 in a concentration-dependent manner. After immunoprecipitation of Lgl-GFP and saturation of the phosphorylation state by AurA, we performed dephosphorylation assays using GST-PP1γ (Moreira *et al*., 2019). B) PP1 dephosphorylates MBP- Lgl previously phosphorylated by AurA in a time-dependent manner. λ phosphatase used at the same units as PP1 (1U, according to their activity towards a non-specific substrate (p-nitrophenyl phosphate)) is unable to dephosphorylate Lgl as efficiently (assay performed by Guilherme Ventura, one of the authors of the paper Moreira *et al*., 2019).

3.5. Lgl contains an evolutionarily conserved PP1 docking site

Our results support the hypothesis that PP1 dephosphorylates Lgl. To access the functional relevance of this dephosphorylation *in vivo* we designed a strategy to interfere with the ability of PP1 to dephosphorylate Lgl. PP1 associates with its target proteins by docking site motifs, such as the RVxF, which allows binding to the hydrophobic pocket of PP1 (Wakula *et al*., 2003). We analyzed Lgl amino acid sequence to search for PP1 docking site motifs and we found three that match the consensus [KR] $[X]_{0-1}$ [VI] {P} [FW] (where $[X]_{0-1}$ may be residues any residue and {P} any residue except Pro). The localization of each motif is illustrated in Figure 3.14A, together with a prediction of the domains where they may be localized based on the crystallographic structure of *S. cerevisae* Sro7 (Figure 3.14A). Then we analyzed the conservation of each motif in *Drosophila* and we found that two of them (named by 1 or 3) are conserved in all the sequenced *Drosophila* species. To predict the functional relevance of these motifs, we analyzed their conservation in other metazoans.

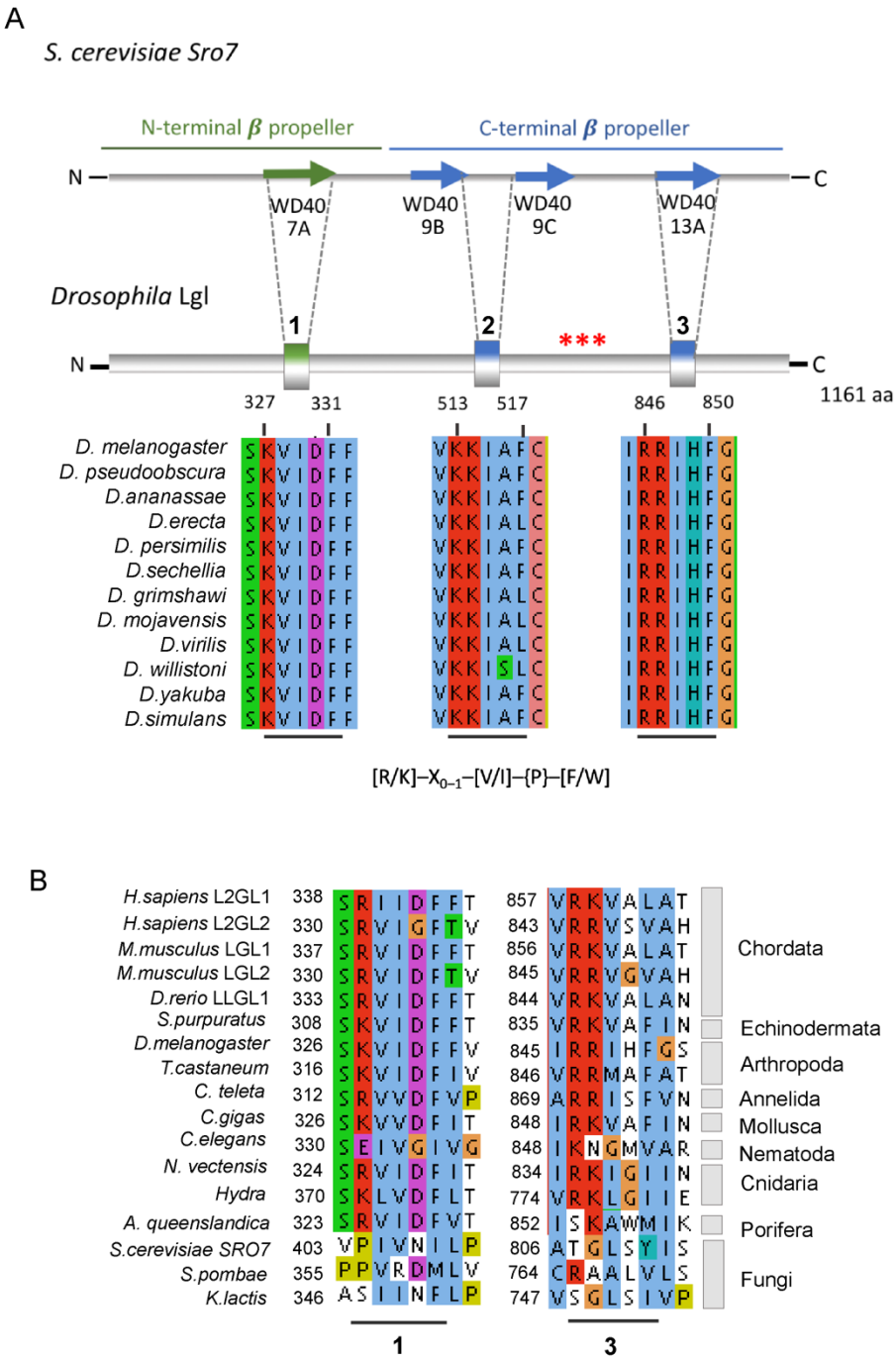

Figure 3.14: *Drosophila melanogaster* has two putative RVxF docking site motifs conserved in *Drosophila*, one of which is evolutionarily conserved in Metazoa. A) Localization of the three RVxF motifs found in Lgl and the respective predicted position based in the Sro7 structure. The red asterisks (*) correspond to the approximate localization of the three evolutionarily conserved serines phosphorylated by aPKC/AurA. The alignment for all the sequenced *Drosophila* species is shown. B) One of the motifs (the more N-terminal one) is evolutionarily conserved in sponges and is not conserved in Fungi.

Our alignments show that one of these motifs, the number 1, localized in the N-terminal β propeller of Lgl, is conserved in Metazoans, including in *H. sapiens* (Figure 3.14B). Interestingly, this motif is not present in Sro7, the closest Lgl orthologue in yeast, and also in other fungi species (Figure 3.14B). This suggests that the motif only appeared with the emergence of Metazoa. Curiously, Lgl in yeast, Sro7, also lacks the polybasic domain where the evolutionarily conserved aPKC phosphorylation sites are localized (Hattendorf *et al*, 2007), suggesting that the presence of this docking site motif is linked with the regulation of Lgl phosphorylation. However, further phylogenetic analyses are required to validate this hypothesis.

We disrupted this evolutionarily conserved motif by mutating two essential residues (**K**VID**F** to **A**VID**A**) for the PP1 docking site function (Meiselbach *et al*., 2006) (Figure 3.15A). Remarkably, $Lgl^{KA,FA}$ displays high cytoplasmic localization in comparison to Lgl-GFP. This phenocopies PP1 depletion and is consistently observed from early stages of oogenesis onwards(Figure 3.15A). The cytoplasmic localization of $Lgl^{KA,FA}$-GFP is not related with the amount of protein expressed, as we did not detect differences in signal intensity compared to Lgl-GFP in the same stages, suggesting that protein quantity remains invariable *in vivo* in the developmental stages we usually analyze (stages 7/8) (Figure 3.15B).

The mutation of the docking site motif in $Lgl^{KA,FA}$-GFP should impair PP1 dephosphorylation of Lgl. So, we firstly analysed the phosphorylation status of the protein by western blot using an antibody specific for phosphorylation in serine 656. We found that $Lgl^{KA,FA}$-GFP is more phosphorylated than Lgl-GFP, as observed by the western blot (Figure 3.16A) and the quantifications of the ratio of pLgl/Lgl (Figure 3.16B). Therefore, $Lgl^{KA,FA}$-GFP is hyperphosphorylated in the aPKC or AurA phosphorylation sites, suggesting an inefficient dephosphorylation by PP1. It is worth noting that less protein was consistently detectable in western blots for $Lgl^{KA,FA}$ -GFP (Figure 3.16A). This was surprising because the UAS constructs for the two variants of Lgl are localized in the same genomic region.

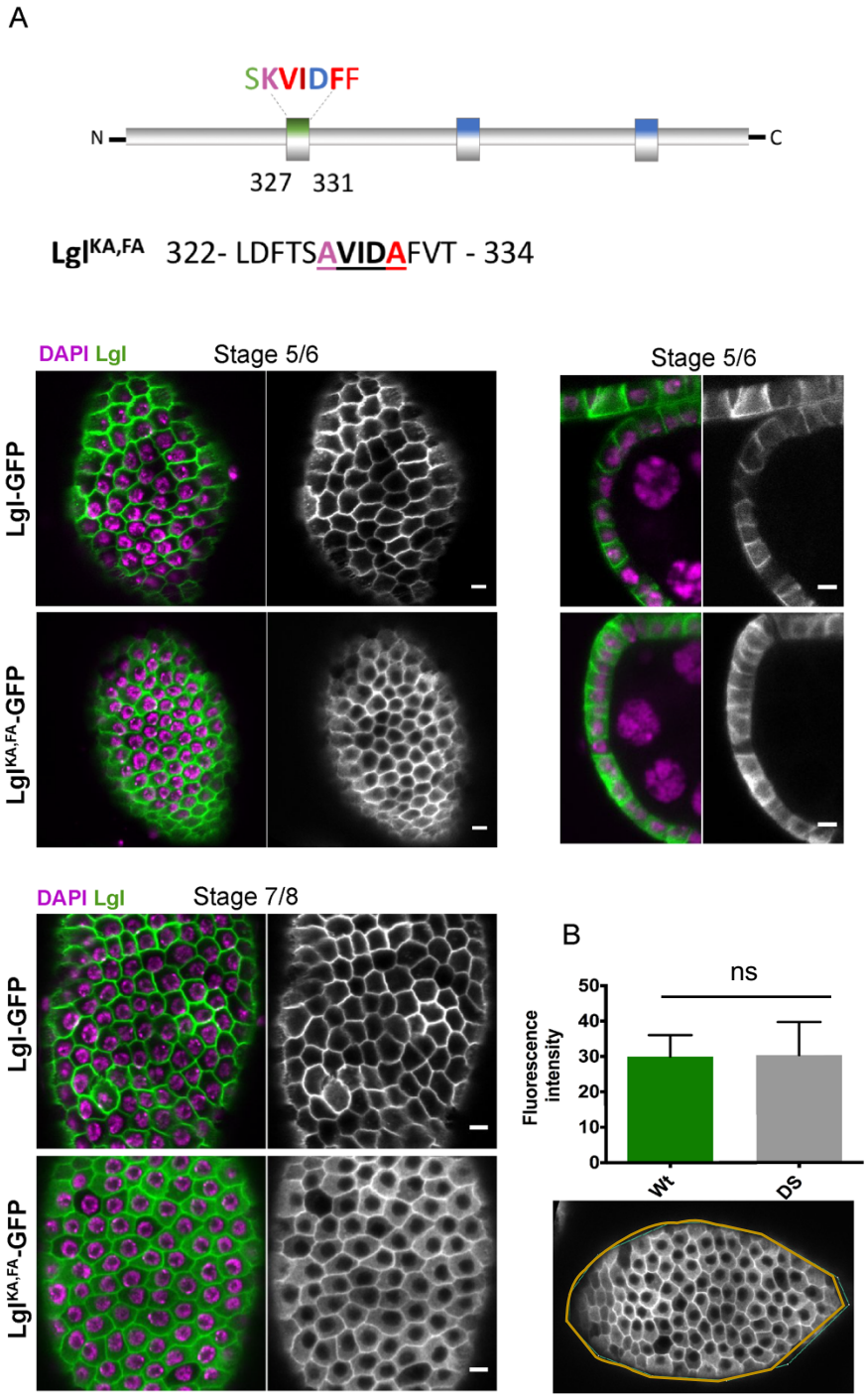

Figure 3.15: Disruption of the conserved PP1 docking leads to cytoplasmic accumulation of Lgl. A) Follicle cells expressing Lgl-GFP or Lgl^{KA,FA}-GFP and stained for DAPI (magenta) at the indicated stages of oogenesis. B) Graph for mean fluorescence intensity of similar staged egg chambers (7/8) expressing Lgl-GFP or Lgl^{KA,FA}-GFP induced at 25ºC (for 2 days) show that there are no significant differences in the levels of both forms during these developmental stages (n=5 egg chambers, mean ± SD). Statistical significance was assayed using an unpaired t test (ns-not significant). Scale bars: 5 μm

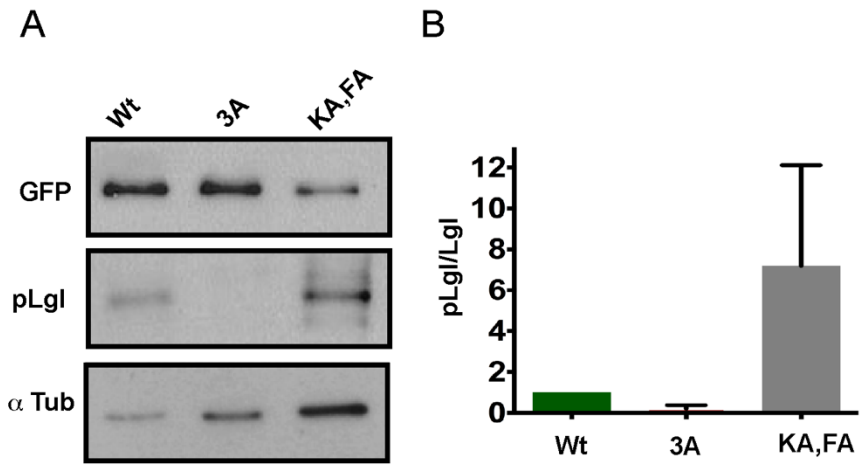

Figure 3.16: Lgl^{KA,FA}-GFP is hyperphosphorylated in *Drosophila* ovaries. A) Western Blot from ovaries expressing Lgl-GFP, Lgl^{3A}-GFP (unphosphorylatable form) and Lgl^{KA,FA}-GFP (docking site mutant form), at 25ºC for 1 day, shows that Lgl^{KA,FA}-GFP is more phosphorylated, as detected by the S656 phosphospecific antibody. Quantification shows the pLgl/Lgl-GFP ratio from three independent experiments and normalized to the WT (mean ± SEM) (Moreira *et al*., 2019).

According to the previous result that Lgl^{KA,FA}-GFP is hyperphosphorylated, we raised the possibility that this is related with the inability of PP1 to properly bind Lgl^{KA,FA}-GFP. To test this hypothesis, we performed an immunoprecipitation assay using ovary extracts to access the ability of Lgl^{KA,FA}-GFP to bind overexpressed Pp1-87B-HA. Contrarily to what expected, we found that Lgl^{KA,FA}-GFP was co-immunoprecipitated with Pp1-87B-HA (Figure 3.17A). On the other hand, an unphosphorylatable form of Lgl, Lgl^{3A}-GFP, can barely bind to PP1, suggesting that phosphorylation of the protein is important for interaction with PP1. We raised the possibility that the other docking site motif evolutionarily conserved in *Drosophila* could account for this result, allowing an interaction between Lgl^{KA,FA}-GFP and PP1. In fact, it was previously shown that secondary PP1 binding sites present in Par-3 might explain the sparse differences observed in the ability of a wild-type and a RVXF mutant version of Par-3 to bind PP1 (Traweger *et al*., 2008). Interestingly, we saw an unexpected increase in the interaction with PP1 in Lgl^{KA,FA}-GFP when compared to Lgl-GFP. We thought that this could be explained by the presence of Lgl^{KA,FA}-GFP in the cytoplasm, allowing a larger pool of this protein to interact with the cytoplasmic pool of Pp1-87B-HA previously shown (Figure 3.6). In order to validate this hypothesis, we performed an experiment where Lgl-GFP mislocalization to the cytoplasm was induced in ovaries treated with ionomycin, which disrupts plasma membrane phosphoinositides (Dong *et al*., 2015). We observed a high

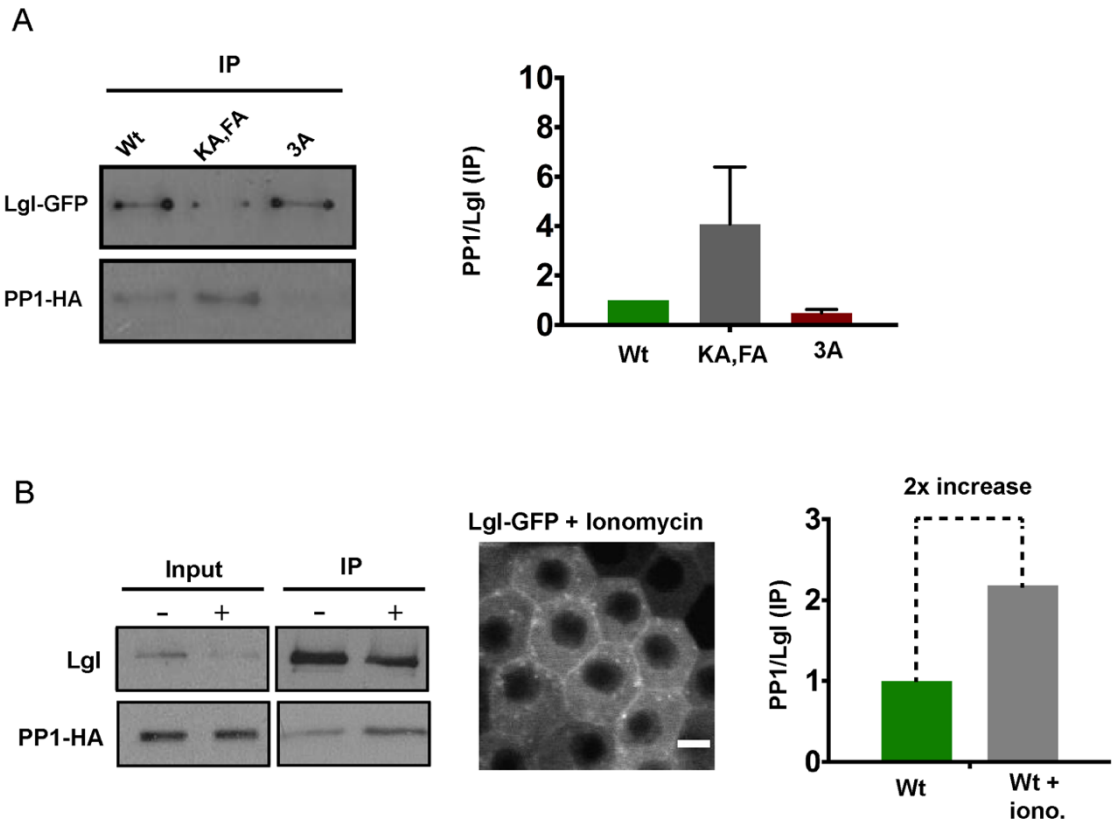

Figure 3.17: PP1 interaction with Lgl is not dependent on the docking site motif. A) Immunoprecipitation (IP) using magnetic beads coupled with a nanobody for GFP reveal that the interaction of PP1 with Lgl does not require the docking motif but is dependent on Lgl phosphorylation. Quantifications obtained from three independent experiments are the ratio PP1/Lgl from the IP (mean ± SEM). B) IP from ovaries extract expressing Lgl-GFP, with or without previous treatment with ionomycin (0.08 μM for 25 min at room temperature) reveal that ionomycin treatment increases the ability of Lgl-GFP to interact with Pp1-87B-HA. Graph represents the quantification of the PP1/Lgl ratio from the IP presented. Scale bar: 5 μm

increase of Lgl-GFP binding to Pp1-87B-HA, which suggests that cytoplasmic localization of Lgl is sufficient to increase the amount of Lgl co-immunoprecipitated with PP1, therefore explaining the unexpected results observed for the $Lgl^{KA,FA}$-GFP (Figure 3.17A). This could also partially explain the inability of Lg^{3A}-GFP to binding PP1, since this unphosphorylatable form has a lower cytoplasmic pool. Curiously, cytoplasmic Lgl induced by treatment with ionomycin is less stable when compared with the Lgl in the control (input of Figure 3.17B). This suggests that mislocalized cytoplasmic Lgl becomes more unstable in ovaries extracts, even in an context where it is not hyperphosphorylated.

To further validate that $Lgl^{KA,FA}$-GFP is cytoplasmic due to hyperphosphorylation, we depleted aPKC by RNAi in the follicular epithelium. Despite the efficiency of the aPKC depletion in the follicular epithelium, $Lgl^{KA,FA}$-GFP remains in the cytoplasm in follicle cells depleted of aPKC (Figure 3.18). This could be attributed to the effect of phosphorylation of Lgl during mitosis by Aurora A, which shares the same phosphorylation sites of aPKC (Carvalho *et al*., 2015), associated to an inefficient PP1 dephosphorylation of $Lgl^{KA,FA}$-GFP. Thus we used a non-proliferative epithelial tissue in the salivary glands to exclude the contribution of Lgl cortical release during mitosis. In these cells, $Lgl^{K327A,F331A}$–GFP was also detected in the cytoplasm, whereas Lgl-GFP was mostly cortical (Figure 3.19). This suggests that Lgl is likely to be under the same phosphoregulation mechanisms in the two systems. RNAi-mediated depletion of aPKC was also efficient in this system, since aPKC cannot be detected in the duct of salivary glands as found in the control (Figure 3.19, non-expressing - yellow arrow). More importantly, aPKC depletion reallocates $Lgl^{K327A,F331A}$–GFP to the cortex of epithelia of salivary glands, indicating that cytoplasmic localization results of Lgl hyperphosphorylation.

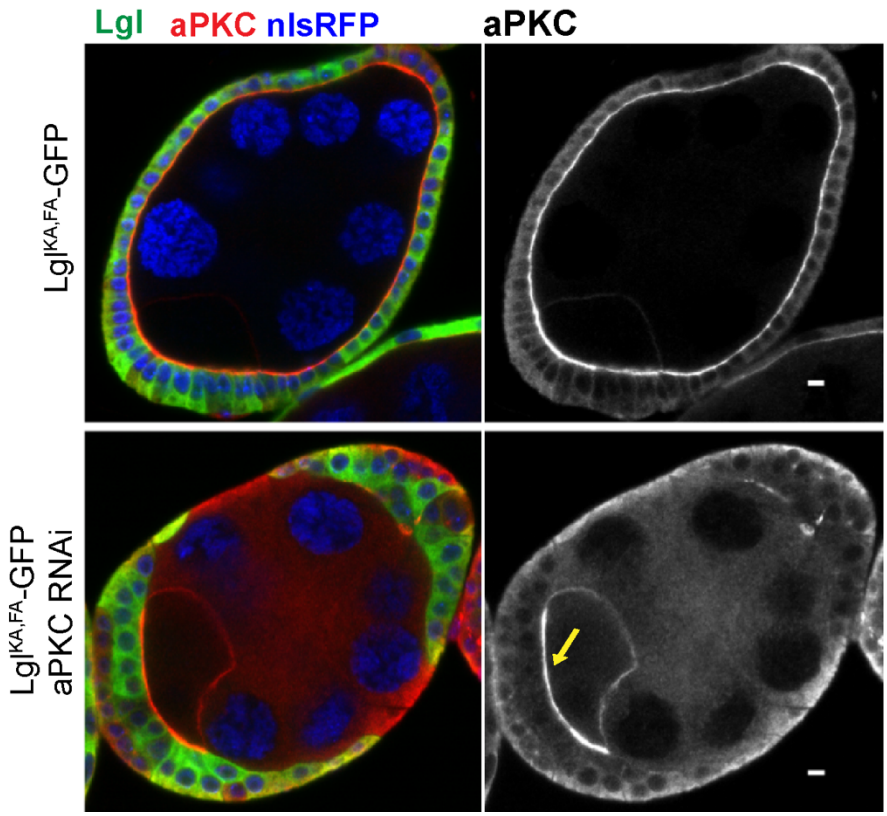

Figure 3.18: Lgl^{KA,FA}-GFP is maintained in the cytoplasm when aPKC is depleted in the follicular epithelium. The efficiency of depletion is confirmed by aPKC staining. Arrow (yellow) shows that aPKC is only observed in the oocyte upon UAS-driven RNAi depletion specifically in follicle cells, confirming also the efficiency of the staining. Scale bars: 5μm

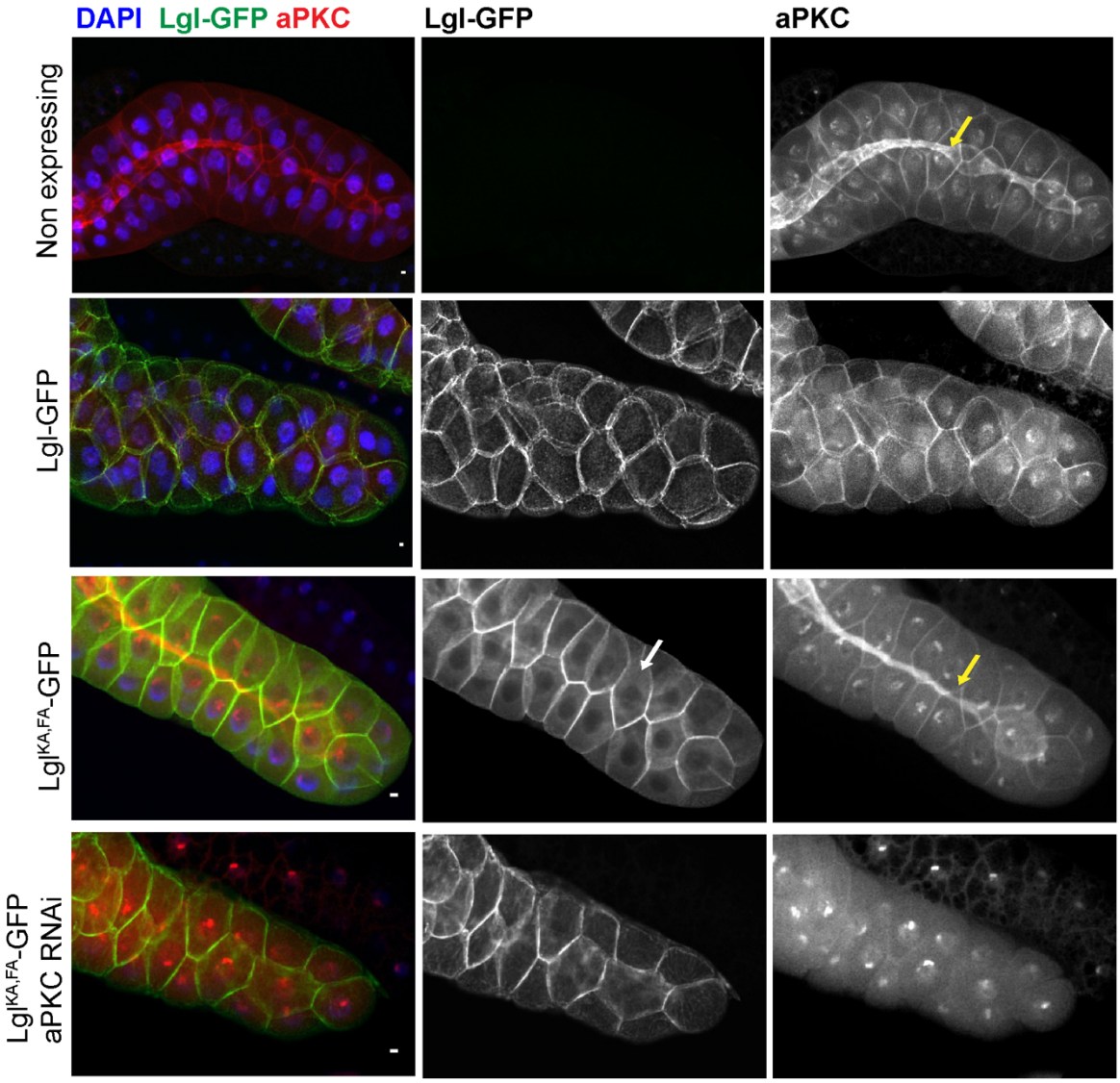

Figure 3.19: Depletion of aPKC promotes cortical localization of Lgl^{KA,FA}-GFP in salivary gland epithelium. UAS-Lgl versions were expressed using *ey*>Gal4 driver. Arrow (white) depict the cytoplasmic localization of Lgl^{KA,FA}-GFP, which is not visible when depleting aPKC. Yellow arrows point out the detection of aPKC in the duct of salivary glands non-expressing or expressing Lgl^{KA,FA}-GFP. Scale bars: 5μm

3.6. Lgl^{KA,FA}-GFP is unable to maintain epithelial organization

Disruption of the PP1 docking site motif of Lgl induces displacement to the cytoplasm, which is dependent on aPKC phosphorylation. This is expected to have strong implications for tissue organization since, as mentioned earlier, Lgl function in cell polarity relies on its ability to be localized at the cortex to antagonize apical polarity complexes. To analyze the ability of the Lgl^{KA,FA}-GFP to support epithelial cell polarity, we induced *lgl* mutant clones and expressed the different forms of Lgl in the follicular epithelium. We found that Lgl^{KA,FA}-GFP is unable to support epithelial monolayer organization (about 80% of the egg chambers have a multilayering epithelium in the mutant, while it is rarely present when expressing the wild-type version, Figure 3.20A and Figure 3.20C). Consistent with a failure of Lgl^{KA,FA}-GFP in supporting cell polarity, we also observed the mislocalization of aPKC and of the adherens junction protein Armadillo, mainly in multilayered tissues but also in some cells still integrated in a monolayer (Figure 3.20B).

Our results suggest that PP1-mediated cortical localization of Lgl is important to sustain apical-basal cell polarity. To understand whether this function is related with the ability to antagonize the apical domain, we performed overexpression-based functional analyses to test the capacity of the two forms of Lgl to interfere with aPKC localization. When we induced positively marked clones expressing the two Lgl versions to compare the localization of aPKC with wild-type cells, we found that Lgl-GFP is able to disrupt aPKC localization (Figure 3.20D, arrows). On the other hand, Lgl^{KA,FA}-GFP overexpression is unable to disrupt aPKC localization to the apical side or cause defects in the follicular epithelium (Figure 3.20D). Curiously, and consistently with these data, we detected aPKC in the duct of Lgl^{KA,FA}-GFP expressing salivary glands, as well as in non-expressing glands, but not in the Lgl-GFP (Figure 3.19). Together, these results suggest that Lgl^{KA,FA}-GFP, contrarily with Lgl-GFP, is not able to antagonize aPKC and sustain cell polarity in the absence of the endogenous Lgl. As an additional experiment, we tested the ability of the two variants of Lgl to interfere with border cell migration. Border cells originate from specialized follicular cells that start to migrate between the nurse cells towards the oocyte, and this migration is essential for female fertility (Duchek, 2001). They are also a very useful model to understand the collective cell migration processes that are associated with cancer invasion and metastasis (Ilina and Friedl, 2009). They can be used to adress the antagonism between aPKC and the two Lgl variants, since aPKC was found to be a key polarity molecule in border cell migration (Wang *et al*., 2018).

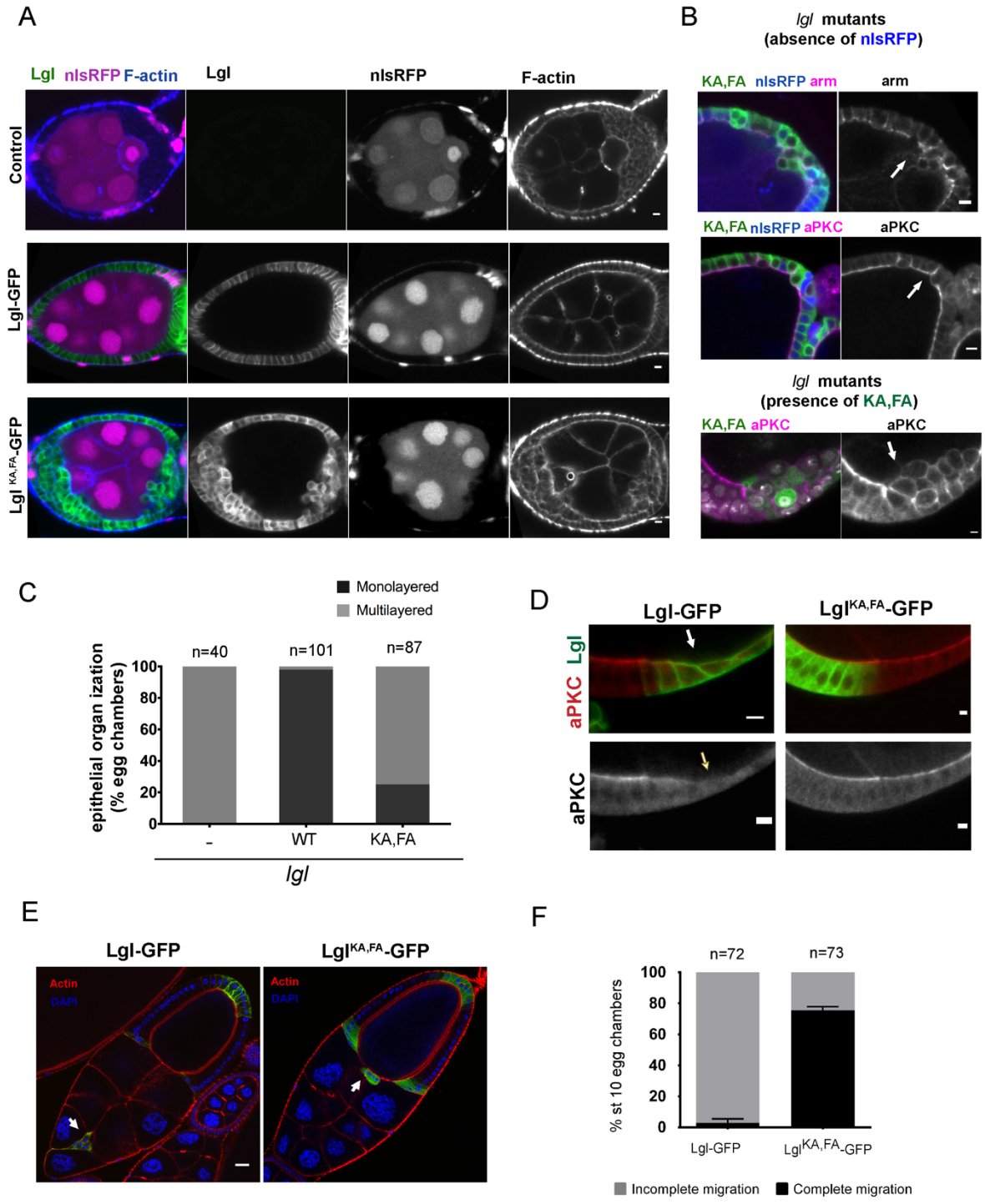

Figure 3.20: Lgl^{KA,FA}-GFP does not support epithelial cell polarity and tissue architecture. A) General expression of Lgl^{KA,FA}-GFP using GR1>Gal4 driver does not rescue the multilayering phenotype observed in *lgl^{27S3}* mutant clones (absence of magenta, nlsRFP), in contrast to Lgl-GFP. Expression was performed at 29ºC, for 1 day. Quantifications in C) show the % of egg chambers with multilayered epithelia (from stage 6 to 8 of oogenesis). The graph includes data from 3 independent experiments, taking only into account mutant clones bigger than ¼ (Moreira *et al.*, 2019). B) Lgl^{KA,FA}-GFP is not able to sustain epithelial cell polarity in *lgl^{27S3}* mutant clones generated by Flp-FRT system marked by the absence of RFP, as indicated by mislocalization of

armadillo and aPKC in mutant clones. The same mislocalization for aPKC is observed in a multilayering tissue of *lgl*^{27S3} mutant follicle cells originated using the Flp-FRT system combined with the ability of Gal80 to inhibit the Gal4 expression in non-expressing cells. Then, positive clones are marked by the positive expression of Lgl^{KA,FA}-GFP (Gal80 absence). D) Strong overexpression of Lgl^{KA,FA}-GFP does not interfere with apical polarization. Positive clones for two Lgl forms using the act-Flp-out strategy shows that strong overexpression of Lgl-GFP disrupts aPKC localization contrarily to Lgl^{KA,FA}-GFP. E) F) Using a *Slbo>GAL4* driver specific for border cells we found that overexpression of Lgl-GFP strongly delays border cell migration (in 97% of the egg chambers, as indicated by the graph in F) while in the Lgl^{KA,FA}-GFP only 25 % fail to migrate (see white arrows indicating the position of border cells). N=3 independent experiments (performed by Margarida Gonçalves, one of the authors of the paper Moreira *et al.*, 2019). Scale bars: 5 μm; 10 μm (in B).

We observed that, when expressing Lgl-GFP in border cells using a specific driver, *slbo>GAL4*, the migration of border cells is delayed, in contrast with overexpression of Lgl^{KA,FA}-GFP (Figure 3.20 E,F). Taken together, our results suggest that PP1-mediated dephosphorylation of Lgl relies on an evolutionarily conserved PP1 docking site which promotes Lgl localization in the cortex, where it antagonizes apical proteins to maintain epithelial architecture (Figure 3.21).

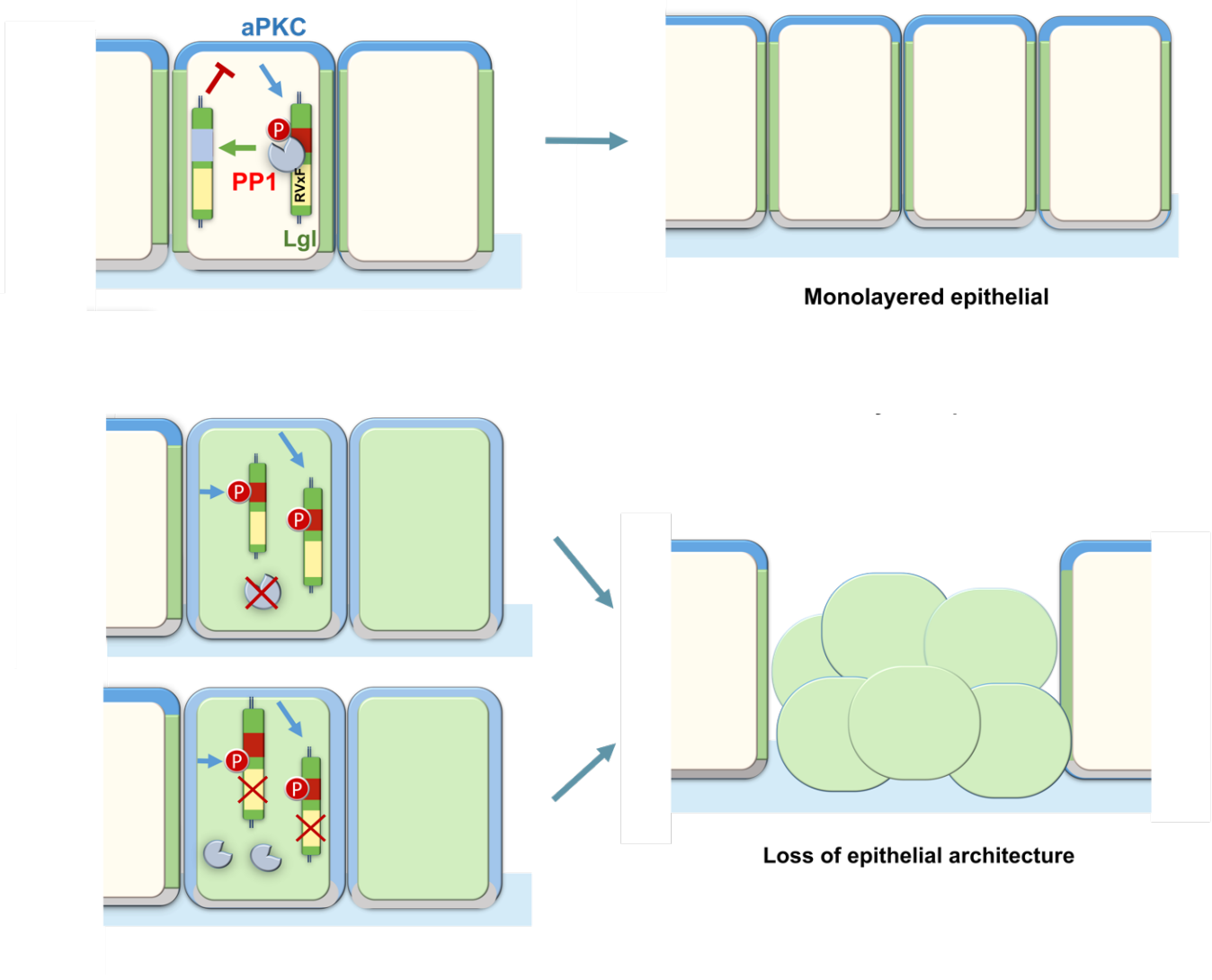

Figure 3.21: Proposed model for PP1 regulation of Lgl cortical localization during interphase and antagonism of apical aPKC for maintenance of epithelial polarity. PP1 dephosphorylates Lgl through the Lgl PP1 docking site, maintaining Lgl localization in the basolateral cortical domain and ensuring the monolayered organization of the epithelia. Depletion of PP1 or interference with PP1's ability to dephosphorylate Lgl induces extension of aPKC in the basolateral domain, with consequent disruption of cell polarity and epithelial architecture.

3.7. Discussion

PP1 phosphatase antagonizes aPKC-mediated phosphorylation to promote cortical localization of Lgl

In this study, we propose that PP1 reverses aPKC phosphorylation to maintain the cortical localization of Lgl and proper tissue architecture. In particular, we found that Lgl cytoplasmic mislocalization in a context of PP1 depletion relies on aPKC-mediated phosphorylation of Lgl. Second, our *in vitro* dephosphorylation results combined with an *in vivo* functional characterization of the Lgl docking site mutant indicate that PP1 directly dephosphorylates Lgl to support epithelial cell polarity.

Associated with a highly penetrant Lgl mislocalization phenotype, loss of PP1 results in the disruption of epithelial architecture with consequent multilayering, resembling the *lgl* loss-of-function phenotypes observed in the follicular epithelium (Bilder *et al*, 2000). Thus, could the multilayering phenotype induced by PP1 depletion arise from loss of cortical Lgl with consequent unbalance of the apical-basolateral activities? In fact, it is reported that *lgl* mutant phenotypes in imaginal discs and brain, including cell polarity defects and tumorigenesis, are suppressed by reducing aPKC levels, showing that aPKC activity antagonizes Lgl activity to maintain epithelia architecture (Ilina and Friedl, 2009). Using a similar approach, we modified the aPKC levels in a context of PP1 downregulation and analyzed the consequences in tissue architecture. We found that removing one copy of aPKC suppresses the multilayering phenotype associated with PP1 depletion, whereas adding an extra-copy induces a more aggressive multilayering. Our results therefore indicate that a reduction of aPKC levels is sufficient to repress the multilayering phenotype of PP1 depletion. Could this rescue be associated with a recovery of Lgl cortical localization? Indeed, we found that overexpression of Lgl-GFP partially rescues the multilayering phenotype associated with loss of PP1, possibly by restoring Lgl localization in the cortex and re-establishing the apical-basal mutual antagonism.

In line with these results, we found different abilities of Lgl-GFP and $Lgl^{KA,FA}$-GFP in supporting epithelial apical-basal polarity in *lgl* null mutant clones. Whereas the wild-type version restores almost completely the monolayer epithelium in the analyzed egg chambers, the docking site mutant, $Lgl^{KA,FA}$-GFP, found to be hyperphosphorylated and mostly localized in the cytoplasm, displays a much lower rescue efficiency. Our results

therefore suggest that PP1 dephosphorylation of Lgl through this docking motif increases Lgl affinity to the cortex/plasma membrane and, consequently, might restore the ability to antagonize aPKC and maintain epithelial polarity. Curiously, we observed that $Lgl^{KA,FA}$-GFP is still able to rescue the *lgl* mutant multilayering in about 20% of the egg chambers. This result is consistent with some association of $Lgl^{KA,FA}$-GFP with the cortex/plasma membrane possibly induced by PP1-mediated dephosphorylation through the other predicted docking site motif conserved in *Drosophila* species or by a PP1-independent mechanism.

Consistent with the idea that PP1-mediated dephosphorylation of Lgl is important for Lgl basolateral function in the repression of aPKC, we found evidences that overexpression of the two Lgl versions, Lgl-GFP and $Lgl^{KA,FA}$-GFP, has a distinct impact on the inhibition of aPKC function and localization. Our overexpression-based functional analyses show that only Lgl-GFP is able to disrupt aPKC localization or function in both follicle cells, salivary glands and border cells. The capacity of Lgl-GFP in inhibiting aPKC when overexpressed could also explain the consistent observation that PP1 depletion induces a stronger cytoplasmic localization of endogenous Lgl than the overexpressed Lgl-GFP. In fact, aPKC inhibition caused by Lgl-GFP overexpression could reduce the availability of active kinase to phosphorylate Lgl when PP1 is downregulated. Together, our functional assays suggest that cortical localization promoted by PP1 not only counteracts aPKC phosphorylation, but is also an important mechanism to promote Lgl-mediated inhibition of aPKC activity.

Our results strongly suggest that PP1 dephosphorylates directly Lgl to induce its localization in the cortex. However, one consistent phenotype associated with PP1 depletion is a dramatic change in the cortical shape of follicle cells, which is curiously one of the essential steps towards cell invasion behavior (Friedl and Alexander, 2011). In fact, we observed epithelial cells invading the germline in a context of PP1 RNAi. These morphological changes are particularly evident when epithelial cells are imaged live, where PP1 depletion induces visible cortical deformations (see Movie 2). The cortical effects observed in PP1 depletion have been attributed to its role on moesin dephosphorylation and control of cortical stiffness (Kunda *et al*., 2008). Moreover, the PP1 regulatory subunit Sds22 has been reported to have an important role in epithelial cell shape and polarity by controlling the phosphorylation of moesin and Spaghetti Squash, the non-muscle myosin II regulatory light chain in *Drosophila* (Grusche *et al*, 2009). Since homology searches combined with biochemical assays suggest that Lgl was found to bind Myosin-II in the cortex (Betschinger *et al*., 2005), could cortical effects originated from PP1 depletion, such as hyperphosphorylation of myosin, induce Lgl mislocalization to the cytoplasm? Our results contradict this hypothesis, since the cortical localization of Lgl^{3A}, an unphosphorylatable

form of Lgl which should also bind NMII (Betschinger *et al*., 2005; Barros *et al*., 2003), remains unaffected in cells depleted for PP1. Additionally, previous work have shown that Lgl recruitment to the cytoskeleton fraction seems to be partially independent of myosin (Betschinger *et al*., 2005).

Taken our results together, we propose a model where the balanced activities of PP1 and aPKC maintain the basolateral cortical localization of Lgl. This allows Lgl antagonization of the apical domain, an essential condition for the maintenance of the polarity and architecture of the follicular epithelia.

PP1 role towards other canonical polarity proteins

PP1 participates in several cellular processes, targeting multiple substrates and specific subcellular components by interacting with a variety of regulatory subunits. PP1-mediated dephosphorylation of cortical components, such as myosin and moesin, has been shown to be required for the maintenance of epithelial cell polarity (Grusche *et al*, 2006; Jiang *et al*, 2011). But also canonical polarity proteins have been found to be targeted by PP1. The basolateral protein Scribble, for instance, was shown to interact and be dephosphorylated by PP1 in human cells (Nagasaka *et al*., 2013). However, a PP1-binding site shown to be important for PP1 interaction with human Scrib is absent in *Drosophila*, remaining unknown if PP1 is also able to dephosphorylate Scrib in the follicular epithelium.

While the cortical localization of Scrib is not significantly affected in PP1 depleted epithelial cells, Dlg is partly mislocalized to the cytoplasm. Although this phenotype could be indirectly associated with loss of cell polarity, it raises the hypothesis of a PP1-direct regulation of Dlg in the follicular epithelia. In a possible scenario, Dlg localization could be regulated by the antagonistic activities of PP1 and a Dlg-targeting kinase, similarly to what we have described for Lgl. So far, *Drosophila* Dlg was found to be phosphorylated by three kinases: CamKII (Koh *et al*., 1999), Par-1 (Zhang *et al*., 2007) and, more recently, aPKC (Golub *et al*., 2017). While aPKC phosphorylation of Dlg was only shown to have an impact on its conformation by disrupting the intramolecular interaction between SH3 and GUK domains (Golub *et al*., 2017), Par-1 and CamKII phosphorylation regulates the synaptic distribution of Dlg in *Drosophila* larval Neuromuscular Junction (Koh *et al*., 1999; Zhang *et al*., 2007). Wild-type and unphosphorylatable forms of Dlg are able to localize efficiently in synapses in homeostatic conditions, but overexpression of Par-1 mislocalizes endogenous Dlg to the muscle cytoplasm (Zhang *et al*, 2007). Similarly, constitutive CamKII activation leads to

abnormal localization of Dlg in synaptic membrane in a manner dependent on CamKII phosphorylation (Koh *et al*., 1999). Therefore, it would be interesting to explore whether PP1 could antagonize Par-1 or CamKII phosphorylation on Dlg to maintain its localization in the cortex in the follicular epithelia. Alternatively, Dlg cytoplasmic localization in PP1-depleted cells could be an indirect consequence of Lgl mislocalization, since Lgl and Dlg were found to possibly interact *in vitro* (Zhu *et al*, 2014). Moreover, in *Drosophila* embryos, Dlg and Lgl are mutual dependent for their proper subcellular localization (Bilder *et al*., 2000). Thus, whether this is an indirect consequence of loss of cell polarity or a direct consequence of a *in vivo* interaction between these two proteins remains still unknown. Curiously, in the epithelium of *Drosophila* midgut, *dlg* mutants disrupt the normal localization of Lgl at the septate junction without affecting apical-basal polarity (Chen *et al*, 2018), further suggesting a possible interaction between Dlg and Lgl.

Previous studies also report an interaction of PP1 with the apical protein Par-3. In mammalian cells, PP1α binds directly Par-3 to control its phosphorylation state and to allow the establishment of a functional Par-3/aPKC complex (Traweger *et al*., 2008). It remains to be known if the same mechanism operates in *Drosophila*. Our results instead indicate that PP1 suppresses aPKC signaling in the basolateral domain by promoting Lgl cortical localization. Lgl was also suggested to inhibit aPKC activity in *Drosophila* neuroblasts, although the way it represses aPKC activity is still unclear (Atwood and Prehoda, 2009; Wirtz-Peitz *et al*., 2008). Another balancing mechanism for aPKC signaling was proposed in *Drosophila* neuroblasts, where PP2A dephosphorylation of Par-6 allows its interaction with aPKC and inhibits its signaling during asymmetric cell division (Ogawa *et al*., 2009). Curiously, in the same study, Pp1-87B was identified as a potential inhibitor of the aPKC signaling, since mutants for this phosphatase enhance the membrane tethered aPKC-induced eye phenotype. In light of our model, an interesting possibility is that PP1 could balance aPKC signaling by dephosphorylating Lgl for the regulation of asymmetric cell division.

In conclusion, this chapter of my thesis contributes to the understanding of how cortical localization of Lgl is regulated in epithelial tissues. In an homeostatic condition, Lgl cortical localization should be regulated through an equilibrium between aPKC phosphorylation and PP1 dephosphorylation activities. In a context where homeostasis is compromised by loss or reduction of PP1 expression (reported in some human cancers cells) (Jiang *et al*., 2011) this equilibrium is unbalanced towards a more phosphorylated and cytoplasmic form of Lgl. Curiously, Lgl was also found to be mislocalized in gastric cancer (Lisovsky *et al*., 2009; Nam *et al*., 2014). Also, PP1γ (related to fly PP1α genes) is downregulated under hypoxia

(Comerford *et al*., 2006), a common phenomenon in the majority of malignant tumors and found to strongly induce Lgl to the cytoplasm though disruption of plasma membrane PIP_2 (Dong *et al*., 2015). Our findings provide an additional mechanism to explain Lgl reallocation to the cytoplasm under hypoxia by disruption of the PP1-dependent cortical localization of Lgl. Therefore, Lgl might be an important link for the understanding of PP1 misregulation and cancer.

Chapter 4

Molecular mechanisms controlling the recovery of cortical Lgl at mitotic exit

4.1. Introduction

In the previous chapter, we identified PP1 as the phosphatase that promotes Lgl cortical localization, preserving apical-basal cell polarity and the integrity of epithelia. Many epithelial tissues proliferate to ensure tissue growth and homeostasis and must therefore orchestrate cell division with the maintenance of epithelial cell polarity. Similarly to what has been shown during asymmetric cell division (Wirtz-Peitz *et al*., 2008), previous studies on epithelial cells describe that core components of the apical-basal polarity machinery are also spatially reorganized during symmetric cell division. Activation of Aurora A kinase induces cortical release of Lgl at early mitosis by phosphorylation of Lgl (Carvalho *et al*., 2015; Bell *et al*., 2015) (Figure 4.1A). This process was found to be important for planar spindle orientation in follicular epithelia, thus linking cell cycle-dependent reorganization of polarity complexes with the propagation of tissue architecture.

In the current chapter, we aim to understand how epithelial cell polarity is restored at mitotic exit in proliferative epithelial tissues. Regardless of the importance of Lgl phosphorylation and cortical exclusion during mitosis, its cortical localization must be re-established at mitotic exit to propagate cell polarity and preserve epithelial architecture (Figure 4.1B). Several questions arise: what happens to the Lgl pool that was phosphorylated and excluded to the cytoplasm during mitosis? How is Lgl cortical localization re-established? In the previous chapter, we found a role for PP1 in the control of Lgl cortical localization by acting on the phosphorylation sites that are controlled by aPKC and Aurora A. We therefore asked whether PP1, which is activated at anaphase, could also have a particularly important role for a timely Lgl cortical reloading at mitotic exit, since cells have to deal with the complete pool of Lgl in a phosphorylated form. In fact, we uncovered an essential role for PP1/Sds22 phosphatase holoenzyme in controlling reloading to the cortex at mitotic exit and consequently the maintenance of apical-basal polarity in the new daughter cells.

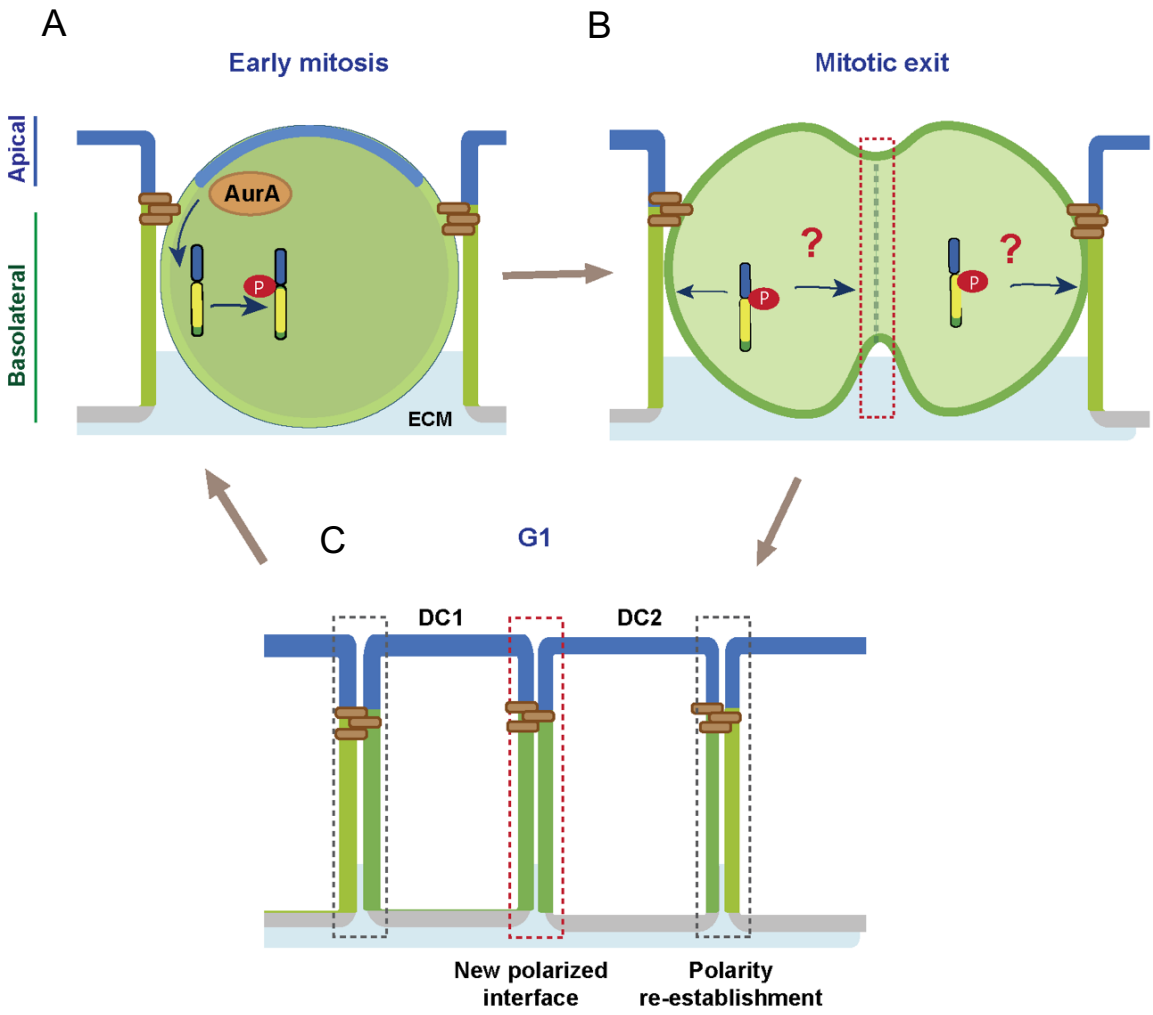

Figure 4.1: Understanding Lgl re-establishment in the cortex of daughter cells at mitotic exit. A) In early prophase, Lgl changes its localization from the cortex to the cytoplasm in a process dependent on phosphorylation by Aurora A. Thus, Aurora A activation at mitotic entry provides temporal control to the spatial regulation of Lgl exerted by aPKC (Carvalho *et al.*, 2015; Bell *et al.*, 2015). B),C) Additional regulatory mechanisms should restore Lgl cortical localization in the new daughter cells, not only in the new polarized interface between the two daughter cells (DC1 and DC2) but also in the pre-existing membranes. These mechanisms are predicted to be essential for the maintenance of monolayered tissue architecture in proliferating epithelial tissues.

4.2. Lgl is reloaded from the cytoplasm to the cortex at mitotic exit

To understand how Lgl localization is restored in the cortex of the new daughter cells, we started by characterizing the localization of Lgl-GFP at mitotic exit in follicular epithelial cells. As observed in time-lapse images and kymographs, Lgl starts to disappear from the cytoplasm after anaphase (Figure 4.2A) (Movie 1). In turn, Lgl signal progressively increases at the cortex of the new interface from 2 minutes until about 15 min after anaphase, which inversely correlates with the cytoplasmic decay (Figure 4.2B). As observed by the midsagittal perspective of the follicular epithelia, recovering of Lgl at the new interface occurs asymmetrically from the basal to the apical side, following the direction of the cleavage ingression typically observed in this epithelia (Morais-de-Sá and Sunkel, 2013). Moreover, Lgl accumulates in the apical extremity of the membrane, possibly corresponding to the midbody, a transient structure formed at the end of cytokinesis (Thieleke-Matos *et al*., 2017) (kymograph of the new interface in Figure 4.2A). Additionally, the absence of signal in neighboring cells due to clonal expression of Lgl-GFP allows visualization of a progressive accumulation of Lgl in the old membranes (Figure 4.2A, red arrows). Similarly to the follicular epithelium, we found that Lgl also disappears from the cytoplasm while accumulating in the cortex at mitotic exit in the embryonic epithelium of *Drosophila* (Figure 4.2D, blue arrows). Moreover, Lgl cytoplasmic decay in this epithelium has similar dynamics to the follicular epithelium (graph in Figure 4.2D), suggesting that Lgl localization and dynamics at mitotic exit might be controlled by similar mechanisms.

Despite the inverse correlation observed between Lgl signal increase in the new interface and the disappearance from the cytoplasm, the rate of variation between 4 min and 8 min is different (-12.75 for the cytoplasmic decay and 8.229 for the new interface accumulation), suggesting faster cytoplasmic decay than accumulation in the new interface (Figure 4.2C). This delay might be a consequence of *de novo* and progressive establishment of the new interface, contrasting with a rapid redistribution of cytoplasmic Lgl to the pre-existent ones.

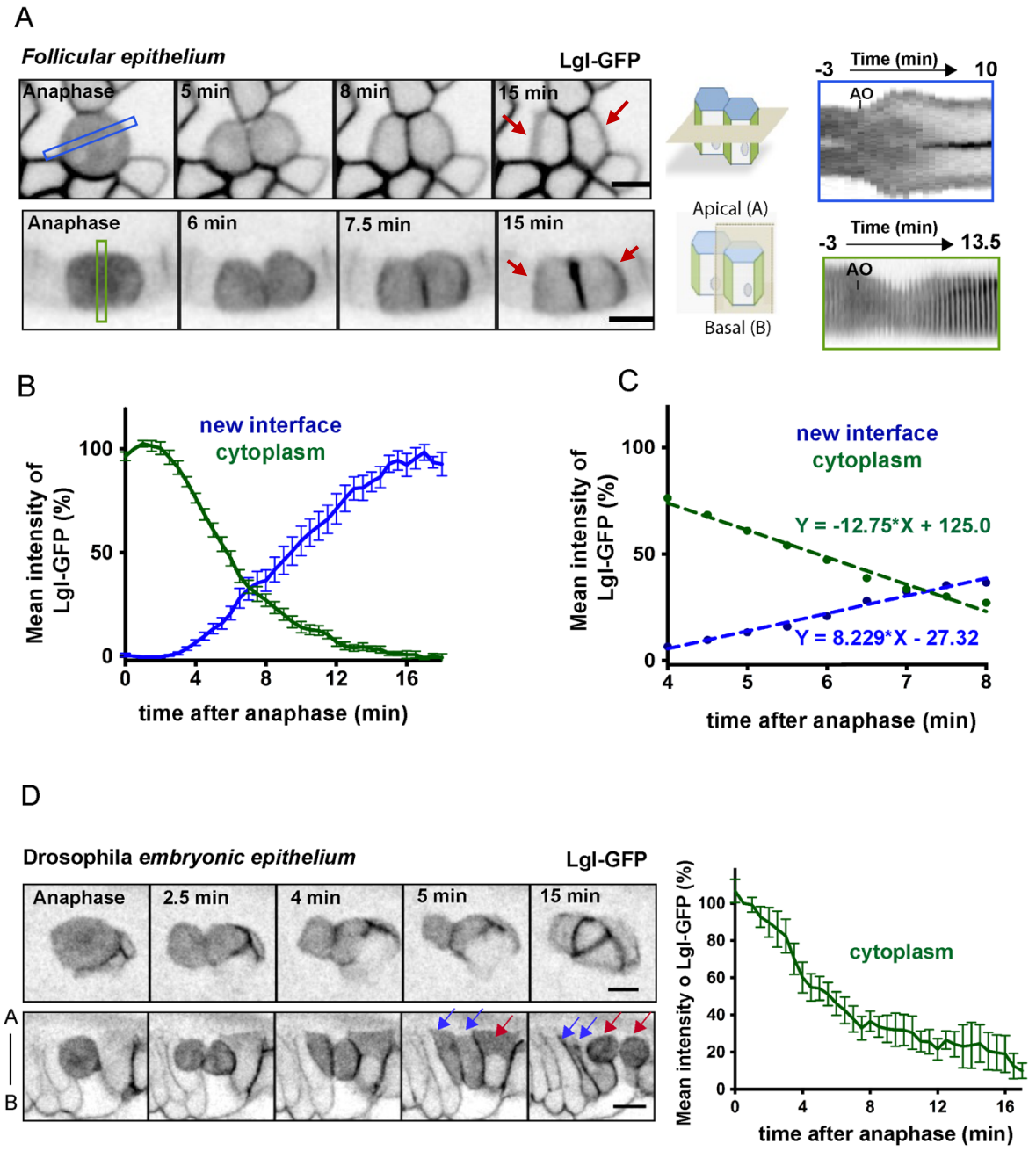

Figure 4.2: Characterization of Lgl-GFP localization and dynamics at mitotic exit in epithelial cells. A) Clonal expression of Lgl-GFP in the follicular epithelia shows that cytoplasmic Lgl-GFP starts to disappear after anaphase while it accumulates in the new interface and in the pre-existent cortex (red arrows). A midsagittal perspective shows Lgl accumulating in the new interface from the basal towards the apical side, following the formation of the new interface. Kymographs from the regions indicated in colored boxes are shown. B) Quantification of the Lgl signal at mitotic exit suggests an inverse correlation between Lgl decay in the cytoplasm (n=21, green) and its accumulation in the new interface (n=16, blue). C) Graphic representation of the linear regression obtained from values between 4 min and 8 min, when there is linear variation of fluorescence intensity, but at different rates for Lgl cytoplasmic decay and Lgl recovering in the new interface. D) Analyses of Lgl-GFP in embryonic epithelium, where Lgl is also reallocated from the cytoplasm (as showed by cytoplasmic decay quantifications) to the cortex (blue arrows) (n=11). Error bars: mean ± SEM. Scale bars: 5 μm

Alternatively, the different rates observed between cytoplasmic decay and new interface accumulation could indicate that phosphorylated cytoplasmic Lgl is degraded and replaced by newly synthesized Lgl with more affinity to the cortex, thus restoring Lgl cortical localization. To address this possibility, we generated a photoconvertible version of Lgl-Dendra2 to express in *Drosophila* S2 cells, where Lgl also decays in the cytoplasm and accumulates in the cortex at mitotic exit (Figure 4.3A). Photoconversion of Lgl-Dendra2 at metaphase labels the pre-existent protein in red, allowing one to track its localization at mitotic exit. As observed by the time lapse images and the quantifications of cytoplasmic decay, we found that cytoplasmic Lgl is reloaded to the cortex (Figure 4.3B). Additionally, quantifications of the overall intensity of the photoconverted protein suggest that Lgl intensity remains stable during mitotic exit (Figure 4.3B, graph). Our results thus support the idea that the cytoplasmic and phosphorylated pool of Lgl is fully reloaded to the cortex at mitotic exit.

4.3. The impact of Aurora A and aPKC kinases in Lgl cortical reloading

4.3.1. Aurora A degradation is not the timer for Lgl cortical reloading

Reloading of Lgl to the cortex at mitotic exit might be controlled by cell-cycle dependent processes, common to both polarized and unpolarized cells. Due to the importance of Aurora A activation in Lgl phosphorylation and cortical exclusion (Bell *et al*.,2015; Carvalho *et al*., 2015), we postulated that Aurora A degradation at the end of mitosis could play a role in Lgl cortical reloading. Aurora A degradation is critical for the regulation of Aurora A activity at mitotic exit (Lindon *et al*., 2016) and relies on ubiquitin-mediated proteolysis promoted by the coactivator of anaphase promoting complex (APC), Cdh1 (Castro *et al*., 2002). We generated FRT/FLP mutant clones for the *Drosophila* Cdh1 homologue, *rap/Fzr,* in the follicular epithelia, as an approach to characterize Lgl dynamics in the context of stabilized AurA. Firstly, we characterized the phenotype of these mutants and found that cell polarity in *rap* mutant clones is not affected, as the localization of the apical polarity protein aPKC and the basolateral localization of Lgl are indistinguishable in mutants comparing with control (Figure 4.4A).

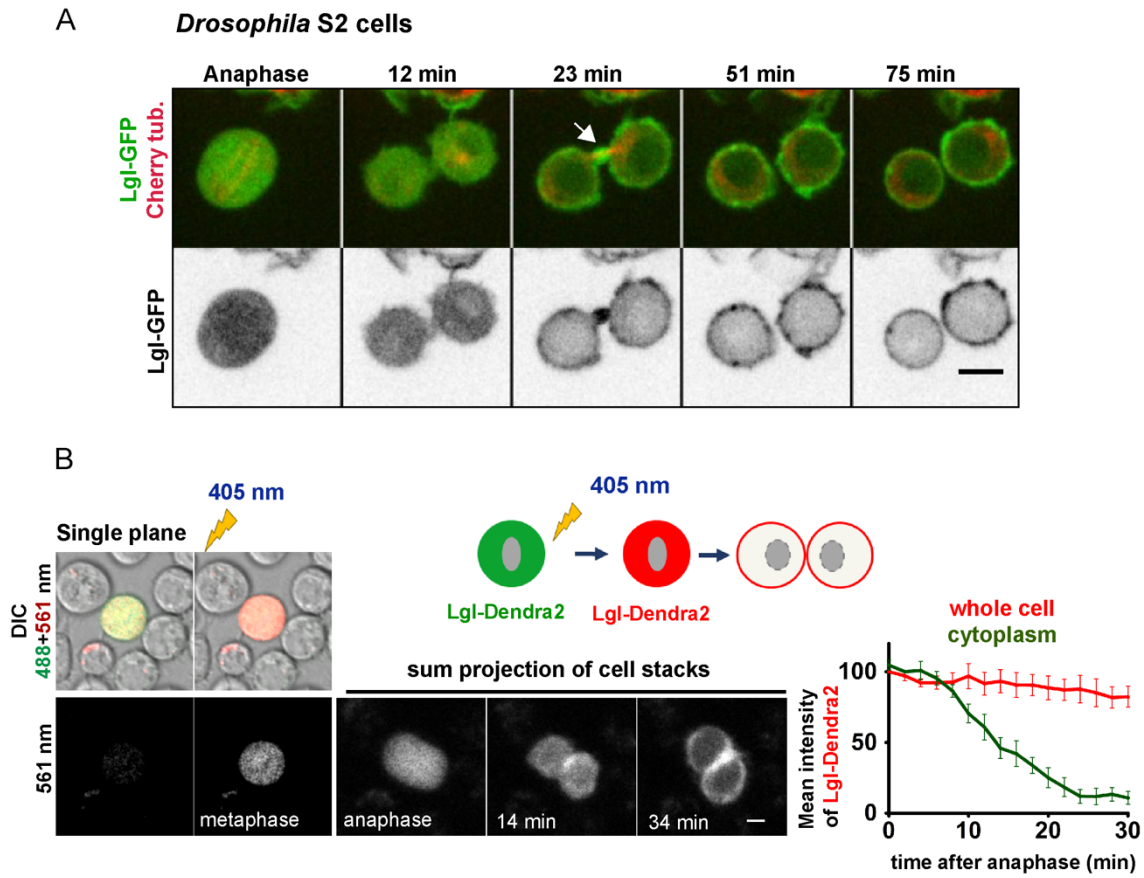

Figure 4.3: Cytoplasmic Lgl returns to the cortex at mitotic exit in S2 cells. A) Lgl-GFP disappears from the cytoplasm after anaphase and progressively accumulates in the cortex of S2 cells (white arrow pinpoints the strong accumulation of Lgl-GFP in a bridge linking the two daughter cells). B) Photoconversion of Lgl-Dendra2 using a 405 nm laser in S2 cells at metaphase shows that cytoplasmic Lgl returns to the cortex at mitotic exit. We observed a decay of the signal in the cytoplasm and an accumulation in the cortex at mitotic exit, suggesting that the cytoplasmic pool is reloaded to the cortex This is confirmed by quantifications of the cytoplasmic decay and the integrated density (cell area x mean intensity value) in sum projections of the whole cells (n=6), which suggests that the Lgl photoconverted after anaphase is not degraded at mitotic exit. Error bars: mean ± SEM. Scale bars: 5 μm

Despite this, we detected small and high condensed nuclei in mutant clones (Figure 4.4A). We also confirmed whether AurA is stabilized in *rap* mutants using the presence of AurA-GFP at the centrosomes as a readout for its stability. At mitotic exit, AurA-GFP signal progressively disappears from the centrosomes which are labeled with an RFP-tagged version of centrosomin, cnnRFP, a protein required for centrosome assemble and function in *Drosophila* (Megraw *et al*., 1999; Vaizel-Ohayon and Schejter, 1999) (Figure 4.4B). In mutant cells for *rap*, we observe a higher stabilization of AurA-GFP at centrosomes, since the signal of AurA-GFP at centrosomes is present 46 min after anaphase while it is only slightly visible at 11 min after anaphase in wild-type cells (Figure 4.4B). Finally, we quantified Lgl cytoplasmic decay in *rap* mutant clones as a readout for Lgl reloading dynamics at mitotic exit. As observed by the time-lapse images and quantifications of cytoplasmic decay, there were no significant changes in Lgl reloading (Figure 4.4C), indicating that AurA degradation is not the driving mechanism for cortical reallocation of Lgl at mitotic exit.

To confirm these results, we overexpressed AurA-GFP and AurA$^{\Delta Abox}$-GFP, a version of AurA which lacks the A-Box that is recognized by APC/C-rap, and so remains stable at mitotic exit without interfering with the catalytic domain (Meghini *et al*., 2016;Lindon *et al*., 2016). Accordingly, AurA$^{\Delta Abox}$-GFP signal is still observed 14 min after anaphase, when AurA-GFP has already disappeared (Figure 4.5A). Despite being stabilized at mitotic exit, is AurA$^{\Delta Abox}$-GFP active and able to phosphorylate its substrates? To confirm that, we analyzed the phosphorylation status of a substrate of AurA, TACC, in follicle cells expressing AurA$^{\Delta Abox}$-GFP, using a pTACC antibody (Barros *et al*., 2005). Performing clonal analysis to compare cells expressing AurA$^{\Delta Abox}$-GFP with non-expressing cells, we found that accumulation of pTAAC at centrosomes only occurs in cells expressing AurA$^{\Delta Abox}$-GFP (Figure 4.5B). However, overexpression of this stabilized and the active version of AurA does not change the dynamics of Lgl reloading to the cortex at mitotic exit, as observed by the time-lapse images and the kymographs of Lgl-RFP (Figure 4.5A) and also the corresponding quantification of cytoplasmic decay (Figure 4.5C). Thus, stabilization of an active form of AurA at mitotic exit is not sufficient to impact Lgl cortical reloading.

Conversely, we also analysed the impact of AurA in Lgl reloading, based on the AurA depletion or inactivation, which could cause a premature reloading of Lgl if Aurora A degradation had a major role in Lgl cortical reloading. To address this question, we used two systems, the polarized follicular epithelium and the unpolarized S2 cells.

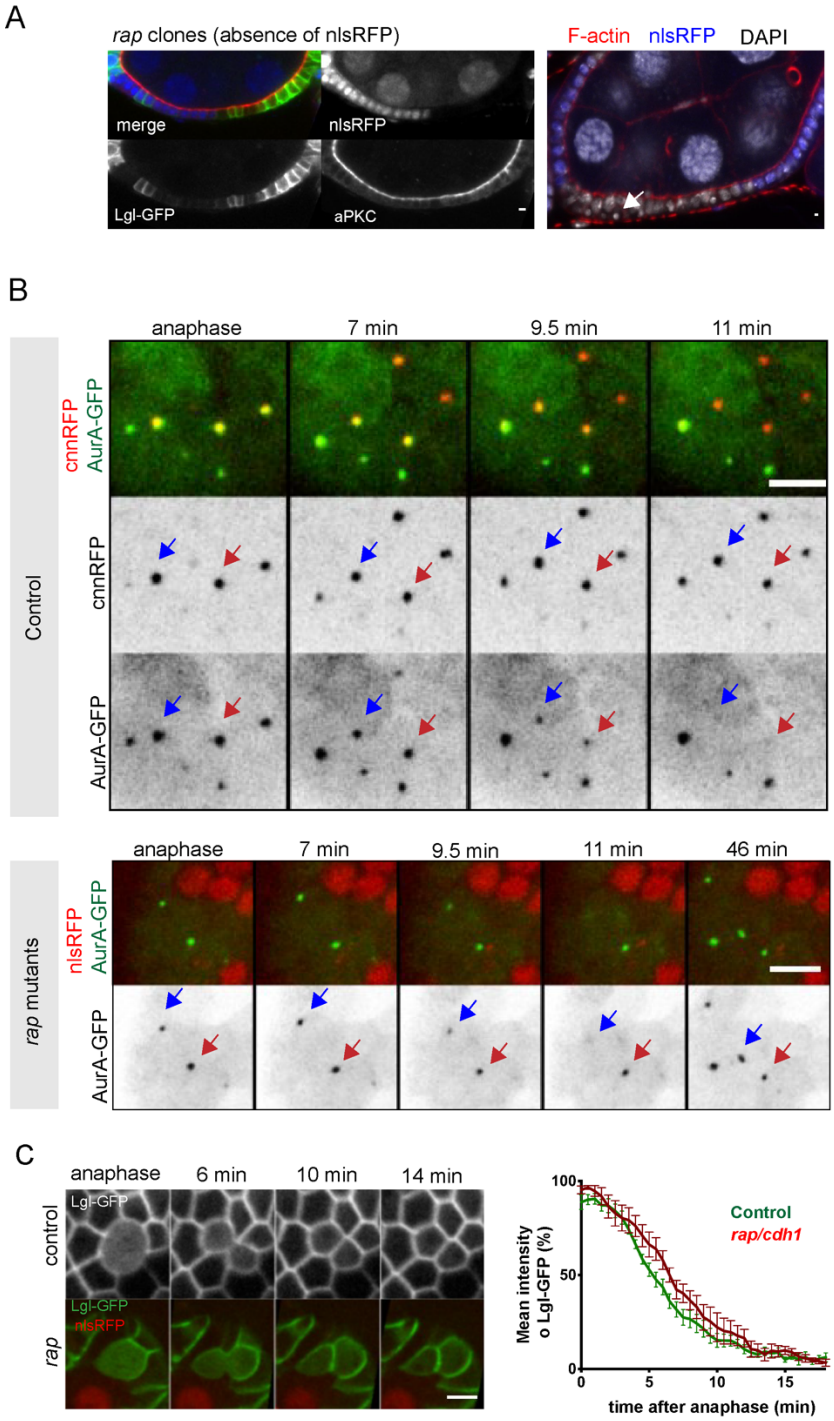

Figure 4.4: Stabilization of AurA at mitotic exit does not affect Lgl reloading. A) *rap* mutant cells are not affected in polarity, but display some micronuclei**.** B) Time-lapse images of follicle cells showing a stabilization of AurA-GFP in the centrosomes of *rap* mutant cells when compared with controls (arrows pinpoint the centrosomes of the followed cell). C) Lgl reloading dynamics are not significantly affected in *rap* mutant clones as shown by time-lapse images and quantifications of the cytoplasmic decay (n=12 control; n=6 *rap* mutant cells). A non-parametric Mann-Whitney statistical test was performed to compare control and *rap* mutants at two time-points, 6 min and 7 min, but the data were not statistically different. Error bars: mean ± SEM Scale bars: 5 μm

In the follicular epithelium, we induced *aurA* mutant clones to analyze the dynamics of Lgl at mitotic exit. As anticipated from the role of AurA at mitotic entry, Lgl cytoplasmic exclusion was strongly delayed (data not shown) (Carvalho *et al*., 2015). However, at mitotic exit, no changes were detected in the dynamics of Lgl cytoplasmic decay, which still progressively accumulates in the cortex (Figure 4.5 D, E). Similarly, depletion of AurA in S2 cells also interferes with cortical release at mitotic exit (Figure 4.5 F, arrows), but does not affect Lgl cortical reloading (Figure 4.5 G). Taken together, our results support the conclusion that regulation of Aurora A degradation is not the main mechanism controlling the reloading of Lgl at mitotic exit.

4.3.2. aPKC does not repress Lgl cortical reloading at mitotic exit in the follicular epithelia

Mutant cells for aPKC show a slight delay in Lgl cortical release at mitotic entry, suggesting that aPKC participates in Lgl reallocation to the cytoplasm during this period (Carvalho *et al*., 2015). Moreover, since aPKC represses Lgl cortical localization, we analyzed the possible relevance of aPKC for the Lgl reloading at the basolateral cortex during mitotic exit. For that, we overexpressed Lgl-GFP in the follicular epithelium of cells harbouring both the $aPKC^{K06403}$ null and the temperature sensitive allele $aPKC^{ts}$ (Guilgur *et al*., 2012). When compared with control cells, Lgl reloading is not affected in $aPKC^{ts}$/ $aPKC^{K06403}$ in follicle cells imaged at a restrictive temperature (Figure 4.6A and 4.6C), despite the loss of epithelial integrity (Figure 4.6B). Our results therefore suggest that aPKC-mediated phosphorylation is unable to repress Lgl reloading to the lateral cortex at mitotic exit in the follicular epithelia.

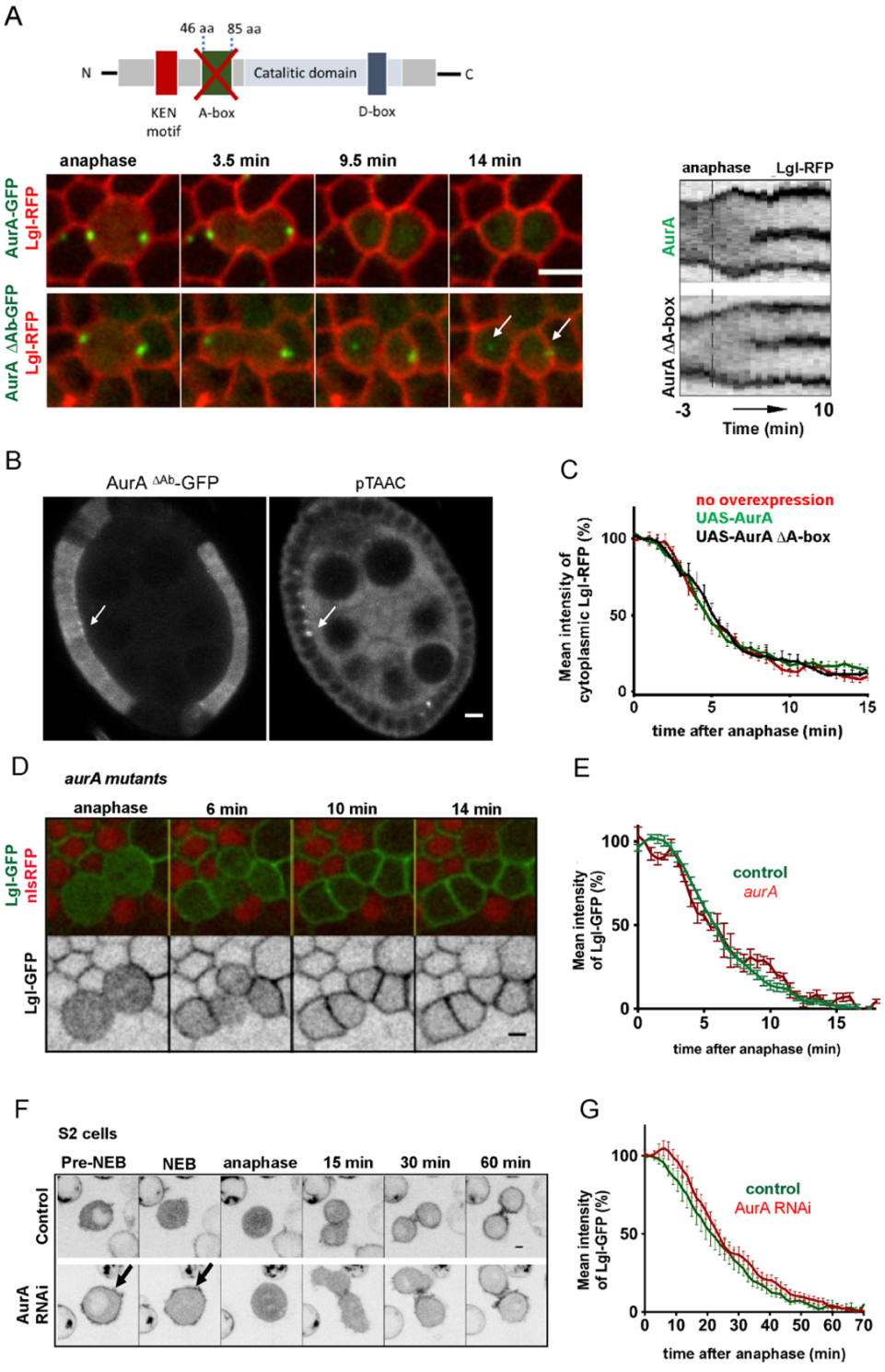

Figure 4.5. Overexpression of a stabilized version of AurA, AurA$^{\Delta Ab\text{-}GFP}$, or depletion of AurA does not change the kinetics of Lgl cortical reloading. A) Overexpression of a version of AurA deleted for the A-box degron motif, inducing its stabilization at mitotic exit (as indicated by the white arrows in the centrosomes), does not change Lgl cortical reloading when compared with overexpression of AurA wild-type. B) The pTAAC antibody is detected in centrosomes of interphase cells overexpressing AurA$^{\Delta Ab}$-GFP in a clonal manner,

suggesting that stabilized AurA$^{\Delta Ab}$-GFP is active C) Quantifications of Lgl cytoplasmic decay in cells overexpressing AurA$^{\Delta Ab\text{-}GFP}$ (n=9), AurA-GFP (n=13) or non-expressing cells (n=14). D), E) Lgl reloading is not affected in *aurA* mutant cells (generated by FRT/FLP system and marked by the absence of nlsRFP) (n=3), as observed in the time-lapse images and quantifications of cytoplasmic decay (n=16 control cells). F) G) Depletion of AurA in S2 cells delays Lgl release from the cortex (indicated by the black arrows), but does not affect cortical reloading (n=23 control cells; n=17 AurA RNAi cells) . Error bars: mean ± SEM Scale bars: 5 μm

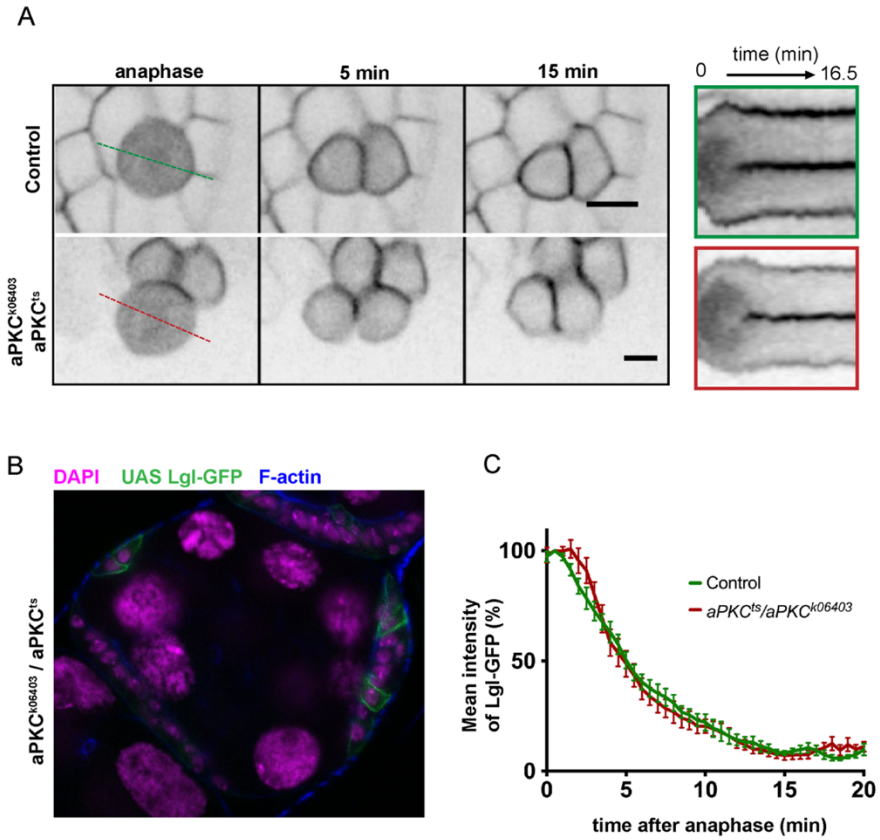

Figure 4.6: aPKC inactivation does not affect Lgl cortical reloading at mitotic exit in the follicular epithelium. A) Lgl reloading in control and *aPKC^{K06403}/aPKC^{ts}* follicle cells is not disrupted or filmed at a restrictive temperature. B) *aPKC^{K06403}/aPKC^{ts}* raised at restrictive temperature show disruption of the epithelial monolayer. C) No changes in the dynamics of cytoplasmic decay were observed when interfering with aPKC in the follicular epithelium (n=10 control cells; n=10 *aPKC^{K06403}/aPKC^{ts}* cells). Error bars: mean ± SEM Scale bars: 5 μm

4.4. PP1/Sds22 is involved in Lgl cortical reloading at mitotic exit

At mitotic exit, cells have to deal with all Lgl in the phosphorylated form to promote quick cortical reallocation. We thus explored the hypothesis that cortical reloading is dependent on the activation of phosphatases which could dephosphorylate Lgl. In the previous chapter, we found that Protein phosphatase 1 (PP1) dephosphorylates Lgl, targeting the same sites that block Lgl interaction with the membrane when phosphorylated (Dong *et al*., 2015). Therefore, PP1 is a strong candidate as a regulator of Lgl reloading, since it was found to be activated at mitotic exit to control several events (Bollen *et al*., 2009) and could dephosphorylate Lgl to re-establish its affinity with the membrane. To explore this hypothesis, we analyzed Lgl-GFP dynamics at mitotic exit in cells depleted for the major PP1 isoform, Pp1-87B. We found that these cells show a strong delay in Lgl reloading when compared with control cells (~70% of the Lgl remains in the cytoplasm 35 min after anaphase versus ~20% in control cells) (Figure 4.7B) (Movie 2). Since PP1 depletion continuously disrupts Lgl localization in interphase, we tried to analyze more specifically the role of this phosphatase on Lgl reloading by depleting the regulatory subunit Sds22, whose RNAi does not have a strong effect on Lgl in interphase but which is known to regulate PP1 activity at mitotic exit (Chapter 3) (Kunda *et al*., 2012). Depletion of Sds22 strongly delays Lgl reloading in the follicular epithelium, although less efficiently than depletion of PP1 (~40% of Lgl remains in the cytoplasm of depleted cells) (Figure 4.7B). Conversely, we overexpressed the Pp1-87B-HA catalytic subunit of *Drosophila* reasoning that it could dephosphorylate Lgl and induce a premature reloading by anticipating Lgl dephosphorylation and binding to the cortex/plasma membrane. However, overexpression of Pp1-87B-HA does not alter the Lgl reloading at mitotic exit when compared with control cells (Figure 4.7B). It is worth noting that although overexpression of the *Drosophila* PP1-HA did not effect Lgl reloading, phosphatases do not act as free catalytic subunits alone, but together with non-catalytic regulatory subunits (Moura and Conde, 2019; Barr *et al*., 2011) and so it is possible that overexpression of Pp1-87B-HA is insufficient to increase PP1 activity.

Since PP1/Sds22 control cell-cycle events, the effect observed in Lgl reloading to the cortex when depleting this phosphatase in follicle cells should also occur in non-polarized cells. To test this idea, we depleted PP1 in S2 cells and analyzed the reloading at mitotic exit. Similarly to epithelial cells, depletion of Pp1-87B using a dsRNA specific for the 5'UTR of Pp1-87B (Figure 3.5, Chapter 3) induces a delay in Lgl reloading (Figure 4.8A). Moreover, using a dsRNA able to target all PP1 isoforms (Figure 3.5, Chapter 3) we found a

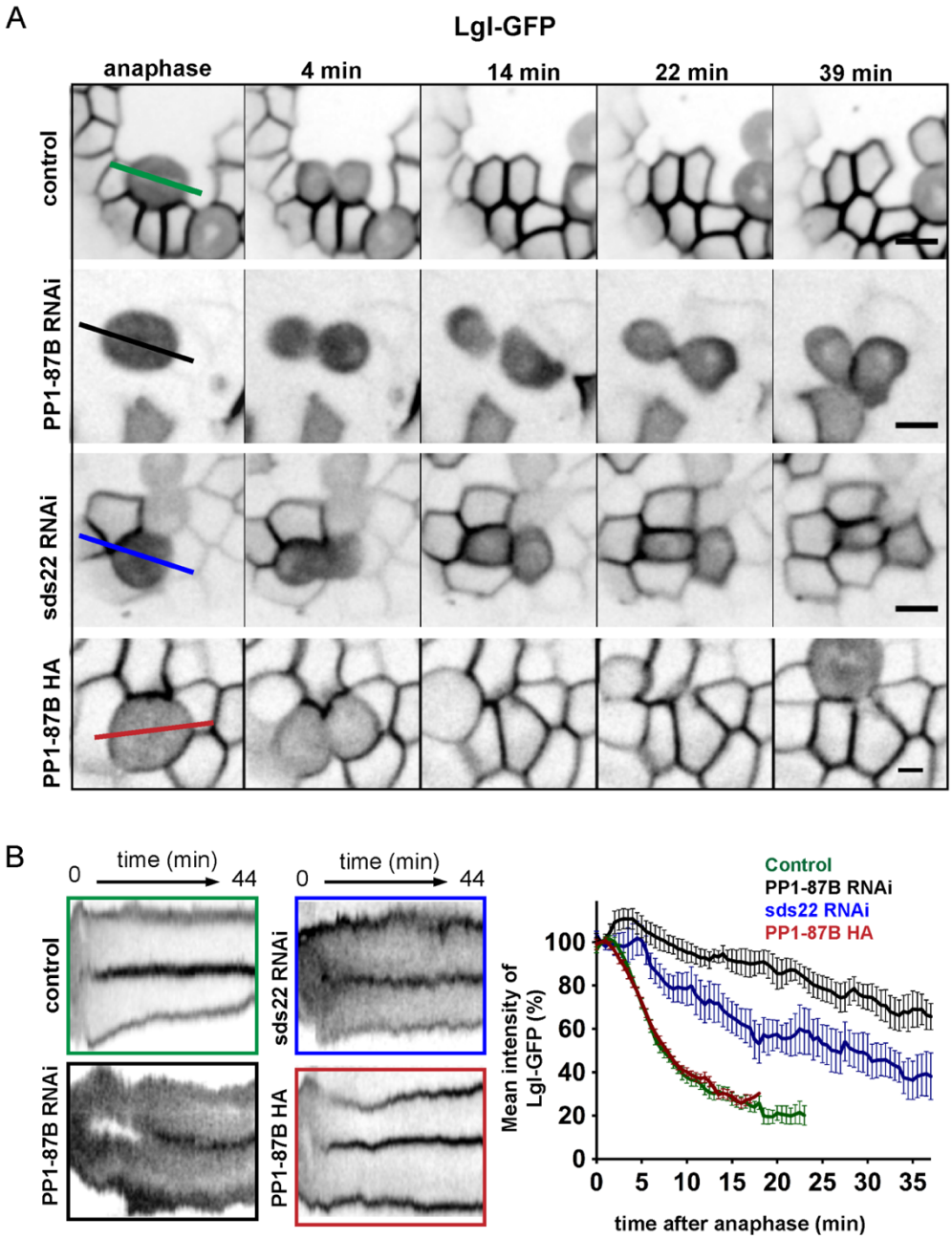

Figure 4.7: PP1/Sds22 regulates Lgl cortical reloading at mitotic exit in follicle cells. A) Depletion of Pp1-87B (2 days at 29ºC) and the regulatory subunit Sds22 (1 days at 29ºC) strongly delays Lgl cortical reloading. Overexpression of Pp1-87B-HA (1 day at 25ºC) does not affect cortical reloading. B) Kymographs of the cells represented in A from regions indicated by different colored lines and quantifications of Lgl cytoplasmic decay (n=21 control; n=17 Pp1-87B-HA; n= 11 sds22 RNAi; n=8 Pp1-87B RNAi). Error bars: mean ± SEM Scale bars: 5 μm

stronger disruption in Lgl cortical reloading (Figure 4.8A). This function is specific to PP1, since depletion of the catalytic subunit of PP2A, the other major serine/threonine phosphatase involved in events at mitotic-exit, only have a slight effect on Lgl reloading (Figure 4.8A). Therefore, PP1/Sds22 seems to be involved in Lgl cortical reloading in different cells in a cell-cycle dependent manner. Curiously, and in contrast to what we observed in the follicular epithelia, depletion of aPKC induces premature reloading of Lgl (Figure 4.8B) suggesting that aPKC can inhibit Lgl cortical reloading at mitotic exit in S2 cells. Despite the importance of aPKC for repressing Lgl reloading, PP1 depletion still delays Lgl reloading when co-depleted with aPKC (Figure 4.8B). This result is expected due to the existence of a second kinase, Aurora A, that also phosphorylates Lgl during mitosis. Thus, our results suggests that PP1 and aPKC counteract each other activity to control Lgl cortical reloading at mitotic exit in S2 cells, but confirm that PP1 is also required to regulate Lgl reloading independently of aPKC.

To confirm that cortical delay of Lgl at mitotic exit is directly related with Lgl dephosphorylation by PP1/Sds22, we took advantage of the Lgl mutated in the PP1 docking site characterized in Chapter 3. We expressed this form in the follicular epithelia and we found a strong delay in the reloading, which is enhanced by depletion of Sds22 (Figure 4.9A). This suggests that this PP1-docking motif promotes robust dephosphorylation and reloading of Lgl but is dispensable for partial PP1 activity when the PP1/Sds22 complex is available. Curiously, in the embryonic epithelium, the reloading of the mutant form for PP1-docking site is strongly delayed (Figure 4.9C, red arrows).

We also found that, both in S2 cells and in the follicular epithelia, Lgl strongly accumulates at the end of the contractile ring constriction, near the midbody (Figure 4.3A; Figure 4.10A). To explore the contribution of cytokinesis for Lgl cortical reloading, we initially used Latranculin A, a drug that interferes with actin polymerization and consequently with the assembly of the contractile ring (O'Shaughnessy and Thiyagarajan, 2018). Epithelial cells treated with LatA show recovery of Lgl-GFP at the cortex, even when cytokinesis failed (Figure 4.10B). However, there is a delay in cortical reloading, which suggests that cytokinesis promotes Lgl reloading. Since Lgl binds to cortical actin, LatA treatment may not only interfere with cytokinesis but reduce the affinity of Lgl binding to the actomyosin cortex, which would compromise its cortical reloading. We therefore interfered with cytokenisis by depleting Pavarotti, a member of a kinesin-like protein family of microtubule-dependent molecular motors, which is a specifically important protein to assemble the

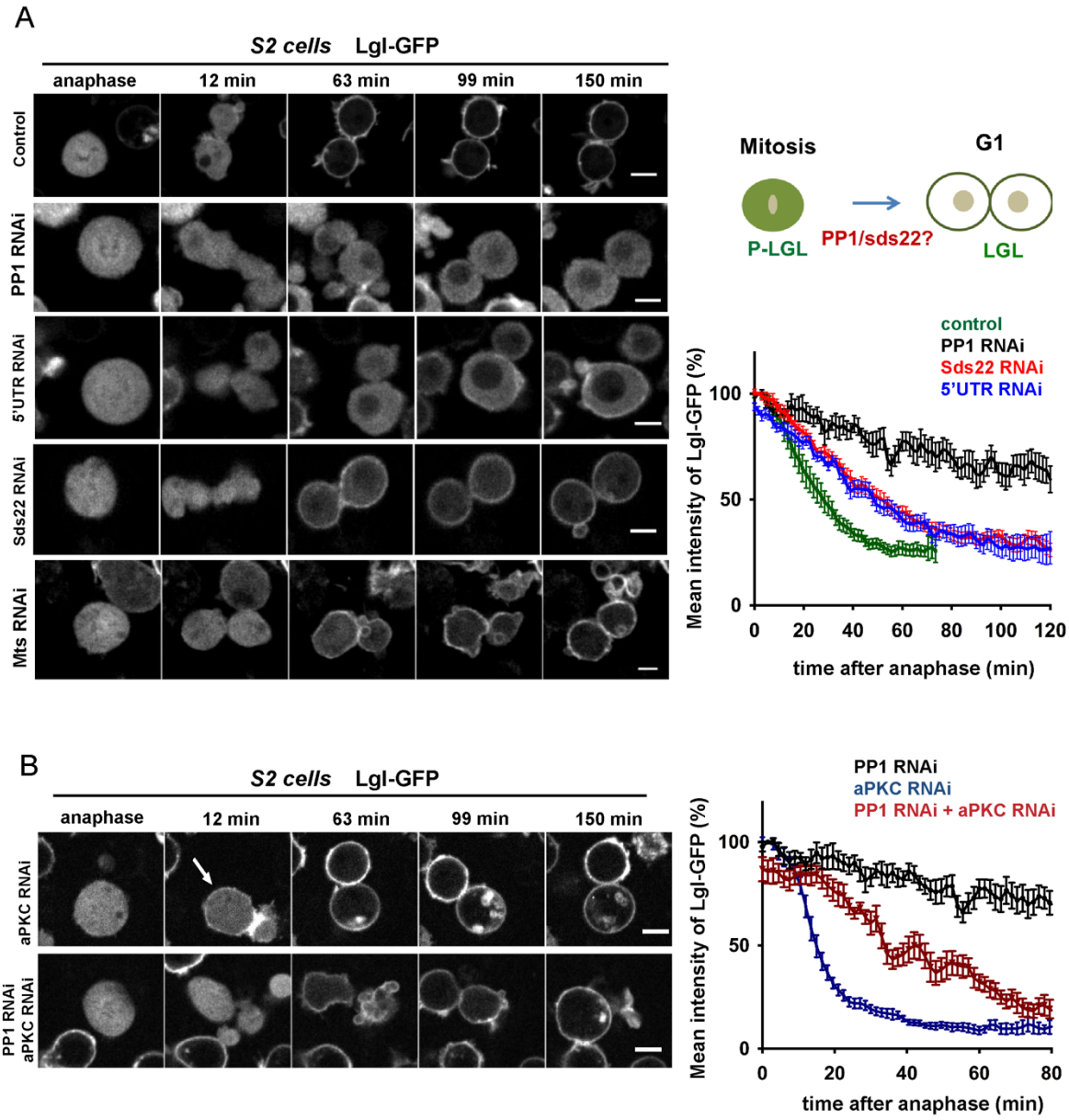

Figure 4.8: Depletion of PP1 and Sds22 delays Lgl reloading in S2 cells. A) Depletion of PP1 and Sds22 strongly delays Lgl cortical reloading, as observed by quantifications of the cytoplasmic decay and the time-lapse images. Mts RNAi only induces a slight effect on Lgl reloading. B) aPKC represses Lgl reloading to the cortex at mitotic exit in S2 cells, counteracting the action of PP1. In aPKC depleted cells, Lgl starts to accumulate very early when compared with control, as indicated by the white arrow. Error bars: mean ± SEM Scale bars: 5 μm

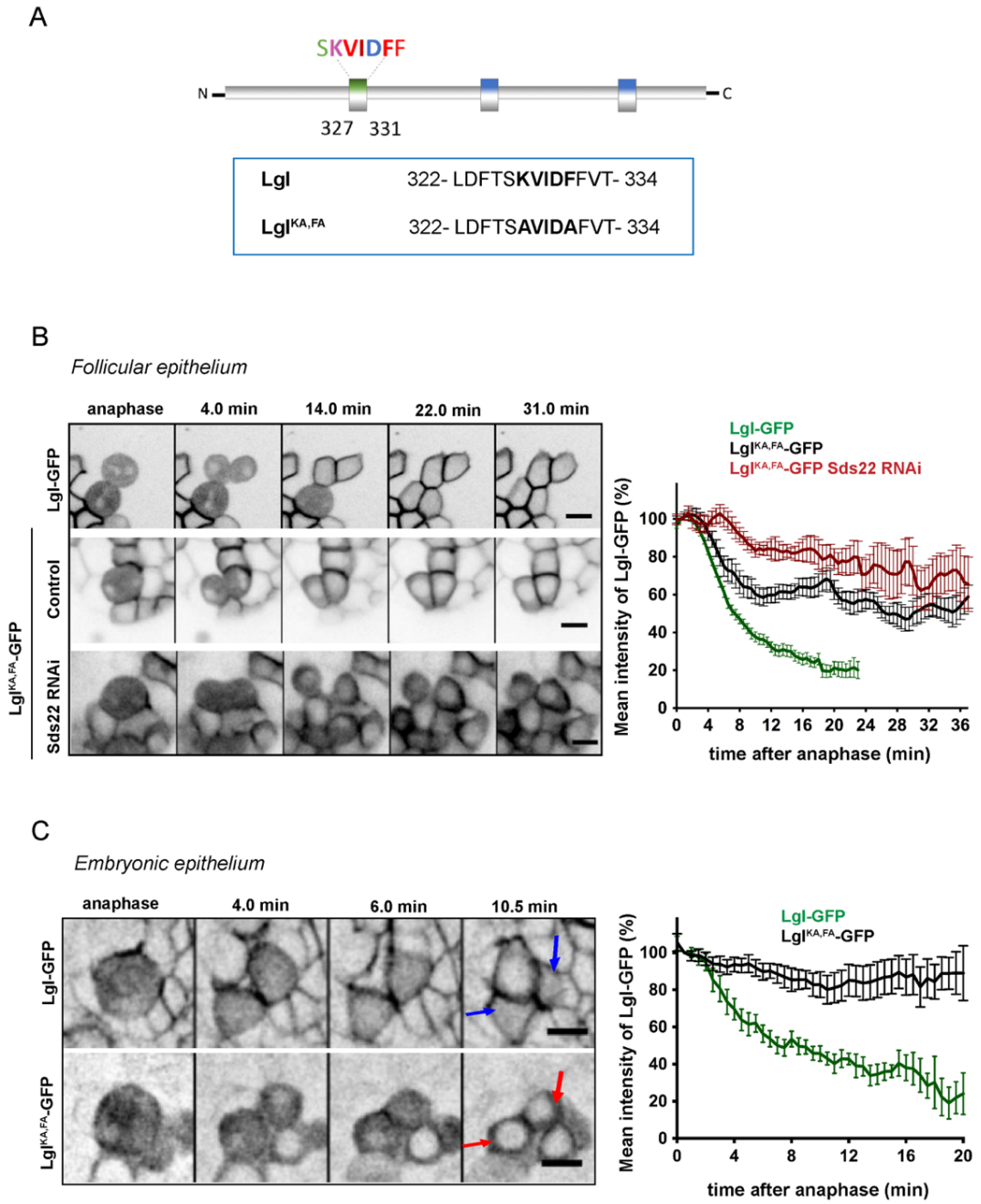

Figure 4.9: Lgl^{KA,FA} -GFP is delayed in reloading to the cortex in epithelia. A) Schematic representation of the mutation in the PP1 docking site motif of Lgl, Lgl^{KA,FA} -GFP, where the first and last aminoacids were replaced by alanines (see Chapter 3 for details). B) In the follicular epithelium, Lgl^{KA,FA} -GFP reloading is also strongly delayed, which is enhanced by depletion of Sds22 (n=21 control cells; n=11 Lgl^{KA,FA} -GFP cells; n=12 Lgl^{KA,FA} -GFP in sds22 RNAi cells for 3 days at 25ºC). C) Lgl^{KA,FA} -GFP does not accumulate at the cortex at mitotic exit in embryonic epithelia, as pointed out by the red arrows (compare with cells indicated by the blue arrows in the control). Quantification of cytoplasmic decay is represented in the graph (n=13 control cells; n= 11 Lgl^{KA,FA} -GFP expressing cells). Error bars: mean ± SEM Scale bars: 5 μm

contractile ring but does not generally interfere with the actomyosin cytoskeleton (Adams *et al*., 1998). Lgl cortical reloading also seems to be delayed in this context (Figure 4.10C), suggesting that cytokinesis promotes Lgl reloading to the cortex, but it is not an essential process.

Could a delay in Lgl reloading observed in a context of PP1 or Sds22 depletion be associated with a prolonged anaphase (Kunda *et al*., 2012) and then to a delayed mitotic exit and cytokinesis? In fact, previous studies in mammalian cells suggest a role for PP1 in the control of cytokinesis (Fernandez *et al*., 1992) and PP1γ was found associated with the cleavage furrow and midbody in HeLa cells (Trinkle-Mulcahy *et al*., 2003). Moreover, in *Drosophila*, PP1 or Sds22 depletion causes cortical instability during cytokinesis in the notum (Kunda *et al*., 2012). A decrease in anaphase elongation rate or cytokinesis could possibly be responsible for an initial delay in Lgl reloading when interfering with PP1 or Sds22, as observed in the graph of Figure 4.7B (in the first 5 minutes after anaphase), but cannot explain the strong delay in Lgl reloading kinetics that is observed afterwards or the strong delay observed in Lgl^{KA,FA}-GFP.

4.5. Lgl cortical localization at mitotic exit is required for correct polarization of daughter cells

A new interface between daughter cells is established upon cell division in the follicular epithelium. Thus, we analyzed the importance of Lgl cortical reloading and PP1 dephosphorylation for *de novo* polarization of the new interface between daughter cells. Firstly, we filmed epithelial cells expressing simultaneously Lgl-mCherry and aPKC-GFP. As suggested by the time-lapse images and kymographs (Figure 4.11 A, B), Lgl starts to localize to the new interface before apical accumulation of aPKC. Moreover, Lgl reloading is completed before aPKC reaches its maximum levels, as suggested by the graph in Figure 4.11C, where the minimum plateau of Lgl cytoplasmic decay occurs before aPKC has reached its maximum. To complement our results, we analyzed the localization of Par6-mCherry simultaneously with Lgl-GFP in an midsagittal perspective. As observed by the time-lapse images, Lgl-GFP accumulates in the new interface before Par6-mcherry has fully polarized to the apical side (Figure 4.11D, black arrows).

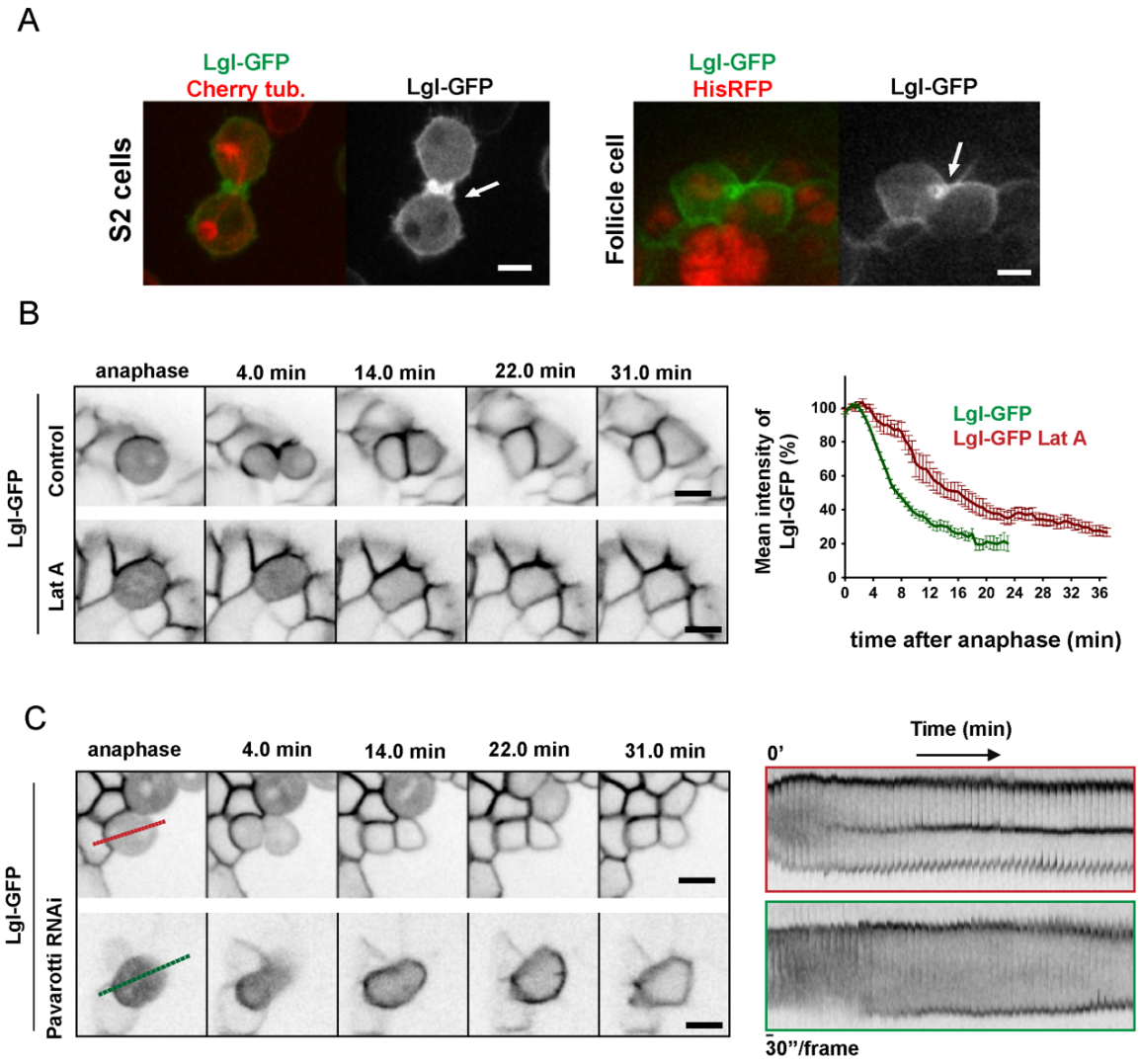

Figure 4.10: The role of cytokinesis in Lgl cortical reloading. A) As indicated by the white arrows, Lgl strongly accumulates in the bridge linking the two daughter cells, termed midbody, in both S2 cells and follicle cells. B) Treatment of epithelial cells with Lat A (5 μg/μl) induces failure in cytokinesis and delays Lgl cortical reloading (n=21 Lgl-GFP; n=14 Lgl-GFP LatA). C) RNAi-mediated depletion of the protein Pavarotti (for 1 day at 29ºC) also delays Lgl cortical reloading in the follicular epithelium. Error bars: mean ± SEM Scale bars: 5 μm

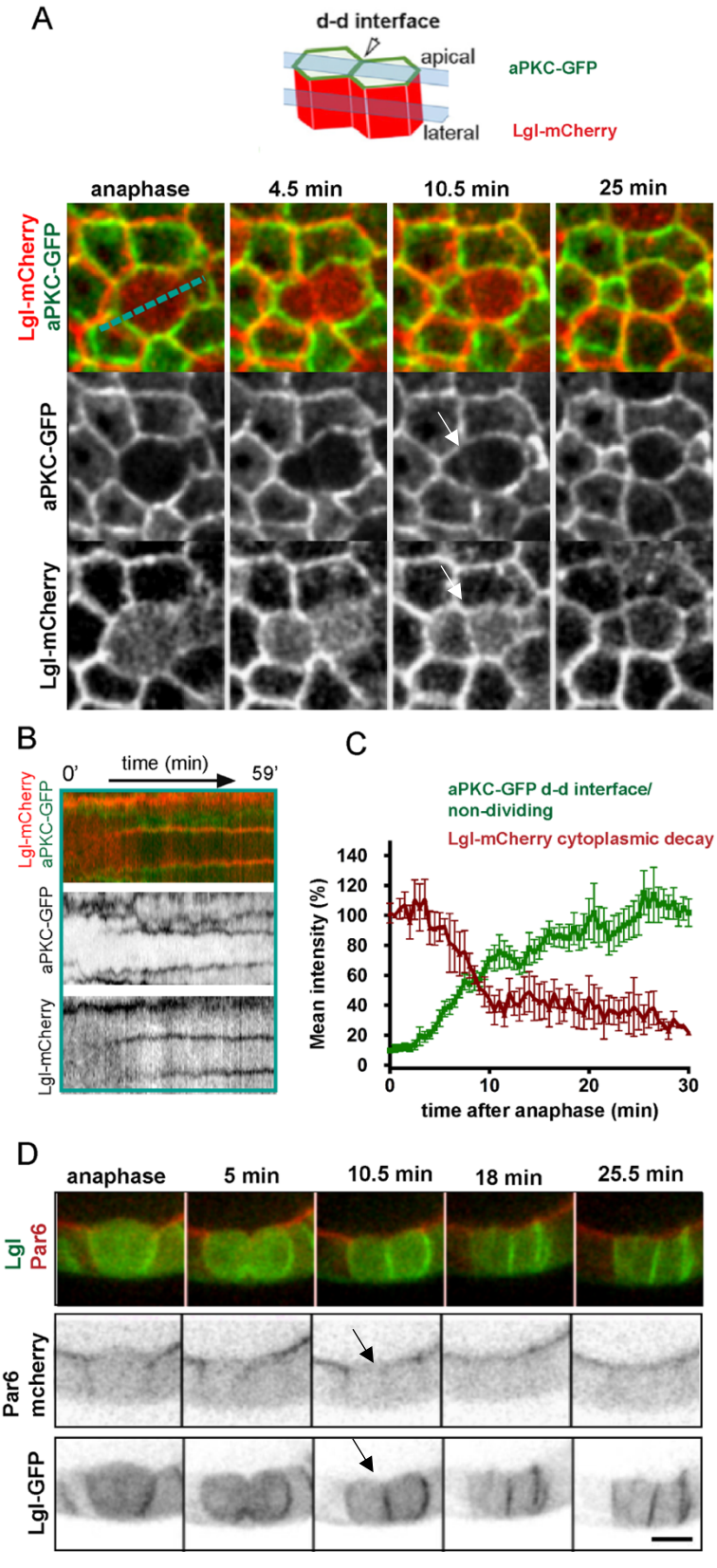

Figure 4.11: Lgl reloading to the cortex precedes aPKC accumulation in the new daughter-daughter interface. A) Time-lapse images of follicle cells expressing aPKC-GFP and Lgl-mCherry at endogenous levels. Maximum projections of selected apical and basolateral planes are shown. Lgl reloading occurs before aPKC accumulation in the apical daughter-daughter (d-d) interface (white arrows). B) Kymographs obtained from the place indicated by the green dashed line in A. C) Graph showing the quantifications of Lgl -mCherry cytoplasmic decay and aPKC-GFP accumulation in the new interface. Lgl in the cytoplasm reaches its minimum when aPKC-GFP its not yet totally established in the apical side (n=12 cells for aPKC-GFP accumulation in the new interface; n=5 cells for Lgl cytoplasmic decay). D) Midsagittal perspective of a follicle cell expressing Par6-mCherry and Lgl-GFP shows that Lgl-GFP accumulates in the new cortical interface before Par6-mcherry is fully accumulated at the apical side (black arrow). Error bars: mean ± SEM. Scale bars: 5 μm

We hypothesized that Lgl cortical reloading could be important to antagonize aPKC in the basolateral side, thereby promoting its accumulation in the apical domain. For that, we examined the segregation of endogenously tagged aPKC-GFP to the apical domain while interfering with Lgl reloading to the cortex. First, we tested the importance of PP1-mediated Lgl reloading in aPKC apical polarization. As shown before (Chapter 3, Figure 3.11), PP1 RNAi disrupts aPKC-GFP localization and induces defects in epithelial architecture. Nevertheless, we quantified the accumulation of aPKC-GFP in the new interface of cells depleted for Pp1-87B but maintaining a correct plan of division. Quantifications of the Lgl accumulation in the new interface of dividing cells were normalized for the signaling of Lgl in neighbor non-dividing cells, whose aPKC-GFP localization was also affected due to the depletion of PP1. Despite this, we observed a delay in its recovery (Figure 4.12A,B). To confirm the importance of Lgl reloading for aPKC polarization, we used a temperature-sensitive allele of Lgl, lgl^{ts3} , which was shown to reallocate to the cytoplasm at restrictive temperature (Manfruelli *et al*., 1996) and thus allows a temporal control of Lgl localization. We confirmed that lgl^{ts3} reallocates to the cytoplasm at 29ºC, but the tissue maintains its monolayered organization during the first 2 hours (Figure 4.12C), allowing access to the specific impact of Lgl localization for aPKC-GFP polarization. We therefore tracked aPKC-GFP accumulation in the apical interface between daughter cells in lgl^{ts3}/lgl^{4} filmed at the restrictive temperature for a maximum of 2 hours at 29ºC. aPKC-GFP accumulation in the apical daughter-daughter interface is strongly impaired in lgl^{ts3}/lgl^{4} cells when compared with control cells harbouring only a mutant allele (Figure 4.12 D,E). Moreover, in an apical-basal perspective, we observed that aPKC is ectopically localized to the basolateral domain in the new daughter-daughter interface of lgl^{ts3}/lgl^{4} mutant cells (Figure 4.12E). These results suggest that Lgl cortical reloading to the new interface restricts aPKC localization to the apical side.

Taken together, our results suggest that by controlling the timing of Lgl cortical reloading, PP1 activation coordinates Lgl dephosphorylation and reloading to the cortex with the apical-basal polarization of the new daughter cells at mitotic exit (Figure 4.13).

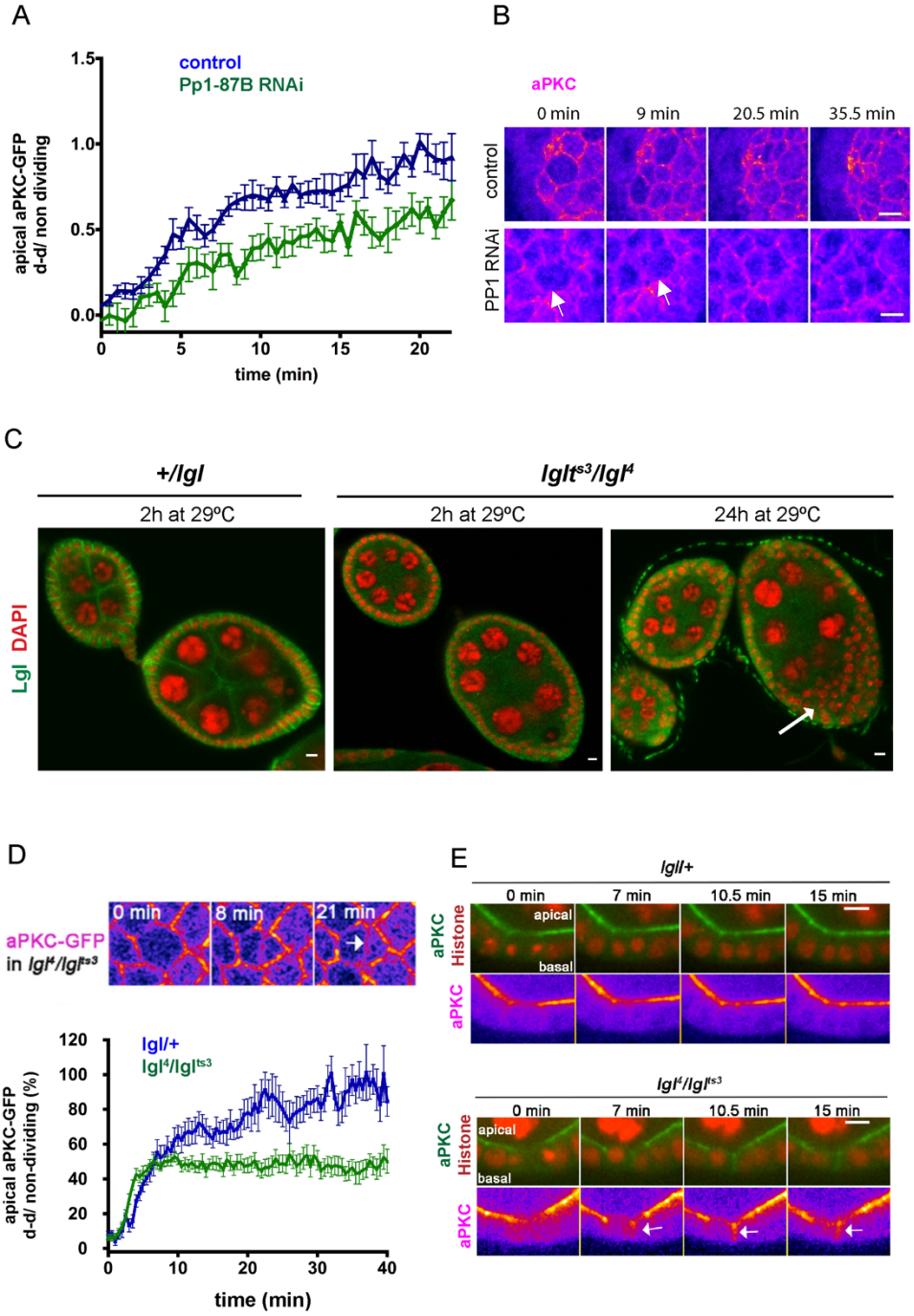

Figure 4.12: Lgl cortical reloading represses the lateral localization of aPKC in the new daughter-daughter interface. A), B) Depletion of Pp1-87B delays Lgl accumulation in the new interface after anaphase (white arrows). Data show mean ± SEM. Scale bars: 5 μm. C) Lgl immunofluorescence in egg chambers of lgl^{ts3}/lg^{4} flies after 2h or 24h at 29ºC, showing that lgl^{ts3} is completely reallocated to the cytoplasm after 2h at 29ºC without affecting the architecture of the epithelia, when compared with epithelial tissue of sibling flies carrying a wild-type copy of Lgl ($lgl^{ts3\ or\ 4}$/+). Mutant flies incubated at 29ºC for 24h display a multilayered

epithelium (arrow). Scale bars: 20 μm. D) aPKC-GFP accumulation at the new interface is strongly impaired in *lgl*^{ts3}/*lgl*^{4} mutant cells from ovaries filmed at restrictive temperature (n= 40 *lgl*^{4}/*lgl*^{ts3} cells; n= 21 *lgl*/+ cells). E) Midsagittal egg chamber sections showing aPKC-GFP mislocalization in the new daughter-daughter interface in *lgl*^{4}/*lgl*^{ts3} mutant cells (arrows), imaged at restrictive temperature. Time 0 min at anaphase. Note: Figures C, D, E are adapted from Moreira *et al.*, 2019; the movies in experiments A), B) and D) were performed by Mariana Osswald, co-author in Moreira *et al.*, 2019.

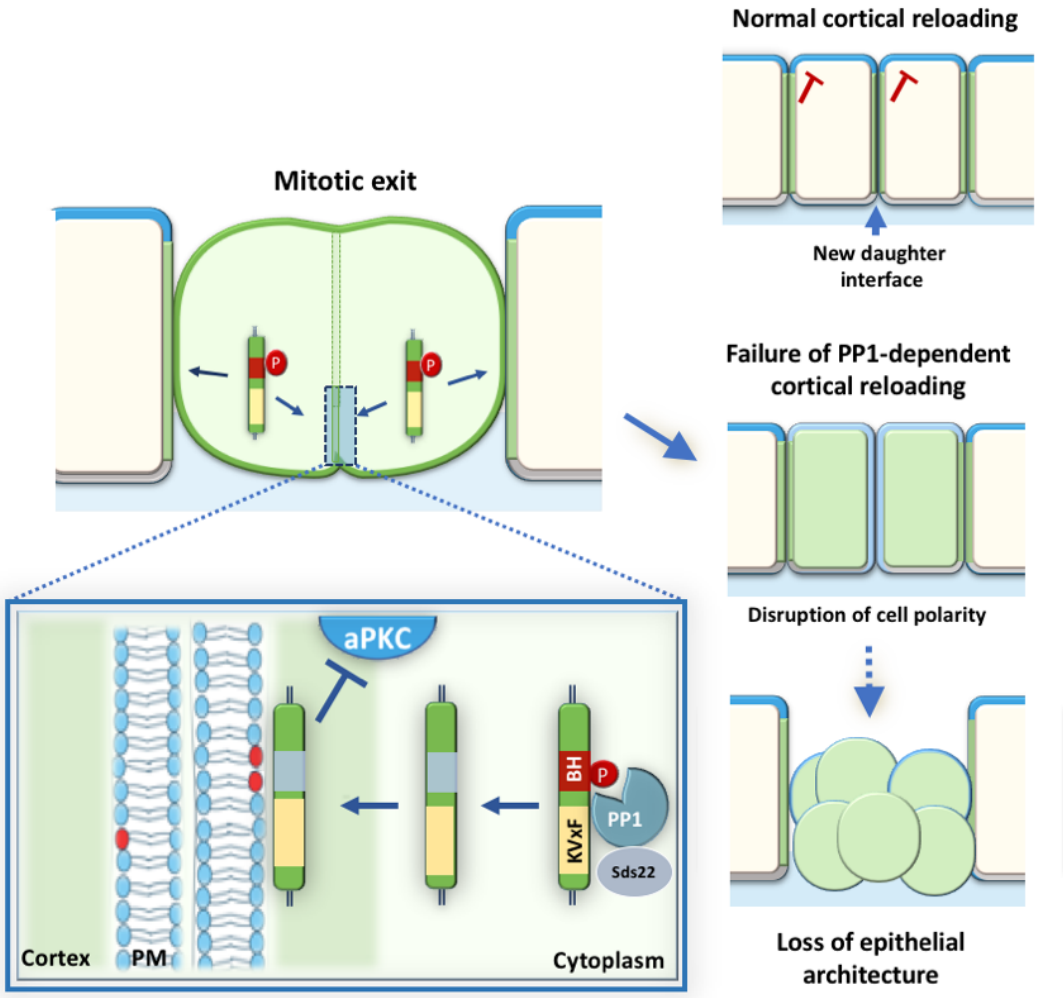

Figure 4.13. Model for how PP1/Sds22 controls Lgl cortical reloading at mitotic exit in epithelial cells (adapted from Moreira *et al.*, 2019). Lgl reloading to the cortex at mitotic exit relies on PP1/Sds22 dephosphorylation through a PP1 docking site motif in Lgl. This mechanism allows the restriction of aPKC in the apical domain of the new interphase between daughter cells and the maintenance of tissue monolayer. Disruption of the docking site motif or depletion of PP1 or Sds22 induces a failure in Lgl reloading to the cortex and disruption of epithelial architecture.

4.6. Discussion

PP1/Sds22 coordinates apical-basal polarization of new daughter cells with mitotic exit

The role of the PP1/Sds22 holoenzyme complex in coordinating events at mitotic exit has been widely described across species. From early studies performed in yeast (Ohkura *et al*., 1991; MacKelvie *et al*., 1995) to later studies in mammalian cells (Posh *et al*., 2010), PP1/Sds22 has been shown to be essential for successful mitotic exit, allowing proper chromosome segregation and timely completion of mitosis. In *Drosophila*, mutations in the *Pp1-87B* locus are lethal at late larval stage, inducing several defects including a delay in mitotic progression and abnormal sister chromatid segregation in neuroblasts (Axton *et al*, 1990). Afterwards, PP1/Sds22 was described to regulate moesin phosphorylation status and induce polar relaxation during anaphase for a proper chromosome segregation in *Drosophila melanogaster* (Kunda *et al*., 2012). Our work unveils a new role for PP1/Sds22, which links cell-cycle regulation at the end of mitosis with the propagation of cell polarity to daughter cells. Upon depletion of Pp1-87B or its regulatory subunit Sds22 in both follicle and S2 cells, we found that Lgl cortical reloading is strongly impaired. How can PP1/Sds22 induce Lgl cortical reloading at mitotic exit? Previous work reveal that Lgl phosphorylation disrupts binding to the plasma membrane by adding negative charges to the basic and hydrophobic (BH) motif of Lgl and weakening electrostatic interactions with phospholipids (Dong *et al*., 2015). Therefore, dephosphorylation by PP1/Sds22 would revert the process, re-establishing the bulk electrostatic charge of the BH domain and then reloading Lgl to all the membranes by increasing its affinity to phospholipids. Moreover, it was shown that Lgl interacts with non-muscle myosin II (NMII) in a manner dependent on Lgl phosphorylation status (Betschinger *et al*., 2005), being also described that Lgl binds electrostatically to a negatively charged region of NMII in mamalian cells (Dahan *et al*., 2011). Therefore, dephosphorylation might increase the electrostatic attraction and binding of Lgl to the plasma membrane and the cortex.

Our experiments in S2 cells allow us to conclude that Lgl reloading at mitotic exit is also mediated by PP1/Sds22 in this system, thus reflecting a cell-cycle dependent process. In these cells, we observed a delay in Lgl cortical reloading using a dsRNA specific for Pp1-87B, which is even more pronounced when depleting all the PP1 isoforms, similarly to what

was observed for Lgl localization in interphase (see Chapter 3). Thus, other PP1 isoforms could act redundantly to allow a more efficient reloading of Lgl excluded by phosphorylation to the cytoplasm during mitosis. In fact, flapwing has also been suggested to have a role at mitotic exit in *Drosophila*, since depletion induces lagging chromosomes and chromosome bridges at anaphase (Bollen *et al*., 2009). The direct role of PP1/Sds22 in regulating Lgl localization is also supported by the delay in cortical reloading observed when the evolutionarily conserved PP1 docking site KVIDF is disrupted. Despite the delay, this mutant form of Lgl is partially reloaded in follicular epithelial cells, suggesting that it is only partially required for PP1-mediated Lgl localization. The other two RVxF motifs found in *Drosophila melanogaster* (Chapter 3) could also play a role in binding to the surface groove of PP1, since the interaction of PP1 with its binding proteins can occur through several binding motifs in different regions of the phosphatase surface to provide more stability to the complex (Moura and Conde, 2019).

I have described in separate chapters the importance of PP1 in Lgl cortical localization during interphase and at mitotic exit. However, these two cell-cycle stages are intimately interconnected, so that the PP1's effect on Lgl cortical reloading at mitotic exit could influence the localization of Lgl in the two daughter cells in interphase and *vice versa*. As an attempt to uncouple the role PP1 in interphase from its role at mitotic exit, we depleted Sds22, a PP1 regulatory subunit described to be important for PP1-mediated events at mitotic exit (Kunda *et al*., 2012). We only observe a mild effect on Lgl localization in interphase, but Sds22 induces a major delay in Lgl cortical reloading in follicle and S2 cells. Curiously, we found that in epithelial cells, Sds22-GFP strongly accumulates in the nucleus, being released to the cytoplasm during mitosis (data not shown), thus supporting a predominant role for Sds22 in the cytoplasm at mitotic exit. Consistent with this, Sds22-GFP was also strongly detected in the nucleus of follicle cells in a previous study (Grusche *et al*., 2009). Despite the delay in Lgl reloading observed in cells depleted for Sds22, Sds22 depletion induces a milder effect on Lgl reloading when compared with Pp1-87B depletion in epithelial cells, which could suggest one of two different scenarios: 1) Pp1-87B downregulation could potentiate the delay in Lgl reloading due to its function during interphase, while Sds22 could act specifically and transiently at a particular time, similarly to what was observed for moesin dephosphorylation at the anaphase cell cortex (Kunda *et al*., 2012); 2) Sds22 could act redundantly with other regulatory subunits to allow robust dephosphorylation of Lgl at mitotic exit and, in this case, other regulatory subunits would act together with PP1 since early interphase. Thus, it is possible that Sds22 could act in a transient time-window to boost PP1 activity, which is necessary to deal with the complete pool of Lgl in the phosphorylated form during mitosis.

Curiously, in the follicular epithelia, we observed a higher delay in $Lgl^{KA,FA}$-GFP reloading when depleting Sds22, which supports the importance of Sds22 for a robust PP1 dephosphorylation at mitotic exit, particularly when the evolutionarily conserved docking site is perturbed. There is no evidence for a direct interaction between Lgl and Sds22, and so we cannot put forward the hypothesis that Sds22 acts as a redundant recruitment factor for Lgl. Alternatively, it was shown that Sds22 is important for PP1 activity by regulating the metal recruitment at the active site of PP1 (Heros *et al*., 2013) and bringing a chaperone complex that promotes PP1 folding (Brautigan *et al*, 2018). Another possible hypothesis is that other regulatory subunits might control PP1-mediated dephosphorylation of Lgl through the evolutionarily conserved motif KVIDF, whereby Sds22 acts separately in Lgl recruitment to the complex.

The impact of Aurora A and aPKC kinases in Lgl cortical reloading

Our work suggests that Aurora A degradation at the end of mitosis is unnecessary for proper Lgl reloading. In *Drosophila* eye imaginal discs (a monolayer of epithelial cells that will give rise to the adult eye), the APC/C co-activator *rap/Fzr* was shown to be important for the correct pattern formation of the developing eye, allowing a timely degradation of cell cycle regulators and proper mitotic exit of precursor cells (Pimentel and Venkatesh, 2005). In the follicular epithelia, however, mutant clones for *rap* do not show polarity defects or disruption of the tissue organization. A possible explanation could rely on the different intrinsic nature or origin of the two epithelia, or simply on different mutant alleles used or the fact that all wing disc cells are mutant, contrasting with our mutant clonal analyses. Despite this, we observed what seems to be some micronuclei in the mutant *Fzr* clones, which could result from a mis-regulation of cell cycle events reported in *rap/Fzr* mutants (Pimentel and Venkatesh, 2005). Accordingly, a study in human fibroblasts describe a role for APC^{Cdh1} in preventing chromosomal instability and micronuclei formation (Engelbert *et al*., 2008).

Regarding aPKC, the other important kinase for Lgl phosphorylation, we have shown that it does not repress Lgl reloading in the follicular epithelium, while it has an inhibitory role towards Lgl reloading in S2 cells. In epithelial cells, aPKC is localized at the apical side during interphase, being physically separated from the basolateral Lgl at mitotic entry, but progressively spreads throughout the cortex of dividing cells (Morais-de-Sá and Sunkel, 2013). However, aPKC does not play a major role on Lgl cortical exclusion in epithelial cells, because interfering with this kinase only causes a minor delay in Lgl accumulation in the cytoplasm (Carvalho *et al*., 2015). Lgl cortical release is therefore mainly attributed to

Aurora A, which is critical to ensure Lgl cortical release at early stages of mitosis (Carvalho *et al*., 2015). By contrast, in S2 cells, aPKC was shown to be able to phosphorylate and partially exclude Lgl from the cortex from early mitosis (Carvalho *et al*., 2015). In this system, aPKC is distributed in the cytoplasm throughout the cell cycle (Kono *et al*., 2019; Osswald *et al*., 2019), allowing the kinase to easily phosphorylate Lgl. These results suggest that aPKC activity towards Lgl is significantly higher in S2 cells, potentially explaining the naturally occurring delay of Lgl reloading to the cortex in unpolarized cells when compared with epithelial cells (note that cytoplasmic decay of Lgl-GFP in epithelial cells is much faster than in S2 cells – compare Figure 4.2B for decay in epithelial cells with Figure 4.5G for decay in S2 cells). In S2 cells depleted for aPKC, downregulation of PP1 still delays Lgl cortical reloading, suggesting a role for PP1 towards Lgl independent of aPKC. However, the delay observed is higher in cells depleted for PP1 in which aPKC is active. This suggests the existence of an equilibrium between PP1 and aPKC activities towards Lgl for reloading to the cortex in S2 cells.

In epithelial cells, we have seen that Lgl cortical reloading precedes the apical accumulation of aPKC in the new interface. This result suggests that Lgl reloading is the timer for aPKC polarization in the new interface. As a way to adress the impact of PP1-mediated dephosphorylation of Lgl for the polarization of aPKC, we depleted PP1 and quantified the apical accumulation of aPKC-GFP in the new interface between daughter cells. Due to the effects of PP1 on cell polarity, the neighboring non-dividing cells were significantly affected regarding aPKC-GFP polarization, and since aPKC intensity values in the new interface were normalized to the neighboring cells, the intensity values observed do not reflect the real impact of downregulating Pp1-87B. As an alternative, this experiment should be performed using clonal depletion of Pp1-87B to compare aPKC-GFP with neighboring cells not affected by the Pp1-87B depletion during interphase. Nevertheless, we used another strategy to analyze the impact of Lgl reloading on the polarization of aPKC using a temperature-sensitive allele, lgl^{ts3}, that induces cytoplasmic accumulation of Lgl. Curiously, disrupting Lgl cortical localization at mitotic exit induces defects in aPKC polarization in the new interface, but not in pre-existent ones. The new interface between daughter cells has to be polarized *de novo*, and so this result suggests that some other polarized factors antagonize aPKC redundantly with Lgl to repress aPKC accumulation at the lateral cortex of the pre-existing membranes. As I will discuss in the next chapter, other basolateral proteins, namely Dlg and Scrib, also have the ability to antagonize aPKC independently of Lgl, and these proteins are maintained in the cortex throughout the cell division (Carvalho *et al*., 2015) so they may provide the polarizing cues in the new daughter cells.

Cytokinesis and formation of a new interface: does it matter for Lgl cortical reloading?

Cytokinesis is the constriction of the actomyosin contractile ring that is connected to the plasma membrane at the equator of the cell. In most epithelial tissues, this process generates a new interface between the daughter where new polarity domains and adhesive contacts must be established *de novo*. We found that Lgl accumulates in this new interface from the basal to the apical side in follicular and embryonic epithelium, following the ingression towards the apical side of the cleavage furrow typically observed in these epithelial tissues (Morais de Sá *et al*., 2013; Bras and Borgne, 2014). A strong possibility is that, as soon as Lgl is dephosphorylated, it can bind to high affinity partners of the contractile ring, such as the phosphoinositides (PIPs) of the ingressing plasma membrane.

The second step of cytokinesis consists in the formation of the midbody, composed by the central spindle and contractile ring components present at the end of ring constriction. We found that both in S2 cells and in the follicular epithelia, Lgl seems to accumulate strongly in the midbody, which is positioned apically close to the apical domain in the follicular epithelium (Morais de Sá *et al*., 2013). The midbody is a structure strongly rich in PIP_2 and actin (Thieleke-Matos *et al*., 2017) two of the major binding partners of Lgl (Betschinger *et al*., 2005; Dong *et al*., 2015) and maybe therefore an important place for Lgl accumulation for a faster redistribution to the rest of the plasma membrane. In fact, Lgl is a protein that binds to plasma membrane and has a very high mobility (as will be discussed in Chapter 5), and so it can be redistributed faster to the rest of the membranes once strongly accumulated in the midbody. However, the accumulation of Lgl at the midbody is not required for reloading, since disruption of cytokinesis does not prevent cortical accumulation of Lgl at mitotic exit. Despite this, Lgl reloading is slightly delayed in these conditions, suggesting that the midbody could in fact promote faster recruitment to the plasma membrane. Curiously, in S2 cells, the midbody formation occurs around 12 minutes after anaphase (Kechad *et al*., 2012) much latter than the formation of the midbody in follicle cells, which takes about 3-4 minutes (Morais de Sá *et al*., 2013). Also, according to our data in S2 cells, Lgl reloading becomes faster after ~ 12 min (the rate of the linear regression obtained for values between anaphase and 12 min is -1.74, while the rate obtained after the linear regression of values between 12 min and 30 min is -2.545). This might overlap with Lgl accumulation in the midbody, allowing a faster redistribution to the membrane

(Movie 3). In the follicular epithelium, the midbody formation occurs earlier, which might be correlated with a faster Lgl reloading in these cells when comparing with S2 cells.

Concluding, our results identify an essential role for PP1/Sds22 dephosphorylation in Lgl reloading at mitotic exit and the contribution of the midbody formation to accelerate Lgl redistribution to the new daughter cell membranes. This PP1-mediated cortical reloading of Lgl also aids the polarization of the new apical domain at the interface between daughter cells. Hence, our study indicates that cell-cycle dependent control of PP1 activity plays a key role in apical-basal polarity, coupling cell division with the polarization of the new daughter cells to maintain epithelial function during proliferation.

Chapter 5

Exploring the potential interaction of Lgl with Dlg *in vivo* using FRAP

5.1. Introduction

As described in the previous chapter, Lgl is reloaded to the cortex at mitotic exit, rebuilding the basolateral domain of the daughter cells. In this domain, Lgl cooperates with other two basolateral polarity proteins, Dlg and Scrib, to establish and maintain the apical-basal polarity. However, how exactly these three proteins work together for basolateral determination and which individual functions they may perform remain open questions in the cell polarity field.

The idea that Lgl, Dlg and Scrib proteins cooperate in a common pathway to control cell polarity came from early studies in *Drosophila*, based on their similar localization and on genetic interactions observed between them (Bilder and Perrimon, 2000; Wodarz, 2000). Moreover, an interdependence observed between the localization of these proteins led to assumption that the three could form the so-called "Scrib complex". This terminology has lately been replaced by the term *module* due to lack of evidence for physical interactions between them. In fact, although the three proteins depend on each other for their correct cellular localization, whether this results from direct physical interaction or indirect effects of loss of cell polarity remains unknown. Nevertheless, physical interactions were reported between Scrib and Dlg in the *Drosophila* neuromuscular synapses, although indirectly mediated through a protein termed GUK-holder (GUKH) (Mathew *et al*., 2002). Until now, a physical interaction between Scrib and Lgl was reported in mammalian epithelial cells (Kallay *et al*., 2006), whereas Lgl was found to interact directly with the GUK domain of Dlg in a phosphorylation-dependent manner (Zhu *et al*., 2014). However, there is not direct evidences for the *in vivo* interaction between any of the three components of the basolateral module in epithelial tissue.

In our lab, we used FRAP (**F**luorescence **R**ecovery **A**fter **P**hotobleaching) for a detailed analysis on the dynamics of the three basolateral proteins, Dlg, Lgl, and Scrib, in the follicular epithelia tissue (Figure 5.1). This technique is based on the irreversible photobleaching of a fluorescent-tagged protein in a region of interest and the subsequent monitoring of the rate at which a new steady-state is established by replacement of bleached proteins by unbleached ones. The use of FRAP has been widely reported in several contexts to study protein mobility *in vivo* and can answer a huge number of questions. In our group, it was implemented and optimized as part of the master thesis work of Guilherme Ventura to address the interaction of Lgl with its multiple cortical binding

partners in the follicular epithelium and the implication of Lgl phosphoregulation in these interactions (Ventura *et al*, unpublished results). Combining the FRAP technique with genetic and pharmacological manipulation, previous work performed by Guilherme Ventura describes the impact of phosphoinositides (PIPs) and cortical actomyosin on Lgl dynamics at the cortex of the follicular epithelium (Figure 5.1C). Here I describe some of my contributions to this work which is centered on the use of FRAP to understand Lgl's interaction with Dlg. This question will be deeply addressed in the current chapter, starting from the observation that Dlg delays Lgl recovery dynamics in the basolateral domain.

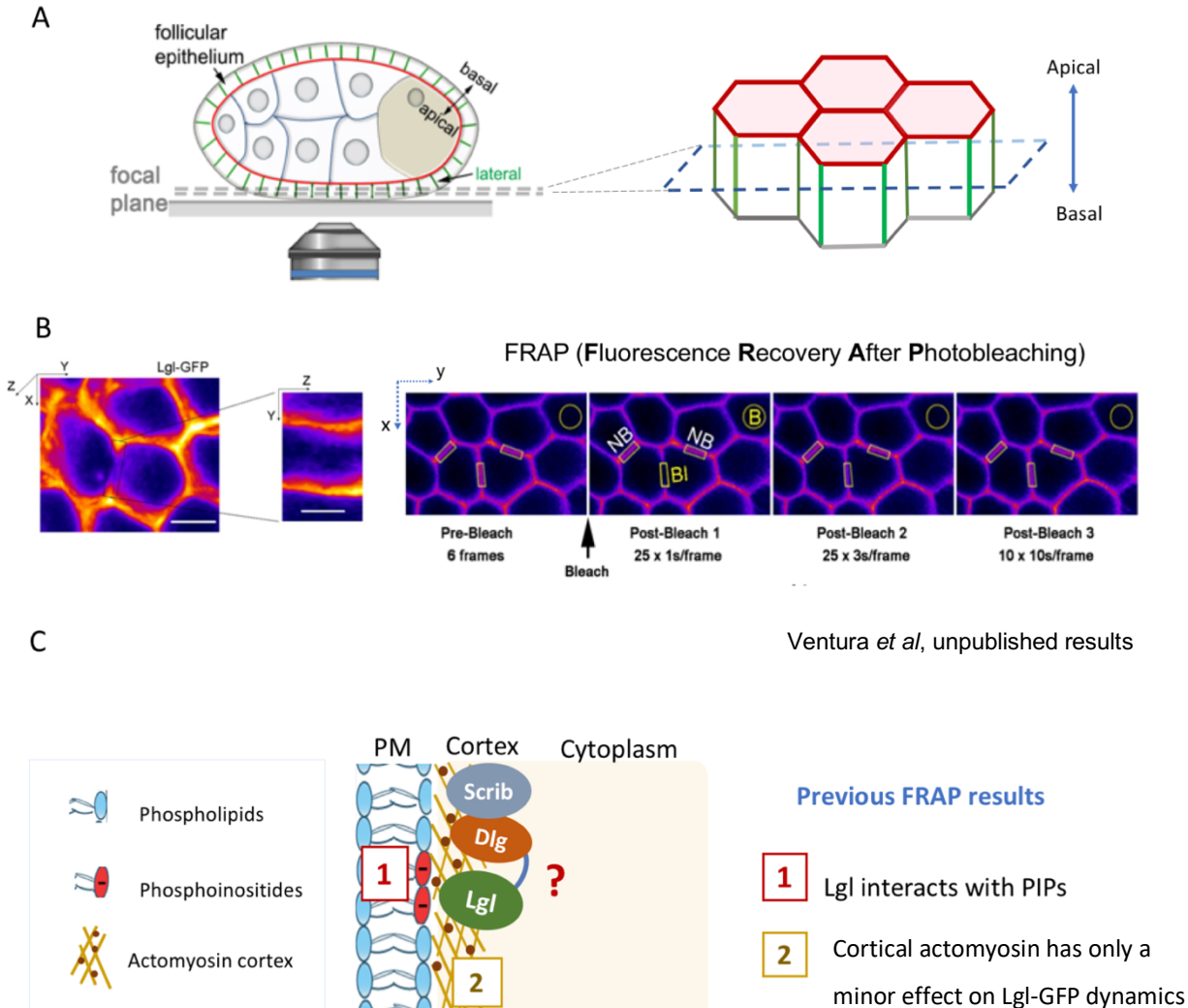

Figure 5.1: Implementation of a FRAP (Fluorescence Recovery After Photobleaching) protocol to study Lgl-Dlg interaction *ex vivo*. A) Schematic representation of an egg chamber and the selected basolateral plan of the follicular epithelium for FRAP experiments. B) An example of the FRAP protocol applied for the basolateral protein Lgl-GFP. The efficient photobleaching of Lgl-GFP along the Z axis is observed by the maximum intensity Z-stack projection and by the orthogonal YZ view of the bleached region. An example of a photobleaching experiment for Lgl-GFP is also shown: in the basolateral section of the follicular epithelium, an interface between two cells was bleached using a ROI 3 µm x 1 µm (BI) and recovery was measured in this region. Two non-adjacent interfaces (NB) were also measured to correct for changes in plane or fluorescence loss during the acquisition. The background (B) was measured in the nucleus position of a non-adjacent cell and subtracted from the output measurements. These results are previous unpublished data (Ventura *et al.*). C) Previous results from the lab report the impact of PIPs and cortical actomyosin in the recovery dynamics of Lgl-GFP. How Dlg impacts Lgl dynamics will be addressed in this chapter.

5.2. Characterization of basolateral polarity protein dynamics using FRAP

In theory, if Dlg, Lgl and Scrib proteins would form a stable immobile complex at the cortex, they should display similar FRAP dynamics. We analysed the dynamics of each protein in the follicular epithelium using GFP-tagged proteins at endogenous levels (Figure 5.2) and we focused on egg chamber stages ranging from 7 to 9 to avoid any contribution of mature septate junctions (SJ) at later stages (Mahowald, 1972). After photobleaching and data acquisition, fluorescence intensity (average of all pixels within the bleached spot) was measured through time and normalized to neighboring interfaces to correct for photobleaching and plane change (see *Chapter 2* for details in the quantification method). We observed very different half-times in the recovery dynamics for the three proteins (mean half-time values: Lgl-GFP$^{t1/2}$= 10.98 s, Dlg-GFP$^{t1/2}$= 42.87 s; Scrib-GFP $^{t1/2}$= 60.83 s) (Figure 5.2 A,B). These distinct half-times are detectable in the time-lapse images and kymographs of bleached regions in representative cells (Figure 5.2C) and are likely to reflect the independent roles for each protein in the basolateral domain.

Another relevant observation in the FRAP recovery profiles is the existence of a fraction that is not recovered (≈ 10% for Lgl; ≈ 20% for Dlg and ≈30% for Scrib), which is normally termed the immobile fraction since it can reflect a protein pool that is stably bound to its partners and cannot be replaced by unbleached protein. Since this parameter could be valuable to access protein interactions with cortical or plasma membrane components we accessed if lack of full fluorescence recovery could also be an artifact of the bleaching process and acquisition. We addressed this issue by performing two consecutive bleaching experiments in the same bleached ROI. If fluorescence loss was due to the disappearance of the immobile fraction after the first photoperturbation, it would be anticipated that the second recovery curve would reach about 100% of the fluorescence that remained after the first bleach (Figure 5.3A). However, the recovery plateau that resulted from the photobleaching experiment is identical to the first one, suggesting that the apparent immobile fraction (≈ 10%) is induced by the bleaching and data acquisition process, which could give rise to a false immobile fraction as a result of protein damage and crosslinking induced by free radical species (Lippincott-Schwartz and Patterson, 2003).

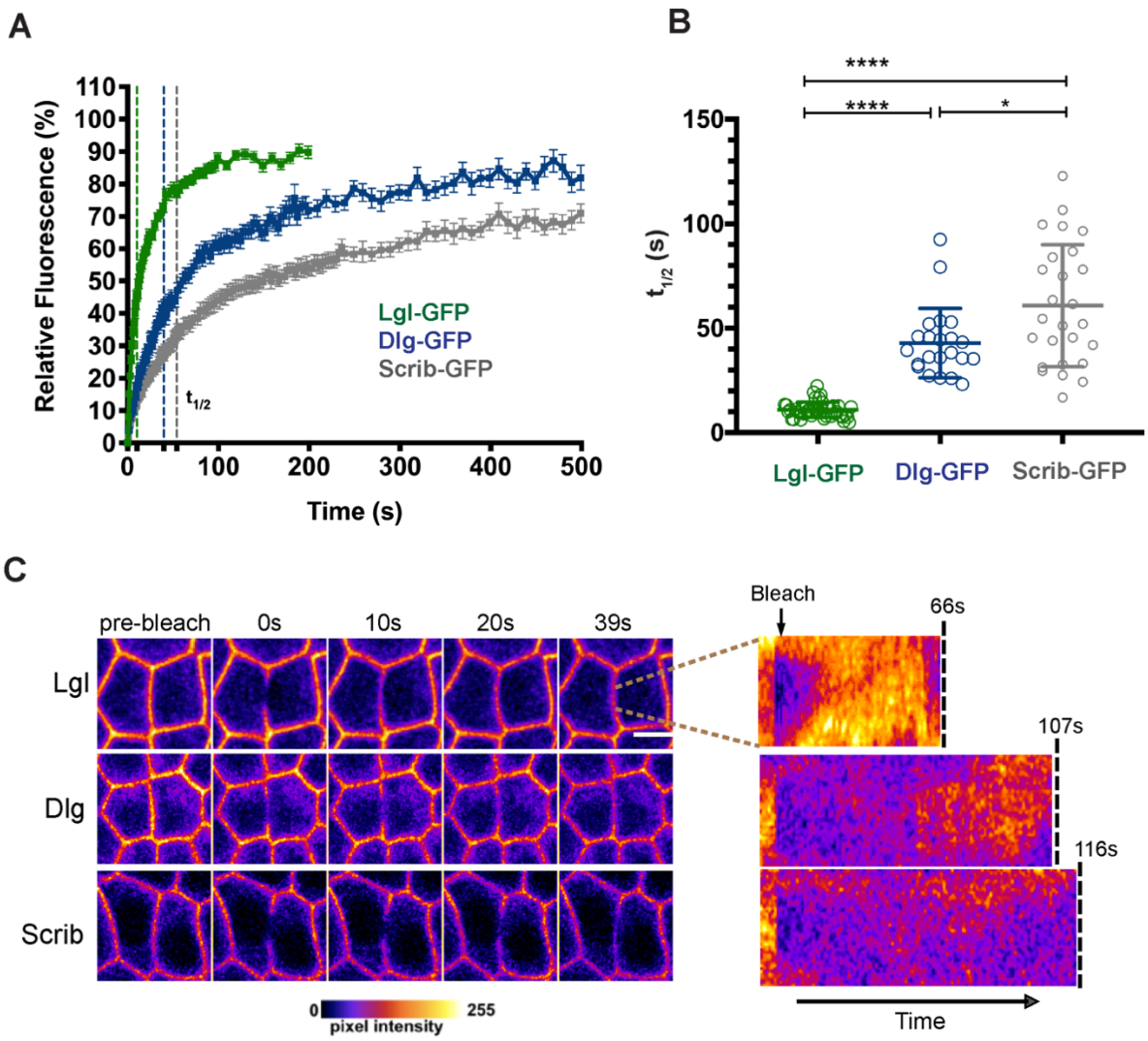

Figure 5.2: Characterization of the dynamics of Dlg, Lgl and Scribble using FRAP.

A) Quantifications of the recovery dynamics of Lgl-GFP, Dlg-GFP and Scrib-GFP reveal very distinct mobility between the three basolateral proteins in the follicular epithelium. Error bars: mean ± SEM. B) Scatter plots showing the half-time ($t_{1/2}$) distribution of Lgl-GFP ($t_{1/2}$= 10.98 s, n= 44), Dlg-GFP ($t_{1/2}$= 42.87 s, n= 22) and Scrib-GFP ($t_{1/2}$=60.83 s, n= 26). The Shapiro-Wilk was used to test the normal distribution of the data and the Bartlett's test was used to test for the heteroscedasticity, to check the assumptions of the ANOVA. The Shapiro-Wilk test was significant for Lgl-GFP and Dlg-GFP (p=0.0257 for Lgl-GFP; p=0.0020 for Dlg-GFP). The Bartlett's test was also significant (p<0.0001). Since the two tests indicate that the data distribution is not normal and that the variances are not equal, we used a non-parametric multiple comparison test, the Kruskal-Wallis test, to perform the statistical analysis. Mean and error bars indicating SD are shown. C) Time-lapse images and kymographs showing the different recovery dynamics in the bleached region. Images and kymographs are pseudo-colored to reflect the intensity levels of fluorescence in the bleached region (the scale of intensities is represented below the time-lapse images). Time after photobleaching is also indicated. Scale bar= 5 μm

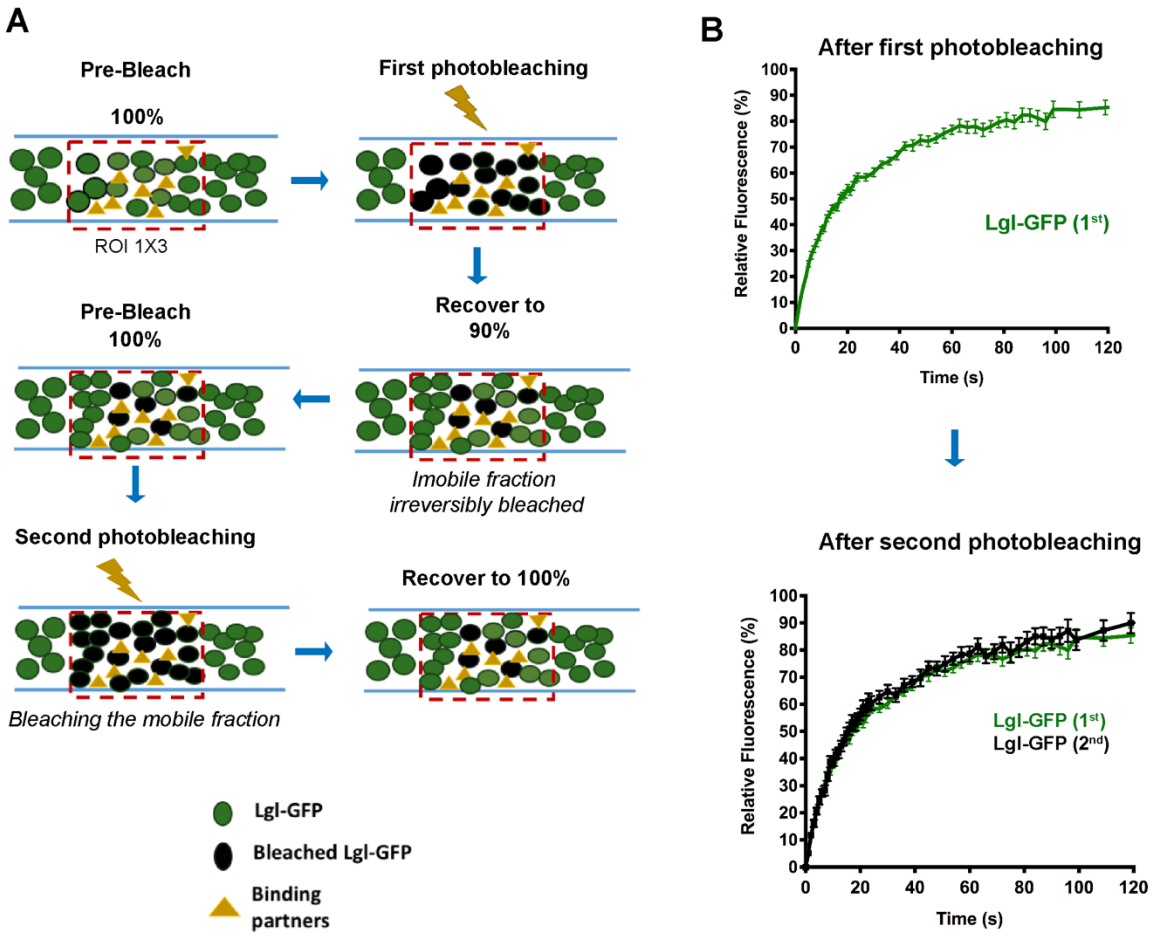

Figure 5.3: FRAP protocol used to analyze the biological relevance of the immobile fraction of Lgl. A) Schematic representation of the method used to address the significance of the immobile fraction detected in the recovery plots. Two consecutive photobleaching pulses in the same region are performed using the same FRAP protocol and ROI dimension. After the fluorescence recovery of the first photobleaching reaches an equilibrium, only the mobile fraction should account for the second photobleaching experiment. Therefore, if the immobile fraction is real, the recovery after the second photobleaching is expected to reach a plateau of 100%. B) The recovery plots obtained after two consecutive photobleaching are identical (n=12 cells), suggesting that the immobile fraction (≈ 10%) observed in Lgl-GFP may result from an artifact of the bleaching process. Error bars: Mean ± SEM.

We therefore decided to focus only on the evaluation of the fluorescence recovery kinetics (half-time) of the proteins to analyze the impact of Dlg on Lgl dynamics. Fluorescence recovery time in a certain ROI can be influenced by protein interaction with binding partners and its dissociation rate, which hinder molecules to diffuse freely (Sprague and McNally, 2005). Diffusion of a protein can be defined by the rate of movement of particles due to random motion, and can generally be the result of lateral diffusion (when protein movements occur in the lipid membrane) or cytoplasm-membrane exchange. According to Sprague and

McNally, 2005, FRAP recovery is diffusion-coupled when the time to diffuse across the bleached ROI is comparable to or longer than the time necessary to bind its partners. On the other hand, when diffusion is much faster than the binding component, it is considered diffusion-uncoupled and the initial diffusion can be negligible since only contributes for a very small initial fraction of the fluorescence recovery. Therefore, in a diffusion-uncoupled recovery, the diffusion phase is short and is followed by a much longer binding phase. To test if recovery of each protein is diffusion-coupled, we took advantage of an already validated strategy based on the use of different sized ROIs in the photoperturbation step (Goehring *et al*., 2010; Rino *et al*., 2014). Since the distance fluorescent molecules must diffuse will increase using a larger box for photobleaching, changing the box size will alter the recovery kinetics of diffusion-coupled proteins. Therefore, diffusion is influenced by the space dimension, and if it is rate-limiting, larger ROIs should result in slower dynamics. On the other hand, diffusion-uncoupled proteins will exhibit no differences in recovery dynamics using the two ROIs of distinct size since the initial diffusion component would be negligible and the dynamics will mainly rely on the reaction kinetics of binding/unbinding to its partners. As schematically represented in Figure 5.4A, we used two distinct ROIs for photoperturbation, one 3 µm x 1 µm and a smaller one, 1.5 µm x 1 µm. Based on this analysis, we concluded that Lgl-GFP and Dlg-GFP have a diffusion-coupled dynamics, since they exhibit faster recovery using the small ROI for photobleaching (Figure 5.4B-F). Additionally, membrane diffusion can be detected by the recovery profile in kymographs, where it becomes evident that Lgl and Dlg molecules diffuses laterally, since fluorescence recovery initiates at the edge of the photobleached region and not uniformly as expected for proteins mainly exchanging between the plasma membrane and cytoplasm. Thus, we conclude that lateral diffusion has a significant contribution to the dynamics of Lgl and Dlg recovery. Similar observations regarding Dlg-GFP spreading from lateral regions in embryos were previously described (Oshima and Fehon, 2011). To further confirm the lateral diffusion of Lgl, we did a simple test, measuring the fluorescence intensity in an interface adjacent to the photobleached ROI, as illustrated in Figure 5.5A. In the case of lateral-diffusion, it would be expected that the bleached proteins will diffuse to the adjacent region, thereby decreasing the fluorescence intensity in an adjacent interface. In fact, while we observed that Lgl-GFP fluorescence increases in the photoperturbed region, a decrease is observed in the second ROI measured in the adjacent interface (Figure 5.5B). This decrease is not related with acquisition or bleaching damage of this interface since values were corrected to the loss of fluorescence in the imaging plane at each time-point.

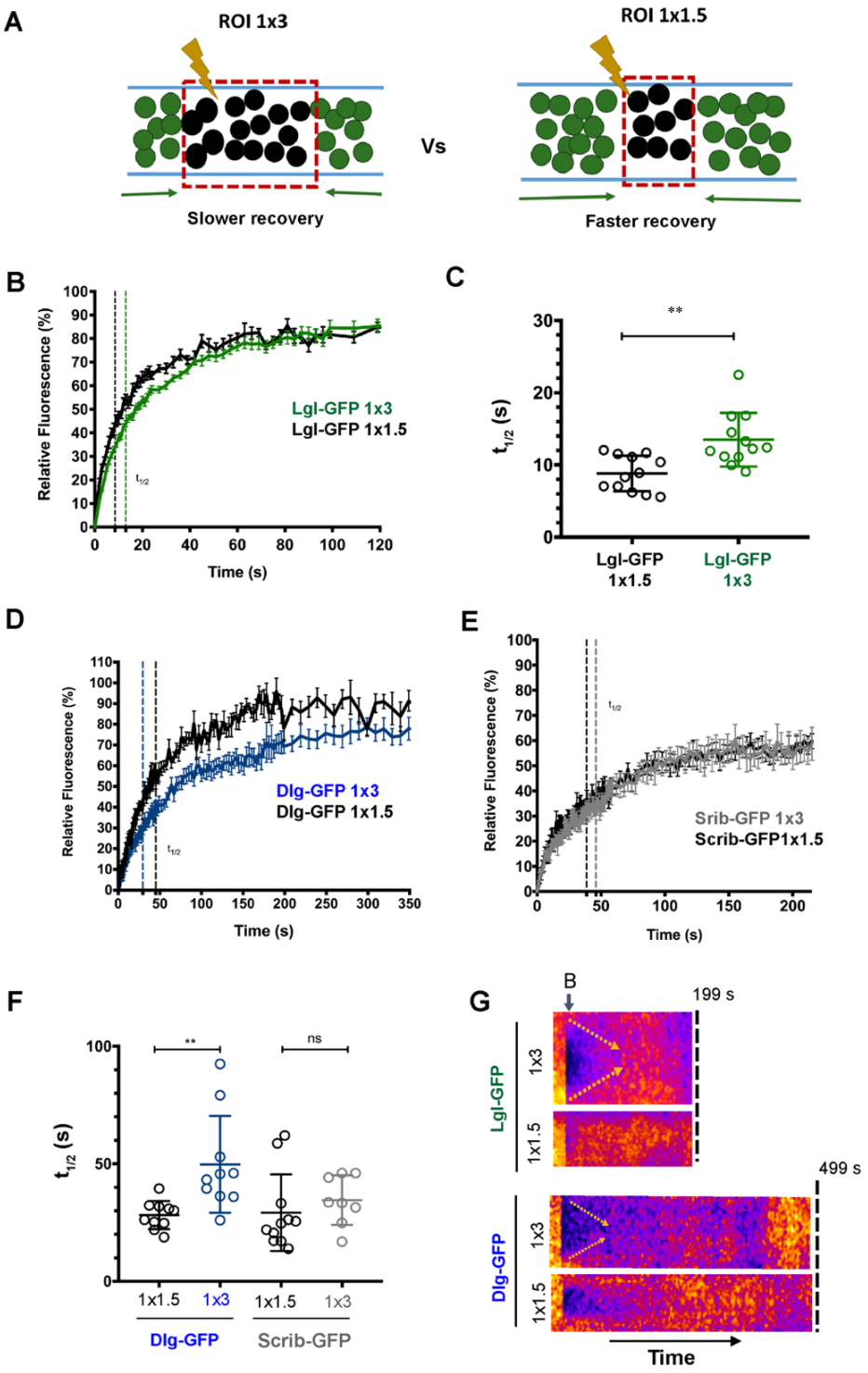

Figure 5.4: Lgl and Dlg dynamics are coupled to lateral membrane diffusion. A) We used two ROI with different size to test if protein diffusion played a significant role in the fluorescence recovery dynamics. B) Fluorescence recovery profiles of Lgl-GFP using two differently sized ROIs. Error bars: Mean ± SEM. C) Scatter plots showing the half-time ($t_{1/2}$) distribution of Lgl-GFP using different ROIs ($t_{1/2}$ (1.5x1)= 8.80 s; $t_{1/2}$ (1x3)=13.48 s). We used the Shapiro-Wilk's to test the normal distribution of the data. The Shapiro-Wilk test was not significant for both conditions (Lgl-GFP (1x1.5) p=0.1059; Lgl-GFP (3x1) p=0.3810), and so the null-hypothesis that data

are normally distributed is not rejected. Therefore we used a parametric unpaired t-test with 95% CI and found that the two groups are statistically different (**p=0.0015). Mean and error bars indicating SD are shown. D,E) Recovery profiles of (D) Dlg-GFP and (E) Scrib-GFP, using two differently sized ROIs. Error bars: Mean ± SEM. F) Scatter plots showing the half-time ($t_{1/2}$) distribution of Dlg-GFP and Scrib-GFP using different ROIs (Dlg-GFP: $t_{1/2}$ (1.5x1)=28.17 s; $t_{1/2}$ (1x3)= 49.73 s; Scrib-GFP: $t_{1/2}$ (1.5x1)= 29.17 s; $t_{1/2}$ (1x3)= 34.44s). The Shapiro-Wilk test was not significant for Dlg-GFP experiments (Dlg-GFP (1x1.5) p=0.9073; Dlg-GFP (3x1) p=0.0520), therefore we used a parametric unpaired t-test with 95% CI and found that the two groups are statistically different (**p=0.0052). Regarding Scrib-GFP, since one of the group has a significant p value for Shapiro-Wilk test (Scrib-GFP (1x1.5) **p=0.0046; Scrib-GFP (3x1) p=0.3743), meaning that it does not follow a Gaussian distribution, we used a non-parametric Mann-Whitney test and found that the two conditions are not statistically significant (p=0.1986). ns-non significant. Mean and error bars indicating SD are shown. G) Kymographs of the bleached region, showing Lgl-GFP and Dlg-GFP recovering using two different sized ROIs. As indicated by the arrows, recovery initiates at the edges, as anticipated by the impact of lateral-diffusion in Lgl recovery dynamics. B indicates the bleach time-point.

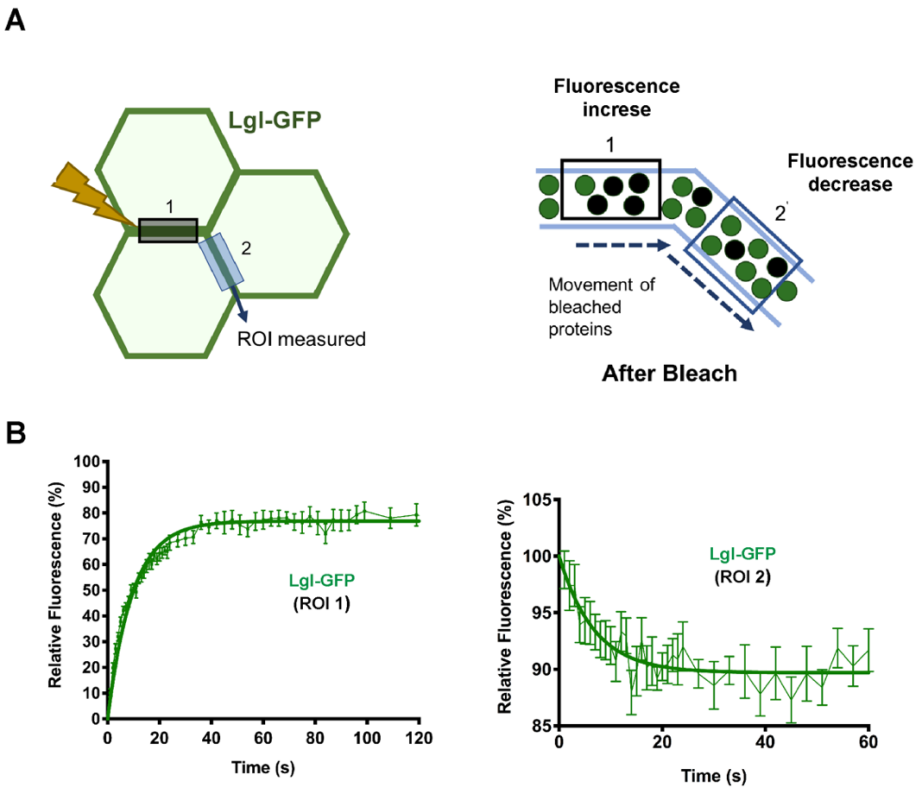

Figure 5.5: Exploring the lateral-diffusion properties of Lgl. A) Schematic representation of the method used to confirm the lateral-diffusion of Lgl-GFP. A decrease in the fluorescence in an interface region adjacent to the bleached region should be expected due to the diffusion of bleached molecules. B) Plots showing the fluorescence intensity of Lgl-GFP recovery in the bleach region and in the adjacent region. Intensity values obtained from the adjacent ROI were normalized to the mean intensity in the entire image to take into account the photobleaching occurring during live imaging process. Initial decrease in fluorescence is shown in the first 20s after photobleaching. Error bars: mean ± SEM.

Taken together, this first set of data indicate that the polarity proteins Dlg, Lgl and Scrib display very distinct mobility in the basolateral domain. Lgl is the most mobile protein and displays a lateral diffusion-coupled dynamics. Dlg is less mobile than Lgl and has a similar mean half-time recovery to Scrib. However, while Dlg also displays a lateral diffusion-coupled dynamics, Scrib recovery seems to result mostly from cytoplasmic-membrane exchange. These different recovery behaviors might suggest distinct roles between the three proteins.

5.3. Loss of Dlg accelerates Lgl recovery due to increased aPKC phosphorylation and not by disruption of Dlg-Lgl complexes

We then explored the possible significance of an interaction between Dlg and Lgl for Lgl dynamics, since *in vitro* experiments and X-ray crystallography studies provided evidence for interaction between Lgl and the guanylate kinase domain (GUK) of Dlg (Zhu *et al*, 2014). According to this study, this interaction is dependent on Lgl phosphorylation, since an unphosphorylated form of Lgl is unable to interact with the GUK domain of Dlg. Thus, we took advantage of the already available aPKC-unphosphorylatable mutants for Lgl, in which the five serines predicted to be phosphorylated by aPKC and Aurora kinases were mutated to alanines (Dong *et al*, 2015). The existence of a relevant interaction of Lgl with Dlg is expected to interfere with the mobility of the protein. Therefore, we performed FRAP in an unphosphorylatable Lgl, Lgl^{5A}, raising the possibility that the expected inability to interact with Dlg would accelerate Lgl. As observed in Figure 5.6A, no significant differences in the half-time recovery were observed between the two forms of Lgl. Similarly, no differences were detected between overexpressed Lgl-GFP and overexpressed Lgl^{3A}-GFP (Figure 5.6B), in which the three serines necessary for Lgl binding to the GUK domain were mutated to alanines (Zhu *et al*, 2014).

A possibility would be that Lgl could bind Dlg in a phosphorylation-independent manner. In fact, we can co-immunoprecipitate Lgl^{3A}-GFP together with Dlg using ovaries extracts (Figure 5.6C). Thus, to further understand the putative role of Dlg in Lgl dynamics, we performed FRAP experiments in *dlg* mutant follicle cells. As anticipated from previous work showing the interdependence between the localization of these basolateral proteins (Bilder *et al*., 2000) endogenous Lgl-GFP is strongly mislocalized in the cytoplasm in *dlg* mutant clones (Figure 5.7A). This result could suggest that Dlg is an important partner for anchoring Lgl in the cortex. However, the unphosphorylatable form, Lgl^{5A}-GFP, remains properly localized in *dlg* mutant clones (Figure 5.7A), suggesting that Dlg is not necessary to enable the localization of Lgl at the cortex or plasma membrane.

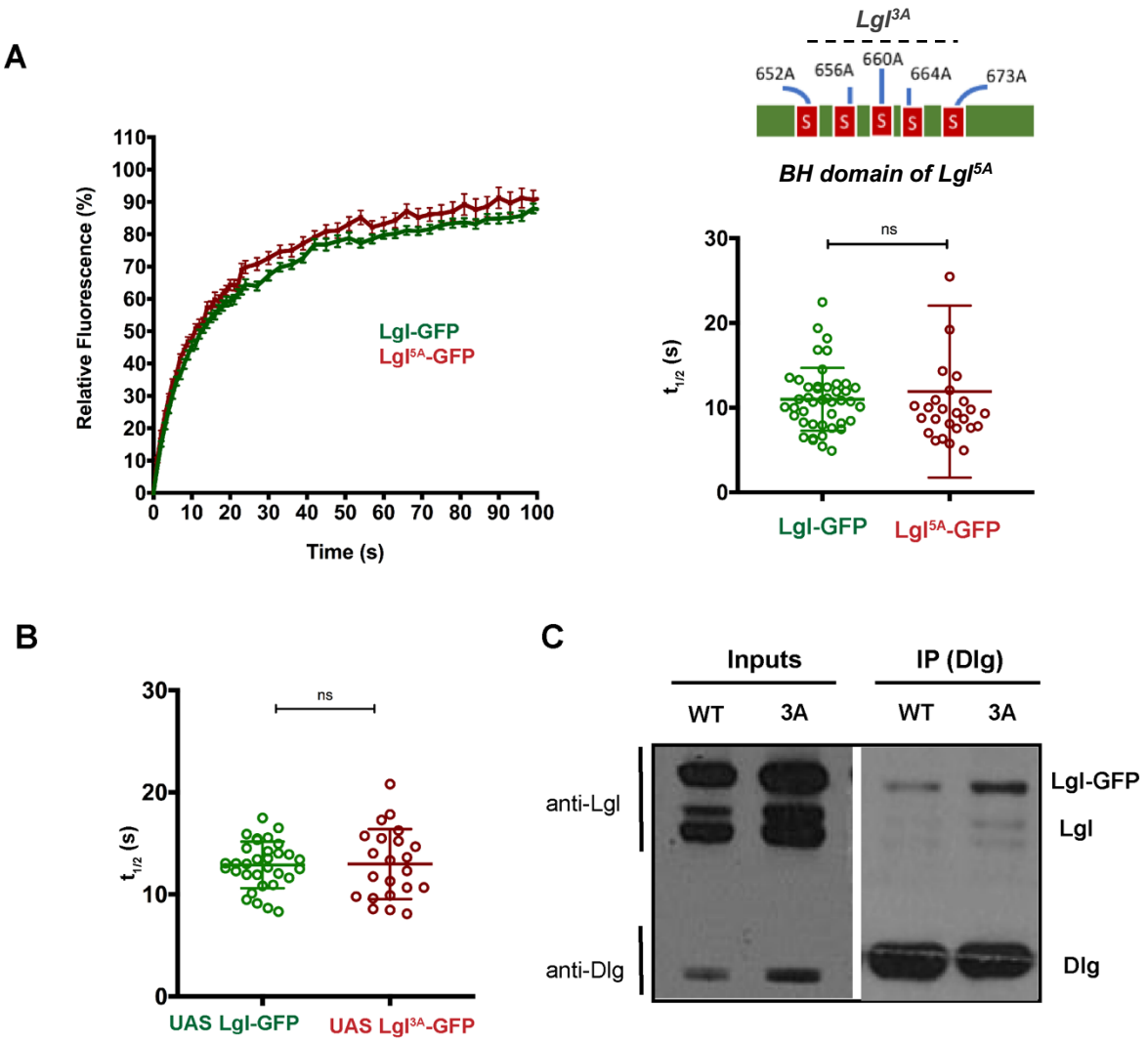

Figure 5.6: Unphosphorylatable forms of Lgl display similar dynamics to the wild-type form in the basolateral domain. A) The recovery dynamics of Lgl^{5A}-GFP, an unphosphorylatable form in which the five putative aPKC phosphorylation sites were replaced by alanines, is similar to the recovery dynamics of Lgl-GFP. No significant difference in the half-time recovery were found. Error bars: mean ± SEM for the recovery graph. B) Mutation of the three main serines found to be phosphorylated by aPKC do not affect the dynamics of Lgl recovery at the basolateral cortex. C) IP of Dlg shows that both forms of Lgl, Lgl-GFP and Lgl^{3A}-GFP, can be co-immunoprecipitated with Dlg. Statistical analysis of the half-time mean in A) was performed using a non-parametric test, the Mann-Whitney test, since data do not follow a Gaussian distribution according to the Shapiro-Wilk test (Lgl-GFP *p=0.0257; Lgl^{5A}-GFP ****p <0.0001). Since the Shapiro-Wilk was not significant for the value in B), we used a t-test to compare the two groups and we found non-statistical differences between them (p=0.9078). ns – non significant.

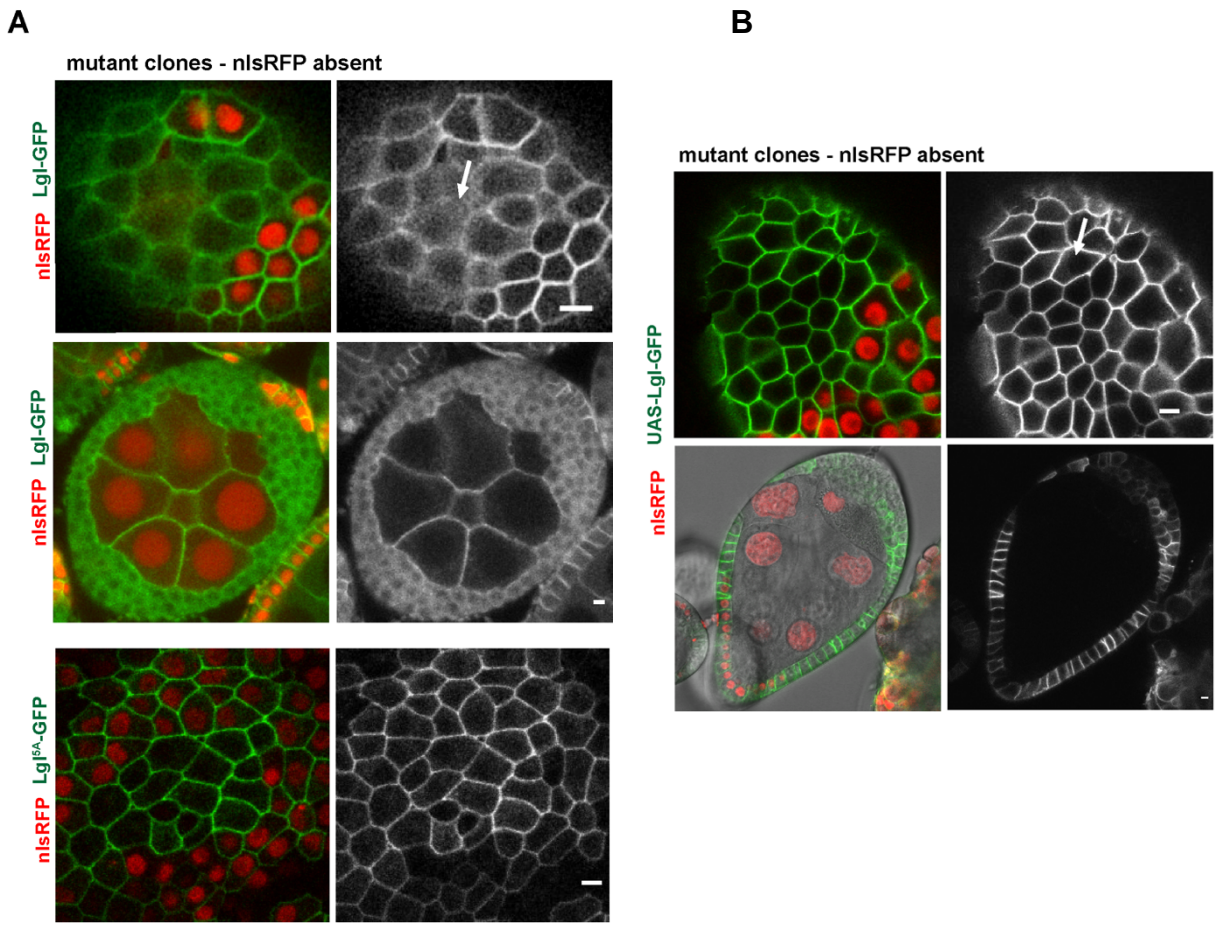

Figure 5.7: Mutation of the aPKC phosphorylation sites prevents Lgl cytoplasmic localization in *dlg* mutants. A) Mutant clones for dlg^{A} (labelled by absence of nuclear RFP (red)) show strong localization of endogenous Lgl-GFP to the cytoplasm, in contrast to Lgl^{5A}-GFP. As expected, *dlgA* mutant clones induce strong multilayering in the follicular epithelia. B) UAS-induced expression of Lgl-GFP enables Lgl cortical localization in *dlgA* mutants for FRAP experiments. Note that although less pronounced, some cytoplasmic localization of Lgl-GFP is still detected in *dlg* mutants (white arrow). Similarly, a multilayering phenotype is also observed in mutant clones for Dlg. Scale bars: 5 µm.

aPKC extends along the cortex due to loss of cell polarity (Franz and Riechmann, 2010), and so should be able to phosphorylate Lgl all over the cortex of *dlg* mutants. Thus, Lgl cytoplasmic localization in the absence of Dlg could be just the result of phosphorylation by mislocalized aPKC and unrelated to any possible ability of Dlg to anchor Lgl at the cortex? We therefore used FRAP as a more sensitive method to evaluate the impact of Lgl-Dlg binding, which should be detected through alterations in Lgl cortical dynamics. Since endogenously expressed Lgl-GFP is strongly localized in the cytoplasm and can barely be detected in the cortex of *dlg* mutant cells, we resorted to UAS-driven Lgl-GFP expression, which restores Lgl cortical localization (Figure 5.7B). We found that UAS-Lgl-GFP dynamics strongly increases in *dlg* mutants (mean half-time values: UAS-Lgl$^{t1/2}$ (control)= 12.89s; UAS-Lgl$^{t1/2}$ (*dlgA*)=8.95s), indicating a role for Dlg in regulating Lgl dynamics.

As PIP_2 was shown to be an important binding component of Lgl to the plasma membrane (Dong *et al*, 2015), one possible explanation for the acceleration of Lgl recovery is a change in PIP_2 composition in *dlg* mutants. In fact, previous work show that Lgl-GFP dynamics is also accelerated when PIP_2 is depleted by using a recently developed optogenetic tool (Guglielmi *et al*., 2015). This technique is based on targeting a lipid phosphatase to the plasma membrane, the 5-phosphatase OCRL (pm-OCRL), after exposure to light, which induces an efficient PIP_2 depletion (indicated by accumulation of PH-mCherry, a lipid sensor, in aggregates in the cytoplasm – white arrow on Figure 5.9). As an alternative approach to test the significance of PIP_2 binding for Lgl dynamics, I generated mutant clones for the kinase that produces PIP_2 from PI(4)P, *skittles* (Figure 5.8B). *skittles* mutant clones show an increase in cytoplasmic PH-mCherry, a marker of PIP_2 localization (as indicated in Figure 5.8C, yellow arrow). By performing FRAP in mutant cells where Lgl-GFP can still be detected in the cortex, we observed a significant increase in the recovery dynamics of Lgl-GFP (Figure 5.8B). Although this result further validates the acceleration of Lgl dynamics when PIP_2 is depleted, time-controlled depletion of PIP_2 using optogenetics enables more analysis of the direct consequences of PIP_2 depletion (Figure 5.9A). Since unphosphorylated versions of Lgl are expected to bind phosphoinositides equally to wild-type Lgl (Dong *et al*, 2015), we so anticipated to see an accelerated recovery of this proteins in cells depleted for PIP_2 by OCRL. Indeed, we observed a significant decrease in the mean half-time of Lgl^{5A} and Lgl^{3A} in this context, when compared to their respective controls, suggesting that PIP_2 depletion also accelerates the dynamics of these two unphosphorylatable forms of Lgl. In contrast, the dynamics of these mutant proteins is not affected by removing Dlg (UAS-Lgl$^{3A(t1/2)}$ (control)= 12.98s; UAS-Lgl$^{3A(t1/2)}$ (*dlgA*)= 11.77s) and Lgl$^{5A(t1/2)}$ (control)= 11.89s; Lgl$^{5A(t1/2)}$ (*dlgA*)= 11.00s) (Figure 5.8A,B). Together, these results suggest that the increase in Lgl dynamics observed in *dlg* mutants is not induced by

decreasing PIP_2 levels in these cells, but it is instead influenced by the phosphorylation status of Lgl.

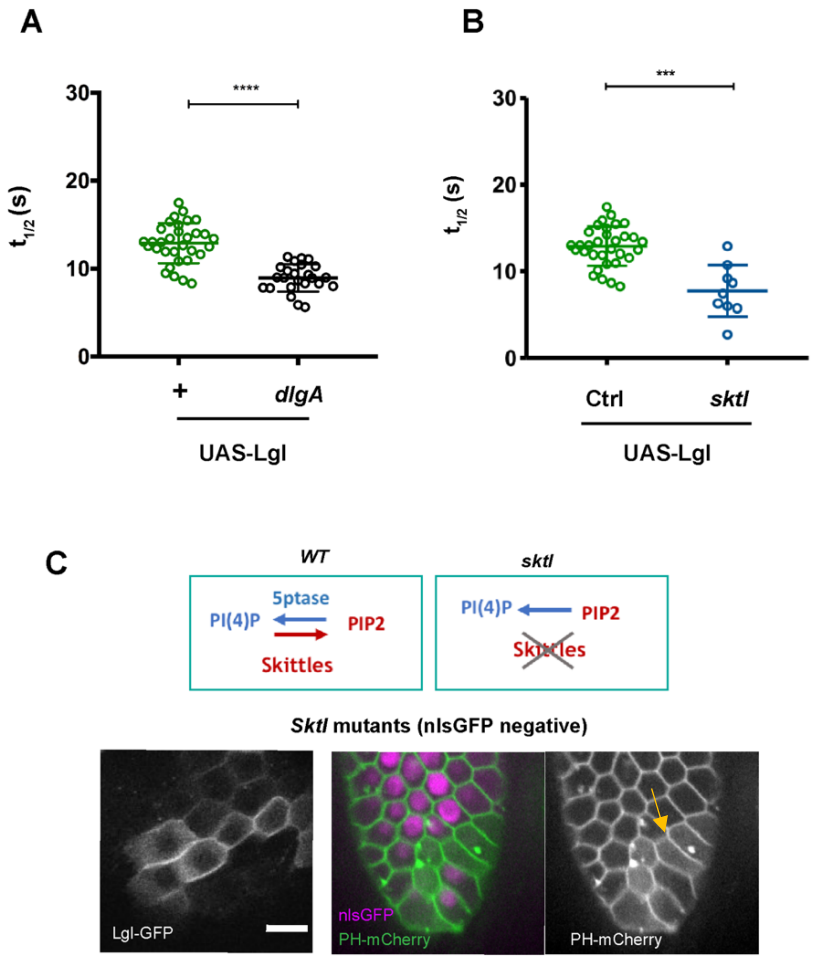

Figure 5.8: The rate of Lgl recovery after photobleaching increases in *dlgA* mutants in a similar extent to depletion of PIP_2. A) Scatter-plot representing the half-time recovery of Lgl-GFP in *dlgA* mutant cells comparing with the control. Statistical analysis was performed using a t-test (****p<0.0001). B) Mutants for the kinase Skittles, important for PIP_2 production from PI(4)P, induce a significant increase in Lgl-GFP dynamics. Statistical analysis was performed using a t-test (***p=0.0007). C) *skittles* mutants display a strong Lgl-GFP cytoplasmic localization and a decrease in the localization of the PIP_2 sensor PH-mCherry, even in small clones (yellow arrow). Experiments in A) were performed by Guilherme Ventura.

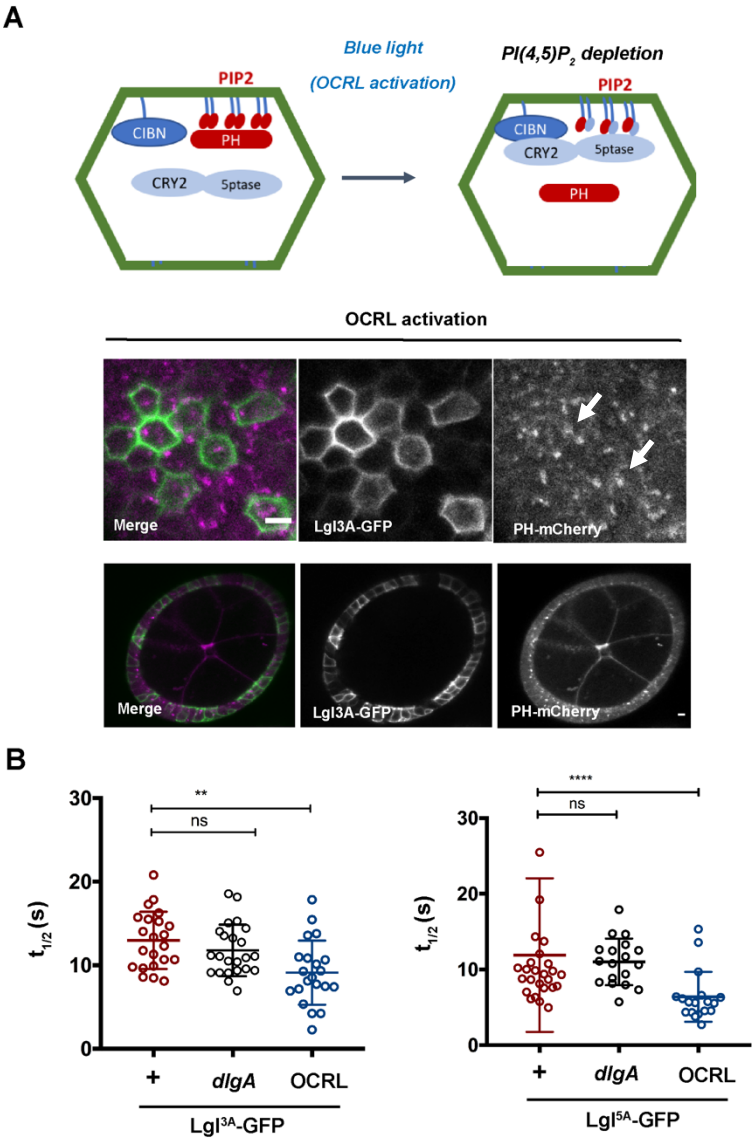

Figure 5.9: Increase in Lgl dynamics is not related with PIP_2 levels in *dlg* mutant clones. A) Schematic representation of PIP_2 depletion based on OCRL light-induced activation at the membrane. An example of an egg chamber where OCRL activation induces a slight decrease of Lgl^{3A}-GFP in the cortex, as well as a typical aggregation of PH-mCherry in the cytoplasm as a confirmation of efficient PIP_2 depletion. Sagittal section of an egg chamber shows that the OCRL light-induced system to deplete PIP_2 does not affect the architecture of the epithelia, as exemplified in the egg chamber where PIP_2 depletion was efficiently induced due to the presence of PH-mCherry aggregates in the cytoplasm. B) Scatter-plot representing the similar half-time recoveries of Lgl^{3A} in *dlgA* mutant cells and wild-type cells. Statistical analysis was performed using a t-test (UAS-GFP: ****p<0.0001; UAS-Lgl^{3A}-GFP: p=0.2225). ns- non significant. Lgl^{5A}-GFP dynamics is not altered in *dlgA* mutants. Statistical analysis was performed using a t-test (p=0.6760). ns-non significant. Optogenetic-induced depletion of PIP_2 by OCRL activation in the plasma membrane induces an increase of the dynamics of two unphosphorylatable forms of Lgl, Lgl^{3A}-GFP and Lgl^{5A}-GFP. Statistical analysis in Lgl^{3A}-GFP was performed using the t-test (**p=0.0012). Statistical analysis in Lgl^{5A}-GFP was performed using the Mann-Whitney test (****p<0.0001). Experiments for analyzing the Lgl^{5A}-GFP and Lgl^{3A}-GFP dynamics in *dlgA* mutants were performed by Guilherme Ventura. Scale bars: 5 μm.

Together, these experiments support the hypothesis that ectopic aPKC phosphorylation is the main cause of the increase in Lgl dynamics in *dlgA* mutants. Previous results from the lab have shown that *aPKC,dlg* double mutants have normal cortical localization of Lgl (data not shown), suggesting that Lgl cortical localization is rescued if aPKC activity is also abrogated. We then tested if the *dlg* phenotype could be quickly reverted by inhibition of aPKC activity, and therefore performed live imaging of epithelial cells mutant for *dlgA* after adding an aPKC inhibitor (CRT0103390) at 5 µM, which was shown to inhibit 80% of LLGL2 *in vitro* phosphorylation by aPKC (Rodriguez *et al.*, 2017). If Lgl cytoplasmic accumulation in *dlgA* mutant clones was solely due to continuous phosphorylation by aPKC, we would expect an increased Lgl localization to the cortex upon addition of the inhibitor due to the action of PP1 phosphatase (Figure 5.10A) (see Chapter 3). However, Lgl-GFP remained in the cytoplasm even about 2h30 after the addition of the drug (Figure 5.10B). Although drug treatment was sufficient to mislocalize Lgl-GFP to the apical side in some wild-type epithelial cells, as expected in a context of aPKC inhibition (Figure 5.10C), we detected the accumulation of cytoplasmic Lgl in wild-type cells 2h30 after adding the inhibitor (Figure 5.10B, white arrow), which suggests that unspecific drug-effects may interfere with the ability of Lgl to reallocate to the cortex in mutant cells. Nevertheless, assuming that the drug is efficiently inhibiting aPKC, this result would suggest that Lgl localization to the cytoplasm in *dlg* mutants results of a role of Dlg in the repression of aPKC that does not require sustained aPKC activity.

5.4. Role of Dlg and Scribble in the repression of Lgl phosphorylation by aPKC

In this section, I explore possible mechanisms that could underlie the role of Dlg in the repression of aPKC activity, either directly or indirectly. Recent work has shown that Dlg is an aPKC substrate in *Drosophila* neuroblasts (Golub *et al.*, 2017). Based on this work, we raised the possibility that the competition of Dlg with Lgl for the same kinase could inhibit aPKC-mediated phosphorylation of Lgl, somewhat similarly to asymmetric cell division, where Lgl competes with Bazooka for aPKC phosphorylation (Wirtz-Peitz *et al.*, 2008). Basically, as illustrated in Figure 5.11A, Dlg phosphorylation would buffer aPKC activity, which would protect Lgl from phosphorylation in the basolateral domain.

Therefore, when Dlg is lost, all the active pool of aPKC is available to phosphorylate Lgl and exclude it to the cytoplasm (Figure 5.11A). To explore this possibility, we took advantage of two *Drosophila* stocks produced in the context of the work of Golub *et al*, 2017. One line harbors UAS-Dlg-GFP, which is able to be phosphorylated by aPKC in the SH3 domain, and another line in which one of the phosphorylatable serines (S662) was replaced by an aspartate (D). Therefore, this form is expected to be less phosphorylatable by aPKC (Figure 5.11B). To address if Dlg could act as a competitor for aPKC phosphorylation of Lgl, we overexpressed the two forms of Dlg (Wt and S662D) in *Drosophila* ovaries. Overexpression conditions can be used to evaluate the phosphorylation status of Lgl in a context where aPKC remains correctly localized to the apical side of follicle cells (Figure 5.11C). We thus tested the impact of Dlg-GFP and Dlg^{S662D}-GFP overexpression in Lgl phosphorylation status by western blot. As observed by the western blot (Figure 5.11D) and the graph from quantification of two independent experiments, a slight decrease in Lgl phosphorylation is detected when overexpressing Dlg, particularly the form which has the two phosphorylation site available for phosphorylation by aPKC.

We then analysed the ability to rescue Lgl cortical localization using versions of Dlg with distinct ability to act as aPKC substrates. Preliminarily, we observed that whereas overexpression of Dlg-GFP rescues Lgl cortical localization in *dlgA* mutant clones (Figure 5.11F), Dlg^{S662D}-GFP is less efficient in restoring cortical localization of Lgl in *dlg* mutant clones. Moreover, we observed a complete rescue of *dlgA* multilayering phenotype when overexpressing Dlg-GFP wild-type, while some clones still have multilayering when overexpressing Dlg^{S662D}-GFP (data not show). Together, these results suggest that Dlg^{S662D}-GFP has less ability to support epithelial cell polarity in *dlg* mutants and rescue Lgl cortical localization than Dlg-GFP, which may result from their distinct ability to buffer aPKC activity in the basolateral domain.

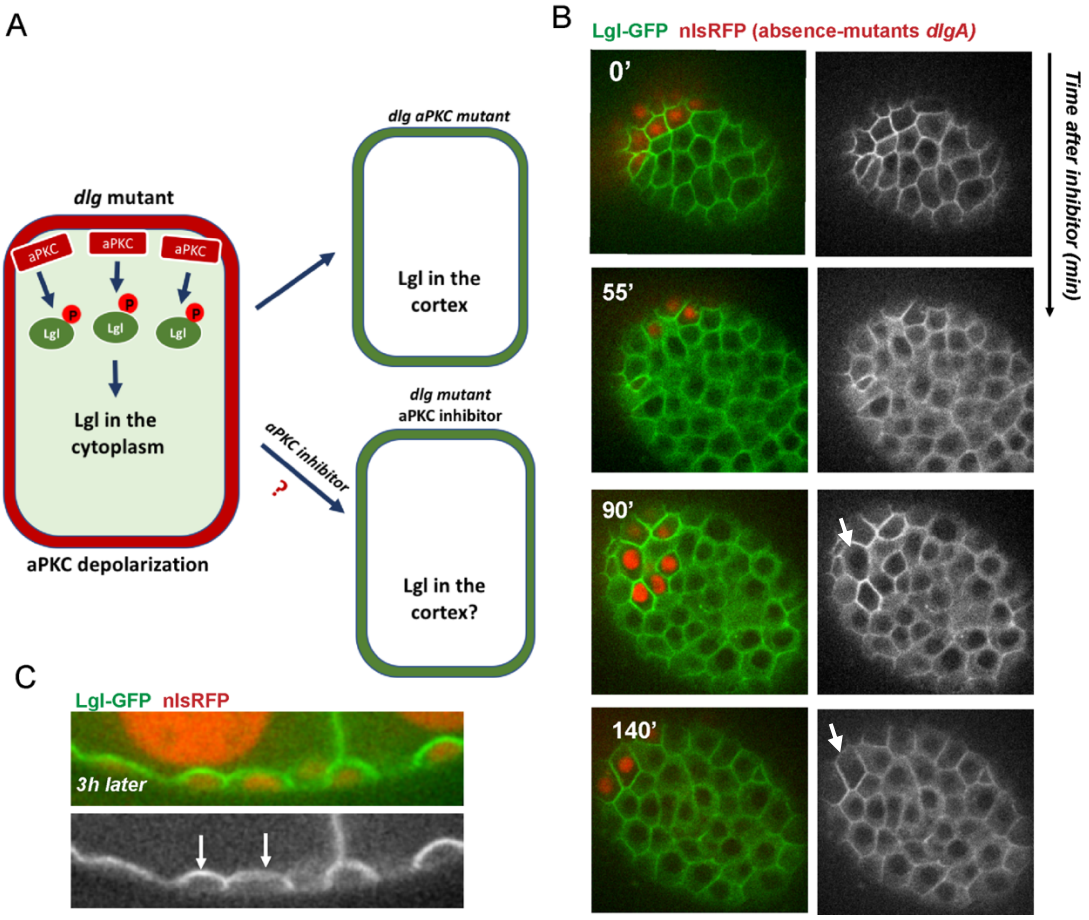

Figure 5.10: Acute inhibition of aPKC activity does not rescue Lgl cortical localization in *dlgA* epithelia mutants. A) Schematic representation of the hypothesis that Lgl cytoplasmic localization is a consequence of ectopic aPKC localization. Previous results from the lab have shown that lack of Lgl phosphorylation by aPKC in double mutants for Dlg and aPKC rescue Lgl localization in the cortex. Here I tested if inhibition of Lgl phosphorylation would also be sufficient to restore Lgl localization. B) 5 μM of an aPKC inhibitor, CRT0103390, were added to live imaging media containing *Drosophila* egg chambers with *dlgA* mutant clones expressing Lgl-GFP. Mutant clones for *dlgA* (lacking nlsRFP) show cytoplasmic localization of Lgl-GFP when the inhibitor is added and cytoplasmic accumulation increases since the addition of the inhibitor in both mutant and wild type cells (nlsRFP positive, white arrow). C) Lgl-GFP is observed in the apical side of wild-type epithelial cells, as expected in a context of aPKC inhibition.

Overexpression of Scrib-GFP, which has not been described to be phosphorylated by aPKC, has even a stronger ability to suppress Lgl phosphorylation by aPKC (Figure 5.11D), suggesting a possible role for Scrib as a direct or indirect inhibitor of aPKC. Since loss of Dlg induces a strong mislocalization of Scrib-GFP in embryos (Mathew *et al*, 2002) and also in the follicular epithelia (data not shown), this finding raises the possibility that Dlg role is required to inhibit aPKC-mediated phosphorylation of Lgl due to its role on Scrib localization. In fact, FRAP analysis show that *scrib* mutants also induce an acceleration of Lgl mobility, even higher than *dlg* mutants (Figure 5.12). In the future, it would be interesting to adress this question further and understand how Dlg and Scrib cooperate to restrict aPKC phosphorylation of Lgl in the basolateral domain.

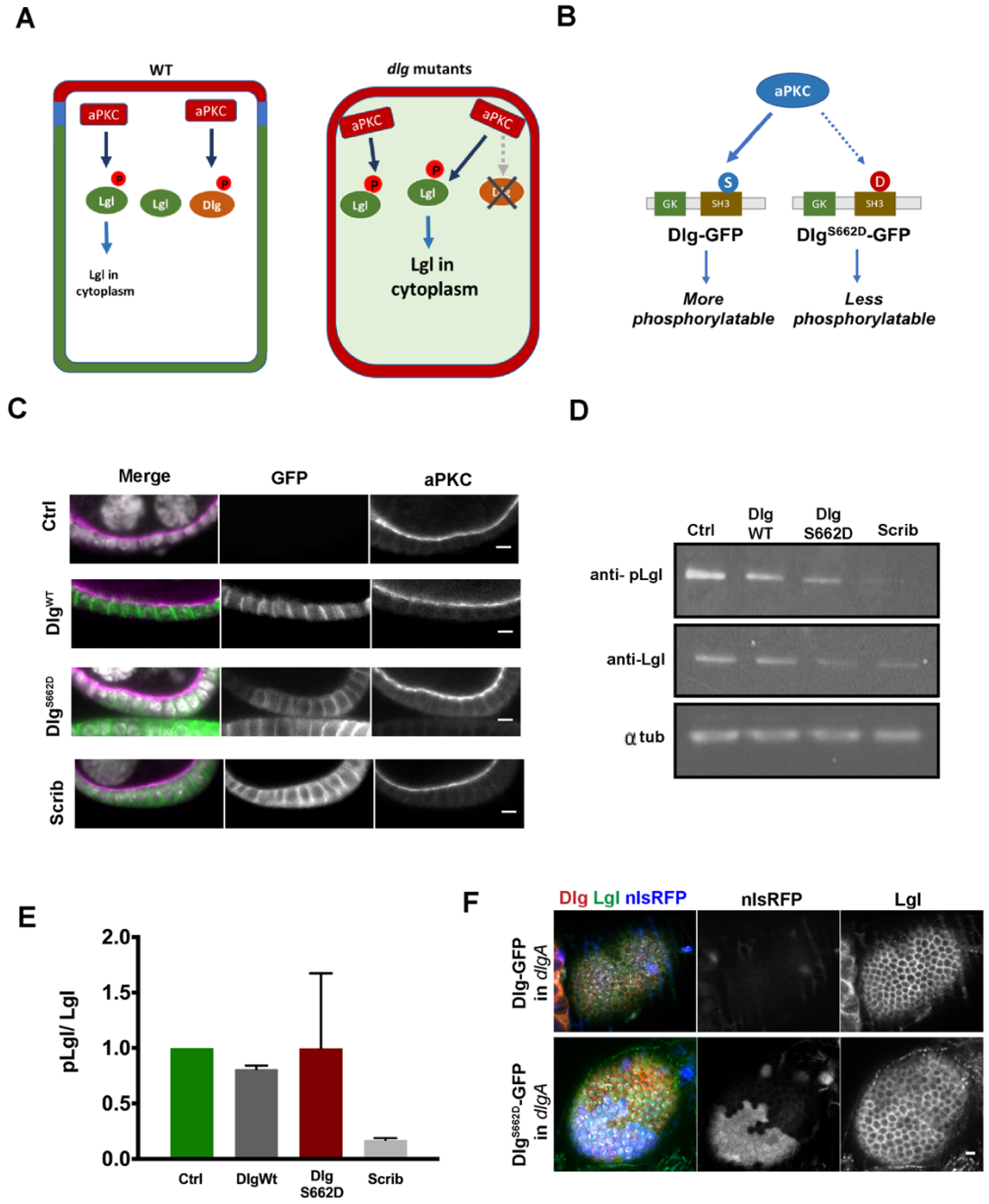

Figure 5.11: Exploring Dlg and Scribble as competitors/inhibitors of Lgl phosphorylation by aPKC. A) Schematic representation of the proposed hypothesis relying on aPKC phosphorylation of Dlg in the basolateral domain and competition with Lgl for phosphorylation. B) Two forms of Dlg-GFP previously produced (Golub *et al*, 2017) were used to explore this hypothesis: Dlg-GFP, the wild-type form which has a serine in SH3 domain available for phosphorylation and Dlg^{S662D}-GFP, in which this serine is replaced by an aspartate (D) to mimic the phosphorylation and therefore rendering it less phosphorylatable. C) Stainings for aPKC in follicular epithelium expressing Dlg forms or Scribble show that aPKC localization is not perturbed in these conditions. D) Western blot showing that overexpression of Dlg-GFP and Scrib-GFP for 1 day at 25ºC inhibits Lgl phosphorylation in ovaries extracts. E) Quantification of the ratio pLgl/Lgl (each one normalized for α-tub) in two independent experiments and normalized for the control ratio show that Dlg-GFP and Scrib-GFP (specially Scrib) is able to reduce Lgl phosphorylation in ovaries extracts. F) Staining for Lgl in mutant clones *dlgA*

overexpressing Dlg-GFP or Dlg^{S662D}-GFP using GR1 for 1 day at 25ºC. This preliminary experiment shows that Lgl is localized in the cytoplasm in mutant clones expressing Dlg^{S662D}-GFP, while it rescues the cortical Lgl localization when overexpressing Dlg-GFP.

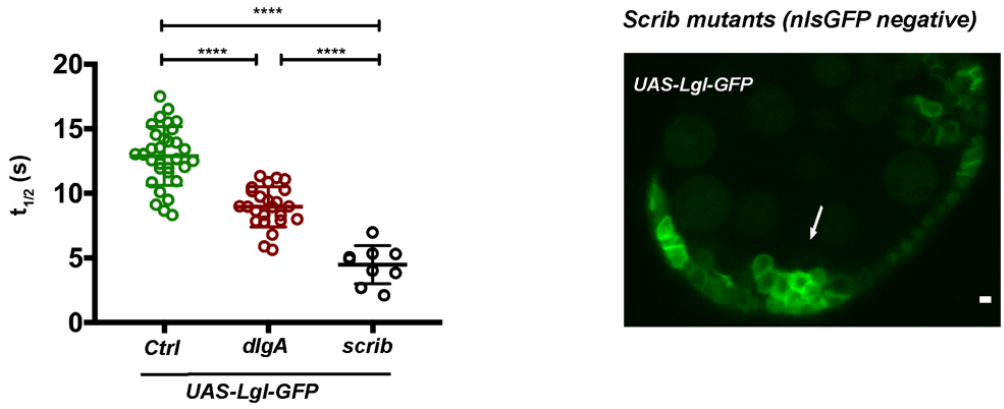

Figure 5.12. Lgl-GFP recovery fluorescence dynamics is strongly increased in mutants for *scrib*. Mutant clones for scrib display a faster recovery of Lgl-GFP after FRAP, even higher than observed in *dlgA* mutants. Statistical analyses were performed using ordinary one-way ANOVA. Egg chamber containing mutant clones for scrib (absence of nlsGFP) and showing the multilayering phenotype and also the localization of Lgl-GFP in the cytoplasm. Scale bars: 5 μm.

5.5. Discussion

Distinct mobility of Lgl, Dlg and Scribble at the basolateral cortex

This chapter reports the use of FRAP in the *Drosophila* follicular epithelium to explore the impact of putative binding partners of Lgl in its mobility at the lateral cortex, centering on its potential to detect interaction between Lgl and Dlg *in vivo*. The use of FRAP as a means to evaluate the formation of stable complexes was already reported to characterize the organization of the *Drosophila* septate junctions (SJ), the analogue of vertebrate tight junctions (TJs) (Oshima and Fehon, 2011). The authors found that, while some SJ components display very similar dynamics, Dlg is much more mobile, despite being localized at the SJ level in *Drosophila* embryos and required for SJ formation (Bilder *et al*., 2003). Together with the finding that Dlg dynamics do not change in mutants for core SJ components, the authors conclude that Dlg is not a structural component of these junctions.

Similarly, our first set of results suggests that Lgl does not form a stable immobile tripartite basolateral complex with Dlg and Scrib in the follicular epithelia, since these three proteins display very distinct florescence recovery dynamics. Moreover, we could not detect any significant immobile fraction of Lgl-GFP. Scrib-GFP displays slowest fluorescence recovery rate and it is curiously the protein with the higher molecular weight. However, protein weight might not severely impact protein dynamics, since it was previously shown that diffusion is largely independent on protein mass (Sprague and McNally, 2005). Protein size can be nevertheless considered in the context of the "molecular sieving" effect imposed by dense actin-based meshwork of the cytoskeleton, which can influence protein dynamics (Sprague and McNally, 2005; Trimple and Gristein, 2015). Spectrin, or other proteins of the cytoskeleton, such as septins, can trap the random movement of proteins (Trimple and Gristein, 2015) and influence Scrib-GFP dynamics in the basolateral epithelium. In fact, a role for septins in restricting the lateral diffusion at membranes was previously reported in yeast and might be also conserved in higher eukaryotes (Caudron and Barral, 2009). In the future, it would be interesting to interfere with the actin cytoskeleton (either with actin polymerization, using LatA, or genetically remove the contribution of cytoskeleton proteins) and analyse its consequence on the dynamics of Dlg-GFP and Scrib-GFP.

Since FRAP measures the off rate of proteins which is influenced by the affinity of protein-protein interactions (Garbett and Bretscher, 2014), the distinct recovery profiles also

depend on the distinct protein interactions associated with independent functions for each protein. All three basolateral proteins contain several domains that mediate the interaction with a plethora of distinct proteins (Stephens *et al*., 2018). Scrib, for example, was shown to have much slower recovery dynamics than Lgl, which could reflect a more stable binding to some immobile components. Interestingly, Scrib interacts with the cytoskeleton protein spectrin in mammalian cells, but not with Dlg or Lgl, according to the Venn diagrams based on interactions validated in several studies (Stephens *et al*., 2018). This interaction was found to slowdown the Scrib dynamics measured by FRAP (Boëda and Etienne-Manneville, 2015). It is still unknown whether β2-Spectrin binds Scrib in *Drosophila*, but the C-terminal domain used for this interaction in mammalian cells is poorly conserved (Boëda and Etienne-Manneville, 2015). Part of the slower recovery dynamics observed for Dlg and Scrib when compared with Lgl may rely on their preferential binding to other proteins, including the junctional protein E-cadherin, which is largely immobile after recruitment to cell-cell contact in epithelial cells (Adams *et al*., 1998) and does not diffuse in the plasma membrane in mature junctions (de Beco *et al*., 2009; Huang *et al*., 2011). Although we have tried to measure the dynamics of Dlg and Scrib specifically on the basolateral domain, it is possible that we also measured some pool that is bound to AJ. On the other hand, Lgl preferential binding to plasma membrane phosphoinositides, such as PIP_2 (Dong *et al*, 2015; Bailey and Prehoda, 2015) may account for the faster recovery rate observed for this protein. In fact, results from our lab show that the recovery dynamics of PLCδPH-GFP, a GFP tagged Pleckstrin Homology (PH) domain that interacts specifically with PIP_2 in the plasma membrane (Stauffer *et al*., 1998; Szentpetery *et al*., 2009), is extremely fast, displaying a mean half-time recovery of about 3 seconds (Ventura *et al.*, unpublished results).

Septate junctions (SJ) proteins display a high stability and very slow dynamics, as already discussed (Oshima *et al*, 2011). We reduced the possible impact of SJ in protein dynamics through the selection of the developmental stage of oogenesis used for FRAP analysis. Specifically, we used earlier stages (from 7 do 9) to perform our FRAP experiments since junctions only fully mature during oogenesis from stages 10B to 14 (Mahowald, 1972). However, insipient SJ are already detected in early stages of oogenesis, appearing on stage 6 when follicle cells stop to proliferate (Müller, 2000). Therefore, the presence of these so called *pre-septate* junctions could differently influence the dynamics of these proteins. Curiously, the two less dynamic proteins, Scrib and Dlg, are latter co-localized at SJ (Bilder *et al*., 2000) and are earlier enriched in the membrane region where SJ will be latter formed (Zeitler *et al*, 2004). Moreover, a role for Scrib in predetermining the site of SJ by mediating the recruitment of other SJ components has been suggested (Zeitler *et al*., 2004) and could influence the dynamics of this protein. Additionally, a possible interaction of Dlg with Scrib

might impact its dynamics. In fact, a slight increase in Dlg-GFP dynamics was detected in *scrib* zygotic mutants (Oshima and Fehon, 2011) and, recently, a study in the endodermal epithelium of *Drosophila* midgut shows that Dlg localization in SJ depends on Scrib (Chen *et al*., 2018).

Much more remains to be known about what controls the distinct dynamics of these three proteins in the basolateral domain, but our results regarding the different FRAP recovery dynamics further go in line with the current idea that, although the three proteins function in a common pathway to regulate cell polarity and growth, they also have independent functions.

Using FRAP to explore Lgl-Dlg interaction and Dlg-dependent inhibition of aPKC activity towards Lgl

Our FRAP experiments reveal that Lgl-GFP mobility significantly increases in *dlgA* mutants. This result could suggest that Dlg and Lgl interact in the basolateral domain, similarly to what was previously concluded about the increase in Dlg-GFP mobility in *scrib* mutant background of *Drosophila* embryos (Oshima and Fehon, 2011). However, our complementary experiments instead favor the idea that the increase in Lgl-GFP dynamics in *dlgA* mutants is mainly related with an ectopic activity of aPKC in the basolateral domain.

The similar dynamics of Lgl-GFP and the unphosphorylatable forms of Lgl, Lgl^{3A}-GFP and Lgl^{5A}-GFP, suggests that, in the steady-state of epithelial organization, aPKC is efficiently restricted in the apical side and does not influence the dynamics of Lgl in the basolateral cortex. However, in *dlgA* mutants, aPKC depolarizes, spreading into the lateral membrane of epithelial cells (Franz *et al.*, 2010), thus inducing cytoplasmic accumulation of Lgl-GFP, but not of the Lgl unphosphorylatable forms. Importantly, overexpression of Lgl-GFP in *dlgA* mutants rescues the cortical localization of Lgl. This further suggests that Lgl mislocalization to the cytoplasm results from ectopic aPKC activity towards Lgl, which is reduced by overexpression of its inhibitor Lgl (Betschinger *et al*., 2003; Fletcher *et al*., 2012; Wirtz-Peitz *et al*., 2008). Alternatively, aPKC overactivation may be simply rescued by the presence of an excess of substrate. Despite of this, FRAP analysis revealed that there is still an increase in Lgl recovery dynamics in *dlg* mutants. Moreover, we show that the dynamics of Lgl fluorescence recovery in versions insensitive to aPKC phosphorylation are affected by PIP_2 depletion, but are unaffected by loss of Dlg. Thus, Dlg does not affect Lgl dynamics through

its ability to bind Lgl, or by indirect regulation of the electrostatic interactions established between the BH domain of Lgl and PIP_2 (Dong *et al*, 2015; Bailey and Prehoda, 2015). Instead, Dlg seems to repress the activity of aPKC, preventing Lgl-GFP hyperphosphorylation and the concomitant disruption of plasma membrane and cortical interactions. In fact, aPKC phosphorylation of Lgl potentiates the off rate of binding to PIP_2 and cytoskeleton proteins, such as Myosin II, whose binding to Lgl is also regulated by electrostatic interactions (Dahan *et al*., 2014). So, the higher dynamics of Lgl in *dlgA* mutant cells likely results from a faster lateral diffusion, together with an increase in the membrane to cytoplasm exchange.

Previous work in our lab has shown that mutation for *aPKC* restores Lgl cortical localization in *dlg* mutants, supporting the idea that Dlg is not necessary for maintaining Lgl in the cortex if the activity of aPKC is abolished. However, since these mutant clones have long-term disruption of both Dlg and aPKC, it is possible that the rescue in cortical localization is solely associated with the complete disruption of any phosphorylation of Lgl by aPKC regardless Dlg´s role in aPKC regulation. We thus performed a temporal analysis by chemically inhibiting aPKC in *dlgA* mutants. However, after 2h30min, we did not observe a rescue of Lgl in the cortex of *dlgA* mutant cells. Assuming that aPKC was efficiently inhibited, this result suggests that Lgl does not require sustained phosphorylation by aPKC to remain mislocalized in the cytoplasm. This idea is in agreement with our previous results that aPKC does not influence Lgl reloading in epithelial cells and that a counteracting phosphatase activity is important for Lgl cortical localization (Chapter 3). However, while at mitotic exit Lgl reloading occurs in less than 20 min, in *dlg* mutants treated with aPKC inhibitor, PP1 was unable to induce Lgl reloading at the end of 2h30min. One possibility is that the activity of PP1 towards Lgl dephosphorylation during interphase is reduced when compared with the activity at the end of mitosis. In fact, while in interphase a balance between the kinase and phosphatase should be sufficient to maintain Lgl in the cortex, at mitotic exit, when Lgl is already in the cytoplasm by Aurora A/aPKC phosphorylation during mitosis, PP1 activity should be sufficiently high to allow a timely dephosphorylation and reload of the protein to the cortex of the new daughter cells. Additionally, it is possible that the kinase inhibition was not efficient enough to revert the phosphorylation of Lgl induced by aPKC depolarization. aPKC activity would be expected to be reduced to less than 20% in the presence of the aPKC inhibitor, according to *in vitro* data (Rodriguez *et al*., 2017), but this may not reflect what happens *in vivo*. Another hypothesis is related with the existence of a second kinase able to phosphorylate Lgl when aPKC is inhibited and which could also be misregulated in *dlg* mutant cells. This kinase could be Pak1, which was reported to have overlapping roles with aPKC, being also able to phosphorylate Lgl *in vitro* (Aguilar-Aragon *et al*., 2018).

However, since double mutants for aPKC and Dlg completely rescue the cortical localization of Lgl, it is unlikely that Pak1 would have a relevant role in excluding Lgl from the cortex in *dlgA* mutants. A third hypothesis could be that inhibition of aPKC activity by this drug could induce a conformational change and mislocalization of aPKC into the cytoplasm, where it could bind Lgl. This hypothesis could also explain the unexpected Lgl cytoplasmic localization observed in wild-type cells in ovaries treated with the aPKC inhibitor. The aPKC inhibitor used (CRT0103390) is a derivate of another one, CRT0066854, having a bifunctional inhibitory effect over PKCι as suggested by crystallographic analysis of PKCι bound to the inhibitor: first, it acts as a competitive ATP inhibitor for a nucleotide-binding pocket of aPKC and additionally also prevents the formation of a catalytically competent conformation (Kjær *et al*., 2013). These changes could induce an aPKC mislocalization to the cytoplasm, but further analyses must be performed to test this hypothesis.

Dlg and Scribble as inhibitors/competitors for aPKC-mediated phosphorylation of Lgl

The basolateral module Lgl/Dlg/Scrib has long been proposed to antagonize aPKC complex (Bilder and Perrimon, 2000; Bilder *et al*., 2003; Tanentzapf and Tepass, 2003), but how this antagonization occurs is still unclear. aPKC repression has been centered on Lgl ability to act as a buffer of aPKC activity towards other substrates (Wirtz-Peitz *et al*., 2008). A recent study suggests that Dlg is an aPKC substrate (Golub *et al*., 2017) and previous studies in embryonic and follicular epithelia suggest that Dlg prevents the lateral localization of apical proteins, including aPKC (Bilder and Perrimon, 2000; Franz *et al* 2010). We thus hypothesized that Dlg could inhibit aPKC activity towards Lgl by its ability to compete as a substrate of phosphorylation. In fact, a recent study shows that all aPKC substrates can inhibit, with different efficiencies, the ability of the kinase to phosphorylate other substrates (Holly and Prehoda, 2019), consistent with the notion that substrates compete with each other for the access to the kinase active site (Fersht, 1999). Part of our results corroborate this hypothesis. First, a Dlg^{S662D}-GFP variant, which is less phosphorylatable and therefore a weaker competitor for aPKC phosphorylation is unable to rescue Lgl cortical localization in *dlgA* mutants. Accordingly, Dlg-GFP overexpression was found to inhibit Lgl phosphorylation in ovaries extracts, but Dlg^{S662D}-GFP does not interfere with Lgl phosphorylation. However, this result does not provide evidence for a direct role of Dlg in buffering aPKC activity, since Lgl mislocalization may result indirectly from the multilayering phenotype associated with Dlg^{S662D}-GFP expression in *dlg* clones. Therefore, we are

currently testing the direct role of Dlg as a competing substrate for aPKC phosphorylation using immunoprecipitated aPKC/Par6/Bazooka complex from ovaries as kinase source for *in vitro* competition assays. In case Dlg could be able to compete with Lgl for aPKC phosphorylation, it should be expected a decrease in phosphorylation of recombinant Lgl in the presence of Dlg when using aPKC complex as a kinase source.

Instead of acting as a competing substrate, could Dlg inhibit aPKC directly by accessing the catalitic site of the kinase, as proposed for the human Par3 CR3 inhibitory arm (Soriano *et al*., 2016)? Although this hypothesis cannot be excluded, the correct polarization of aPKC observed when overexpressing Dlg-GFP in the follicular epithelium suggests that aPKC activity is not being perturbed. Otherwise, polarity should be affected in this context due to the inability of aPKC to phosphorylate important polarity substrates. Moreover, what is known for Lgl is not a function related with inhibition of aPKC catalytic activity, but rather buffering aPKC activity towards other substrates (Wirtz-Peitz *et al*., 2008). This could also be the case of Dlg, which is also a substrate of aPKC.

Dlg may also work more indirectly as a repressor of aPKC ectopic localization in the basolateral domain. For instance, loss of Dlg could induce defects in zonula adherens formation and promote aPKC depolarization to the basolateral cortex. In fact, Dlg was proposed to inhibit the localization of apical proteins in the basolateral domain and prevent ectopic adherens junction formation (Franz *et al* 2010). Therefore, Dlg could act together with AJ to restrict the apical activity of aPKC, preventing the spreading of this kinase to the basolateral cortex. In fact, adherens junctions could work as an important fence for the inhibition of aPKC extension. Consistent with this, the localization of Bazooka and Par6 is lost in *arm* mutants, which are defective in adherens junction formation (Bilder *et al*., 2003; Franz and Riechmann, 2010) and, recently, a study suggests that adherens junctions provide a diffusion barrier that restricts the localization of apical and basolateral polarity proteins to control domain sizes (Aguilar-Aragon *et al*., 2019). Interestingly, we found that aPKC is extended in the basolateral cortex of the new interface formed between daughter cells when Lgl is not reloaded to the cortex (Figure 4.12E), but it is properly restricted apically in older interfaces, possibly through adherens junctions maintained during mitosis.

Another possibility is that loss of Dlg could induce mislocalization of other basolateral components that inhibit aPKC activity. In fact, beyond Lgl, loss of Dlg causes a strong mislocalization of Scrib-GFP (Mathew *et al*, 2002). The same result was also observed in the follicular epithelium (data not shown). According to our western blot assays using ovary extracts, overexpression of Scrib-GFP strongly inhibits Lgl phosphorylation. Could Scrib

play a role in aPKC inhibition? Mutants for *scribble* were found to increase Lgl-GFP accumulation in the cytoplasm, which could be related to an extension of aPKC and ectopic activity over Lgl. Surprisingly, Lgl dynamics at the lateral cortex is faster in *scrib* mutants than in *dlg* mutants, and Lgl cytoplasmic localization is more pronounced in *scrib* mutants. Alternatively, Scrib could also play a role in Lgl recruitment to the cortex, since it was found to co-IP via Scrib's LRR domain in mammalian cells (Kallay *et al*, 2006).

Concluding, our work suggests that basolateral proteins might have distinct roles in apical-basal polarity. We show that Lgl dynamics is not dependent on direct interactions with Dlg and propose a model where Dlg and Scrib may cooperate to antagonize aPKC localization or activity in the basolateral domain. Our work may therefore contribute for a better understanding of how the basolateral proteins exclude the apical polarity complex to maintain the boundaries of basolateral and apical domains in epithelial cells.

Chapter 6

General Discussion

General Discussion

The explorer who will not come back or send back his ships to tell his tale is not an explorer, only an adventurer; and his sons are born in exile.

Ursula K. Le Guin
In The Dispossessed

After exploring how Lgl phosphoregulation controls the dynamic subcellular localization of Lgl and its interaction with cortical partners in different stages of the cell-cycle, here are our "ships" to science: **1)** the identification of a phosphatase, PP1, that dephosphorylates Lgl to promote its cortical localization, antagonizing aPKC and Aurora A phosphorylation (Figure 6 - Chapter 3); **2)** an important role for the phosphatase holoenzyme, PP1-Sds22, in the regulation of Lgl phosphorylation status and cortical reloading for the propagation of cell polarity to the daughter cells (Figure 6 - Chapter 4); **3)** the identification of an evolutionarily conserved PP1 docking site motif (Figure 6 – Chapter 3), which is important for PP1-mediated dephosphorylation of Lgl and whose disruption induces a strong mislocalization of Lgl in the cytoplasm and consequent disruption of epithelial architecture; **4)** FRAP analyses which revealed that Lgl is much more dynamic than the other two basolateral proteins, Dlg and Scribble, and also that these may control Lgl mobility through their ability to repress aPKC activity towards Lgl (Figure 6 – Chapter 5).

In this study, we have shown that Lgl is reloaded to the cortex at mitotic exit by a PP1-mediated dephosphorylation mechanism, allowing epithelial cells to deal with the complete pool of Lgl in the cytoplasmic and phosphorylated form at mitotic exit. Lgl dynamic phosphoregulation is similarly coordinated with the cell-cycle in unpolarized S2 cells, suggesting that epithelial cells have taken advantage of basic cell-cycle regulated processes to orchestrate polarity remodeling and polarization of the new daughter cells. Importantly, we found that Lgl reloading restricts aPKC to the apical side in the new interface, which is important to maintain tissue architecture. Interestingly, Lgl cortical reloading is not required for the apical localization of aPKC at mitotic exit in interfaces contacting the neighboring cells. A possible explanation would be that other polarity components, such as Scrib, Dlg and adherens junctions, could have important roles in preventing aPKC extension in these pre-existent interfaces, where basolateral Scrib and

Dlg remain in the cortex (Carvalho *et al*., 2015) and adherens junctions are maintained during mitosis to mechanically connect the dividing cell to the neighbors (Bras and Le Borgne, 2014). On the other hand, the new interface between daughter cells has to be polarized *de novo*, and Lgl reloading could be a particularly important cue to prevent aPKC extension while the new interface is not fully established. Since maintaining Lgl in the cytoplasm in lgl^{ts3} mutants at restrictive temperature induces mislocalization of aPKC in the basolateral side of the new interface, future work should also focus on the analysis of the segregation of aPKC at the end of mitosis in *lgl* mutant cells expressing $Lgl^{KA,FA}$-GFP, to access specifically the relevance of PP1-mediated Lgl reloading for aPKC localization in the newly formed interface.

Missense mutations in PP1-docking site residues of human LLGL1 and LLGL2 were detected in some cancers. In gastric adenocarcinoma was detected a change in the first aminoacid of the PP1-docking motif (p.R339H) in LLGL1 whereas a mutation in the third aminoacid (p.I341M) was found in lung carcinoma (data from COSMIC - Catalogue of Somatic Mutations in Cancer, https://cancer.sanger.ac.uk/cosmic). In LLGL2, missense mutations were found to change the first and the last aminoacids of the docking site motif (p.R331L and p.G334C) in bile duct carcinoma and in liver tumor samples, respectively. Future work could be performed to understand the prevalence of mutations in the docking site motif in several types of cancer and which ones are associated with a mislocalization of Lgl in the cytoplasm. Moreover, this PP1 docking site on Lgl is immediately adjacent to an evolutionarily conserved serine (see Figure 3.14), whose phosphorylation could eventually regulate PP1 binding to Lgl, similarly to what was found for phosphorylation of serine residues inside RVxF motifs (Nasa and Kettenbach, 2018). Searching the impact of this phosphorylation for PP1 interaction with Lgl in this docking site motif and identification of the kinase that targets this residue could be important to improve our understanding of Lgl phosphoregulation by PP1.

In this study, we also propose a new mechanism by which balanced PP1 and aPKC activities is essential for proper Lgl basolateral cortical localization where it restricts the apical localization of aPKC for the maintenance of proper epithelial architecture. In fact, the multilayering phenotype associated with PP1-depletion is rescued by a decrease of aPKC levels or when Lgl-GFP is overexpressed, possibly by buffering and inhibiting aPKC activity. Curiously, aPKC is overexpressed in several types of cancers, including lung cancer (Halaoui and McCaffrey, 2015), where recently PP1 was also found to be downregulated (Verdugo-Sivianes *et al*., 2017). Whether Lgl mislocalization is the common link underlying the impact of these two modifications in lung cancer, or cancers with other origins, could be

an important question to address in the future. Furthermore, restoring Lgl cortical localization by PP1 or Sds22 expression could be a potential approach for treatment of certain types of cancer. In fact, pharmaceutical companies have been encouraged to pursue approaches for the activation of PP1 holoenzymes (Felgueiras and Fardilha, 2014). Some compounds have been identified to enhance the activity of PP1 *in vitro* and strategies based on RVxF-mimetic peptides that generate a cellular pool of PP1:activator complex to dephosphorylate several substrates have been explored (Chatterjee and Köhn, 2013). Furthermore, understanding how aPKC is inhibited by other basolateral proteins could contribute for the design of new and more specific drugs or peptide-based strategies for aPKC signaling inhibition in cancer cells where this kinase is overexpressed.

Despite the focus on the role of PP1 in interphase and at mitotic exit in two independent chapters of this thesis, events occurring during interphase and at mitotic exit are strongly interconnected, and so interfering specifically with PP1 regulatory subunits acting in a time-restricted window can help to discern the role of the phosphatase in different cell-cycle phases. Accordingly, we have identified Sds22 as a regulatory subunit able to potentiate PP1-activity towards Lgl at mitotic exit. PP1/Sds22 phosphatase was also found to be an important regulator of metaphase-anaphase elongation by dephosphorylating and clearing p-Moesin specifically in the two poles of the cell (Kunda *et al*., 2012). In our work, however, we did not find a specific accumulation of Lgl-GFP in the cell poles as a result of PP1/Sds22 intensive dephosphorylation near cell poles. Possibly, failure in detecting such specific cortical accumulation of Lgl is related with the very dynamic redistribution of this protein to the overall cortex/membrane, as observed in Chapter 5.

Previous studies reported that loss of Sds22 function promotes neoplastic tumor development in *Drosophila* imaginal discs, similarly to mutations in the canonical basolateral polarity proteins (Jiang *et al*., 2011). This Sds22 role in maintaining epithelial architecture and integrity has been mainly associated with an effect on myosin or moesin hyperphosphorylation (Grusche *et al*., 2009; Jiang *et al*., 2011). Although reducing the levels of active myosin II can suppress some Sds22 loss of function phenotypes, including invasion and cell death, blocking myosin II activity does not totally abolish the Sds22/PP1-mediated JNK kinase activation nor epithelial polarity defects (Jiang *et al*., 2011), suggesting that other targets might be involved. Curiously, overexpression of Sds22 was found to be able to largely suppress the loss of function phenotypes of Scrib polarity gene (Jiang *et al*., 2011). One of the phenotypes associated with loss of Scrib is a strong mislocalization of Lgl-GFP in the cytoplasm, as observed in the Chapter 5. In light of our results, a possible explanation for the rescue of *scrib* mutant phenotypes when

overexpressing Sds22 could be through its ability to promote Lgl dephosphorylation, localizing Lgl to the cortex. Thus, our work provides an additional interpretation for the tumor-suppressive role of Sds22 and its human homolog PPP1R7. In fact, PP1-Sds22 can exert a tumor-suppressive role and inhibit the JNK activation by regulating the cortical localization of Lgl, since JNK pathway activation has been reported in mutant cells for *lgl* in imaginal discs. Future experiments could be done for further understanding if Lgl mislocalization in the cytoplasm is similar to loss of Lgl function regarding hyperactivation of the JNK pathway. This question could be addressed by analyzing the activation of the JNK pathway when $Lgl^{KA,FA}$, which is mostly cytoplasmic, is expressed in *lgl* mutant clones.

In conclusion, our findings will add an important piece to the unfinished puzzle that depicts how epithelial cell polarity is regulated during the cell-cycle. I anticipate that our results may establish the groundwork for future researches, paving the way to find new solutions for human health problems. I thus hope that “good winds” blow in the cell polarity field to bring back more “ships” full of knowledge.

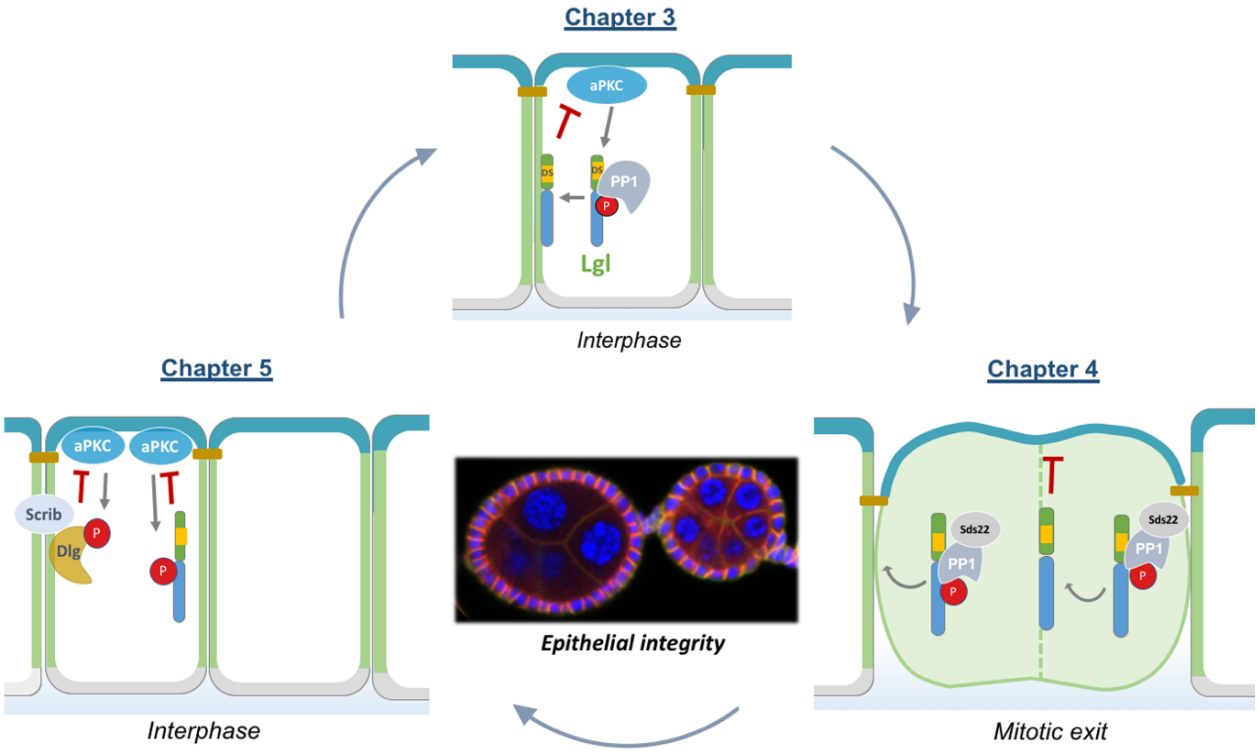

Figure 6: Graphic illustration of the main results of this thesis

And once the storm is over you won't remember how you made it through. You won't even be sure, in fact, whether the storm is really over. But one thing is certain. When you come out of the storm you won't be the same person who walked in.

That's what this storm is all about.

Haruki Murakami, in Kafka on the Shore

References

Adams, C.L., Chen, Y.-T., Smith, S.J., and James Nelson, W. (1998). Mechanisms of Epithelial Cell–Cell Adhesion and Cell Compaction Revealed by High-resolution Tracking of E-Cadherin– Green Fluorescent Protein. J. Cell Biol. *142*, 1105–1119.

Adams, M.D., Celniker, S.E., Holt, R.A., Evans, C.A., Gocayne, J.D., Amanatides, P.G., Scherer, S.E., Li, P.W., Hoskins, R.A., Galle, R.F., et al. (2000). The genome sequence of *Drosophila melanogaster*. Science *287*, 2185–2195.

Aguilar-Aragon, M., Elbediwy, A., Foglizzo, V., Fletcher, G.C., Li, V.S.W., and Thompson, B.J. (2018). Pak1 Kinase Maintains Apical Membrane Identity in Epithelia. Cell Rep. *22*, 1639–1646.

Aguilar-Aragon, M., Tournier, A., and Thompson, B.J. (2019). A fence function for adherens junctions in epithelial cell polarity. BioRxiv 605808.

Almagor, L., Ufimtsev, I.S., Ayer, A., Li, J., and Weis, W.I. (2019). Structural insights into the aPKC regulatory switch mechanism of the human cell polarity protein lethal giant larvae 2. Proc. Natl. Acad. Sci. U. S. A. *116*, 10804–10812.

Amine, N.E., Kechad, A., Jananji, S., and Hickson, G.R.X. (2013). Opposing actions of septins and Sticky on Anillin promote the transition from contractile to midbody ring. J. Cell Biol. *203*, 487–504.

Assémat, E., Bazellières, E., Pallesi-Pocachard, E., Le Bivic, A., and Massey-Harroche, D. (2008). Polarity complex proteins. Biochim. Biophys. Acta *1778*, 614–630.

Atwood, S.X., and Prehoda, K.E. (2009). Phosphorylation-mediated cortical displacement of fate determinants by aPKC during neuroblast asymmetric cell division. Curr. Biol. CB *19*, 723–729.

Axton, J.M., Dombrádi, V., Cohen, P.T.W., and Glover, D.M. (1990). One of the protein phosphatase 1 isoenzymes in *Drosophila* is essential for mitosis. Cell *63*, 33–46.

Bachmann, A., Grawe, F., Johnson, K., and Knust, E. (2008). *Drosophila* Lin-7 is a component of the Crumbs complex in epithelia and photoreceptor cells and prevents light-induced retinal degeneration. Eur. J. Cell Biol. *87*, 123–136.

Bailey, M.J., and Prehoda, K.E. (2015). Establishment of Par-Polarized Cortical Domains via Phosphoregulated Membrane Motifs. Dev. Cell *35*, 199–210.

Barr, F.A., Elliott, P.R., and Gruneberg, U. (2011). Protein phosphatases and the regulation of mitosis. J. Cell Sci. *124*, 2323–2334.

Barros, C.S., Phelps, C.B., and Brand, A.H. (2003). *Drosophila* Nonmuscle Myosin II Promotes the Asymmetric Segregation of Cell Fate Determinants by Cortical Exclusion Rather Than Active Transport. Dev. Cell *5*, 829–840.

Barros, T.P., Kinoshita, K., Hyman, A.A., and Raff, J.W. (2005). Aurora A activates D-TACC–Msps complexes exclusively at centrosomes to stabilize centrosomal microtubules. J. Cell Biol. *170*, 1039–1046.

Bastock, R., and St Johnston, D. (2008). *Drosophila* oogenesis. Curr. Biol. CB *18*, R1082-1087.

de Beco, S., Gueudry, C., Amblard, F., and Coscoy, S. (2009). Endocytosis is required for E-cadherin redistribution at mature adherens junctions. Proc. Natl. Acad. Sci. U. S. A. *106*, 7010–7015.

Bell, G.P., Fletcher, G.C., Brain, R., and Thompson, B.J. (2015). Aurora Kinases Phosphorylate Lgl to Induce Mitotic Spindle Orientation in *Drosophila* Epithelia. Curr. Biol. *25*, 61–68.

Bellen, H.J., Tong, C., and Tsuda, H. (2010). 100 years of *Drosophila* research and its impact on vertebrate neuroscience: a history lesson for the future. Nat. Rev. Neurosci. *11*, 514–522.

Bennett, D., and Alphey, L. (2006). Yeast Two-Hybrid Screens to Identify *Drosophila* PP1-Binding Proteins. In Protein Phosphatase Protocols, (New Jersey: Humana Press), pp. 155–180.

Bennett, D., Szöor, B., Gross, S., Vereshchagina, N., and Alphey, L. (2003). Ectopic expression of inhibitors of protein phosphatase type 1 (PP1) can be used to analyze roles of PP1 in *Drosophila* development. Genetics *164*, 235–245.

Bennett, D., Lyulcheva, E., and Alphey, L. (2006). Towards a Comprehensive Analysis of the Protein Phosphatase 1 Interactome in *Drosophila*. J. Mol. Biol. *364*, 196–212.

Benton, R., and Johnston, D.S. (2003). *Drosophila* PAR-1 and 14-3-3 Inhibit Bazooka/PAR-3 to Establish Complementary Cortical Domains in Polarized Cells. Cell *115*, 691–704.

Berdnik, D., and Knoblich, J.A. (2002). *Drosophila* Aurora-A Is Required for Centrosome Maturation and Actin-Dependent Asymmetric Protein Localization during Mitosis. Curr. Biol. *12*, 640–647.

Bergstralh, D.T., Lovegrove, H.E., and St Johnston, D. (2013). Discs large links spindle orientation to apical-basal polarity in *Drosophila* epithelia. Curr. Biol. CB *23*, 1707–1712.

Bergstralh, D.T., Lovegrove, H.E., Kujawiak, I., Dawney, N.S., Zhu, J., Cooper, S., Zhang, R., and St Johnston, D. (2016). Pins is not required for spindle orientation in the *Drosophila* wing disc. Development *143*, 2573–2581.

Bergstralh, D.T., Dawney, N.S., and St Johnston, D. (2017). Spindle orientation: a question of complex positioning. Development *144*, 1137–1145.

Berns, N., Woichansky, I., Friedrichsen, S., Kraft, N., and Riechmann, V. (2014). A genome-scale in vivo RNAi analysis of epithelial development in *Drosophila* identifies new proliferation domains outside of the stem cell niche. J. Cell Sci. *127*, 2736–2748.

Besson, C., Bernard, F., Corson, F., Rouault, H., Reynaud, E., Keder, A., Mazouni, K., and Schweisguth, F. (2015). Planar Cell Polarity Breaks the Symmetry of PAR Protein Distribution prior to Mitosis in *Drosophila* Sensory Organ Precursor Cells. Curr. Biol. CB *25*, 1104–1110.

Betschinger, J., Mechtler, K., and Knoblich, J.A. (2003). The Par complex directs asymmetric cell division by phosphorylating the cytoskeletal protein Lgl. Nature *422*, 326–330.

Betschinger, J., Eisenhaber, F., and Knoblich, J.A. (2005). Phosphorylation-Induced Autoinhibition Regulates the Cytoskeletal Protein Lethal (2) giant larvae. Curr. Biol. *15*, 276–282.

Bi, P., and Kuang, S. (2015). Notch signaling as a novel regulator of metabolism. Trends Endocrinol. Metab. TEM *26*, 248–255.

Bilder, D. (2004). Epithelial polarity and proliferation control: links from the *Drosophila* neoplastic tumor suppressors. Genes Dev. *18*, 1909–1925.

Bilder, D., and Perrimon, N. (2000). Localization of apical epithelial determinants by the basolateral PDZ protein Scribble. Nature *403*, 676–680.

Bilder, D., Li, M., and Perrimon, N. (2000). Cooperative regulation of cell polarity and growth by *Drosophila* tumor suppressors. Science *289*, 113–116.

Bilder, D., Schober, M., and Perrimon, N. (2003). Integrated activity of PDZ protein complexes regulates epithelial polarity. Nat. Cell Biol. *5*, 53.

Bischoff, J.R., Anderson, L., Zhu, Y., Mossie, K., Ng, L., Souza, B., Schryver, B., Flanagan, P., Clairvoyant, F., Ginther, C., et al. (1998). A homologue of *Drosophila* aurora kinase is oncogenic and amplified in human colorectal cancers. EMBO J. *17*, 3052–3065.

Blankenship, J.T., Fuller, M.T., and Zallen, J.A. (2007). The *Drosophila* homolog of the Exo84 exocyst subunit promotes apical epithelial identity. J. Cell Sci. *120*, 3099–3110.

Bøe, R., Gjertsen, B.T., Vintermyr, O.K., Houge, G., Lanotte, M., and Døskeland, S.O. (1991). The protein phosphatase inhibitor okadaic acid induces morphological changes typical of apoptosis in mammalian cells. Exp. Cell Res. *195*, 237–246.

Boëda, B., and Etienne-Manneville, S. (2015). Spectrin binding motifs regulate Scribble cortical dynamics and polarity function. ELife *4*.

Bollen, M., Gerlich, D.W., and Lesage, B. (2009). Mitotic phosphatases: from entry guards to exit guides. Trends Cell Biol. *19*, 531–541.

Bollen, M., Peti, W., Ragusa, M.J., and Beullens, M. (2010). The extended PP1 toolkit: designed to create specificity. Trends Biochem. Sci. *35*, 450–458.

Bonello, T.T., and Peifer, M. (2019). Scribble: A master scaffold in polarity, adhesion, synaptogenesis, and proliferation. J. Cell Biol. *218*, 742–756.

Brand, A.H., and Perrimon, N. (1993). Targeted gene expression as a means of altering cell fates and generating dominant phenotypes. Dev. Camb. Engl. *118*, 401–415.

Bras, S.L., and Borgne, R.L. (2014). Epithelial cell division – multiplying without losing touch. J Cell Sci *127*, 5127–5137.

Brautigan, D.L., and Shenolikar, S. (2018). Protein Serine/Threonine Phosphatases: Keys to Unlocking Regulators and Substrates. Annu. Rev. Biochem. *87*, 921–964.

Brumby, A.M., and Richardson, H.E. (2003). scribble mutants cooperate with oncogenic Ras or Notch to cause neoplastic overgrowth in *Drosophila*. EMBO J. *22*, 5769–5779.

Brumby, A.M., and Richardson, H.E. (2005). Using *Drosophila melanogaster* to map human cancer pathways. Nat. Rev. Cancer *5*, 626–639.

Brumby, A., Secombe, J., Horsfield, J., Coombe, M., Amin, N., Coates, D., Saint, R., and Richardson, H. (2004). A Genetic Screen for Dominant Modifiers of a cyclin E Hypomorphic Mutation Identifies Novel Regulators of S-Phase Entry in *Drosophila*. Genetics *168*, 227–251.

Bubici, C., and Papa, S. (2014). JNK signalling in cancer: in need of new, smarter therapeutic targets. Br. J. Pharmacol. *171*, 24–37.

Bulgakova, N.A., and Knust, E. (2009). The Crumbs complex: from epithelial-cell polarity to retinal degeneration. J. Cell Sci. *122*, 2587–2596.

Buszczak, M., Paterno, S., Lighthouse, D., Bachman, J., Planck, J., Owen, S., Skora, A.D., Nystul, T.G., Ohlstein, B., Allen, A., et al. (2007). The Carnegie Protein Trap Library: A Versatile Tool for *Drosophila* Developmental Studies. Genetics *175*, 1505–1531.

Calin, G.A., Iasio, M.G. di, Caprini, E., Vorechovsky, I., Natali, P.G., Sozzi, G., Croce, C.M., Barbanti-Brodano, G., Russo, G., and Negrini, M. (2000). Low frequency of alterations of the α (PPP2R1A) and β (PPP2R1B) isoforms of the subunit A of the serine-threonine phosphatase 2A in human neoplasms. Oncogene *19*, 1191.

Cao, F., Miao, Y., Xu, K., and Liu, P. (2015). Lethal (2) Giant Larvae: An Indispensable Regulator of Cell Polarity and Cancer Development. Int. J. Biol. Sci. *11*, 380–389.

Carvalho, C.A., Moreira, S., Ventura, G., Sunkel, C.E., and Morais-de-Sá, E. (2015). Aurora A Triggers Lgl Cortical Release during Symmetric Division to Control Planar Spindle Orientation. Curr. Biol. *25*, 53–60.

Castilho, P.V., Williams, B.C., Mochida, S., Zhao, Y., and Goldberg, M.L. (2009). The M Phase Kinase Greatwall (Gwl) Promotes Inactivation of PP2A/B55δ, a Phosphatase Directed Against CDK Phosphosites. Mol. Biol. Cell *20*, 4777–4789.

Castro, A., Arlot-Bonnemains, Y., Vigneron, S., Labbé, J.-C., Prigent, C., and Lorca, T. (2002). APC/Fizzy-Related targets Aurora-A kinase for proteolysis. EMBO Rep. *3*, 457–462.

Caudron, F., and Barral, Y. (2009). Septins and the lateral compartmentalization of eukaryotic membranes. Dev. Cell *16*, 493–506.

Ceulemans, H., Vulsteke, V., De Maeyer, M., Tatchell, K., Stalmans, W., and Bollen, M. (2002). Binding of the Concave Surface of the Sds22 Superhelix to the α4/α5/α6-Triangle of Protein Phosphatase-1. J. Biol. Chem. *277*, 47331–47337.

Chabu, C., and Doe, C.Q. (2009). Twins/PP2A regulates aPKC to control neuroblast cell polarity and self-renewal. Dev. Biol. *330*, 399–405.

Chatterjee, J., and Köhn, M. (2013). Targeting the untargetable: recent advances in the selective chemical modulation of protein phosphatase-1 activity. Curr. Opin. Chem. Biol. *17*, 361–368.

Chen, F., Archambault, V., Kar, A., Lio', P., D'Avino, P.P., Sinka, R., Lilley, K., Laue, E.D., Deak, P., Capalbo, L., et al. (2007). Multiple Protein Phosphatases Are Required for Mitosis in *Drosophila*. Curr. Biol. *17*, 293–303.

Chen, J., Sayadian, A.-C., Lowe, N., Lovegrove, H.E., and Johnston, D.S. (2018). An alternative mode of epithelial polarity in the *Drosophila* midgut. PLOS Biol. *16*, e3000041.

Cheng, Y., Liu, W., Kim, S.-T., Sun, J., Lu, L., Sun, J., Zheng, S.L., Isaacs, W.B., and Xu, J. (2011). Evaluation of PPP2R2A as a prostate cancer susceptibility gene: comprehensive germline and somatic study. Cancer Genet. *204*, 375–381.

Clark, B.S., Cui, S., Miesfeld, J.B., Klezovitch, O., Vasioukhin, V., and Link, B.A. (2012). Loss of Llgl1 in retinal neuroepithelia reveals links between apical domain size, Notch activity and neurogenesis. Dev. Camb. Engl. *139*, 1599–1610.

Clevers, H. (2006). Wnt/β-Catenin Signaling in Development and Disease. Cell *127*, 469–480.

Clyne, P.J., Certel, S.J., de Bruyne, M., Zaslavsky, L., Johnson, W.A., and Carlson, J.R. (1999). The Odor Specificities of a Subset of Olfactory Receptor Neurons Are Governed by Acj6, a POU-Domain Transcription Factor. Neuron *22*, 339–347.

Dahan, I., Yearim, A., Touboul, Y., and Ravid, S. (2012). The tumor suppressor Lgl1 regulates NMII-A cellular distribution and focal adhesion morphology to optimize cell migration. Mol. Biol. Cell *23*, 591–601.

Dahan, I., Petrov, D., Cohen-Kfir, E., and Ravid, S. (2014). The tumor suppressor Lgl1 forms discrete complexes with NMII-A and Par6α-aPKCζ that are affected by Lgl1 phosphorylation. J. Cell Sci. *127*, 295–304.

De Lorenzo, C., Strand, D., and Mechler, B.M. (1999). Requirement of *Drosophila* l(2)gl function for survival of the germline cells and organization of the follicle cells in a columnar epithelium during oogenesis. Int. J. Dev. Biol. *43*, 207–217.

Doggett, K., Grusche, F.A., Richardson, H.E., and Brumby, A.M. (2011). Loss of the *Drosophila* cell polarity regulator Scribbled promotes epithelial tissue overgrowth and cooperation with oncogenic Ras-Raf through impaired Hippo pathway signaling. BMC Dev. Biol. *11*, 57.

Dollar, G.L., Weber, U., Mlodzik, M., and Sokol, S.Y. (2005). Regulation of Lethal giant larvae by Dishevelled. Nature *437*, 1376–1380.

Dombrádi, V., and Cohen, P.T. (1992). Protein phosphorylation is involved in the regulation of chromatin condensation during interphase. FEBS Lett. *312*, 21–26.

Dombrádi, V., Axton, J.M., Brewis, N.D., Silva, E.F.D.C.E., Alphey, L., and Cohen, P.T.W. (1990). *Drosophila* contains three genes that encode distinct isoforms of protein phosphatase 1. Eur. J. Biochem. *194*, 739–745.

Dombrádi, V., Mann, D.J., Saunders, R.D., and Cohen, P.T. (1993). Cloning of the fourth functional gene for protein phosphatase 1 in *Drosophila melanogaster* from its chromosomal location. Eur. J. Biochem. *212*, 177–183.

Dong, W., Zhang, X., Liu, W., Chen, Y., Huang, J., Austin, E., Celotto, A.M., Jiang, W.Z., Palladino, M.J., Jiang, Y., et al. (2015). A conserved polybasic domain mediates plasma membrane targeting of Lgl and its regulation by hypoxia. J. Cell Biol. *211*, 273–286.

Dong, W., Lu, J., Zhang, X., Wu, Y., Lettieri, K., Hammond, G.R., and Hong, Y. (2019). A Polybasic Domain in aPKC Mediates Par-6-Dependent Control of Plasma Membrane Targeting and Kinase Activity. BioRxiv 588624.

Dow, L.E., Brumby, A.M., Muratore, R., Coombe, M.L., Sedelies, K.A., Trapani, J.A., Russell, S.M., Richardson, H.E., and Humbert, P.O. (2003). hScrib is a functional homologue of the *Drosophila* tumour suppressor Scribble. Oncogene *22*, 9225–9230.

Dragsten, P.R., Blumenthal, R., and Handler, J.S. (1981). Membrane asymmetry in epithelia: is the tight junction a barrier to diffusion in the plasma membrane? Nature *294*, 718.

Duchek, P. (2001). Guidance of Cell Migration by EGF Receptor Signaling During *Drosophila* Oogenesis. Science *291*, 131–133.

Duffy, J.B. (2002). GAL4 system in *Drosophila*: A fly geneticist's swiss army knife. Genesis *34*, 1–15.

Dunagan, M., Chaudhry, K., Samak, G., and Rao, R.K. (2012). Acetaldehyde disrupts tight junctions in Caco-2 cell monolayers by a protein phosphatase 2A-dependent mechanism. Am. J. Physiol. Gastrointest. Liver Physiol. *303*, G1356-1364.

Eder, A.M., Sui, X., Rosen, D.G., Nolden, L.K., Cheng, K.W., Lahad, J.P., Kango-Singh, M., Lu, K.H., Warneke, C.L., Atkinson, E.N., et al. (2005). Atypical PKCı contributes to poor prognosis through loss of apical-basal polarity and Cyclin E overexpression in ovarian cancer. Proc. Natl. Acad. Sci. U. S. A. *102*, 12519–12524.

Edgar, B.A., and Orr-Weaver, T.L. (2001). Endoreplication Cell Cycles: More for Less. Cell *105*, 297–306.

Eiteneuer, A., Seiler, J., Weith, M., Beullens, M., Lesage, B., Krenn, V., Musacchio, A., Bollen, M., and Meyer, H. (2014). Inhibitor-3 ensures bipolar mitotic spindle attachment by limiting association of SDS22 with kinetochore-bound protein phosphatase-1. EMBO J. *33*, 2704–2720.

Engelbert, D., Schnerch, D., Baumgarten, A., and Wäsch, R. (2008). The ubiquitin ligase APCCdh1 is required to maintain genome integrity in primary human cells. Oncogene *27*, 907–917.

Etienne-Manneville, S., Manneville, J.-B., Nicholls, S., Ferenczi, M.A., and Hall, A. (2005). Cdc42 and Par6-PKCzeta regulate the spatially localized association of Dlg1 and APC to control cell polarization. J. Cell Biol. *170*, 895–901.

Feigin, M.E., Akshinthala, S.D., Araki, K., Rosenberg, A.Z., Muthuswamy, L.B., Martin, B., Lehmann, B.D., Berman, H.K., Pietenpol, J.A., Cardiff, R.D., et al. (2014). Mislocalization of the cell polarity protein Scribble promotes mammary tumorigenesis and is associated with basal breast cancer. Cancer Res. *74*, 3180–3194.

Felgueiras, J., and Fardilha, M. (2014). Phosphoprotein phosphatase 1-interacting proteins as therapeutic targets in prostate cancer. World J. Pharmacol. *3*, 120–139.

Feng, X., Chen, K., Ye, S., Wang, H., Wei, G., Tan, W., Cheng, S., Zhang, Y., Liu, S., and Zhou, Y. (2012). MPP3 inactivation by promoter CpG islands hypermethylation in colorectal carcinogenesis. Cancer Biomark. *11*, 99–106.

Fernandez, A., Brautigan, D.L., and Lamb, N.J. (1992). Protein phosphatase type 1 in mammalian cell mitosis: chromosomal localization and involvement in mitotic exit. J. Cell Biol. *116*, 1421–1430.

Fletcher, G.C., Lucas, E.P., Brain, R., Tournier, A., and Thompson, B.J. (2012). Positive Feedback and Mutual Antagonism Combine to Polarize Crumbs in the *Drosophila* Follicle Cell Epithelium. Curr. Biol. *22*, 1116–1122.

Flores-Benitez, D., and Knust, E. (2016). Dynamics of epithelial cell polarity in *Drosophila*: how to regulate the regulators? Curr. Opin. Cell Biol. *42*, 13–21.

Franz, A., and Riechmann, V. (2010). Stepwise polarisation of the *Drosophila* follicular epithelium. Dev. Biol. *338*, 136–147.

Fersht, A. (1999). Structure and mechanism in protein science: a guide to enzyme catalysis and protein folding (W.H. Freeman).

Friedl, P., and Alexander, S. (2011). Cancer Invasion and the Microenvironment: Plasticity and Reciprocity. Cell *147*, 992–1009.

Froldi, F., Ziosi, M., Garoia, F., Pession, A., Grzeschik, N.A., Bellosta, P., Strand, D., Richardson, H.E., Pession, A., and Grifoni, D. (2010). The lethal giant larvae tumour suppressor mutation requires dMyc oncoprotein to promote clonal malignancy. BMC Biol. *8*, 33.

Funke, L., Dakoji, S., and Bredt, D.S. (2005). Membrane-associated guanylate kinases regulate adhesion and plasticity at cell junctions. Annu. Rev. Biochem. *74*, 219–245.

Gamblin, C.L., Hardy, É.J.-L., Chartier, F.J.-M., Bisson, N., and Laprise, P. (2014). A bidirectional antagonism between aPKC and Yurt regulates epithelial cell polarity. J. Cell Biol. *204*, 487–495.

Gangar, A., Rossi, G., Andreeva, A., Hales, R., and Brennwald, P. (2005). Structurally conserved interaction of Lgl family with SNAREs is critical to their cellular function. Curr. Biol. CB *15*, 1136–1142.

Garbett, D., and Bretscher, A. (2014). The surprising dynamics of scaffolding proteins. Mol. Biol. Cell *25*, 2315–2319.

Gardiol, D., Kühne, C., Glaunsinger, B., Lee, S.S., Javier, R., and Banks, L. (1999). Oncogenic human papillomavirus E6 proteins target the discs large tumour suppressor for proteasome-mediated degradation. Oncogene *18*, 5487–5496.

Gardiol, D., Zacchi, A., Petrera, F., Stanta, G., and Banks, L. (2006). Human discs large and scrib are localized at the same regions in colon mucosa and changes in their expression patterns are correlated with loss of tissue architecture during malignant progression. Int. J. Cancer *119*, 1285–1290.

Gateff, E. (1978). Malignant neoplasms of genetic origin in *Drosophila melanogaster*. Science *200*, 1448–1459.

Gateff, E., and Schneiderman, H.A. (1974). Developmental capacities of benign and malignant neoplasms of*Drosophila* . Wilhelm Roux Arch. Fur Entwicklungsmechanik Org. *176*, 23–65.

Germani, F., Bergantinos, C., and Johnston, L.A. (2018). Mosaic Analysis in *Drosophila* . Genetics *208*, 473–490.

Goehring, N.W., Chowdhury, D., Hyman, A.A., and Grill, S.W. (2010). FRAP Analysis of Membrane-Associated Proteins: Lateral Diffusion and Membrane-Cytoplasmic Exchange. Biophys. J. *99*, 2443–2452.

Goentoro, L.A., Yakoby, N., Goodhouse, J., Schüpbach, T., and Shvartsman, S.Y. (2006). Quantitative analysis of the GAL4/UAS system in *Drosophila* oogenesis. Genes. N. Y. N 2000 *44*, 66–74.

Goepfert, T.M., Adigun, Y.E., Zhong, L., Gay, J., Medina, D., and Brinkley, W.R. (2002). Centrosome Amplification and Overexpression of Aurora A Are Early Events in Rat Mammary Carcinogenesis. Cancer Res. *62*, 4115–4122.

Goldstein, B., and Macara, I.G. (2007). The PAR Proteins: Fundamental Players in Animal Cell Polarization. Dev. Cell *13*, 609–622.

Golub, O., Wee, B., Newman, R.A., Paterson, N.M., and Prehoda, K.E. (2017). Activation of Discs large by aPKC aligns the mitotic spindle to the polarity axis during asymmetric cell division. ELife *6*.

Grammont, M., and Irvine, K.D. (2002). Organizer activity of the polar cells during *Drosophila* oogenesis. Dev. Camb. Engl. *129*, 5131–5140.

Graybill, C., and Prehoda, K.E. (2014). Ordered Multisite Phosphorylation of Lethal Giant Larvae by Atypical Protein Kinase C. Biochemistry *53*, 4931–4937.

Graybill, C., Wee, B., Atwood, S.X., and Prehoda, K.E. (2012). Partitioning-defective protein 6 (Par-6) activates atypical protein kinase C (aPKC) by pseudosubstrate displacement. J. Biol. Chem. *287*, 21003–21011.

Grifoni, D., Garoia, F., Schimanski, C.C., Schmitz, G., Laurenti, E., Galle, P.R., Pession, A., Cavicchi, S., and Strand, D. (2004). The human protein Hugl-1 substitutes for *Drosophila* Lethal giant larvae tumour suppressor function in vivo. Oncogene *23*, 8688–8694.

Grusche, F.A., Hidalgo, C., Fletcher, G., Sung, H.-H., Sahai, E., and Thompson, B.J. (2009). Sds22, a PP1 phosphatase regulatory subunit, regulates epithelial cell polarity and shape [Sds22 in epithelial morphology]. BMC Dev. Biol. *9*, 14.

Grzeschik, N.A., Parsons, L.M., Allott, M.L., Harvey, K.F., and Richardson, H.E. (2010). Lgl, aPKC, and Crumbs Regulate the Salvador/Warts/Hippo Pathway through Two Distinct Mechanisms. Curr. Biol. *20*, 573–581.

Guglielmi, G., Barry, J.D., Huber, W., and De Renzis, S. (2015). An Optogenetic Method to Modulate Cell Contractility during Tissue Morphogenesis. Dev. Cell *35*, 646–660.

Guilgur, L.G., Prudencio, P., Ferreira, T., Pimenta-Marques, A.R., and Martinho, R.G. (2012). *Drosophila* aPKC is required for mitotic spindle orientation during symmetric division of epithelial cells. Development *139*, 503–513.

Gupta, T., and Schüpbach, T. (2003). Cct1, a phosphatidylcholine biosynthesis enzyme, is required for *Drosophila* oogenesis and ovarian morphogenesis. Development *130*, 6075–6087.

Häcker, U., and Perrimon, N. (1998). DRhoGEF2 encodes a member of the Dbl family of oncogenes and controls cell shape changes during gastrulation in *Drosophila*. Genes Dev. *12*, 274–284.

Halaoui, R., and McCaffrey, L. (2015). Rewiring cell polarity signaling in cancer. Oncogene *34*, 939–950.

Halaoui, R., Rejon, C., Chatterjee, S.J., Szymborski, J., Meterissian, S., Muller, W.J., Omeroglu, A., and McCaffrey, L. (2017). Progressive polarity loss and luminal collapse disrupt tissue organization in carcinoma. Genes Dev. *31*, 1573–1587.

Halder, G., and Johnson, R.L. (2011). Hippo signaling: growth control and beyond. Dev. Camb. Engl. *138*, 9–22.

Hales, K.G., Korey, C.A., Larracuente, A.M., and Roberts, D.M. (2015). Genetics on the Fly: A Primer on the *Drosophila* Model System. Genetics *201*, 815–842.

Hannaford, M.R., Ramat, A., Loyer, N., and Januschke, J. (2018). aPKC-mediated displacement and actomyosin-mediated retention polarize Miranda in *Drosophila* neuroblasts. ELife *7*.

Hannus, M., Feiguin, F., Heisenberg, C.-P., and Eaton, S. (2002). Planar cell polarization requires Widerborst, a B' regulatory subunit of protein phosphatase 2A. Dev. Camb. Engl. *129*, 3493–3503.

Hao, Y., Du, Q., Chen, X., Zheng, Z., Balsbaugh, J.L., Maitra, S., Shabanowitz, J., Hunt, D.F., and Macara, I.G. (2010). Par3 Controls Spindle Pole Orientation in Epithelial Cells by aPKC-Mediated Phosphorylation of Pins at the Apical Cortex. Curr. Biol. CB *20*, 1809–1818.

Harris, T.J.C., and Peifer, M. (2004). Adherens junction-dependent and -independent steps in the establishment of epithelial cell polarity in *Drosophila*. J. Cell Biol. *167*, 135–147.

Hattendorf, D.A., Andreeva, A., Gangar, A., Brennwald, P.J., and Weis, W.I. (2007). Structure of the yeast polarity protein Sro7 reveals a SNARE regulatory mechanism. Nature *446*, 567–571.

Hazelett, D.J., Bourouis, M., Walldorf, U., and Treisman, J.E. (1998). decapentaplegic and wingless are regulated by eyes absent and eyegone and interact to direct the pattern of retinal differentiation in the eye disc. Dev. Camb. Engl. *125*, 3741–3751.

Hazelrigg, T., Levis, R., and Rubin, G.M. (1984). Transformation of white locus DNA in *Drosophila*: dosage compensation, zeste interaction, and position effects. Cell *36*, 469–481.

Heim, A., Konietzny, A., and Mayer, T.U. (2015). Protein phosphatase 1 is essential for Greatwall inactivation at mitotic exit. EMBO Rep. *16*, 1501–1510.

Heller, D., Hoppe, A., Restrepo, S., Gatti, L., Tournier, A.L., Tapon, N., Basler, K., and Mao, Y. (2016). EpiTools: An Open-Source Image Analysis Toolkit for Quantifying Epithelial Growth Dynamics. Dev. Cell *36*, 103–116.

Hendrickx, A., Beullens, M., Ceulemans, H., Den Abt, T., Van Eynde, A., Nicolaescu, E., Lesage, B., and Bollen, M. (2009). Docking motif-guided mapping of the interactome of protein phosphatase-1. Chem. Biol. *16*, 365–371.

Heroes, E., Lesage, B., Görnemann, J., Beullens, M., Van Meervelt, L., and Bollen, M. (2013). The PP1 binding code: a molecular-lego strategy that governs specificity: The PP1 binding code. FEBS J. *280*, 584–595.

Herszterg, S., Leibfried, A., Bosveld, F., Martin, C., and Bellaiche, Y. (2013). Interplay between the dividing cell and its neighbors regulates adherens junction formation during cytokinesis in epithelial tissue. Dev. Cell *24*, 256–270.

Holly, R.W., and Prehoda, K.E. (2019). Phosphorylation of Par-3 by Atypical Protein Kinase C and Competition between Its Substrates. Dev. Cell *49*, 678–679.

Hong, Y. (2018). aPKC: the Kinase that Phosphorylates Cell Polarity. F1000Research *7*, 903.

Huang, J., Huang, L., Chen, Y.-J., Austin, E., Devor, C.E., Roegiers, F., and Hong, Y. (2011). Differential regulation of adherens junction dynamics during apical-basal polarization. J. Cell Sci. *124*, 4001–4013.

Humbert, P.O., Grzeschik, N.A., Brumby, A.M., Galea, R., Elsum, I., and Richardson, H.E. (2008). Control of tumourigenesis by the Scribble/Dlg/Lgl polarity module. Oncogene *27*, 6888–6907.

Humbert, P.O., Russell, S.M., Smith, L., and Richardson, H.E. (2015). The Scribble–Dlg–Lgl Module in Cell Polarity Regulation. In Cell Polarity 1: Biological Role and Basic Mechanisms, K. Ebnet, ed. (Cham: Springer International Publishing), pp. 65–111.

Hutterer, A., Betschinger, J., Petronczki, M., and Knoblich, J.A. (2004). Sequential roles of Cdc42, Par-6, aPKC, and Lgl in the establishment of epithelial polarity during *Drosophila* embryogenesis. Dev. Cell *6*, 845–854.

Ilina, O., and Friedl, P. (2009). Mechanisms of collective cell migration at a glance. J. Cell Sci. *122*, 3203–3208.

Janssens, V., and Goris, J. (2001). Protein phosphatase 2A : a highly regulated family of serine/threonine phosphatases implicated in cell growth and signalling. 23.

Jennings, B.H. (2011). *Drosophila* – a versatile model in biology & medicine. Mater. Today *14*, 190–195.

Jiang, Y., Scott, K.L., Kwak, S.-J., Chen, R., and Mardon, G. (2011). Sds22/PP1 links epithelial integrity and tumor suppression via regulation of myosin II and JNK signaling. Oncogene *30*, 3248–3260.

Johnston, D.S., and Ahringer, J. (2010). Cell Polarity in Eggs and Epithelia: Parallels and Diversity. Cell *141*, 757–774.

Johnston, C.A., Hirono, K., Prehoda, K.E., and Doe, C.Q. (2009). Identification of an Aurora-A/PinsLINKER/Dlg spindle orientation pathway using induced cell polarity in S2 cells. Cell *138*, 1150–1163.

Johnston, C.A., Doe, C.Q., and Prehoda, K.E. (2012). Structure of an Enzyme-Derived Phosphoprotein Recognition Domain. PLoS ONE *7*.

Kallay, L.M., McNickle, A., Brennwald, P.J., Hubbard, A.L., and Braiterman, L.T. (2006). Scribble associates with two polarity proteins, Lgl2 and Vangl2, via distinct molecular domains. J. Cell. Biochem. *99*, 647–664.

Kechad, A., Jananji, S., Ruella, Y., and Hickson, G.R.X. (2012). Anillin acts as a bifunctional linker coordinating midbody ring biogenesis during cytokinesis. Curr. Biol. CB *22*, 197–203.

Kinoshita, N., Ohkura, H., and Yanagida, M. (1990). Distinct, essential roles of type 1 and 2A protein phosphatases in the control of the fission yeast cell division cycle. Cell *63*, 405–415.

Kirchner, J., Gross, S., Bennett, D., and Alphey, L. (2007). Essential, Overlapping and Redundant Roles of the *Drosophila* Protein Phosphatase 1α and 1β Genes. Genetics *176*, 273–281.

Kjær, S., Linch, M., Purkiss, A., Kostelecky, B., Knowles, P.P., Rosse, C., Riou, P., Soudy, C., Kaye, S., Patel, B., et al. (2013). Adenosine-binding motif mimicry and cellular effects of a thieno[2,3- *d*]pyrimidine-based chemical inhibitor of atypical protein kinase C isoenzymes. Biochem. J. *451*, 329–342.

Klämbt, C., and Schmidt, O. (1986). Developmental expression and tissue distribution of the lethal (2) giant larvae protein of *Drosophila melanogaster.* EMBO J. *5*, 2955–2961.

Klezovitch, O., Fernandez, T.E., Tapscott, S.J., and Vasioukhin, V. (2004). Loss of cell polarity causes severe brain dysplasia in Lgl1 knockout mice. Genes Dev. *18*, 559–571.

Klinkert, K., Levernier, N., Gross, P., Gentili, C., von Tobel, L., Pierron, M., Busso, C., Herrman, S., Grill, S.W., Kruse, K., et al. (2019). Aurora A depletion reveals centrosome-independent polarization mechanism in Caenorhabditis elegans. ELife *8*.

Koh, Y.H., Popova, E., Thomas, U., Griffith, L.C., and Budnik, V. (1999). Regulation of DLG Localization at Synapses by CaMKII-Dependent Phosphorylation. Cell *98*, 353–363.

Kollareddy, M., Dzubak, P., Zheleva, D., and Hajduch, M. (2008). Aurora kinases: structure, functions and their association with cancer. Biomed. Pap. Med. Fac. Univ. Palacky Olomouc Czechoslov. *152*, 27–33.

Krahn, M.P., Egger-Adam, D., and Wodarz, A. (2009). PP2A Antagonizes Phosphorylation of Bazooka by PAR-1 to Control Apical-Basal Polarity in Dividing Embryonic Neuroblasts. Dev. Cell *16*, 901–908.

Kunda, P., Pelling, A.E., Liu, T., and Baum, B. (2008). Moesin controls cortical rigidity, cell rounding, and spindle morphogenesis during mitosis. Curr. Biol. CB *18*, 91–101.

Kunda, P., Rodrigues, N.T.L., Moeendarbary, E., Liu, T., Ivetic, A., Charras, G., and Baum, B. (2012). PP1-Mediated Moesin Dephosphorylation Couples Polar Relaxation to Mitotic Exit. Curr. Biol. *22*, 231–236.

Kuphal, S., Wallner, S., Schimanski, C.C., Bataille, F., Hofer, P., Strand, S., Strand, D., and Bosserhoff, A.K. (2006). Expression of Hugl-1 is strongly reduced in malignant melanoma. Oncogene *25*, 103–110.

Kwon, Y.-G., Lee, S.Y., Choi, Y., Greengard, P., and Nairn, A.C. (1997). Cell cycle-dependent phosphorylation of mammalian protein phosphatase 1 by cdc2 kinase. Proc. Natl. Acad. Sci. *94*, 2168–2173.

Lahuna, O., Quellari, M., Achard, C., Nola, S., Méduri, G., Navarro, C., Vitale, N., Borg, J.-P., and Misrahi, M. (2005). Thyrotropin receptor trafficking relies on the hScrib–βPIX–GIT1–ARF6 pathway. EMBO J. *24*, 1364–1374.

Laprise, P., Beronja, S., Silva-Gagliardi, N.F., Pellikka, M., Jensen, A.M., McGlade, C.J., and Tepass, U. (2006). The FERM Protein Yurt Is a Negative Regulatory Component of the Crumbs Complex that Controls Epithelial Polarity and Apical Membrane Size. Dev. Cell *11*, 363–374.

Laprise, P., Lau, K.M., Harris, K.P., Silva-Gagliardi, N.F., Paul, S.M., Beronja, S., Beitel, G.J., McGlade, C.J., and Tepass, U. (2009). Yurt, Coracle, Neurexin IV and the Na(+),K(+)-ATPase form a novel group of epithelial polarity proteins. Nature *459*, 1141–1145.

Lee, M., and Vasioukhin, V. (2008). Cell polarity and cancer - cell and tissue polarity as a non-canonical tumor suppressor. J. Cell Sci. *121*, 1141–1150.

Lindon, C., Grant, R., and Min, M. (2016). Ubiquitin-Mediated Degradation of Aurora Kinases. Front. Oncol. *5*.

Lippincott-Schwartz, J., and Patterson, G.H. (2003). Development and use of fluorescent protein markers in living cells. Science *300*, 87–91.

Lisovsky, M., Dresser, K., Baker, S., Fisher, A., Woda, B., Banner, B., and Lauwers, G.Y. (2009). Cell polarity protein Lgl2 is lost or aberrantly localized in gastric dysplasia and adenocarcinoma: an immunohistochemical study. Mod. Pathol. *22*, 977–984.

Lisovsky, M., Ogawa, F., Dresser, K., Woda, B., and Lauwers, G.Y. (2010). Loss of cell polarity protein Lgl2 in foveolar-type gastric dysplasia: correlation with expression of the apical marker aPKC-zeta. Virchows Arch. Int. J. Pathol. *457*, 635–642.

Littlepage, L.E., and Ruderman, J.V. (2002). Identification of a new APC/C recognition domain, the A box, which is required for the Cdh1-dependent destruction of the kinase Aurora-A during mitotic exit. Genes Dev. *16*, 2274–2285.

Lohia, M., Qin, Y., and Macara, I.G. (2012). The Scribble Polarity Protein Stabilizes E-Cadherin/p120-Catenin Binding and Blocks Retrieval of E-Cadherin to the Golgi. PLoS ONE *7*, e51130.

Lorenzo, C., Liao, Q., Hardwicke, M.A., and Ducommun, B. (2009). Pharmacological inhibition of Aurora-A but not Aurora-B impairs interphase microtubule dynamics. Cell Cycle *8*, 1733–1737.

Luxenburg, C., Pasolli, H.A., Williams, S.E., and Fuchs, E. (2011). Developmental roles for Srf, cortical cytoskeleton and cell shape in epidermal spindle orientation. Nat. Cell Biol. *13*, 203–214.

Ma, S., Vigneron, S., Robert, P., Strub, J.M., Cianferani, S., Castro, A., and Lorca, T. (2016). Greatwall dephosphorylation and inactivation upon mitotic exit is triggered by PP1. J. Cell Sci. *129*, 1329–1339.

Macara Ian G., and McCaffrey Luke (2013). Cell polarity in morphogenesis and metastasis. Philos. Trans. R. Soc. B Biol. Sci. *368*, 20130012.

MacKelvie, S.H., Andrews, P.D., and Stark, M.J. (1995). The Saccharomyces cerevisiae gene SDS22 encodes a potential regulator of the mitotic function of yeast type 1 protein phosphatase. Mol. Cell. Biol. *15*, 3777–3785.

Mahowald, A.P. (1972). Ultrastructural observations on oogenesis in *Drosophila*. J. Morphol. *137*, 29–48.

Manfruelli, P., Arquier, N., Hanratty, W.P., and Sémériva, M. (1996). The tumor suppressor gene, lethal(2)giant larvae (1(2)g1), is required for cell shape change of epithelial cells during *Drosophila* development. Dev. Camb. Engl. *122*, 2283–2294.

Margolis, B., and Borg, J.-P. (2005). Apicobasal polarity complexes. J. Cell Sci. *118*, 5157–5159.

Martins, T., Eusebio, N., Correia, A., Marinho, J., Casares, F., and Pereira, P.S. (2017). TGFβ/Activin signalling is required for ribosome biogenesis and cell growth in *Drosophila* salivary glands. Open Biol. *7*, 160258.

Massimi, P., Gammoh, N., Thomas, M., and Banks, L. (2004). HPV E6 specifically targets different cellular pools of its PDZ domain-containing tumour suppressor substrates for proteasome-mediated degradation. Oncogene *23*, 8033–8039.

Mathew, D., Gramates, L.S., Packard, M., Thomas, U., Bilder, D., Perrimon, N., Gorczyca, M., and Budnik, V. (2002). Recruitment of scribble to the synaptic scaffolding complex requires GUK-holder, a novel DLG binding protein. Curr. Biol. CB *12*, 531–539.

Matsumine, A., Ogai, A., Senda, T., Okumura, N., Satoh, K., Baeg, G.H., Kawahara, T., Kobayashi, S., Okada, M., Toyoshima, K., et al. (1996). Binding of APC to the human homolog of the *Drosophila* discs large tumor suppressor protein. Science *272*, 1020–1023.

Mayer-Jaekel, R.E., Baumgartner, S., Bilbe, G., Ohkura, H., Glover, D.M., and Hemmings, B.A. (1992). Molecular cloning and developmental expression of the catalytic and 65-kDa regulatory subunits of protein phosphatase 2A in *Drosophila*. Mol. Biol. Cell *3*, 287–298.

McGill, M.A., McKinley, R.F.A., and Harris, T.J.C. (2009). Independent cadherin–catenin and Bazooka clusters interact to assemble adherens junctions. J. Cell Biol. *185*, 787–796.

McLaughlin, J.M., and Bratu, D.P. (2015). *Drosophila melanogaster* Oogenesis: An Overview. In *Drosophila* Oogenesis: Methods and Protocols, D.P. Bratu, and G.P. McNeil, eds. (New York, NY: Springer New York), pp. 1–20.

McLaughlin, S., and Murray, D. (2005). Plasma membrane phosphoinositide organization by protein electrostatics. Nature *438*, 605–611.

van Meer, G., and Simons, K. (1986). The function of tight junctions in maintaining differences in lipid composition between the apical and the basolateral cell surface domains of MDCK cells. EMBO J. *5*, 1455–1464.

Meghini, F., Martins, T., Tait, X., Fujimitsu, K., Yamano, H., Glover, D.M., and Kimata, Y. (2016). Targeting of Fzr/Cdh1 for timely activation of the APC/C at the centrosome during mitotic exit. Nat. Commun. *7*.

Megraw, T.L., Li, K., Kao, L.R., and Kaufman, T.C. (1999). The centrosomin protein is required for centrosome assembly and function during cleavage in *Drosophila*. Dev. Camb. Engl. *126*, 2829–2839.

Meiselbach, H., Sticht, H., and Enz, R. (2006). Structural analysis of the protein phosphatase 1 docking motif: molecular description of binding specificities identifies interacting proteins. Chem. Biol. *13*, 49–59.

Menéndez, J., Pérez-Garijo, A., Calleja, M., and Morata, G. (2010). A tumor-suppressing mechanism in *Drosophila* involving cell competition and the Hippo pathway. Proc. Natl. Acad. Sci. U. S. A. *107*, 14651–14656.

Miles, C.M., Lott, S.E., Hendriks, C.L.L., Ludwig, M.Z., Manu, Williams, C.L., and Kreitman, M. (2011). Artificial Selection on Egg Size Perturbs Early Pattern Formation in *Drosophila melanogaster*. Evolution *65*, 33–42.

Mirzoyan, Z., Sollazzo, M., Allocca, M., Valenza, A.M., Grifoni, D., and Bellosta, P. (2019). *Drosophila melanogaster*: A Model Organism to Study Cancer. Front. Genet. *10*.

Morais-de-Sá, E., and Sunkel, C. (2013). Adherens junctions determine the apical position of the midbody during follicular epithelial cell division. EMBO Rep. *14*, 696–703.

Morais-de-Sá, E., Mirouse, V., and St Johnston, D. (2010). aPKC phosphorylation of Bazooka defines the apical/lateral border in *Drosophila* epithelial cells. Cell *141*, 509–523.

Moreira, S., and Morais-de-Sá, E. (2016). Spatiotemporal phosphoregulation of Lgl: Finding meaning in multiple on/off buttons. BioArchitecture *6*, 29–38.

Moura, M., and Conde, C. (2019). Phosphatases in Mitosis: Roles and Regulation. Biomolecules *9*, 55.

Müller, H.-A.J. (2000). Genetic control of epithelial cell polarity: Lessons from *Drosophila*. Dev. Dyn. *218*, 52–67.

Müsch A., Cohen, D., Yeaman, C., Nelson, W.J., Rodriguez-Boulan, E., and Brennwald, P.J. (2002). Mammalian Homolog of *Drosophila* Tumor Suppressor Lethal (2) Giant Larvae Interacts with Basolateral Exocytic Machinery in Madin-Darby Canine Kidney Cells. Mol. Biol. Cell *13*, 158–168.

Murray, N.R., Kalari, K.R., and Fields, A.P. (2011). Protein Kinase Cι Expression and Oncogenic Signaling Mechanisms in Cancer. J. Cell. Physiol. *226*, 879–887.

Nagasaka, K., Seiki, T., Yamashita, A., Massimi, P., Subbaiah, V.K., Thomas, M., Kranjec, C., Kawana, K., Nakagawa, S., Yano, T., et al. (2013). A Novel Interaction between hScrib and PP1γ Downregulates ERK Signaling and Suppresses Oncogene-Induced Cell Transformation. PLOS ONE *8*, e53752.

Nakagawa, S., and Huibregtse, J.M. (2000). Human scribble (Vartul) is targeted for ubiquitin-mediated degradation by the high-risk papillomavirus E6 proteins and the E6AP ubiquitin-protein ligase. Mol. Cell. Biol. *20*, 8244–8253.

Nakajima, Y., Meyer, E.J., Kroesen, A., McKinney, S.A., and Gibson, M.C. (2013). Epithelial junctions maintain tissue architecture by directing planar spindle orientation. Nature *500*, 359–362.

Nam, K.H., Kim, M.A., Choe, G., Kim, W.H., and Lee, H.S. (2014). Deregulation of the cell polarity protein Lethal giant larvae 2 (Lgl2) correlates with gastric cancer progression. Gastric Cancer *17*, 610–620.

Nam, S.-C., Mukhopadhyay, B., and Choi, K.-W. (2007). Antagonistic functions of Par-1 kinase and protein phosphatase 2A are required for localization of Bazooka and photoreceptor morphogenesis in *Drosophila*. Dev. Biol. *306*, 624–635.

Naora, H., and Montell, D.J. (2005). Ovarian Cancer Metastasis: Integrating insights from disparate model organisms. Nat. Rev. Cancer *5*, 355.

Nasa, I., and Kettenbach, A.N. (2018). Coordination of Protein Kinase and Phosphoprotein Phosphatase Activities in Mitosis. Front. Cell Dev. Biol. *6*.

Ng, B.F., Selvaraj, G.K., Santa-Cruz Mateos, C., Grosheva, I., Alvarez-Garcia, I., Martín-Bermudo, M.D., and Palacios, I.M. (2016). α-Spectrin and integrins act together to regulate actomyosin and columnarization, and to maintain a monolayered follicular epithelium. Dev. Camb. Engl. *143*, 1388–1399.

Nikonova, A.S., Astsaturov, I., Serebriiskii, I.G., Dunbrack, R.L., and Golemis, E.A. (2013). Aurora-A kinase (AURKA) in normal and pathological cell growth. Cell. Mol. Life Sci. CMLS *70*, 661–687.

Nilsson, J. (2019). Protein phosphatases in the regulation of mitosis. J. Cell Biol. *218*, 395–409.

Nunbhakdi-Craig, V., Machleidt, T., Ogris, E., Bellotto, D., White, C.L., and Sontag, E. (2002). Protein phosphatase 2A associates with and regulates atypical PKC and the epithelial tight junction complex. J. Cell Biol. *158*, 967–978.

Ogawa, H., Ohta, N., Moon, W., and Matsuzaki, F. (2009). Protein phosphatase 2A negatively regulates aPKC signaling by modulating phosphorylation of Par-6 in *Drosophila* neuroblast asymmetric divisions. J. Cell Sci. *122*, 3242–3249.

Ohkura, H., and Yanagida, M. (1991). S. pombe gene sds22+ essential for a midmitotic transition encodes a leucine-rich repeat protein that positively modulates protein phosphatase-1. Cell *64*, 149–157.

Ohshiro, T., Yagami, T., Zhang, C., and Matsuzaki, F. (2000). Role of cortical tumour-suppressor proteins in asymmetric division of *Drosophila* neuroblast. Nature *408*, 593.

Olivieri, D., Sykora, M.M., Sachidanandam, R., Mechtler, K., and Brennecke, J. (2010). An in vivo RNAi assay identifies major genetic and cellular requirements for primary piRNA biogenesis in *Drosophila*. EMBO J. *29*, 3301–3317.

O'Shaughnessy, B., and Thiyagarajan, S. (2018). Mechanisms of contractile ring tension production and constriction. Biophys. Rev. *10*, 1667–1681.

Oshima, K., and Fehon, R.G. (2011). Analysis of protein dynamics within the septate junction reveals a highly stable core protein complex that does not include the basolateral polarity protein Discs large. J. Cell Sci. *124*, 2861–2871.

Osswald, M., Santos, A.F., and Morais-de-Sá, E. (2019). Light-Induced Protein Clustering for Optogenetic Interference and Protein Interaction Analysis in *Drosophila* S2 Cells. Biomolecules *9*, 61.

Ouyang, Z., Zhan, W., and Dan, L. (2010). hScrib, a human homolog of *Drosophila* neoplastic tumor suppressor, is involved in the progress of endometrial cancer. Oncol. Res. *18*, 593–599.

Pagliarini, R.A. (2003). A Genetic Screen in *Drosophila* for Metastatic Behavior. Science *302*, 1227–1231.

Pancratov, R., Peng, F., Smibert, P., Yang, S., Olson, E.R., Guha-Gilford, C., Kapoor, A.J., Liang, F.-X., Lai, E.C., Flaherty, M.S., et al. (2013). The miR-310/13 cluster antagonizes β-catenin function in the regulation of germ and somatic cell differentiation in the *Drosophila* testis. Dev. Camb. Engl. *140*, 2904–2916.

Parker, L., Gross, S., Beullens, M., Bollen, M., Bennett, D., and Alphey, L. (2002). Functional interaction between nuclear inhibitor of protein phosphatase type 1 (NIPP1) and protein phosphatase type 1 (PP1) in *Drosophila*: consequences of over-expression of NIPP1 in flies and suppression by co-expression of PP1. Biochem. J. *368*, 789–797.

Parsons, L.M., Portela, M., Grzeschik, N.A., and Richardson, H.E. (2014). Lgl regulates Notch signaling via endocytosis, independently of the apical aPKC-Par6-Baz polarity complex. Curr. Biol. CB *24*, 2073–2084.

Parsons, L.M., Grzeschik, N.A., Amaratunga, K., Burke, P., Quinn, L.M., and Richardson, H.E. (2017). A Kinome RNAi Screen in *Drosophila* Identifies Novel Genes Interacting with Lgl, aPKC, and Crb Cell Polarity Genes in Epithelial Tissues. G3amp58 GenesGenomesGenetics *7*, 2497–2509.

Pénalva, C., and Mirouse, V. (2012). Tissue-specific function of Patj in regulating the Crumbs complex and epithelial polarity. Development *139*, 4549–4554.

Peyre, E., Jaouen, F., Saadaoui, M., Haren, L., Merdes, A., Durbec, P., and Morin, X. (2011). A lateral belt of cortical LGN and NuMA guides mitotic spindle movements and planar division in neuroepithelial cells. J. Cell Biol. *193*, 141–154.

Pimentel, A.C., and Venkatesh, T.R. (2005). rap gene encodes Fizzy-related protein (Fzr) and regulates cell proliferation and pattern formation in the developing *Drosophila* eye-antennal disc. Dev. Biol. *285*, 436–446.

Plant, P.J., Fawcett, J.P., Lin, D.C.C., Holdorf, A.D., Binns, K., Kulkarni, S., and Pawson, T. (2003). A polarity complex of mPar-6 and atypical PKC binds, phosphorylates and regulates mammalian Lgl. Nat. Cell Biol. *5*, 301–308.

Posch, M., Khoudoli, G.A., Swift, S., King, E.M., DeLuca, J.G., and Swedlow, J.R. (2010). Sds22 regulates aurora B activity and microtubule–kinetochore interactions at mitosis. J. Cell Biol. *191*, 61–74.

Prasad, M., Jang, A.C.-C., Starz-Gaiano, M., Melani, M., and Montell, D.J. (2007). A protocol for culturing *Drosophila melanogaster* stage 9 egg chambers for live imaging. Nat. Protoc. *2*, 2467–2473.

Raghavan, S., Williams, I., Aslam, H., Thomas, D., Szöor, B., Morgan, G., Gross, S., Turner, J., Fernandes, J., VijayRaghavan, K., et al. (2000). Protein phosphatase 1beta is required for the maintenance of muscle attachments. Curr. Biol. CB *10*, 269–272.

Regala, R.P., Weems, C., Jamieson, L., Khoor, A., Edell, E.S., Lohse, C.M., and Fields, A.P. (2005). Atypical Protein Kinase Cı Is an Oncogene in Human Non–Small Cell Lung Cancer. Cancer Res. *65*, 8905–8911.

Rino, J., Martin, R.M., Carvalho, T., and Carmo-Fonseca, M. (2014). Imaging dynamic interactions between spliceosomal proteins and pre-mRNA in living cells. Methods *65*, 359–366.

Roche, J.P., Packard, M., Moeckel-Cole, S.A., and Budnik, V. (2002). Regulation of synaptic plasticity and synaptic vesicle dynamics by the PDZ protein Scribble. J. Neurosci. Off. J. Soc. Neurosci. *22*, 6471–6479.

Rodrigues, N.T.L., Lekomtsev, S., Jananji, S., Kriston-Vizi, J., Hickson, G.R.X., and Baum, B. (2015). Kinetochore-localized PP1-Sds22 couples chromosome segregation to polar relaxation. Nature *524*, 489–492.

Rodríguez, A. del V., Didiano, D., and Desplan, C. (2011). Power tools for gene expression and clonal analysis in *Drosophila*. Nat. Methods *9*, 47–55.

Rodriguez, J., Peglion, F., Martin, J., Hubatsch, L., Reich, J., Hirani, N., Gubieda, A.G., Roffey, J., Fernandes, A.R., St Johnston, D., et al. (2017). aPKC Cycles between Functionally Distinct PAR Protein Assemblies to Drive Cell Polarity. Dev. Cell *42*, 400-415.e9.

Rodriguez-Boulan, E., and Macara, I.G. (2014). Organization and execution of the epithelial polarity programme. Nat. Rev. Mol. Cell Biol. *15*, 225–242.

Rolls, M.M., Albertson, R., Shih, H.-P., Lee, C.-Y., and Doe, C.Q. (2003). *Drosophila* aPKC regulates cell polarity and cell proliferation in neuroblasts and epithelia. J. Cell Biol. *163*, 1089–1098.

Rørth, P. (1998). Gal4 in the *Drosophila* female germline. Mech. Dev. *78*, 113–118.

Rosse, C., Linch, M., Kermorgant, S., Cameron, A.J.M., Boeckeler, K., and Parker, P.J. (2010). PKC and the control of localized signal dynamics. Nat. Rev. Mol. Cell Biol. *11*, 103–112.

Rugjee, K.N., Roy Chaudhury, S., Al-Jubran, K., Ramanathan, P., Matina, T., Wen, J., and Brogna, S. (2013). Fluorescent protein tagging confirms the presence of ribosomal proteins at *Drosophila* polytene chromosomes. PeerJ *1*, e15.

Saadaoui, M., Machicoane, M., di Pietro, F., Etoc, F., Echard, A., and Morin, X. (2014). Dlg1 controls planar spindle orientation in the neuroepithelium through direct interaction with LGN. J. Cell Biol. *206*, 707–717.

Saito, Y., Nakaoka, T., Muramatsu, T., Ojima, H., Sukeda, A., Sugiyama, Y., Uchida, R., Furukawa, R., Kitahara, A., Sato, T., et al. (2018). Induction of differentiation of intrahepatic cholangiocarcinoma cells to functional hepatocytes using an organoid culture system. Sci. Rep. *8*, 2821.

Schimanski, C.C., Schmitz, G., Kashyap, A., Bosserhoff, A.K., Bataille, F., Schäfer, S.C., Lehr, H.A., Berger, M.R., Galle, P.R., Strand, S., et al. (2005). Reduced expression of Hugl-1, the human homologue of *Drosophila* tumour suppressor gene lgl, contributes to progression of colorectal cancer. Oncogene *24*, 3100–3109.

Schindelin, J., Arganda-Carreras, I., Frise, E., Kaynig, V., Longair, M., Pietzsch, T., Preibisch, S., Rueden, C., Saalfeld, S., Schmid, B., et al. (2012). Fiji: an open-source platform for biological-image analysis. Nat. Methods *9*, 676–682.

Schneider, I. (1972). Cell lines derived from late embryonic stages of *Drosophila melanogaster*. J. Embryol. Exp. Morphol. *27*, 353–365.

Schuhmacher, D., Sontag, J.-M., and Sontag, E. (2019). Protein Phosphatase 2A: More Than a Passenger in the Regulation of Epithelial Cell–Cell Junctions. Front. Cell Dev. Biol. *7*, 30.

Sen, A., Nagy-Zsvér-Vadas, Z., and Krahn, M.P. (2012). *Drosophila* PATJ supports adherens junction stability by modulating Myosin light chain activity. J. Cell Biol. *199*, 685–698.

Seth, A., Sheth, P., Elias, B.C., and Rao, R. (2007). Protein phosphatases 2A and 1 interact with occludin and negatively regulate the assembly of tight junctions in the CACO-2 cell monolayer. J. Biol. Chem. *282*, 11487–11498.

Shao, W., Wu, J., Chen, J., Lee, D.M., Tishkina, A., and Harris, T.J.C. (2010). A Modifier Screen for Bazooka/PAR-3 Interacting Genes in the *Drosophila* Embryo Epithelium. PLoS ONE *5*.

Shi, Y. (2009). Serine/Threonine Phosphatases: Mechanism through Structure. Cell *139*, 468–484.

Shiomi, K., Takeichi, M., Nishida, Y., Nishi, Y., and Uemura, T. (1994). Alternative cell fate choice induced by low-level expression of a regulator of protein phosphatase 2A in the *Drosophila* peripheral nervous system. Development *120*, 1591–1599.

Singh, A.P., Bafna, S., Chaudhary, K., Venkatraman, G., Smith, L., Eudy, J.D., Johansson, S.L., Lin, M.-F., and Batra, S.K. (2008). Genome-wide Expression Profiling Reveals Transcriptomic Variation and Perturbed Gene Networks in Androgen-dependent and Androgen-independent Prostate Cancer Cells. Cancer Lett. *259*, 28–38.

Snaith, H.A., Armstrong, C.G., Guo, Y., Kaiser, K., and Cohen, P.T. (1996). Deficiency of protein phosphatase 2A uncouples the nuclear and centrosome cycles and prevents attachment of microtubules to the kinetochore in *Drosophila* microtubule star (mts) embryos. J. Cell Sci. *109 (Pt 13)*, 3001–3012.

Soriano, E.V., Ivanova, M.E., Fletcher, G., Riou, P., Knowles, P.P., Barnouin, K., Purkiss, A., Kostelecky, B., Saiu, P., Linch, M., et al. (2016). aPKC Inhibition by Par3 CR3 Flanking Regions Controls Substrate Access and Underpins Apical-Junctional Polarization. Dev. Cell *38*, 384–398.

Sotillos, S., Díaz-Meco, M.T., Caminero, E., Moscat, J., and Campuzano, S. (2004). DaPKC-dependent phosphorylation of Crumbs is required for epithelial cell polarity in *Drosophila*. J. Cell Biol. *166*, 549–557.

Sprague, B.L., and McNally, J.G. (2005). FRAP analysis of binding: proper and fitting. Trends Cell Biol. *15*, 84–91.

Stauffer, T.P., Ahn, S., and Meyer, T. (1998). Receptor-induced transient reduction in plasma membrane PtdIns(4,5)P2 concentration monitored in living cells. Curr. Biol. CB *8*, 343–346.

Stefanatos, R.K.A., and Vidal, M. (2011). Tumor invasion and metastasis in *Drosophila*: a bold past, a bright future. J. Genet. Genomics Yi Chuan Xue Bao *38*, 431–438.

Stephens, R., Lim, K., Portela, M., Kvansakul, M., Humbert, P.O., and Richardson, H.E. (2018). The Scribble Cell Polarity Module in the Regulation of Cell Signaling in Tissue Development and Tumorigenesis. J. Mol. Biol. *430*, 3585–3612.

Strand, D. (1994). The *Drosophila* lethal(2)giant larvae tumor suppressor protein forms homo-oligomers and is associated with nonmuscle myosin II heavy chain. J. Cell Biol. *127*, 1361–1373.

Strand, D. (1998). The tumour suppresor l(2)gl; a myosin II-binding protein family. G Proteins Cytoskelet. Cancer 61–78.

Sugihara, T., Nakagawa, S., Sasajima, Y., Ichinose, T., Hiraike, H., Kondo, F., Uozaki, H., Fukusato, T., and Ayabe, T. (2016). Loss of the cell polarity determinant human Discs-large is a novel molecular marker of nodal involvement and poor prognosis in endometrial cancer. Br. J. Cancer *114*, 1012–1018.

Sun, Y., Yan, Y., Denef, N., and Schüpbach, T. (2011). Regulation of somatic myosin activity by Protein Phosphatase 1β controls *Drosophila* oocyte polarization. Dev. Camb. Engl. *138*, 1991–2001.

Suzuki, A. (2006). The PAR-aPKC system: lessons in polarity. J. Cell Sci. *119*, 979–987.

Swarup, S., Pradhan-Sundd, T., and Verheyen, E.M. (2015). Genome-wide identification of phospho-regulators of Wnt signaling in *Drosophila*. Development *142*, 1502–1515.

Szentpetery, Z., Balla, A., Kim, Y.J., Lemmon, M.A., and Balla, T. (2009). Live cell imaging with protein domains capable of recognizing phosphatidylinositol 4,5-bisphosphate; a comparative study. BMC Cell Biol. *10*, 67.

Tanaka, T., Kimura, M., Matsunaga, K., Fukada, D., Mori, H., and Okano, Y. (1999). Centrosomal Kinase AIK1 Is Overexpressed in Invasive Ductal Carcinoma of the Breast. Cancer Res. *59*, 2041–2044.

Tanentzapf, G., and Tepass, U. (2003). Interactions between the crumbs, lethal giant larvae and bazooka pathways in epithelial polarization. Nat. Cell Biol. *5*, 46–52.

Tanentzapf, G., Smith, C., McGlade, J., and Tepass, U. (2000). Apical, Lateral, and Basal Polarization Cues Contribute to the Development of the Follicular Epithelium during *Drosophila* Oogenesis. J. Cell Biol. *151*, 891–904.

Tepass, U. (1996). Crumbs, a Component of the Apical Membrane, Is Required for Zonula Adherens Formation in Primary Epithelia of*Drosophila* . Dev. Biol. *177*, 217–225.

Tepass, U. (2012). The Apical Polarity Protein Network in *Drosophila* Epithelial Cells: Regulation of Polarity, Junctions, Morphogenesis, Cell Growth, and Survival. Annu. Rev. Cell Dev. Biol. *28*, 655–685.

Tepass, U., and Knust, E. (1993). Crumbs and stardust act in a genetic pathway that controls the organization of epithelia in *Drosophila melanogaster*. Dev. Biol. *159*, 311–326.

Tepass, U., Tanentzapf, G., Ward, R., and Fehon, R. (2001). Epithelial cell polarity and cell junctions in *Drosophila*. Annu. Rev. Genet. *35*, 747–784.

Thieleke-Matos, C., Osório, D.S., Carvalho, A.X., and Morais-de-Sá, E. (2017). Chapter Seven - Emerging Mechanisms and Roles for Asymmetric Cytokinesis. In International Review of Cell and Molecular Biology, L. Galluzzi, ed. (Academic Press), pp. 297–345.

Thomas, U., Phannavong, B., Müller, B., Garner, C.C., and Gundelfinger, E.D. (1997). Functional expression of rat synapse-associated proteins SAP97 and SAP102 in *Drosophila* dlg-1 mutants: effects on tumor suppression and synaptic bouton structure. Mech. Dev. *62*, 161–174.

Traweger, A., Wiggin, G., Taylor, L., Tate, S.A., Metalnikov, P., and Pawson, T. (2008). Protein phosphatase 1 regulates the phosphorylation state of the polarity scaffold Par-3. Proc. Natl. Acad. Sci. *105*, 10402–10407.

Trinkle-Mulcahy, L., Andrews, P.D., Wickramasinghe, S., Sleeman, J., Prescott, A., Lam, Y.W., Lyon, C., Swedlow, J.R., and Lamond, A.I. (2003). Time-lapse imaging reveals dynamic relocalization of PP1gamma throughout the mammalian cell cycle. Mol. Biol. Cell *14*, 107–117.

Tsukita, S., Furuse, M., and Itoh, M. (2001). Multifunctional strands in tight junctions. Nat. Rev. Mol. Cell Biol. *2*, 285–293.

Tsuruga, T., Nakagawa, S., Watanabe, M., Takizawa, S., Matsumoto, Y., Nagasaka, K., Sone, K., Hiraike, H., Miyamoto, Y., Hiraike, O., et al. (2007). Loss of Hugl-1 expression associates with lymph node metastasis in endometrial cancer. Oncol. Res. *16*, 431–435.

Udho, E., Tedesco, V.C., Zygmunt, A., and Krucher, N.A. (2002). PNUTS (phosphatase nuclear targeting subunit) inhibits retinoblastoma-directed PP1 activity. Biochem. Biophys. Res. Commun. *297*, 463–467.

Uemura, T., Shiomi, K., Togashi, S., and Takeichi, M. (1993). Mutation of twins encoding a regulator of protein phosphatase 2A leads to pattern duplication in *Drosophila* imaginal discs. Genes Dev. *7*, 429–440.

Vaizel-Ohayon, D., and Schejter, E.D. (1999). Mutations in centrosomin reveal requirements for centrosomal function during early *Drosophila* embryogenesis. Curr. Biol. CB *9*, 889–898.

Verdugo-Sivianes, E.M., Navas, L., Molina-Pinelo, S., Ferrer, I., Quintanal-Villalonga, A., Peinado, J., Garcia-Heredia, J.M., Felipe-Abrio, B., Muñoz-Galvan, S., Marin, J.J., et al. (2017). Coordinated downregulation of Spinophilin and the catalytic subunits of PP1, PPP1CA/B/C, contributes to a worse prognosis in lung cancer. Oncotarget *8*, 105196–105210.

Vereshchagina, N., Bennett, D., Gross, S., Vissi, E., White-Cooper, H., and Alphey, L. (2004). The Essential Role of PP1β in *Drosophila* Is to Regulate Nonmuscle Myosin□D. Mol. Biol. Cell *15*, 11.

Virshup, D.M., and Shenolikar, S. (2009). From promiscuity to precision: protein phosphatases get a makeover. Mol. Cell *33*, 537–545.

de Vreede, G., Schoenfeld, J.D., Windler, S.L., Morrison, H., Lu, H., and Bilder, D. (2014). The Scribble module regulates retromer-dependent endocytic trafficking during epithelial polarization. Development *141*, 2796–2802.

Wakula, P., Beullens, M., Ceulemans, H., Stalmans, W., and Bollen, M. (2003). Degeneracy and Function of the Ubiquitous RVXF Motif That Mediates Binding to Protein Phosphatase-1. J. Biol. Chem. *278*, 18817–18823.

Walther, R.F., and Pichaud, F. (2010). Crumbs/DaPKC-Dependent Apical Exclusion of Bazooka Promotes Photoreceptor Polarity Remodeling. Curr. Biol. *20*, 1065–1074.

Wang, N., Leung, H.-T., Mazalouskas, M.D., Watkins, G.R., Gomez, R.J., and Wadzinski, B.E. (2012). Essential Roles of the Tap42-Regulated Protein Phosphatase 2A (PP2A) Family in Wing Imaginal Disc Development of *Drosophila melanogaster*. PLoS ONE *7*.

Wang, S., Mandell, J.D., Kumar, Y., Sun, N., Morris, M.T., Arbelaez, J., Nasello, C., Dong, S., Duhn, C., Zhao, X., et al. (2018). De Novo Sequence and Copy Number Variants Are Strongly Associated with Tourette Disorder and Implicate Cell Polarity in Pathogenesis. Cell Rep. *24*, 3441-3454.e12.

Weith, M., Seiler, J., van den Boom, J., Kracht, M., Hülsmann, J., Primorac, I., del Pino Garcia, J., Kaschani, F., Kaiser, M., Musacchio, A., et al. (2018). Ubiquitin-Independent Disassembly by a p97 AAA-ATPase Complex Drives PP1 Holoenzyme Formation. Mol. Cell *72*, 766-777.e6.

Winter, S.L., Bosnoyan-Collins, L., Pinnaduwage, D., and Andrulis, I.L. (2007). The interaction of PP1 with BRCA1 and analysis of their expression in breast tumors. BMC Cancer *7*, 85.

Wirtz-Peitz, F., Nishimura, T., and Knoblich, J.A. (2008). Linking cell cycle to asymmetric division: Aurora-A phosphorylates the Par complex to regulate Numb localization. Cell *135*, 161–173.

Wodarz, A. (2000). Tumor suppressors: Linking cell polarity and growth control. Curr. Biol. *10*, R624–R626.

Wodarz, A., and Näthke, I. (2007). Cell polarity in development and cancer. Nat. Cell Biol. *9*, 1016–1024.

Wodarz, A., Grawe, F., and Knust, E. (1993). CRUMBS is involved in the control of apical protein targeting during *Drosophila* epithelial development. Mech. Dev. *44*, 175–187.

Wodarz, A., Hinz, U., Engelbert, M., and Knust, E. (1995). Expression of crumbs confers apical character on plasma membrane domains of ectodermal epithelia of *Drosophila*. Cell *82*, 67–76.

Woodhouse, E., Hersperger, E., and Shearn, A. (1998). Growth, metastasis, and invasiveness of *Drosophila* tumors caused by mutations in specific tumor suppressor genes. Dev. Genes Evol. *207*, 542–550.

Woods, D.F., and Bryant, P.J. (1991). The discs-large tumor suppressor gene of *Drosophila* encodes a guanylate kinase homolog localized at septate junctions. Cell *66*, 451–464.

Woods, D.F., Hough, C., Peel, D., Callaini, G., and Bryant, P.J. (1996). Dlg protein is required for junction structure, cell polarity, and proliferation control in *Drosophila* epithelia. J. Cell Biol. *134*, 1469–1482.

Wu, J.Q., Guo, J.Y., Tang, W., Yang, C.-S., Freel, C.D., Chen, C., Nairn, A.C., and Kornbluth, S. (2009). PP1-mediated dephosphorylation of phosphoproteins at mitotic exit is controlled by inhibitor-1 and PP1 phosphorylation. Nat. Cell Biol. *11*, 644–651.

Wu, X., Tanwar, P.S., and Raftery, L.A. (2008). *Drosophila* follicle cells: Morphogenesis in an eggshell. Semin. Cell Dev. Biol. *19*, 271–282.

Wurzenberger, C., and Gerlich, D.W. (2011). Phosphatases: providing safe passage through mitotic exit. Nat. Rev. Mol. Cell Biol. *12*, 469–482.

Wurzenberger, C., Held, M., Lampson, M.A., Poser, I., Hyman, A.A., and Gerlich, D.W. (2012). Sds22 and Repo-Man stabilize chromosome segregation by counteracting Aurora B on anaphase kinetochores. J Cell Biol *198*, 173–183.

Xu, T., and Rubin, G.M. (1993). Analysis of genetic mosaics in developing and adult *Drosophila* tissues. Dev. Camb. Engl. *117*, 1223–1237.

Xu, Z., Vagnarelli, P., Ogawa, H., Samejima, K., and Earnshaw, W.C. (2010). Gradient of Increasing Aurora B Kinase Activity Is Required for Cells to Execute Mitosis. J. Biol. Chem. *285*, 40163–40170.

Yamada, M., Hirotsune, S., and Wynshaw-Boris, A. (2010). The essential role of LIS1, NDEL1 and Aurora-A in polarity formation and microtubule organization during neurogensis. Cell Adhes. Migr. *4*, 180–184.

Yamaguchi, M., and Yoshida, H. (2018). *Drosophila* as a Model Organism. Adv. Exp. Med. Biol. *1076*, 1–10.

Yamamoto, S., Jaiswal, M., Charng, W.-L., Gambin, T., Karaca, E., Mirzaa, G., Wiszniewski, W., Sandoval, H., Haelterman, N.A., Xiong, B., et al. (2014). A *Drosophila* genetic resource of mutants to study mechanisms underlying human genetic diseases. Cell *159*, 200–214.

Yamanaka, T. (2006). Lgl mediates apical domain disassembly by suppressing the PAR-3-aPKC-PAR-6 complex to orient apical membrane polarity. J. Cell Sci. *119*, 2107–2118.

Yamanaka, T., Horikoshi, Y., Suzuki, A., Sugiyama, Y., Kitamura, K., Maniwa, R., Nagai, Y., Yamashita, A., Hirose, T., Ishikawa, H., et al. (2001). PAR-6 regulates aPKC activity in a novel way and mediates cell-cell contact-induced formation of the epithelial junctional complex. Genes Cells *6*, 721–731.

Yamanaka, T., Horikoshi, Y., Sugiyama, Y., Ishiyama, C., Suzuki, A., Hirose, T., Iwamatsu, A., Shinohara, A., and Ohno, S. (2003). Mammalian Lgl Forms a Protein Complex with PAR-6 and aPKC Independently of PAR-3 to Regulate Epithelial Cell Polarity. Curr. Biol. *13*, 734–743.

Yasumi, M., Sakisaka, T., Hoshino, T., Kimura, T., Sakamoto, Y., Yamanaka, T., Ohno, S., and Takai, Y. (2005). Direct Binding of Lgl2 to LGN during Mitosis and Its Requirement for Normal Cell Division. J. Biol. Chem. *280*, 6761–6765.

Yin, D., Huang, P., Wu, J., and Song, H. (2014). *Drosophila* protein phosphatase V regulates lipid homeostasis via the AMPK pathway. J. Mol. Cell Biol. *6*, 100–102.

Zeitler, J., Hsu, C.P., Dionne, H., and Bilder, D. (2004). Domains controlling cell polarity and proliferation in the *Drosophila* tumor suppressor Scribble. J. Cell Biol. *167*, 1137–1146.

Zhan, L., Rosenberg, A., Bergami, K.C., Yu, M., Xuan, Z., Jaffe, A.B., Allred, C., and Muthuswamy, S.K. (2008). Deregulation of Scribble Promotes Mammary Tumorigenesis and Reveals a Role for Cell Polarity in Carcinoma. Cell *135*, 865–878.

Zhang, H., Neimanis, S., Lopez-Garcia, L.A., Arencibia, J.M., Amon, S., Stroba, A., Zeuzem, S., Proschak, E., Stark, H., Bauer, A.F., et al. (2014). Molecular mechanism of regulation of the atypical protein kinase C by N-terminal domains and an allosteric small compound. Chem. Biol. *21*, 754–765.

Zhang, X., Wang, P., Gangar, A., Zhang, J., Brennwald, P., TerBush, D., and Guo, W. (2005). Lethal giant larvae proteins interact with the exocyst complex and are involved in polarized exocytosis. J. Cell Biol. *170*, 273–283.

Zhang, Y., Guo, H., Kwan, H., Wang, J.-W., Kosek, J., and Lu, B. (2007). PAR-1 Kinase Phosphorylates Dlg and Regulates Its Postsynaptic Targeting at the *Drosophila* Neuromuscular Junction. Neuron *53*, 201–215.

Zhao, P., Teng, X., Tantirimudalige, S.N., Nishikawa, M., Wohland, T., Toyama, Y., and Motegi, F. (2019). Aurora-A Breaks Symmetry in Contractile Actomyosin Networks Independently of Its Role in Centrosome Maturation. Dev. Cell *48*, 631-645.e6.

Zhou, W., and Hong, Y. (2012). *Drosophila* Patj plays a supporting role in apical-basal polarity but is essential for viability. Dev. Camb. Engl. *139*, 2891–2896.

Zhou, H., Kuang, J., Zhong, L., Kuo, W.L., Gray, J.W., Sahin, A., Brinkley, B.R., and Sen, S. (1998). Tumour amplified kinase STK15/BTAK induces centrosome amplification, aneuploidy and transformation. Nat. Genet. *20*, 189–193.

Zhu, J., Shang, Y., Xia, C., Wang, W., Wen, W., and Zhang, M. (2011). Guanylate kinase domains of the MAGUK family scaffold proteins as specific phospho-protein-binding modules. EMBO J. *30*, 4986–4997.

Zhu, J., Shang, Y., Wan, Q., Xia, Y., Chen, J., Du, Q., and Zhang, M. (2014). Phosphorylation-dependent interaction between tumor suppressors Dlg and Lgl. Cell Res. *24*, 451–463.

APPENDIX A

Movie legends

Movie 1: Lgl is reloaded from the cytoplasm to the cortex at mitotic exit.

Mosaic follicular epithelium expressing Lgl-GFP in a clonal manner to visualize Lgl reallocation

Movie 2: Pp1-87B phosphatase is important for Lgl cortical reloading

Follicle epithelium depleted for Pp1-87B retains a large fraction of cortical Lgl-GFP (red in merge with HisRFP in green) before mitotic entry but fails to reload it to the cortex at mitotic exit.

Movie 3: Dynamics of Lgl-GFP in an S2 cell expressing mCherry-tubulin (red).

Time represents min after anaphase

APPENDIX B

Original Publications

1. Moreira, S., Osswald, M., Ventura, G., Gonçalves, M., Sunkel, C.E., and Morais-de-Sá, E. (2019). PP1-Mediated Dephosphorylation of Lgl Controls Apical-basal Polarity. Cell Rep. *26*, 293-301.e7.

2. Moreira, S., and Morais-de-Sá, E. (2016). Spatiotemporal phosphoregulation of Lgl: Finding meaning in multiple on/off buttons. BioArchitecture *6*, 29–38

Report

Cell Reports

PP1-Mediated Dephosphorylation of Lgl Controls Apical-basal Polarity

Graphical Abstract

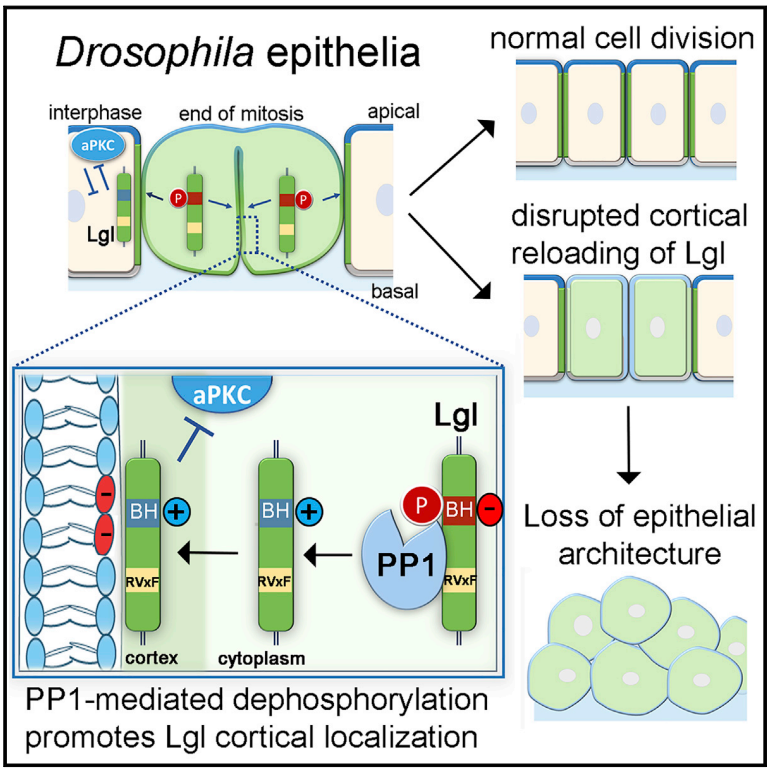

Highlights

- Cytoplasmic Lgl returns to the cortex at mitotic exit in *Drosophila* epithelia
- Lgl cortical localization depends on PP1-mediated dephosphorylation
- PP1 dephosphorylates Lgl to maintain epithelial architecture
- Apical polarization of new daughter cells is coupled with Lgl cortical reloading

Authors

Sofia Moreira, Mariana Osswald, Guilherme Ventura, Margarida Gonçalves, Claudio E. Sunkel, Eurico Morais-de-Sá

Correspondence

eurico.sa@ibmc.up.pt

In Brief

Moreira et al. investigate the post-mitotic polarization of new daughter cells in *Drosophila* epithelia. They identify PP1 phosphatase as a regulator of the conserved basolateral determinant Lgl. Dephosphorylation of Lgl counteracts aPKC/AurA activity, being an essential mechanism to restore Lgl cortical localization and to maintain the architecture of proliferative tissue.

Moreira et al., 2019, Cell Reports *26*, 293–301
January 8, 2019 © 2018 The Author(s).
https://doi.org/10.1016/j.celrep.2018.12.060

CellPress

Cell Reports
Report

OPEN ACCESS
CellPress

PP1-Mediated Dephosphorylation of Lgl Controls Apical-basal Polarity

Sofia Moreira,[1,2] Mariana Osswald,[1,2,3] Guilherme Ventura,[1,2,3,4] Margarida Gonçalves,[1,2] Claudio E. Sunkel,[1,2] and Eurico Morais-de-Sá[1,2,5,*]
[1]Instituto de Biologia Molecular e Celular, Universidade do Porto, Porto, Portugal
[2]Instituto de Investigação e Inovação em Saúde (i3S), Universidade do Porto, Porto, Portugal
[3]These authors contributed equally
[4]Present address: Novo Nordisk Center for Stem Cell Biology (DanStem), University of Copenhagen, Copenhagen, Denmark
[5]Lead Contact
*Correspondence: eurico.sa@ibmc.up.pt
https://doi.org/10.1016/j.celrep.2018.12.060

SUMMARY

Apical-basal polarity is a common trait that underlies epithelial function. Although the asymmetric distribution of cortical polarity proteins works in a functioning equilibrium, it also retains plasticity to accommodate cell division, during which the basolateral determinant Lgl is released from the cortex. Here, we investigated how Lgl restores its cortical localization to maintain the integrity of dividing epithelia. We show that cytoplasmic Lgl is reloaded to the cortex at mitotic exit in *Drosophila* epithelia. Lgl cortical localization depends on protein phosphatase 1, which dephosphorylates Lgl on the serines phosphorylated by aPKC and Aurora A kinases through a mechanism that relies on the regulatory subunit Sds22 and a PP1-interacting RVxF motif of Lgl. This mechanism maintains epithelial polarity and is of particular importance at mitotic exit to couple Lgl cortical reloading with the polarization of the apical domain. Hence, PP1-mediated dephosphorylation of Lgl preserves the apical-basal organization of proliferative epithelia.

INTRODUCTION

Epithelial tissues compartmentalize multicellular organisms and have a variety of specialized roles that rely on asymmetries in protein and lipid composition and the precise positioning of intercellular junctions along its apical-basal axis (Rodriguez-Boulan and Macara, 2014). This polarity axis is defined by conserved apical-basal polarity proteins, which segregate into distinct domains along the epithelial cell cortex (Flores-Benitez and Knust, 2016). One such protein is Lethal giant larvae (Lgl), originally identified as a tumor suppressor in *Drosophila* and often misregulated in human cancer (Gateff, 1978; Halaoui and McCaffrey, 2015). In epithelia, Lgl cooperates with Discs Large (Dlg) and Scribbled as a basolateral determinant to restrict the localization and activity of the atypical protein kinase C (aPKC) and Crumbs complexes to the apical domain (Bilder et al., 2000, 2003; Tanentzapf and Tepass, 2003), possibly by inhibiting aPKC activity (Atwood and Prehoda, 2009; Wirtz-Peitz et al., 2008; Yamanaka et al., 2006) or regulating the trafficking of apical transmembrane proteins (Fletcher et al., 2012; Jossin et al., 2017).

Lgl associates with the actomyosin cytoskeleton (Betschinger et al., 2003; Dahan et al., 2012; Strand et al., 1994), and recent work revealed that its cortical localization is, however, primarily mediated by binding to plasma membrane phosphoinositides through a positively charged basic and hydrophobic (BH) motif (Bailey and Prehoda, 2015; Dong et al., 2015). This motif is phosphorylated by aPKC (Betschinger et al., 2003; Plant et al., 2003) to exclude Lgl from the apical cortex during interphase and by mitotic kinase Aurora A (AurA) to completely release Lgl from the cortex and promote proper mitotic spindle orientation in epithelial tissue (Bell et al., 2015; Carvalho et al., 2015). Interestingly, apical polarity proteins such as aPKC, Par-6, and Par-3 also adjust localization during epithelial mitosis, as shown in *Drosophila* and during early embryogenesis of *Nematostella vectensis* (Bergstralh et al., 2013; Carvalho et al., 2015; Morais-de-Sá and Sunkel, 2013; Ragkousi et al., 2017; Rosa et al., 2015). However, it is unknown how Lgl cortical localization is restored at the end of cell division and how this is coordinated with daughter cell polarization. Moreover, although phosphorylation controls Lgl localization and function, how (and whether) counteracting protein phosphatases actively dephosphorylate Lgl remains undetermined.

Here we report the PP1-Sds22 complex as a critical regulator of Lgl dephosphorylation, promoting its localization at the cortex and plasma membrane. Because dividing cells must deal with the complete pool of Lgl in the cytoplasmic and hyperphosphorylated form, this mechanism has foremost significance to timely polarize daughter cells and maintain the architecture of proliferating epithelia.

RESULTS

Cytoplasmic Lgl Returns to the Cortex at Mitotic Exit

To investigate how Lgl localization is restored in the daughter cells, we examined the dynamics of Lgl subcellular redistribution in the follicular epithelium, a monolayered tissue that envelops the germline in the *Drosophila* ovary. Lgl cytoplasmic levels decline from around 2 min until about 15 min after anaphase onset, with the concomitant accumulation of Lgl at the daughter-daughter (d-d) cell interface just as the new membrane ingresses from the basal side (Figures 1A and 1B; Video S1). This

This is an open access article under the CC BY-NC-ND license (http://creativecommons.org/licenses/by-nc-nd/4.0/).

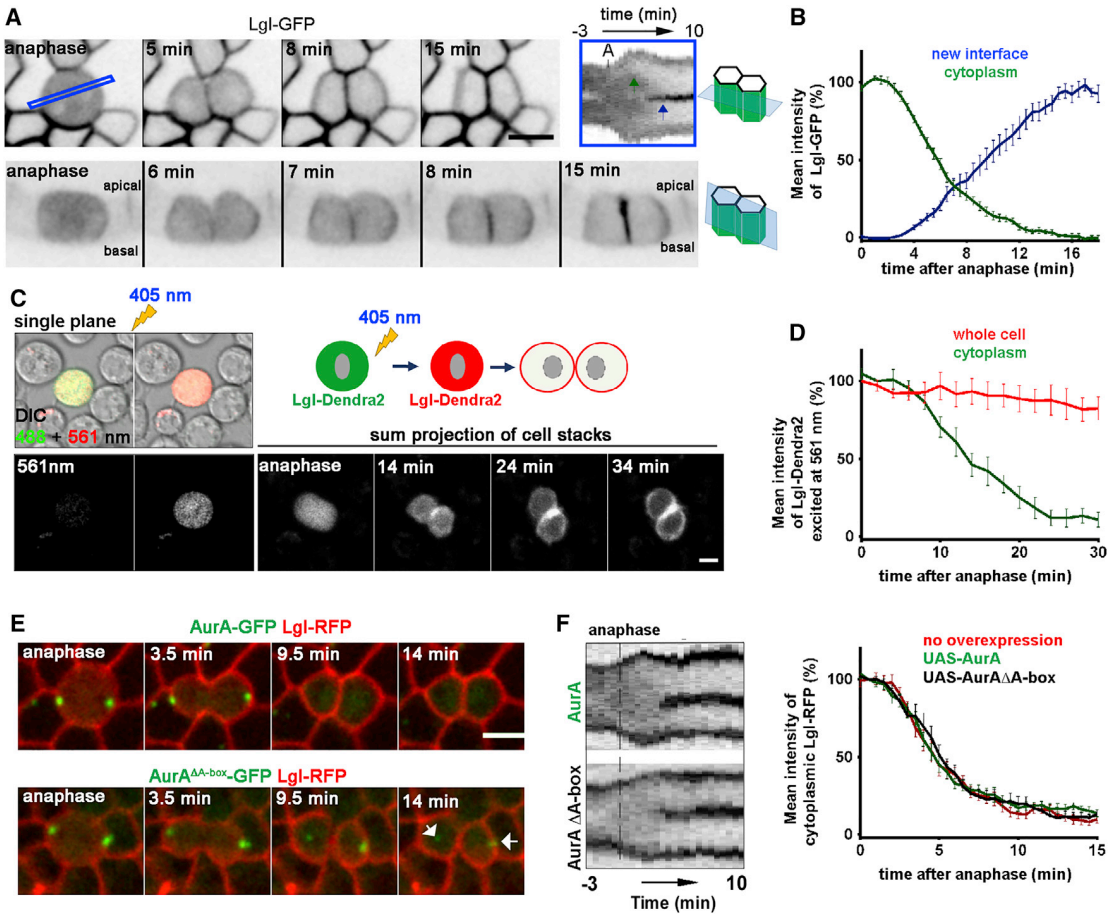

Figure 1. Cytoplasmic Lgl Returns to the Cortex at Mitotic Exit

(A) Dynamic reallocation of Lgl-GFP to the lateral cortex of follicle cells at mitotic exit. A kymograph of the highlighted region shows cytoplasmic decay (green arrow) and Lgl accumulation at the daughter-daughter (d-d) interface (blue arrow).

(B) Normalized mean intensity of Lgl-GFP in the cytoplasm (n = 21) and at the daughter-daughter interface (n = 16) since anaphase.

(C) Photoconversion of Lgl-Dendra2 in mitotic S2 cells shows that cytoplasmic Lgl returns to the cortex at mitotic exit.

(D) Normalized mean intensity of photoconverted Lgl-Dendra2 in the cytoplasm (green) and the integrated density of photoconverted Lgl in the whole cell (red) (n = 6).

(E) Dividing follicle cells expressing Lgl-red fluorescent protein (RFP) and AurA-GFP or AurA$^{\Delta Abox}$-GFP, which is detectable longer at centrosomes (arrows).

(F) Normalized mean intensity of cytoplasmic Lgl-RFP in control cells (red, n = 14) and cells overexpressing AurA-GFP (n = 13) and AurA$^{\Delta Abox}$-GFP (n = 9). The kymographs show the patterns of Lgl-RFP localization.

Data are presented as mean ± SEM. Scale bars, 5 μm.

See also Figure S1.

dynamic reallocation of Lgl-GFP at mitotic exit is also reproduced in the *Drosophila* embryonic epithelium (Figure S1A). To test whether Lgl returns from the cytoplasm to the cortex, we labeled cytoplasmic Lgl through photoconversion during mitosis in S2 cells (Figure 1C). Photoconverted Lgl-Dendra2 accumulates at the cortex when cells exit mitosis (Figure 1C). Moreover, the labeled pool of Lgl-Dendra2 is not degraded during mitotic exit because the total fluorescence of the photoconverted protein remains constant during the period of cytoplasmic signal decay (Figure 1D). Thus, at mitotic exit, Lgl is fully reloaded from the cytoplasm to the cortex. The kinetics of cytoplasmic decay are therefore an accurate readout for the sum of Lgl cortical reloading to the pre-existing cell membranes and to the newly formed daughter-daughter interface.

Lgl release from the cortex at mitotic entry is controlled by AurA (Bell et al., 2015; Carvalho et al., 2015), which is targeted for degradation by the Cdh1-activated anaphase-promoting complex (APC-Cdh1) at mitotic exit (Castro et al., 2002). To investigate whether AurA degradation determines Lgl cortical reloading, we overexpressed AurA-GFP and a stabilized version, AurA$^{\Delta Abox}$-GFP, which lacks the A-box domain and impairs recognition by the APC-Cdh1 complex without interfering with the catalytic domain (Meghini et al., 2016). Stabilization of AurA does not change Lgl dynamics at mitotic exit (Figures 1E and 1F). Moreover, although RNAi depletion of AurA interferes with cortical release at mitotic entry in S2 cells (Carvalho et al., 2015), it does not affect Lgl cortical reloading (Figure S1B). Altogether, we conclude that

regulation of AurA stability is not the timer controlling Lgl reloading to the cortex.

PP1 Antagonizes aPKC and AurA-Mediated Phosphorylation of Lgl

Lgl phosphorylation reduces its affinity to the plasma membrane and to the underlying cortex (Bailey and Prehoda, 2015; Dong et al., 2015; Betschinger et al., 2003). Thus, Lgl cortical reloading should require dephosphorylation, but a phosphatase for Lgl has yet to be described. Two good candidates are PP1 and PP2A, serine and threonine-specific phosphatases activated at mitotic exit (Barr et al., 2011). These phosphatases form multimeric holoenzyme complexes containing catalytic and regulatory subunits. There are four *Drosophila* genes encoding PP1 catalytic subunits: *Pp1β9C* (*flw*), *Pp1-87B*, *Pp1α-96A*, and *Pp1α13C*, which is responsible for negligible PP1 activity, whereas the PP2A catalytic subunit is encoded by *microtubule star* (*mts*). RNAi-mediated depletion of PP1α-96A, Flw, or Mts in the follicular epithelium does not significantly affect Lgl localization (Figures S2A–S2D), whereas PP1-87B depletion leads to Lgl mislocalization to the cytoplasm, as observed by clonal (Figure 2A) and global depletion (Figure 2C).

To confirm whether PP1-87B is the only essential PP1 catalytic subunit required for proper Lgl localization, we generated mutant clones using null alleles of *flw* and *Pp1α-96A*. Lgl localization in these mutant clones is indistinguishable from wild-type cells, whereas Lgl is fully cytoplasmic in double *pp1-87B*, *pp1α-96A* mutant clones (Figure 2B), indicating that PP1-87B enables cortical Lgl localization. This is unlikely to stem from a specific function of PP1-87B but, rather, from it being the most abundant PP1c isozyme because PP1 catalytic subunits have highly overlapping roles (Kirchner et al., 2007). Consistent with this, Lgl cortical localization in PP1-87B-depleted follicle cells is rescued by overexpression of human PPP1cc, whose closest ortholog is *Pp1α-96A* (Figure 2C). Moreover, overexpression of a global PP1 inhibitor, NiPp1, also disrupts Lgl localization (Figure 2D). Thus, overall PP1 activity is essential for proper Lgl localization to the lateral cortex in *Drosophila* epithelia, which is consistent with a role in Lgl dephosphorylation.

We used recombinant MBP-Lgl and Lgl-GFP immunoprecipitated from ovaries to examine whether PP1 could directly dephosphorylate Lgl on S656, an aPKC and AurA phosphorylation site. Incubation of recombinant PP1 with Lgl previously phosphorylated by AurA results in a concentration- and time-dependent decrease in S656 phosphorylation, indicating that Lgl is a substrate for PP1 (Figures 2E and 2F). Importantly, the activity of PP1 toward Lgl is specific compared with λ phosphatase, which fails to dephosphorylate Lgl as efficiently (Figure S2E). Furthermore, we used *Drosophila* S2 cells to dissect whether Lgl mislocalization upon PP1 inactivation results from hyperphosphorylation on the aPKC and AurA phosphorylation sites. Cytoplasmic localization of Lgl is reproduced upon PP1-87B depletion in S2 cells, whereas co-depletion of aPKC rescues Lgl cortical localization (Figures 2G, S2F, and S2G). Moreover, we simultaneously analyzed the localization of Lgl and Lgl^{3A}, which harbors mutations in the serines controlled by aPKC (S656, S660, and S664) and AurA (S656 and S664) (Bell et al., 2015; Betschinger et al., 2003; Carvalho et al., 2015). Strikingly, Lgl^{3A} is retained at the cortex, in contrast with the cytoplasmic accumulation of Lgl in the follicular epithelium and in S2 cells depleted of PP1-87B (Figure 2H). Hence, these results collectively suggest that PP1-mediated dephosphorylation of the aPKC and AurA phosphorylation sites promotes Lgl localization at the lateral cortex.

PP1-Mediated Dephosphorylation of Lgl Maintains Epithelial Architecture and Polarity

PP1-87B RNAi leads to loss of epithelial polarity in the follicular epithelium, with consequent cell invasion and multilayering (Figure S3). This mimics Lgl loss of function phenotypes in the follicular epithelium (Bilder et al., 2000), but PP1 is involved in multiple pathways, which may indirectly contribute to the phenotype. Given that cortical Lgl antagonizes apical determinants, we tested whether reducing aPKC levels could attenuate this phenotype. *aPKC* heterozygosity strongly suppresses the multilayering phenotype of PP1-87B-depleted tissue (Figure 3A), suggesting that PP1 activity balances apical activity by promoting Lgl cortical localization.

Association of PP1 with regulatory subunits and substrates is often mediated by a RVxF docking motif, [KR] [X]$_{0\text{-}1}$[VI]{P} [FW], which binds a PP1 hydrophobic pocket (Wakula et al., 2003). Interestingly, Lgl has a sequence that fits this motif and that is widely conserved in metazoans (Figure 3B). To define the functional significance of Lgl dephosphorylation by PP1, we mutated two critical residues of the PP1 docking motif (Meiselbach et al., 2006). In comparison to Lgl-GFP, Lgl^{K327A,F331A}-GFP accumulates strongly in the cytoplasm of follicle cells and shows increased S656 phosphorylation (Figures 3C and 3D). More importantly, expression of Lgl^{K327A,F331A}-GFP does not support epithelial apical-basal polarity in *lgl*-null mutant clones, leading to multilayered tissue where aPKC is mislocalized (Figures 3E and 3F). Thus, PP1-mediated dephosphorylation promotes Lgl localization to the cortex, where it can act as basolateral determinant to control epithelial organization.

PP1 Orchestrates Apical-basal Polarization at Mitotic Exit

Lgl must be relocated to the epithelial cortex of daughter cells at mitotic exit, making this period particularly challenging for PP1-mediated dephosphorylation of Lgl. Accordingly, Lgl cortical reloading is minor in PP1-87B depleted follicle cells (~70% of mitotic levels remain cytoplasmic 35 min after anaphase onset versus ~20% in the control; Figures 4A and 4B), even for cells that present Lgl largely cortical before mitotic entry (Video S2). Moreover, depletion of the PP1 regulatory subunit Sds22, which enhances PP1 activity during cytokinesis (Kunda et al., 2012; Ohkura and Yanagida, 1991), also delays Lgl reloading at mitotic exit (Figure 4B). Sds22 RNAi has, however, a milder effect than PP1-87B RNAi, culminating in lower levels of cytoplasmic Lgl during early interphase (~40% of mitotic levels). We obtained similar results in *Drosophila* S2 cells (Figure S4A), suggesting that Sds22 is particularly significant to boost PP1 activity to deal with the complete pool of phosphorylated and cytoplasmic Lgl at mitotic exit. Lgl^{K327A,F331A} also shows disrupted cytoplasmic decay in both the embryonic and

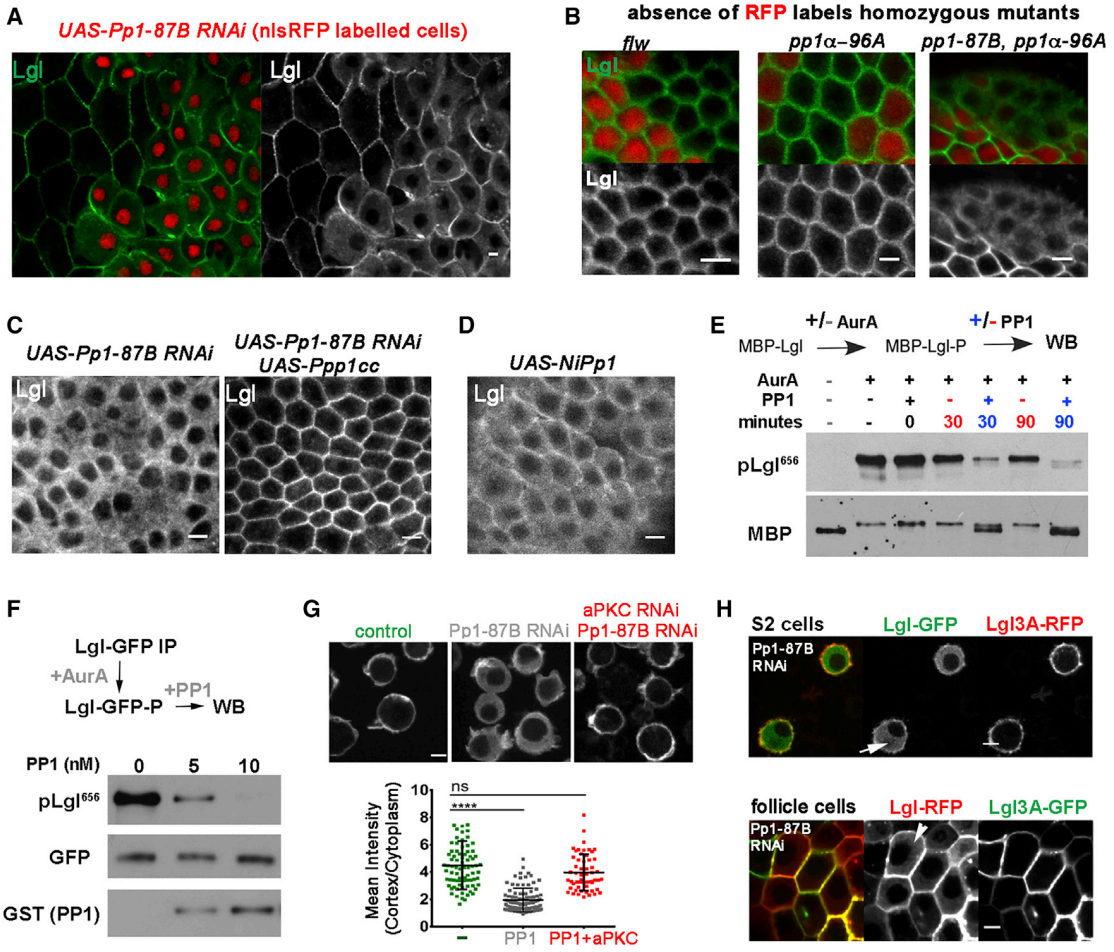

Figure 2. PP1 Antagonizes aPKC/AurA Phosphorylation to Control Lgl Cortical Localization

(A and B) Follicular epithelium stained with anti-Lgl (A) upon clonal depletion of PP1-87B by RNAi (labeled with nuclear localization signal-red fluorescent protein [nlsRFP]) and in (B) egg chambers with mutant clones (absence of nlsRFP) for *flw*^{FP41}, *pp1α-96A*^{2}, or *pp1-87B*$^{87Bg-3}$, *pp1α-96A*^{2}.

(C) Disruption of Lgl localization by PP1-87B RNAi (100%, n = 40) is rescued by overexpression of the human PPP1CC (normal localization, 88%; n = 34).

(D) Overexpression of the PP1 inhibitor NiPp1 induces Lgl-GFP cytoplasmic localization.

(E and F) Western blot analysis of an *in vitro* dephosphorylation assay performed after Lgl phosphorylation by AurA. Dephosphorylation by GST-PP1γ of (E) recombinant maltose binding protein (MBP)-Lgl and (F) Lgl-GFP immunoprecipitated from ovary extracts was detected using a S656 phosphospecific antibody. Blots were also probed for (E) MBP, (F) GFP, and glutathione S-transferase (GST) as controls.

(G) PP1-87B RNAi in S2 cells induces Lgl cytoplasmic mislocalization, which is rescued by simultaneous aPKC depletion. The cortex/cytoplasmic intensity ratio is plotted. Mean ± SD (n = 79 for control, n = 94 for PP1-87B RNAi and n = 74 for PP1-87B RNAi + aPKC RNAi). The p value was calculated with one-way ANOVA ($p < 0.0001$).

(H) Images of S2 cells and follicle cells depleted for PP1-87B by RNAi and co-expressing fluorescently tagged Lgl and Lgl^{3A}.

Scale bars, 5 μm.

See also Figure S2.

follicular epithelium (Figures 4C, 4D, and S4B). Nevertheless, Lgl^{K327A,F331A}-GFP cytoplasmic decay is much faster than Lgl-GFP in PP1-87B-depleted follicle cells. Because Sds22 RNAi induces strong cytoplasmic retention of Lgl^{K327A,F331A}-GFP (Figure 4C and 4D), we conclude that this PP1-docking motif promotes robust dephosphorylation but is dispensable for partial PP1 activity when the PP1-Sds22 complex is available.

In many proliferative tissues, a new daughter-daughter interface is formed upon cell division to hold daughter cells together (Firmino et al., 2016; Herszterg et al., 2014; Olivier et al., 2010). We investigated the importance of Lgl cortical reloading for daughter-daughter interface polarization by examining the segregation of its mutual antagonist aPKC to the apical domain. Simultaneous imaging of Lgl-mCherry with aPKC-GFP shows that Lgl starts localizing to the lateral cortex before apical accumulation of aPKC (Figure 4E, kymographs). This likely results from the basal-to-apical ingression of the cytokinetic furrow, described previously in many epithelia (Herszterg et al., 2014; Morais-de-Sá and Sunkel, 2013). Moreover, Lgl accumulation

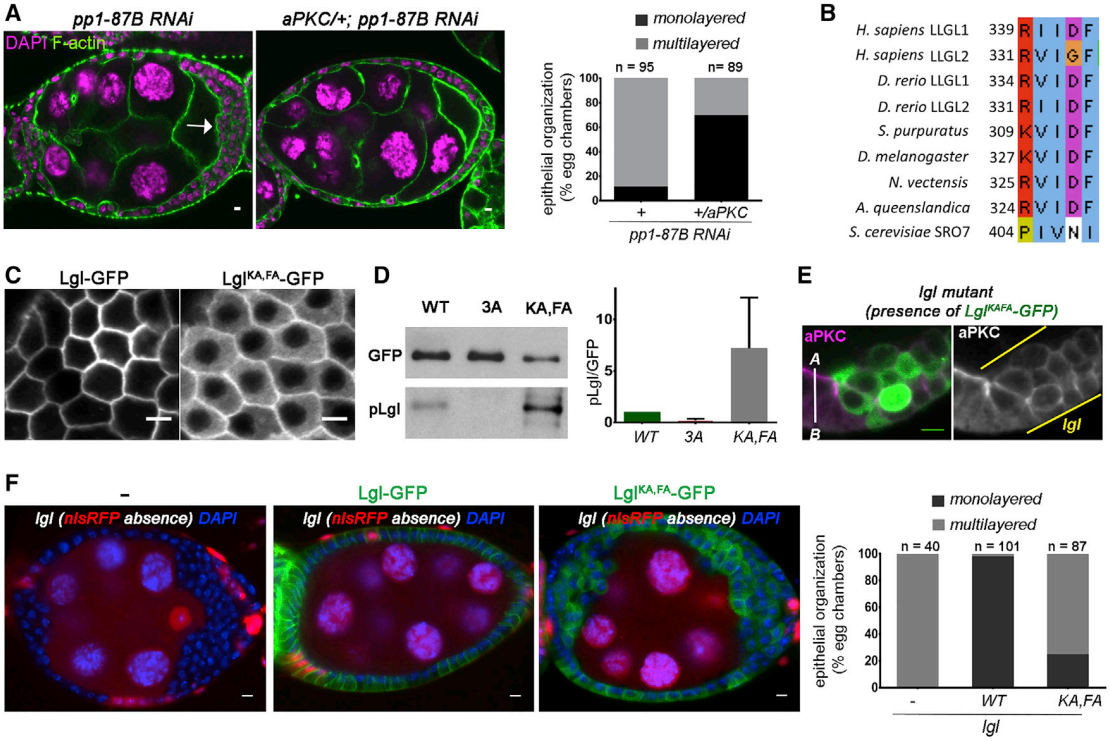

Figure 3. PP1-Mediated Dephosphorylation of Lgl Maintains Epithelial Architecture

(A) Egg chambers stained for F-actin and DAPI. The plot depicts the percentage of egg chambers (stage 4 to stage 8) with multilayered follicular epithelium (arrow) in *tj-Gal4/+;UAS-Pp1-87B RNAi/+* (~88% multilayering) and *tj-Gal4/aPKC^{k06403};UAS-Pp1-87B RNAi/+* (~30% multilayering) flies.

(B) Aligned amino acid sequences of the putative PP1-docking site motif.

(C) Lgl^{K327A,F331A}–GFP shows a stronger accumulation in the follicle cell cytoplasm than Lgl-GFP.

(D) Western blot of protein extracts from ovaries with expression of Lgl-GFP (WT), Lgl^{3A}-GFP (3A), and Lgl^{K327A,F331A}-GFP (KA, FA). Blots were probed with a S656 phosphospecific antibody (pLgl) and anti-GFP. The pLgl/GFP ratio was determined in three independent experiments and normalized to the WT (mean ± SEM is shown).

(E and F) Lgl^{K327A,F331A}-GFP does not sustain epithelial polarity and monolayered organization. Shown are mosaic egg chambers of *lgl^{27S3}* mutant follicle cell clones marked with the expression of Lgl^{K327A,F331A}-GFP (GAL80 absence) and stained for aPKC (E) and *lgl^{27S3}* mutant clones marked by absence of RFP and with general expression of the indicated Lgl variant in the follicular epithelium (F). DAPI staining is also shown. The graph includes data from 3 independent experiments quantifying mutant clones larger than 1/4 of stage 6–stage 8 egg chambers.

Scale bars, 5 μm.

See also Figure S3.

is completed before aPKC reaches maximum apical levels (Figure 4E, kymographs). We therefore hypothesized that loading Lgl to the lateral cortex could be necessary for aPKC accumulation at the apical side. To test this idea, we used an *lgl* temperature-sensitive allele, *lgl^{ts3}*, which reallocates to the cytoplasm at restrictive temperature (Manfruelli et al., 1996), and limited our analysis to the first 2 hr at 29°C, during which the tissue maintains its monolayered organization (Figure S4B). aPKC accumulation in the apical daughter-daughter interface is drastically impaired in *lgl^{ts3}/lgl^{4}* mutant follicle cells (Figure 4F). Moreover, aPKC localizes ectopically in the lateral domain at the daughter-daughter interface of *lgl^{ts3}/lgl^{4}* mutant cells (Figure 4G; Video S3), suggesting that Lgl cortical reloading restricts aPKC to the apical side by limiting its lateral accumulation. Thus, by controlling the timing of Lgl cortical reloading, PP1 activation synchronizes the polarization of apical and basolateral domains at mitotic exit.

DISCUSSION

Apical-basal polarity relies on the asymmetric distribution of the polarity determinant Lgl to the lateral cortex of epithelial cells. Research regarding Lgl regulation has been focused on the modulation of phosphorylation via aPKC and Aurora kinases. Here we found that PP1 provides another layer of regulation, antagonizing Lgl phosphorylation by aPKC or AurA. We show that PP1-mediated dephosphorylation can control Lgl subcellular distribution in both epithelial and non-epithelial cells and is critical to maintain the monolayered organization and apical-basal polarity. Because Lgl is a general cell polarity regulator (Betschinger et al., 2003; Dahan et al., 2012; Raman et al., 2016) and also controls the Notch and Hippo signaling pathways (Grusche et al., 2011; Parsons et al., 2014), it is likely that the significance of Lgl regulation by PP1 extends to a range of processes, including asymmetric cell division, cell migration, fate specification, and growth control.

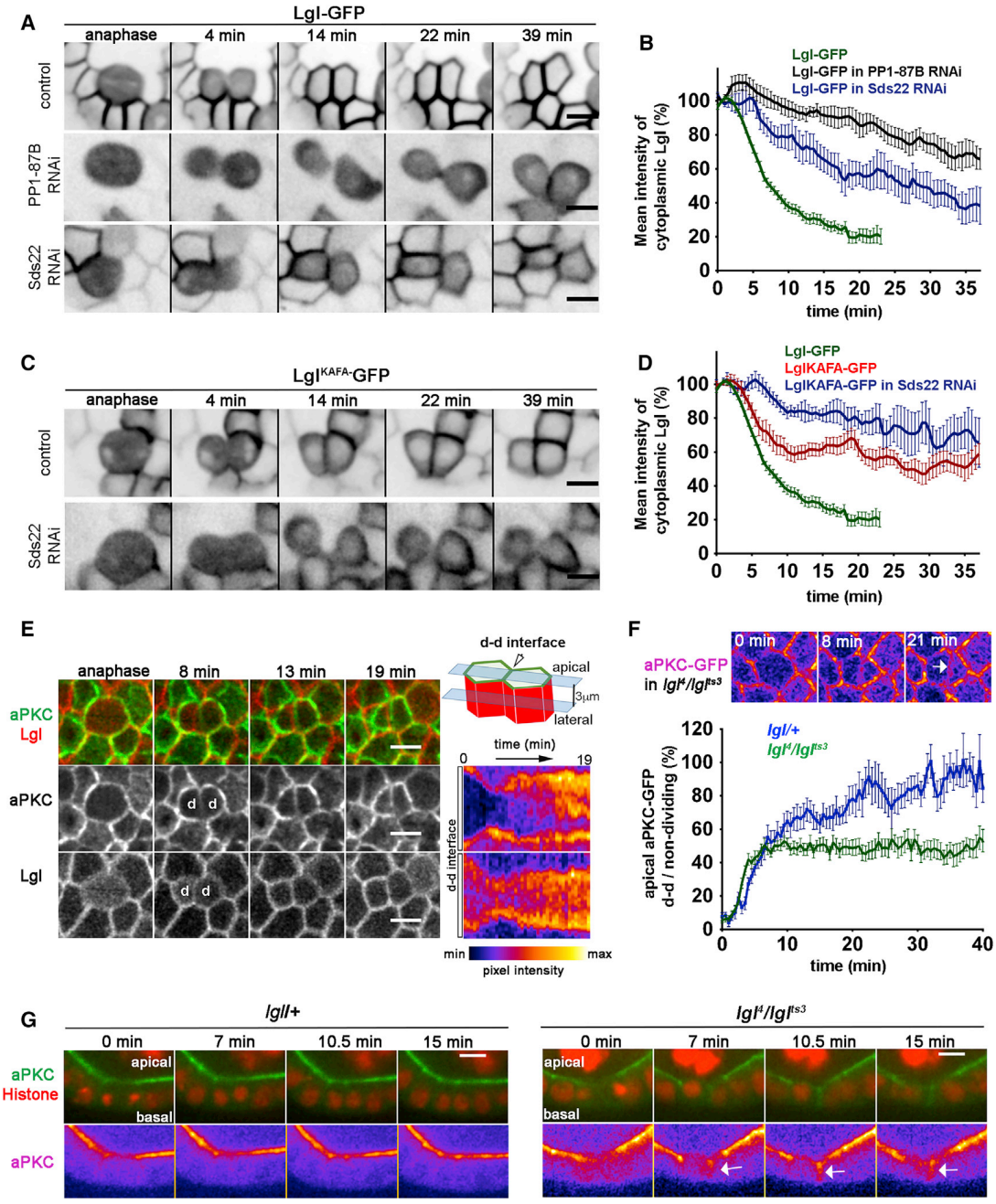

Figure 4. PP1-Mediated Dephosphorylation of Lgl Promotes Apical-basal Polarization at Mitotic Exit

(A) Disrupted cortical reloading of Lgl in PP1-87B- and Sds22-depleted follicle cells.

(B) Normalized mean intensity of cytoplasmic Lgl-GFP in control (n = 22, also in D), PP1-87B RNAi (n = 8), and Sds22 RNAi (n = 11).

(C) Defects in cortical reloading of Lgl^{K327A,F331A}-GFP are enhanced by Sds22 depletion.

(D) Normalized mean intensity of cytoplasmic Lgl^{K327A,F331A}-GFP in control (n = 11) and Sds22 RNAi (n = 12).

(E) Time-lapse images of follicle cells expressing aPKC-GFP and Lgl-mCherry at endogenous levels. The kymographs (pseudocolored to intensity) detail their accumulation at the daughter-daughter interface, projected in the selected apical and lateral planes, respectively.

(F) aPKC-GFP accumulation in the daughter-daughter interface (arrow, fluorescence intensity normalized to non-dividing cells) is strongly reduced in *lgl*^{4}/*lgl*^{ts3} mutant cells imaged at restrictive temperature (n = 40) (~50% of *lgl*/+, n = 21).

(G) Time-lapse images of midsagittal egg chamber sections show that aPKC-GFP accumulates in the lateral side of the new daughter-daughter interface in *lgl*^{4}/*lgl*^{ts3} mutant cells (arrows) imaged at restrictive temperature.

Time is shown since anaphase. Data show mean ± SEM. Scale bars, 5 μm.

See also Figure S4.

PP1 directly dephosphorylates Lgl, and we show that Lgl localization is insensitive to PP1 depletion when the aPKC and AurA phosphorylation sites are mutated. Thus, PP1 dephosphorylation promotes the phosphorylation-inhibited binding between the BH motif of Lgl and plasma membrane phosphoinositides (Bailey and Prehoda, 2015; Dong et al., 2015). This mode of regulation parallels cell polarization in fission yeast, where the protein phosphatase 1 complex Tea4-Dis2 controls dephosphorylation of the polarity regulator Pom1 to expose a basic region with affinity for plasma membrane phospholipids (Hachet et al., 2011). Furthermore, PP1 has been shown to dephosphorylate Par-3 on aPKC phosphorylation sites (Traweger et al., 2008). PP1 is therefore a critical regulator of cell polarity and antagonizes aPKC activity over multiple substrates in epithelial tissues.

We also show that Sds22 promotes Lgl cortical localization. Sds22 has been identified previously as a regulator of epithelial organization, but this function has been mostly linked to the deleterious effect of myosin or moesin hyperphosphorylation (Grusche et al., 2009; Jiang et al., 2011). Interestingly, similarly to loss of function of the basolateral polarity proteins Scrib, Dlg, and Lgl, *sds22* mutation also promotes neoplastic tumor development in *Drosophila* imaginal discs (Jiang et al., 2011). Thus, the role of the PP1-Sds22 complex in Lgl cortical localization provides a possible mechanistic interpretation for the tumor-suppressive role of Sds22 and its human homolog PPP1R7 (Jiang et al., 2011; Narayan et al., 2003).

Lgl becomes fully cytoplasmic because of AurA phosphorylation at mitotic entry (Bell et al., 2015; Carvalho et al., 2015), and since preexisting phosphorylated Lgl is not degraded, PP1-mediated dephosphorylation is critical to reload cytoplasmic Lgl to the cortex of the daughter cells. Moreover, we show that cortically localized Lgl inhibits aPKC accumulation at the lateral domain of the newly formed interface between daughter cells, promoting its apical localization. Hence, although asymmetric furrow ingression and apical midbody positioning may assist with the establishment of apical-basal asymmetries at mitotic exit (Herszterg et al., 2014; Morais-de-Sá and Sunkel, 2013), PP1-mediated cortical reloading of Lgl plays an essential role in the *de novo* polarization of the daughter-daughter interface. PP1 is tightly regulated throughout the cell cycle, being reactivated at mitotic exit to dephosphorylate a number of mitotic proteins (Kunda et al., 2012; Moura et al., 2017; Wu et al., 2009). This study reveals how the cell cycle-dependent control of PP1 activity also plays an essential role in the context of apical-basal polarity, coupling cell division with the post-mitotic polarization of epithelial cells.

STAR★METHODS

Detailed methods are provided in the online version of this paper and include the following:

- KEY RESOURCES TABLE
- CONTACT FOR REAGENT AND RESOURCE SHARING
- EXPERIMENTAL MODEL AND SUBJECT DETAILS
  - *Drosophila* stocks and genetics
  - *Drosophila* cell culture
- METHOD DETAILS
  - S2 cell stable lines and RNA interference
  - Preparation of ovary and S2 cell protein extracts
  - Immunofluorescence and F-actin staining
  - Cloning of Lgl variants
  - RT-PCR
  - Protein purification
  - *in vitro* dephosphorylation assays
  - Photoconversion experiments in S2 cells
  - Multiple sequence alignments
  - Imaging
- QUANTIFICATION AND STATISTICAL ANALYSIS
  - Cytoplasmic decay of Lgl
  - Lgl accumulation in daughter-daughter interface
  - Intensity of Lgl-Dendra2 upon photoconversion
  - aPKC accumulation in the apical interface formed between daughter cells
  - Interphase cortical/cytoplasmic intensity ratio of Lgl in S2 cells

SUPPLEMENTAL INFORMATION

Supplemental Information includes four figures, one table, and three videos and can be found with this article online at https://doi.org/10.1016/j.celrep.2018.12.060.

ACKNOWLEDGMENTS

We thank Daniel St Johnston, François Schweisguth, Guilles Hickson, Jürgen Knoblich, Torcato Martins, Yang Hong, and the Bloomington Drosophila Stock Center for providing plasmids and fly stocks. This work was funded by national funds through Fundação para a Ciência e a Tecnologia (FCT) under project PTDC/BEX-BCM/0432/2014. This work has also received funding from the project Norte-01-0145-FEDER-000029, supported by Norte Portugal Regional Operational Program (NORTE 2020). E.M. holds an FCT Investigator position. S.M. and M.G. are supported by FCT PhD grants. M.O. is supported by a fellowship from FCT and the GABBA PhD program from the University of Porto.

AUTHORS CONTRIBUTIONS

Conceptualization, S.M. and E.M.; Methodology, S.M., M.O., G.V., and E.M.; Formal Analysis, S.M., M.O., G.V., and E.M.; Investigation, S.M., M.O., G.V., M.G., and E.M.; Writing – Original Draft, E.M.; Writing – Review & Editing, S.M., M.O., G.V., C.S., and E.M.; Supervision, C.S. and E.M.; Funding Acquisition, E.M.

DECLARATION OF INTERESTS

The authors declare no competing interests.

Received: August 1, 2018
Revised: November 23, 2018
Accepted: December 13, 2018
Published: January 8, 2019

REFERENCES

Atwood, S.X., and Prehoda, K.E. (2009). aPKC phosphorylates Miranda to polarize fate determinants during neuroblast asymmetric cell division. Curr. Biol. *19*, 723–729.

Bailey, M.J., and Prehoda, K.E. (2015). Establishment of Par-Polarized Cortical Domains via Phosphoregulated Membrane Motifs. Dev. Cell *35*, 199–210.

Barr, F.A., Elliott, P.R., and Gruneberg, U. (2011). Protein phosphatases and the regulation of mitosis. J. Cell Sci. *124*, 2323–2334.

Bell, G.P., Fletcher, G.C., Brain, R., and Thompson, B.J. (2015). Aurora kinases phosphorylate Lgl to induce mitotic spindle orientation in Drosophila epithelia. Curr. Biol. *25*, 61–68.

Berdnik, D., and Knoblich, J.A. (2002). Drosophila Aurora-A is required for centrosome maturation and actin-dependent asymmetric protein localization during mitosis. Curr. Biol. *12*, 640–647.

Bergstralh, D.T., Lovegrove, H.E., and St Johnston, D. (2013). Discs large links spindle orientation to apical-basal polarity in Drosophila epithelia. Curr. Biol. *23*, 1707–1712.

Besson, C., Bernard, F., Corson, F., Rouault, H., Reynaud, E., Keder, A., Mazouni, K., and Schweisguth, F. (2015). Planar Cell Polarity Breaks the Symmetry of PAR Protein Distribution prior to Mitosis in Drosophila Sensory Organ Precursor Cells. Curr. Biol. *25*, 1104–1110.

Betschinger, J., Mechtler, K., and Knoblich, J.A. (2003). The Par complex directs asymmetric cell division by phosphorylating the cytoskeletal protein Lgl. Nature *422*, 326–330.

Bilder, D., Li, M., and Perrimon, N. (2000). Cooperative regulation of cell polarity and growth by Drosophila tumor suppressors. Science *289*, 113–116.

Bilder, D., Schober, M., and Perrimon, N. (2003). Integrated activity of PDZ protein complexes regulates epithelial polarity. Nat. Cell Biol. *5*, 53–58.

Carvalho, C.A., Moreira, S., Ventura, G., Sunkel, C.E., and Morais-de-Sá, E. (2015). Aurora A triggers Lgl cortical release during symmetric division to control planar spindle orientation. Curr. Biol. *25*, 53–60.

Castro, A., Arlot-Bonnemains, Y., Vigneron, S., Labbé, J.C., Prigent, C., and Lorca, T. (2002). APC/Fizzy-Related targets Aurora-A kinase for proteolysis. EMBO Rep. *3*, 457–462.

Dahan, I., Yearim, A., Touboul, Y., and Ravid, S. (2012). The tumor suppressor Lgl1 regulates NMII-A cellular distribution and focal adhesion morphology to optimize cell migration. Mol. Biol. Cell *23*, 591–601.

Dong, W., Zhang, X., Liu, W., Chen, Y.J., Huang, J., Austin, E., Celotto, A.M., Jiang, W.Z., Palladino, M.J., Jiang, Y., et al. (2015). A conserved polybasic domain mediates plasma membrane targeting of Lgl and its regulation by hypoxia. J. Cell Biol. *211*, 273–286.

Firmino, J., Rocancourt, D., Saadaoui, M., Moreau, C., and Gros, J. (2016). Cell Division Drives Epithelial Cell Rearrangements during Gastrulation in Chick. Dev. Cell *36*, 249–261.

Fletcher, G.C., Lucas, E.P., Brain, R., Tournier, A., and Thompson, B.J. (2012). Positive feedback and mutual antagonism combine to polarize Crumbs in the Drosophila follicle cell epithelium. Curr. Biol. *22*, 1116–1122.

Flores-Benitez, D., and Knust, E. (2016). Dynamics of epithelial cell polarity in Drosophila: how to regulate the regulators? Curr. Opin. Cell Biol. *42*, 13–21.

Gateff, E. (1978). Malignant neoplasms of genetic origin in Drosophila melanogaster. Science *200*, 1448–1459.

Grusche, F.A., Hidalgo, C., Fletcher, G., Sung, H.H., Sahai, E., and Thompson, B.J. (2009). Sds22, a PP1 phosphatase regulatory subunit, regulates epithelial cell polarity and shape [Sds22 in epithelial morphology]. BMC Dev. Biol. *9*, 14.

Grusche, F.A., Degoutin, J.L., Richardson, H.E., and Harvey, K.F. (2011). The Salvador/Warts/Hippo pathway controls regenerative tissue growth in Drosophila melanogaster. Dev. Biol. *350*, 255–266.

Hachet, O., Berthelot-Grosjean, M., Kokkoris, K., Vincenzetti, V., Moosbrugger, J., and Martin, S.G. (2011). A phosphorylation cycle shapes gradients of the DYRK family kinase Pom1 at the plasma membrane. Cell *145*, 1116–1128.

Halaoui, R., and McCaffrey, L. (2015). Rewiring cell polarity signaling in cancer. Oncogene *34*, 939–950.

Heller, D., Hoppe, A., Restrepo, S., Gatti, L., Tournier, A.L., Tapon, N., Basler, K., and Mao, Y. (2016). EpiTools: An Open-Source Image Analysis Toolkit for Quantifying Epithelial Growth Dynamics. Dev. Cell *36*, 103–116.

Herszterg, S., Pinheiro, D., and Bellaïche, Y. (2014). A multicellular view of cytokinesis in epithelial tissue. Trends Cell Biol. *24*, 285–293.

Jiang, Y., Scott, K.L., Kwak, S.J., Chen, R., and Mardon, G. (2011). Sds22/PP1 links epithelial integrity and tumor suppression via regulation of myosin II and JNK signaling. Oncogene *30*, 3248–3260.

Jossin, Y., Lee, M., Klezovitch, O., Kon, E., Cossard, A., Lien, W.H., Fernandez, T.E., Cooper, J.A., and Vasioukhin, V. (2017). Llgl1 Connects Cell Polarity with Cell-Cell Adhesion in Embryonic Neural Stem Cells. Dev. Cell *41*, 481–495.e5.

Kirchner, J., Gross, S., Bennett, D., and Alphey, L. (2007). Essential, overlapping and redundant roles of the Drosophila protein phosphatase 1 alpha and 1 beta genes. Genetics *176*, 273–281.

Kunda, P., Rodrigues, N.T., Moeendarbary, E., Liu, T., Ivetic, A., Charras, G., and Baum, B. (2012). PP1-mediated moesin dephosphorylation couples polar relaxation to mitotic exit. Curr. Biol. *22*, 231–236.

Manfruelli, P., Arquier, N., Hanratty, W.P., and Sémériva, M. (1996). The tumor suppressor gene, lethal(2)giant larvae (l(2)g1), is required for cell shape change of epithelial cells during Drosophila development. Development *122*, 2283–2294.

Meghini, F., Martins, T., Tait, X., Fujimitsu, K., Yamano, H., Glover, D.M., and Kimata, Y. (2016). Targeting of Fzr/Cdh1 for timely activation of the APC/C at the centrosome during mitotic exit. Nat. Commun. *7*, 12607.

Meiselbach, H., Sticht, H., and Enz, R. (2006). Structural analysis of the protein phosphatase 1 docking motif: molecular description of binding specificities identifies interacting proteins. Chem. Biol. *13*, 49–59.

Morais-de-Sá, E., and Sunkel, C. (2013). Adherens junctions determine the apical position of the midbody during follicular epithelial cell division. EMBO Rep. *14*, 696–703.

Moura, M., Osswald, M., Leça, N., Barbosa, J., Pereira, A.J., Maiato, H., Sunkel, C.E., and Conde, C. (2017). Protein Phosphatase 1 inactivates Mps1 to ensure efficient Spindle Assembly Checkpoint silencing. eLife *6*, e25366.

Narayan, G., Pulido, H.A., Koul, S., Lu, X.Y., Harris, C.P., Yeh, Y.A., Vargas, H., Posso, H., Terry, M.B., Gissmann, L., et al. (2003). Genetic analysis identifies putative tumor suppressor sites at 2q35-q36.1 and 2q36.3-q37.1 involved in cervical cancer progression. Oncogene *22*, 3489–3499.

Ohkura, H., and Yanagida, M. (1991). S. pombe gene sds22+ essential for a midmitotic transition encodes a leucine-rich repeat protein that positively modulates protein phosphatase-1. Cell *64*, 149–157.

Olivier, N., Luengo-Oroz, M.A., Duloquin, L., Faure, E., Savy, T., Veilleux, I., Solinas, X., Débarre, D., Bourgine, P., Santos, A., et al. (2010). Cell lineage reconstruction of early zebrafish embryos using label-free nonlinear microscopy. Science *329*, 967–971.

Parsons, L.M., Portela, M., Grzeschik, N.A., and Richardson, H.E. (2014). Lgl regulates Notch signaling via endocytosis, independently of the apical aPKC-Par6-Baz polarity complex. Curr. Biol. *24*, 2073–2084.

Plant, P.J., Fawcett, J.P., Lin, D.C., Holdorf, A.D., Binns, K., Kulkarni, S., and Pawson, T. (2003). A polarity complex of mPar-6 and atypical PKC binds, phosphorylates and regulates mammalian Lgl. Nat. Cell Biol. *5*, 301–308.

Ragkousi, K., Marr, K., McKinney, S., Ellington, L., and Gibson, M.C. (2017). Cell-Cycle-Coupled Oscillations in Apical Polarity and Intercellular Contact Maintain Order in Embryonic Epithelia. Curr. Biol. *27*, 1381–1386.

Raman, R., Damle, I., Rote, R., Banerjee, S., Dingare, C., and Sonawane, M. (2016). aPKC regulates apical localization of Lgl to restrict elongation of microridges in developing zebrafish epidermis. Nat. Commun. *7*, 11643.

Rodriguez-Boulan, E., and Macara, I.G. (2014). Organization and execution of the epithelial polarity programme. Nat. Rev. Mol. Cell Biol. *15*, 225–242.

Rosa, A., Vlassaks, E., Pichaud, F., and Baum, B. (2015). Ect2/Pbl acts via Rho and polarity proteins to direct the assembly of an isotropic actomyosin cortex upon mitotic entry. Dev. Cell *32*, 604–616.

Schindelin, J., Arganda-Carreras, I., Frise, E., Kaynig, V., Longair, M., Pietzsch, T., Preibisch, S., Rueden, C., Saalfeld, S., Schmid, B., et al. (2012). Fiji: an open-source platform for biological-image analysis. Nat. Methods *9*, 676–682.

Strand, D., Jakobs, R., Merdes, G., Neumann, B., Kalmes, A., Heid, H.W., Husmann, I., and Mechler, B.M. (1994). The Drosophila lethal(2)giant larvae tumor suppressor protein forms homo-oligomers and is associated with nonmuscle myosin II heavy chain. J. Cell Biol. *127*, 1361–1373.

Tanentzapf, G., and Tepass, U. (2003). Interactions between the crumbs, lethal giant larvae and bazooka pathways in epithelial polarization. Nat. Cell Biol. *5*, 46–52.

Traweger, A., Wiggin, G., Taylor, L., Tate, S.A., Metalnikov, P., and Pawson, T. (2008). Protein phosphatase 1 regulates the phosphorylation state of the polarity scaffold Par-3. Proc. Natl. Acad. Sci. USA *105*, 10402–10407.

Wakula, P., Beullens, M., Ceulemans, H., Stalmans, W., and Bollen, M. (2003). Degeneracy and function of the ubiquitous RVXF motif that mediates binding to protein phosphatase-1. J. Biol. Chem. *278*, 18817–18823.

Wirtz-Peitz, F., Nishimura, T., and Knoblich, J.A. (2008). Linking cell cycle to asymmetric division: Aurora-A phosphorylates the Par complex to regulate Numb localization. Cell *135*, 161–173.

Wu, J.Q., Guo, J.Y., Tang, W., Yang, C.S., Freel, C.D., Chen, C., Nairn, A.C., and Kornbluth, S. (2009). PP1-mediated dephosphorylation of phosphoproteins at mitotic exit is controlled by inhibitor-1 and PP1 phosphorylation. Nat. Cell Biol. *11*, 644–651.

Yamanaka, T., Horikoshi, Y., Izumi, N., Suzuki, A., Mizuno, K., and Ohno, S. (2006). Lgl mediates apical domain disassembly by suppressing the PAR-3-aPKC-PAR-6 complex to orient apical membrane polarity. J. Cell Sci. *119*, 2107–2118.

STAR★METHODS

KEY RESOURCES TABLE

REAGENT or RESOURCE	SOURCE	IDENTIFIER
Antibodies and F-actin staining		
Rabbit anti-Lgl (d-300) (1:100)	Santa Cruz Biotech	Cat#sc-98260; RRID: AB_1564606
Rabbit anti-aPKC (c-20) (1:500)	Santa Cruz Biotech	Cat#sc-216-G; RRID: AB_632241
Rabbit p-Lgl656 (1:500)	Carvalho et al., 2015	N/A
Rabbit anti-GFP (1:1000)	i3S (Biochemical and Biophysical Technologies)	N/A
Anti-MBP-HRP conjugated (1:10000)	New England Biolabs	Cat#E8038; RRID: AB_1559738
Phalloidin-TRITC	SIGMA-ALDRICH	Cat#P1951; RRID: AB_2315148
Mouse anti-GST (B-14) (1:1000)	Santa Cruz Biotech	Cat#sc-138; RRID: AB_627677
Chemicals, Peptides, and Recombinant Proteins		
Phusion High Fidelity DNA polymerase	New England Biolabs	Cat#M0530S
DreamTaq DNA polymerase	Thermo Fisher Scientific	*Cat#EP0701*
DpnI	New England Biolabs	Cat#R0176S
SuperScript II Reverse Transcriptase	Invitrogen (Life technology)	Cat#18064014
Cellfectin II Reagent	Invitrogen (Life technology)	*Cat#10362100*
Effectene Transfection Reagent	QIAGEN	Cat#301425
GFP-Trap_MA system	ChromoTek GmbH	Cat#gtma-10
Aurora A	Millipore	Cat#14-511
GST-PP1γ	MRC-PPU Reagents (University of Dundee)	N/A
Protein Phosphatase 1	New England Biolabs	Cat#P0754
Lambda Phosphatase	New England Biolabs	Cat#P0753S
Aur A inhibitor MLN8237 (Alisertib)	Selleckchem.com	Cat#S1133
VECTASHIELD with DAPI	Vector Laboratories	Cat#H-1200
Halocarbon oil 700	SIGMA-ALDRICH	Cat#H8898
10S VOLTALEF	VWR chemicals	Cat#24627.188
Paraformaldehyde 20%	Electron Microscopy Sciences	Cat#15713
TWEEN 20	SIGMA-ALDRICH	Cat#P9416
Insulin solution from bovine pancreas	SIGMA-ALDRICH	Cat#I0516
Schneider's insect medium	SIGMA-ALDRICH	Cat#S0146
Fetal Bovine Serum (FBS), heat inactivated	Thermo Fisher	Cat#10500-064
Critical Commercial Assays		
Gateway LR Clonase II Enzyme Mix	Invitrogen (Life Technologies)	Cat#11791-020 and 11791-100
RNeasy Mini Kit	QIAGEN	Cat#74104
Megascript T7 kit	Ambion, Austin, TX, USA)	*Cat#AMB13345*
Experimental Models: Cell Lines		
D. melanogaster: Cell line S2: S2-DRSC	Drosophila Genomics Resource Center, Indiana University) (DGRC)	FlyBase: FBtc0000181
S2 cell line co-expressing Lgl-GFP and mCherry-Tubulin	Carvalho et al., 2015	N/A
S2 cell line co-expressing Lgl^{3A} –RFP and Lgl-GFP	This paper	N/A
S2 cell line expressing Lgl-Dendra2	This paper	N/A
Experimental Models: Organisms/Strains		
D. melanogaster: pp1-87B $^{87Bg-3}$, *pp1*α*-96A*^{2}	Bloomington Drosophila Stock Center	BDSC: #23699
		Flybase IDs: FBgn0004103
		FBal0212815

(*Continued on next page*)

Continued

REAGENT or RESOURCE	SOURCE	IDENTIFIER
D. melanogaster: lgl^{27S}	Bloomington Drosophila Stock Center	BDSC: #41561
		FlyBase ID: FBal0175616
D. melanogaster: lgl^{4}	Bloomington Drosophila Stock Center	BDSC: #36289
		FlyBase ID: FBal0009225
D. melanogaster: lglt^{s3}	Semeriva, M. (Manfruelli et al., 1996)	FlyBaseID: FBal0051412
D. melanogaster: aPKC^{k06403}	Bloomington Drosophila Stock Center	BDSC: #10622
		FlyBaseID: FBal0064438
D. melanogaster: Df(3R)Exel7357	Bloomington Drosophila Stock Center	BDSC: #7948
		FlyBase ID: FBab0038319
D. melanogaster: flw^{FP41}	Bloomington Drosophila Stock Center	BDSC: # 51338
		FlyBase ID: FBal0267524
D. melanogaster: UAS-Lgl-GFP (3rd chromossome)	Knoblich, J.A. (Betschinger et al., 2003)	N/A
D. melanogaster: UAS-Lgl-GFP (2rd chromossome – attP-VK18 insertion)	St Johnston D.	N/A
D. melanogaster: UAS-Lgl-RFP	Knoblich, J.A. (Betschinger et al., 2003)	N/A
D. melanogaster: UAS-Lgl^{3A}-GFP	Knoblich, J.A. (Betschinger et al., 2003)	N/A
D. melanogaster: UAS-AurA-GFP	J. Knoblich (Berdnik and Knoblich, 2002)	N/A
D. melanogaster: UAS-Lgl^{K327A,F331A}–GFP (2rd chromossome – attP-VK18 insertion)	This paper	N/A
D. melanogaster: UAS-AurA$^{\Delta Ab}$-GFP	Kimata, Y. (Meghini et al., 2016)	N/A
D. melanogaster: UAS-hPPP1CC	Bloomington Drosophila Stock Center	BDSC: #64394
		FlyBase ID: FBti0182016
D. melanogaster: UAS-NiPp1-HA	Bloomington Drosophila Stock Center	BDSC: #23711
		FlyBase ID: FBti0077905
D. melanogaster: UAS-*Pp1-87B RNAi*	Bloomington Drosophila Stock Center	BDSC: #32414
		FlyBase ID: FBti0132109
D. melanogaster: UAS-*sds22 RNAi*	Vienna Drosophila Resource Center	VDRC: v42051
		FlyBase ID: FBti0081237
D. melanogaster: UAS-*flw* RNAi	Bloomington Drosophila Stock Center	BDSC: #57022
		FlyBase ID:
		FBti0164842
D. melanogaster: UAS-*mts RN*Ai	Bloomington Drosophila Stock Center	BDSC: #38337
		FlyBase ID: FBti0149551
D. melanogaster: Lgl-GFP	Hong, Y. (Dong et al., 2015)	N/A
D. melanogaster: Lgl-mCherry	Hong, Y. (Dong et al., 2015)	N/A
D. melanogaster: aPKC-GFP	Schweisguth, F.(Besson et al., 2015)	N/A
Oligonucleotides		
Primers for dsRNAi (See Table S1)	This paper	N/A
RT-PCR for α-*tub* Sense (5′to 3′): CACACCACCC TGGAGCATTC	This paper	N/A
RT-PCR for α-*tub* Antisense (5′to 3′): CCAATCAG ACGGTTCAGGTTG	This paper	N/A
RT-PCR for *Pp1-87B* Sense (5′to 3′): CGATCTGTT GCGTCTGTTC	This paper	N/A
RT-PCR for *Pp1-87B* Antisense (5′to 3′): CTTGT GGATTTCGACTCGC	This paper	N/A
Cloning of Lgl^{KA,FA} Sense (5′to 3′): CTTGACTTTA CGTCTGCAGTGATTGACGCCTTTGTGAC	This paper	N/A

(*Continued on next page*)

Continued

REAGENT or RESOURCE	SOURCE	IDENTIFIER
Cloning of Lgl^{KA,FA} Antisense (5′to 3′): AGACGT AAAGTCAAGACACACTTTGTGTCCATCGCTGG	This paper	N/A
Recombinant DNA		
pENTR-Lgl	Carvalho et al., 2015	N/A
pENTR-Lgl^{3A}	Carvalho et al., 2015	N/A
pMTW-Dendra	Gilles Hickson, University Montréal, Canada	N/A
pHWG (Drosophila Gateway Vector Collection)	Drosophila Genomics Resource Center	Gateway Collection
pHWR (Drosophila Gateway Vector Collection)	Drosophila Genomics Resource Center	Gateway Collection
pUASt.attb.WG	Brogna. S.	N/A
pMT-Lgl-Dendra2	This paper	N/A
pHW-Lgl-GFP	Carvalho et al., 2015	N/A
pHW-Lgl^{3A}-RFP	This paper	N/A
pUASt.attb.Lgl^{K327A,F331A}-GFP	This paper	N/A
pMAL-LGL$^{402-802}$	Knoblich, J.A. (Betschinger et al., 2003)	N/A
Software and Algorithms		
ImageJ/FIJI	Schindelin et al., 2012	https://fiji.sc/
Icy	Quantitative Image Analysis Unit at Institut Pasteur	http://icy.bioimageanalysis.org
EpiTools	Heller et al., 2016	N/A
MATLAB version R2016a	MathWorks	RRID: SCR_001622
GraphPad Prism	GraphPad Software	https://www.graphpad.com/scientific-software/prism/
PROMALS3D	N/A	http://prodata.swmed.edu
Jalview 2.10.5	N/A	http://www.jalview.org
Other		
Confocal microscope	Leica Microsystems, Germany	TCS SP5 II
Spinning Disk Confocal Microscope	Olympus, UK	Andor Revolution XD

CONTACT FOR REAGENT AND RESOURCE SHARING

Further information and requests for reagents may be directed to and will be fulfilled by the Lead Contact, Eurico Morais-de-Sá (eurico.sa@ibmc.up.pt).

EXPERIMENTAL MODEL AND SUBJECT DETAILS

Drosophila stocks and genetics

Drosophila melanogaster flies were cultured on standard cornmeal/agar/molasses/yeast media at 18°C or 25°C, unless otherwise noted. *tj-GAL4* and *GR1-GAL4* drivers were used to induce expression of UAS transgenes in the follicular epithelium, whereas *matα4*-GAL4-VP16 was used to induce the expression in embryos. The FLP/FRT-mediated mitotic recombination system was used to generate clones, which were induced by heat shock at 37°C. The *GAL80* repressor was used together with FLP/FRT recombination system to control the induction of *Pp1-87B RNAi* in clonal analysis (Figure 2A) and to express UAS-Lgl^{K327A,F331A}-GFP in *lgl* mutant cells (Figure 3E). Crosses were maintained at 18°C and then flies were incubated at 29°C to boost the efficiency of RNAi depletion in experiments with UAS-driven RNAi. Flies were also incubated at 29°C during 1 day for the rescue experiment in Figures 3E and 3F. Both UAS-Lgl^{K327A,F331A}-GFP (this study) and *UAS-Lgl-GFP* (unpublished, gift of Daniel St Johnston, Gurdon Institute, Cambridge, UK) were inserted into the same genomic landing site, attP-VK18. Detailed genotypes are depicted below.

Figure 1

A) *hs-FLP nls-RFP FRT19/hs-FLP tub-Gal80 FRT19; tj-GAL4/+; UAS-Lgl-GFP/+*
(clonal expression to evaluate local Lgl-GFP signal specifically in dividing cell)
B) *w*; *tj-GAL4/+*; *UAS-Lgl-GFP, HisRFP/+*
E, F) Control: *w*; *UAS-Lgl-RFP/ tj-GAL4*

UAS-AurA: *w*; *UAS-Lgl-RFP/ tj-GAL4; UAS-AurA-GFP/+*
UAS-AurAΔAb: *w*; *UAS-Lgl-RFP/ tj-GAL4*; *UAS-AurAΔAb-GFP/+*

Figure 2

A) *hs-FLP nls-RFP FRT19/hs-FLP tub-Gal80 FRT19*; *tj-GAL4/+*; *UAS-Pp1-87B RNAi/+*
B) *hs-FLP ubi-RFP-nls FRT19/flw*^{FP41} *FRT19*; ; *+/+*
hs-FLP/+;; FRT82 RFP/ FRT82 pp1α-96A^{2}
hs-FLP/+;; FRT82 RFP/ FRT82 pp1-87B^{87Bg-3} *e pp1α-96A*^{2}
C) *w; tj-GAL4/+*; *UAS-Pp1-87B RNAi/+*
w; *tj-GAL4/UAS-hPpp1cc*; *UAS-Pp1-87B RNAi/+*
D) *w; tj-GAL4 Lgl-GFP/+*; *UAS-NiPp1-HA/+*
H) *w*; *tj-GAL4/UAS-Lgl-RFP*; *UAS-Pp1-87B RNAi/UAS-Lgl*^{3A}*-GFP*

Figure 3

A) *w*; *tj-GAL4*/CyO; *UAS-Pp1-87B RNAi/+*
w; *tj-GAL4/ aPKC*^{k06403}; *UAS-Pp1-87B RNAi/+*
C) *w*; *tj-GAL4/UAS-Lgl–GFP*
w; *tj-GAL4/UAS-Lgl*^{K327A,F331A}*–GFP*
D) *w*; *tj-GAL4/UAS-Lgl–GFP*
w; *tj-GAL4/+*; *UAS-Lgl*^{3A}*-GFP/+*
w; *tj-GAL4/UAS-Lgl*^{K327A,F331A}*–GFP*
E) *hs-FLP/+*; *lgl*^{27S3} *FRT40 UAS-Lgl*^{K327A,F331A}*–GFP/ tub-GAL80 FRT40*; *GR1-GAL4/+*
(*lgl* homozygous mutant cells are the only ones expressing UAS-Lgl^{K327A,F331A}–GFP)
F) *hs-FLP/+*; *lgl*^{27S3} *FRT40/ RFP FRT40*
hs-FLP/+; *lgl*^{27S3} *FRT40 UAS-Lgl-GFP/ RFP FRT40*; *GR1-GAL4/+*
hs-FLP/+; *lgl*^{27S3} *FRT40UAS-Lgl*^{K327A,F331A}*–GFP/ RFP FRT40*; *GR1-GAL4/+*
(lgl homozygous mutant cells are marked by absence of RFP in a tissue with general expression of UAS-Lgl transgenes)

Figure 4

A,B) *w*; *tj-GAL4/+*; *UAS-Lgl-GFP, HisRFP/+*
w; *tj-GAL4/+*; *UAS-Pp1-87B RNAi/UAS-Lgl-GFP, HisRFP*
w; *tj-GAL4/UAS-sds22 RNAi*; *UAS-Lgl-GFP, HisRFP/+*
C,D) *w*; *tj-GAL4/UAS-Lgl*^{K327A,F331A}*–GFP/*;
w; *tj-GAL4/UAS-Lgl*^{K327A,F331A}*–GFP, UAS-sds22 RNAi*;
E) *aPKC-GFP*; *Lgl-mCherry*
F,G) *aPKC-GFP/+*; *lgl4* or *ts3 /+*; HisRFP/+ (control)
aPKC-GFP/+; *lgl*^{ts3}*/lgl*^{4}; *HisRFP/+* (*lgl* temperature sensitive)

Figure S1

A) embryos from females: *matα4-GAL4* crossed with males: *UAS-Lgl-GFP*

Figure S2

A) *w* (control)
B) *w*; *tj-GAL4/+*; *UAS-mts RNAi/+*
C) *w*; *tj-GAL4/UAS-flw RNAi*; *+/+*
D) *w*; ; *pp1-87B*$^{87Bg-3}$ *e pp1α-96A*^{2} */ Df(3R)Exel7357*

Figure S3

aPKC-GFP/+; *CyO/+*; *UAS-Pp1-87B RNAi/+* (Control)
aPKC-GFP/+; *tj-GAL4/+*; *UAS-Pp1-87B RNAi/+* (PP1-87B RNAi)

Figure S4

B) Embryos from females: *matα4*-GAL4 crossed with males: *UAS-Lgl-GFP or UAS-Lgl*^{KAFA}*-GFP*
C) *aPKC-GFP/+*; *lgl*^{4}*/+* or *lgl*^{ts3}*/+* (Control)
aPKC-GFP/+; *lgl*^{ts3}*/lgl*^{4} (lgl temperature sensitive)

Drosophila cell culture

Drosophila Schneider 2 (S2) cells obtained from *Drosophila* Genomics Resource Center, Indiana University (DGRC) were cultured in Schneider's *Drosophila* media supplemented with 10% FBS (fetal bovine serum), at 25°C.

METHOD DETAILS

S2 cell stable lines and RNA interference

Stable S2 cell lines co-expressing Lgl-GFP and mCherry-Tubulin (Carvalho et al., 2015), co-expressing Lgl^{3A} –RFP and Lgl-GFP, or expressing Lgl-Dendra2 were generated using either Cellfectin® II reagent or Effecten Transfection Reagent**,** according to manufactures' instructions. Gene expression was induced at 37°C for 1 hour in cells expressing Lgl under heat-shock promoter (plasmids: pHW-Lgl-GFP and pHW-Lgl^{3A}-RFP). For double-strand RNAi production, genomic DNA was amplified using primers containing a T7 RNA polymerase-binding site flanked by gene specific sequences (see Table S1). The length of sequences amplified was: 362 bp of *aurA,* 311 bp of *aPKC*, 511 bp of *sds22* and 614 bp of *Pp1-87B.* Megascript® T7 kit was used to transcribe dsRNA from PCR amplified sequences. For RNAi treatment, S2 cells in an exponential growth phase were seeded in a serum-free Schneider media (at a concentration of 1×10^6 cells/ml) and incubated with 30 μg dsRNAi (15 μg in case of *Pp1-87B*) for 1 hour. After that, 2 mL of Schneider's growth media supplemented with 10% of FBS was added and cells analyzed after 96h or 120h.

Preparation of ovary and S2 cell protein extracts

To prepare ovary protein extracts, *Drosophila* ovaries were disrupted through sonication in Lysis Buffer (150 mM KCl, 75 mM HEPES, pH 7.5, 1.5 mM EGTA, 1.5 mM $MgCl_2$, 15% glycerol, 0.1% NP-40) containing 1x protease inhibitors cocktail (Roche) and 1x phosphatase inhibitors cocktail 3 (Sigma). For protein extracts from S2 cells, harvested cells were washed with PBS 1x supplemented with Protease Inhibitors Cocktail (Roche). Lysis buffer was then added and cells were disrupted by sonication. Samples were then centrifuged and supernatant was collected for analyses.

Immunofluorescence and F-actin staining

Drosophila ovaries were fixed using a 4% paraformaldehyde solution (in PBS), followed by washing steps with 0.05% PBT (PBS with 0.05% TWEEN® 20 (Sigma)), 1 hour-blocking with 10% BSA in 0.2% PBT, and overnight incubation at room temperature with primary antibodies diluted in 0.05% PBT (supplemented with 1% BSA). Ovaries were then washed with 0.05% PBT containing 1% BSA, incubated 2 hours with the secondary antibody and washed with 0.05% PBT before mounting in Vectashield with DAPI. The primary antibodies used are indicated in the key resources table. F-actin staining was performed by adding Phalloidin-TRITC at 1 μg/mL to the paraformaldehyde solution during the fixation.

Cloning of Lgl variants

Site-directed mutagenesis in the PP1 - docking site of Lgl was performed using primers containing the desired mutations (see Key Resources Table) and pENTR-Lgl as template (Carvalho et al., 2015). PCRs were performed using Phusion High Fidelity DNA polymerase, followed by a digestion of the template plasmid with DpnI, and transformation of competent bacteria. The Gateway Cloning System (Life Technologies) was used to generate the following plasmids: pMT-Lgl-Dendra2 - recombination of pENTR-Lgl with pMT-W-Dendra2 (gift of Gilles Hickson, University Montréal, Canada); pHW-Lgl^{3A}-RFP - recombination of pENTR-Lgl^{3A} (Carvalho et al., 2015) with pHWR; pUASt.attb.$Lgl^{K327A,F331A}$-GFP, upon recombination of pEntr-$Lgl^{K327A,F331A}$ with pUASt.attb.WG (gift of Saverio Brogna, University of Birmingham, UK). UAS-$Lgl^{K327A,F331A}$-GFP transgene was inserted into the attP-VK18 landing site on chromosome II (BDSC: #9736) via PhiC31 site-specific transgenesis (BestGene Inc).

RT-PCR

Total RNA was isolated using RNeasy Mini Kit from RNAi depleted and control S2 cells ($3x10^6$ cells) following the manufacturer's protocol. RNA samples were then used to synthetize cDNA using SuperScriptTM II Reverse Transcriptase and then PCRs for the required genes were performed using DreamTaq DNA polymerase and primers listed in the Key Resources Table.

Amplified PCR products were resolved in 1% agarose gel electrophoresis.

Protein purification

MBP-$Lgl^{402-802}$ protein was expressed in BL21 Star *E.coli* transformed with pMAL-$Lgl^{402-802}$ ((Betschinger et al., 2003), Gift of Jurgen Knoblich (IMBA, Vienna, Austria)) and purified using amylose magnetic beads according to the manufacturer's instructions (New England Biolabs).

in vitro dephosphorylation assays

For *in vitro* dephosphorylation assays using Lgl from ovary extracts (Figure 2F), Lgl-GFP was immunoprecipitated from ovary extracts using GFP-Trap_MA system according to the manufacturer's instructions. Lgl bound to the beads was then incubated with 200 ng of AurA in kinase reaction buffer (5 mM MOPS, pH 7.2, 2.5 mM β-glycerol-phosphate, 5 mM $MgCl_2$, 1 mM EGTA, 0.4 mM EDTA, 0.25 mM DTT, 100 μM ATP) during 30 min at 30°C to saturate Lgl phosphorylation status. The kinase reaction mix was removed and the phosphatase reaction mix was added, containing 2 μM MLN8237 for inhibition of the AurA kinase, PMP phosphatase buffer (New England Biolabs) containing 50mM HEPES pH 7.5, 100 mM NaCl, 2 mM DTT, 0.01% Brij 35, 1 mM $MnCl_2$ and respective amounts of recombinant human GST-PP1γ. For *in vitro* dephosphorylation assays using recombinant MBP-Lgl (Figure 2E and Figure S2E), the purified protein was first phosphorylated using the kinase assay performed as described above. Dephosphorylation

was then performed in a reaction solution containing 2 μM MLN8237, PMP phosphatase buffer containing 1 mM $MnCl_2$ (New England Biolabs), and 1U of either Protein Phosphatase 1 or Lambda PP (Figure S2E) or GST-PP1γ (Figure 2E). Dephosphorylation reactions were carried at 30°C for 30 min and stopped by addition of SDS Laemmli buffer. p-Lgl656 antibody was used to detect phosphorylation in western blot, whereas anti-GFP, anti-MBP-HRP conjugated or anti-GST were performed to control for the amount of Lgl-GFP, MBP-Lgl or PP1-GST, respectively.

Photoconversion experiments in S2 cells

For photoconversion experiments, expression of Lgl-Dendra2 in S2 cells was induced with 500 μm $CuSO_4$ for at least 12h before live imaging, and cells were plated in glass bottom microwell dishes (MaTek) coated with Poly-L-Lysine. We used Leica TCS SP5 II (Leica Microsystems) confocal microscope and a 405 nm UV laser to perform photoconversion of Lgl-Dendra2. Initial frames were taken using 488 nm and 561 nm lasers to validate photoconversion. Time-lapse stacks covering all the dividing cell were then taken using the 561 nm laser every 2 min, for at least 30 min after anaphase onset.

Multiple sequence alignments

Multiple sequence alignment of Lgl proteins from several species was performed using CLUSTAL format by PROMALS3D (http://prodata.swmed.edu) and the aligned amino acid sequences of the putative PP1-docking site motif were visualized using Jalview 2.10.5 (http://www.jalview.org). Protein sequences used were the following: *H. sapiens* LLGL1 (UniProt:Q15334); *H. sapiens* LLGL2 (UniProt:Q6P1M3); *D. rerio* LLGL1 (UniProt:E7FD67); D. rerio LLGL2 (UniProt:Q7SZE3); *S. purpuratus*predicted L2GL2 (NCBI: XP_011678406.1); *D. melanogaster* L2GL (UniProt:P08111); *N. vectensis* predicted protein (UniProt:A7RKR7); *A.queenslandica* uncharacterized protein (UniProt:A0A1X7U8H8); *S. cerevisiae* SRO7 (UniProt:Q12038).

Imaging

Fixed samples were analyzed using a Leica TCS SP5 II (Leica Microsystems) confocal microscope with HC PL APO CS 40x/NA 1.10 objective or HC PL APO CS 63x /1.30 Glycerine and a LAS 2.6 software. Live imaging was performed using a spinning disc confocal system (Andor Revolution XD) equipped with an electron multiplying charge coupled device camera (iXonEM+; Andor) and a CSU-22 unit (Yokogawa) based on an inverted microscope (IX81; Olympus) with a PLAPON 60x/NA 1.42 objective using iQ software (Andor). Z stacks were collected with serial optical sections separated by 0.5-1 μm. For live imaging of the *Drosophila* follicular epithelia, ovarioles were dissected and incubated in Schneider's media supplemented with 10% FBS and 200 μg/ml insulin (Sigma-Aldrich). Egg chambers with low expression levels of Lgl-RFP (Figures 1E and 1F) were imaged in 10S VOLTALEF® (VWR chemicals) oil for optimization of the fluorescence signal to noise. Live imaging of *Drosophila* embryos (5 to 7 hours of development; stage 10 to stage 11) was performed by immobilizing the embryos in glass bottom microwell dishes (MaTek) containing heptane glue and filled with Halocarbon oil (700) (Sigma-Aldrich). S2 cells were plated on poly-L-lysine-coated culture dishes for live imaging (MatTek). Live imaging experiments were performed at 25°C, except in experiments using the Lgl temperature sensitive mutants (lgl^{ts3}), which were filmed at 29°C.

QUANTIFICATION AND STATISTICAL ANALYSIS

Image processing and quantifications were largely performed using FIJI (Schindelin et al., 2012). All the statistical analysis and graphs were performed using GraphPad Prism 6.

Cytoplasmic decay of Lgl

Cytoplasmic decay of Lgl at mitotic exit in follicular epithelia, S2 cells and embryonic epithelia was quantified by measuring the mean pixel intensity of a manually tracked ROI in the cytoplasm (12x 12 ROI in S2 cells, 8x8 ROI in the follicular epithelia and 6x6 ROI in embryonic epithelia; 1 px = 0.13 μm) in sum-intensity Z projections. To overcome large signal fluctuation that arise from low signal intensity, we averaged 3 consecutive time points in epithelial cells (separated by 30 s) and 2 consecutive time points in S2 cells (separated by 90 s). Background subtracted mean intensity values were presented as a percentage of the anaphase value [average of the first two (in S2 cells) and three (in epithelia) frames after anaphase onset]. Since Lgl invariably reaches a steady-state with neglectable cytoplasmic intensity value in control or upon AurA overexpression/AurA RNAi, the average of the cytoplasmic intensity at the minimum plateau was subtracted in the quantifications of Figures 1 and S1 to represent cytoplasmic decay from 100% to 0%. Cytoplasmic decay has not been normalized to the minimum plateau in Figures 4, S4A, and S4B to enable the analysis of the degree of cytoplasmic accumulation induced by each genetic manipulation.

Lgl accumulation in daughter-daughter interface

To quantify the kinetics of Lgl accumulation in the daughter-daughter interface in epithelia, time-lapse images were aligned using the "StackReg" plugin and we manually tracked the interface to quantify mean intensity values since anaphase. The background subtracted mean intensity value of Lgl in the daughter-daughter interface or dividing cell equator (before cytokinesis) was normalized to the background subtracted mean intensity in the cytoplasm. The resulting anaphase value (average of the first three frames since anaphase) was set to 0% and the average intensities in the plateau of accumulation was set to 100%.

Intensity of Lgl-Dendra2 upon photoconversion

To quantify the overall intensity of Lgl-Dendra2 at mitotic exit after photoconvertion (Figure 1D) we used FIJI to perform a Z sum-projection of all optical sections covering the cell. We then used the active contour protocol of Icy (http://icy.bioimageanalysis.org) for automated cell segmentation. For each time-point, we calculated the background subtracted integrated density (cell area x mean intensity value), which is normalized to the value at anaphase onset (100%).

aPKC accumulation in the apical interface formed between daughter cells

To quantify the accumulation of aPKC in the apical daughter-daughter interface (Figure 4F), we used the image analysis toolkit EpiTools (Heller et al., 2016) to generate selective plane projections of the apical area of the follicular epithelium. The aPKC-GFP signal was then manually tracked in: 1) the equator of dividing cell/daughter-daughter interface (10 pixel width line); 2) four non dividing neighboring cell interfaces (10 pixel width line); 3) three circular ROI with 8 pixel diameter in the cytoplasm, which is used for background subtraction. We generated a custom FIJI script to measure the background subtracted mean intensities of the new daughter-daughter interface and of the non-dividing interfaces, and to normalize the signal of aPKC in the new daughter-daughter interface to the average of non-dividing ones.

Interphase cortical/cytoplasmic intensity ratio of Lgl in S2 cells

To measure the ratio of cortical to cytoplasmic mean intensity of Lgl in S2 cells during interphase (Figure 2G), we used a FIJI macro for automated segmentation of each cell contour (CC) and measured the mean intensity of the region between CC - 1 pixel and CC – 5 pixel (1 px = 0.13 μm) as the cortical intensity. Cytoplasmic intensity was measured using a circular ROI in the cytoplasm. Ratio was obtained after background subtraction.

BioArchitecture

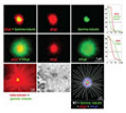

ISSN: 1949-0992 (Print) 1949-100X (Online) Journal homepage: http://www.tandfonline.com/loi/kbia20

Spatiotemporal phosphoregulation of Lgl: Finding meaning in multiple on/off buttons

Sofia Moreira & Eurico Morais-de-Sá

To cite this article: Sofia Moreira & Eurico Morais-de-Sá (2016) Spatiotemporal phosphoregulation of Lgl: Finding meaning in multiple on/off buttons, BioArchitecture, 6:2, 29-38, DOI: 10.1080/19490992.2016.1149290

To link to this article: https://doi.org/10.1080/19490992.2016.1149290

Accepted author version posted online: 26 Feb 2016.
Published online: 26 Feb 2016.

Submit your article to this journal

Article views: 264

View Crossmark data

Citing articles: 1 View citing articles

Full Terms & Conditions of access and use can be found at
http://www.tandfonline.com/action/journalInformation?journalCode=kbia20

BioArchitecture, 6:29–38, 2016
© 2016 Taylor & Francis Group, LLC
ISSN: 1949-0992 print / 1949-100X online
DOI: 10.1080/19490992.2016.1149290

COMMENTARIES

Spatiotemporal phosphoregulation of Lgl: Finding meaning in multiple on/off buttons

Sofia Moreira[1,2] and Eurico Morais-de-Sá[1,2,*]

[1]IBMC, Instituto de Biologia Molecular e Celular, Universidade do Porto, Porto, Portugal
[2]I3S, Instituto de Investigação e Inovação em Saúde, Universidade do Porto, Porto, Portugal

ABSTRACT. Intracellular asymmetries, often termed cell polarity, determine how cells organize and divide to ultimately control cell fate and shape animal tissues. The tumor suppressor Lethal giant larvae (Lgl) functions at the core of the evolutionarily conserved cell polarity machinery that controls apico-basal polarization. This function relies on its restricted basolateral localization via phosphorylation by aPKC. Here, we summarize the spatial and temporal control of Lgl during the cell cycle, highlighting two ideas that emerged from our recent findings: 1) Aurora A directly phosphorylates Lgl during symmetric division to couple reorganization of epithelial polarity with the cell cycle; 2) Phosphorylation of Lgl within three conserved serines controls its localization and function in a site-specific manner. Considering the importance of phosphorylation to regulate the concentration of Lgl at the plasma membrane, we will further discuss how it may work as an on-off switch for the interaction with cortical binding partners, with implications on epithelial polarization and spindle orientation.

KEYWORDS. aPKC, basolateral, cell-cycle, cell polarity, Dlg, Drosophila, epithelial tissue, Lgl, phosphorylation, spindle orientation

The epithelial tissue forms a critical barrier that protects animal organs from the external environment, providing mechanical support and controlling transport and signaling in a polarized manner. Epithelial polarity relies on the asymmetric distribution of cortical protein

*Correspondence to: Eurico Morais-de-Sá; Email: eurico.sa@ibmc.up.pt
Received January 19, 2016; Accepted January 27, 2016.

Color versions of one or more of the figures in this article can be found online at www.tandfonline.com/kbia.

Commentary to: Carvalho CA, Moreira S, Ventura G, Sunkel CE, Morais-de-Sa E. Aurora A triggers Lgl cortical release during symmetric division to control planar spindle orientation. Curr Biol 2015; 25:53-60; PMID:25484294; http://dx.doi.org/10.1016/j.cub.2014.10.053

complexes to define the position of specialized cell junctions, and to orchestrate polarized vesicle trafficking and cytoskeleton organization along the apico-basal axis.[1] Common localization and genetic interactions placed the basolateral proteins Lethal giant larvae (Lgl), Discs large (Dlg) and Scrib in the same pathway that counteracts the activity of apical aPKC and Crumbs polarity complexes[2,3,4] However, how these proteins interact to collaborate as basolateral determinants is still poorly understood. Furthermore, these proteins regulate other pathways that control cell proliferation, migration and cancer.[5] In fact, *lgl* was one of the first tumor suppressors identified and its human paralogues (Hugl-1 and Hugl-2) are now strongly linked to the etiology of cancer.[6-8] Lgl is regulated in a cell-cycle dependent manner as part of the mechanism that produces daughter cells with distinct fates during asymmetric cell division.[9] We and other group have recently discovered that phosphoregulation of Lgl is also required during symmetric division in *Drosophila* epithelial cells, where the cortical release of Lgl promotes planar spindle orientation.[10,11] In this commentary, we will discuss how phosphorylation of Lgl acts as a mechanism to temporally and spatially control its localization, interactions and activity.

LGL INTERACTIONS AT THE PLASMA MEMBRANE AND THE UNDERLYING CORTEX

Early *Drosophila* studies documented Lgl localization in the cytoplasm or in association with the plasma membrane and the underlying actomyosin cortex.[12] Biochemical assays aiming to address the molecular basis for the cortical localization of Lgl revealed a physical interaction with non-muscle myosin II heavy chain,[13,14] which was also validated in mammalian cells.[15,16] However, Lgl recruitment to the cytoskeleton fraction was found to be partially independent of myosin II[14] and, accordingly, other cortical polarity proteins such as aPKC, Dlg and Scrib may form alternative complexes with Lgl.[9,17-20]

aPKC phosphorylation in three evolutionarily conserved residues (S656, S660 and S664 in *Drosophila*) disrupts the localization of Lgl at the cortex and the plasma membrane.[9,17] The combination of *in vitro* studies with the analysis of deletion mutants in *Drosophila* neuroblasts suggested that Lgl phosphorylation induces an intramolecular association between the C- and N-terminus, which masks the domains that mediate cortical and plasma membrane association.[14] However, structural evidences of Lgl conformational changes are still lacking. A comparison with the crystallographic structure of its yeast homolog, Sro7, locates the phosphorylation sites within a flexible loop between two WD40 repeats of Lgl's two-β-propeller fold.[21,22] Importantly, this region is exposed at the surface, forming a platform for electrostatic interactions that provide an alternative mechanism to regulate the Lgl localization, independently of conformational changes. Recent work revealed that the phosphorylation sites are part of a positively charged basic and hydrophobic (BH) motif (Fig. 1A), which interacts with negatively charged plasma membrane phosphoinositides.[22,23] Consistent with this, mutating the basic aminoacids of the BH domain dramatically disrupts Lgl localization and function. Phosphorylation can therefore control plasma membrane localization by rapidly altering the bulk electrostatic charge of the BH domain, thereby weakening the electrostatic attraction to phospholipids.[22,23] Similar electrostatic control of the interaction of this domain with a negatively charged domain in non-muscle myosin II has also been proposed.[15,16] Nevertheless, depletion of plasma membrane phosphoinositides by hypoxia induces full cortical release of Lgl, without affecting other cortical partners of Lgl, such as Myosin and Dlg.[22] Thus, Lgl interactions with other cortical proteins possibly require prior concentration of Lgl near the plasma membrane.

SPATIOTEMPORAL REGULATION OF LGL

aPKC phosphorylates Lgl in epithelial cells during interphase to restrict its localization to the basolateral side[9,24] (Fig. 1B). Additionally,

FIGURE 1. AurA and aPKC control Lgl localization during the cell cycle in epithelia. (A) A conserved Basic and Hydrophobic (BH) domain of Lgl contains the three Serines controlled by aPKC and AurA. Positively charged residues are in blue. (B) Phosphorylation by aPKC on the apical domain controls basolateral restriction of Lgl during interphase. Multisite phosphorylation blocks membrane and cortical interactions, whereas 1P-Lgl may still interact with the plasma membrane, and may be required for interaction with some cortical binding partners. At mitosis onset, activation of Aurora A leads to multisite phosphorylation of Lgl inducing dissociation from the basolateral cortex.

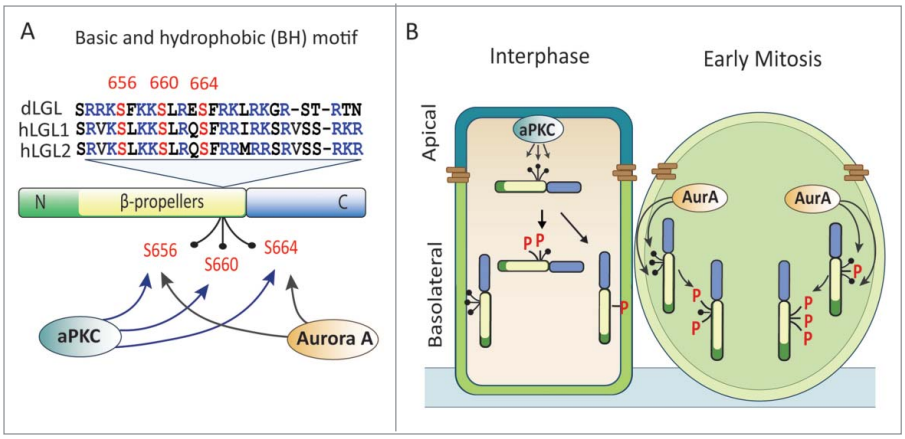

this phosphorylation allows the polarized segregation of cell fate determinants during the asymmetric division of *Drosophila* neuroblasts and sensory organ precursor (SOP) cells.[9,25] Lgl phosphorylation and cortical release breaks its inhibitory effect over aPKC and simultaneously allows association of Bazooka with Par-6/aPKC to induce phosphorylation of the cell fate determinants Numb and Miranda.[25,26] It has been proposed that formation of the aPKC/Par-6/Baz complex is induced by Aurora A (AurA) - mediated phosphorylation of Par-6 and consequent activation of aPKC at mitotic entry.[25] However, a planar asymmetry of these proteins is firstly set during interphase in SOP cells.[27]

The epithelial tissue is in a constant balance between cell death and proliferation to control development and to maintain homeostasis.[28] How epithelial cells maintain overall tissue integrity during division is still largely unknown. Live imaging in *Drosophila* intact tissue recently provided significant insight into the reorganization of polarity complexes, cell junctions and the cytoskeleton during epithelial cell division.[10,11,29-35] The cortical-release of Lgl at mitotic entry represents a striking observation since it differs radically from its known basolateral partners Dlg and Scrib.[10,11,36] Intriguingly, release of Lgl from the basolateral domain occurs in *aPKC* mutant epithelial cells, revealing the involvement of another kinase. The combination of *in vitro* kinase assays with *in vivo* genetic and drug inactivation led to the conclusion that AurA directly controls the release of basolateral Lgl in follicular and wing disc epithelia during mitosis via its ability to phosphorylate Ser656 and Ser664 [10,11] (Fig. 1B). AurA activity is critical to ensure Lgl mitotic release in epithelia since apical aPKC is physically separated from basolateral Lgl at mitotic entry. However, using unpolarized S2 cells, we also demonstrated that Lgl release is a general mitotic event, strongly delayed upon disruption of AurA activity.[11] Furthermore, Bell et al. proposed that Aurora A can directly remove Lgl from the entire cortex of larval neuroblasts during asymmetric cell division, whereas aPKC activation is only involved in the release of apical Lgl.[10] Thus, activation of the mitotic kinase AurA provides cell cycle control to the spatial regulation

exerted by aPKC, maintaining Lgl localization under tight regulation during both symmetric and asymmetric division. Partial redundancy between the two kinases may ensure the robustness of mitotic events where the activity of AurA and aPKC partly overlaps.

SITE-SPECIFIC PHOSPHOREGULATION OF LGL

Both the conformational and electrostatic models imply the existence of two distinct pools of Lgl: an active non-phosphorylated fraction able to interact with actomyosin and the plasma membrane, and an inactive phosphorylated form that should remain in the cytoplasm. But what is the impact of phosphorylation in multiple serine residues? Are these phosphorylation sites equally important for the function, interaction with binding partners and plasma membrane localization? Our analysis of Lgl site-specific phosphoregulation brings out the significance of phosphorylation number and the site-specific importance of each phosphorylation to positively control the activity of Lgl.

Consistent with the importance of phosphorylation to induce cortical release of Lgl, mutation of the three phosphorylatable serines to alanines (Lgl^{3A}) induces extension to the apical domain in *Drosophila* and mammalian epithelial cells and full cortical retention during epithelial and S2 cell mitosis.[10,11,19,24,37] Based on the finding that all double mutants ($Lgl^{S656A,S664A(ASA)}$; $Lgl^{S656A,LglS660A(AAS)}$; $Lgl^{S660A,S664A(SAA)}$) show significant cortical localization during mitosis, we have proposed that at least two phosphorylations are necessary for efficient Lgl cortical exclusion.[11] Another study reached similar conclusions analyzing the localization of equivalent Lgl double mutants upon overexpression of aPKC in S2 cells during interphase.[38] Following the recent work of the Prehoda and Hong labs,[22,23] one possible explanation is that two phosphorylations are required to switch the bulk electrostatic charge of Lgl's BH motif, fully repelling the interaction with phosphoinositides at the plasma membrane and therefore also blocking cortical localization (Fig. 2).

Mutations in any combination of two of the three serines also prevent Lgl cortical exclusion during epithelial mitosis,[11] supporting the importance of multisite phosphorylation during cell division. However, in interphase, single phosphorylatable mutants display distinct abilities to support epithelial polarity or to exert dominant overexpression effects, highlighting the importance of site-specific phosphorylation for Lgl activity (Fig. 3).[11] The presence of phosphorylatable S660 or S664 is sufficient for proper Lgl localization and activity. Furthermore, despite the apical localization of Lgl^{3A} and Lgl^{SAA}, only Lgl^{AAS} has ability to induce loss of apical aPKC when strongly overexpressed, causing a dominant disruption of epithelial polarity.[11,24] Thus, phosphorylation of Lgl on S664 seems to be of major importance for the positive regulation of Lgl as a basolateral factor. We will discuss several factors that may account for the differences in mutants phosphorylatable in each specific serine.

Recent *in vitro* analysis of aPKC phosphorylation indicated that the three phosphorylation sites are not kinetically equivalent.[38] However, the kinetic parameters of singly phosphorylatable peptides expose a preferential order for phosphorylation (S664>S656>S660) that is insufficient on its own to explain the more inefficient apical exclusion of Lgl^{SAA}. Nevertheless, the kinetics of aPKC phosphorylation may differ *in vivo*, where the catalytic activity of aPKC depends on multiple other factors including its interaction with Par-6.[39,40] Moreover, each phosphorylation may have a different impact on the release from the plasma membrane and myosin. Accordingly, singly phosphorylatable mutants have distinct localization during S2 cell mitosis, where Lgl^{SAA} shows much stronger cortical retention (Fig. 3). Thus, regardless of the redundant ability of aPKC and AurA to phosphorylate S656 during S2 cell mitosis, this phosphorylation alone has the weakest effect on the dissociation from myosin and plasma membrane.

It is also unclear how some singly phosphorylatable mutants can be completely removed from the apical cortex (Fig. 3), whereas two phosphorylations are required for efficient cortical exclusion during mitosis. Phosphorylation-dependent interactions that anchor Lgl at

FIGURE 2. Model of phosphorylation as a molecular on/off switch of Lgl interactions. The establishment of electrostatic interactions with phospholipids concentrates Lgl at plasma membrane (PM). Sequential phosphorylation progressively reduces the electrostatic interactions established by Lgl with cortical Myosin and phosphoinositides. In contrast, one phosphorylation seems to be required for the association of Lgl with the GUK domain of Dlg. Phosphorylation may therefore displace Lgl that was bound to the plasma membrane, allowing binding to specific cortical binding partners. Multisite phosphorylation blocks Dlg-Lgl interaction, possibly by further reducing the local concentration of Lgl or by inducing conformational/electrostatic changes that directly block Dlg-Lgl binding.

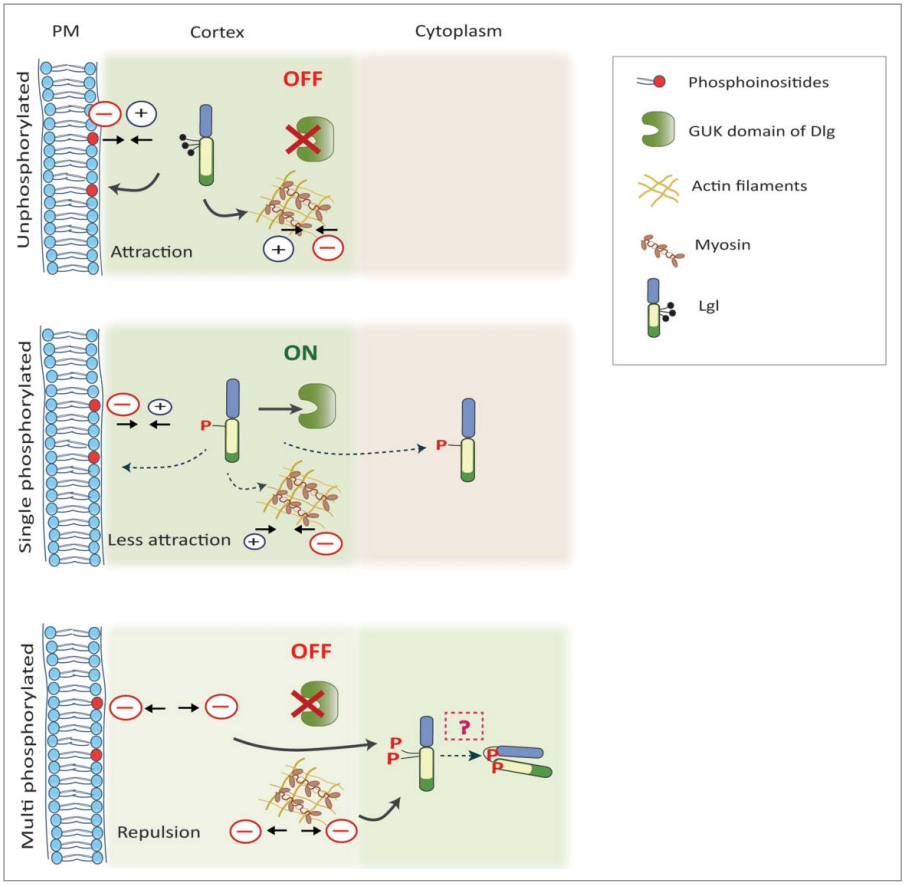

the basolateral cortex of epithelia would reconcile these observations. Dlg could provide these interactions since aPKC phosphorylation in any of the three residues of human Lgl2 induces binding to the Guanylate kinase (GUK) domain of Dlg4 *in vitro*[19] (Fig. 2). Thus, double mutants should bind Dlg's GUK domain in the follicular epithelium through the available phosphorylated serine. However, our study would be consistent with the possibility that each phosphorylated serine confers distinct abilities to bind Dlg and to counteract the activity of apical proteins in the following order: Ser664>Ser660>Ser656 (Fig. 3).[11] Dissociation from myosin and plasma membrane may increase the pool of Lgl available to interact with Dlg, or other cortical proteins, in order to control epithelial polarity (Fig. 2). Thus, the preferential phosphorylation by aPKC on S664[38] allied to its ability to lower the

FIGURE 3. Site-specific control of Lgl function and localization. Schematic overview of the localization of singly phosphorylatable and non-phosphorylatable Lgl mutant forms during epithelial interphase and S2 cell mitosis.[11] Based on the ability of each mutant form to support epithelial polarity or to induce dominant basolateral activity upon strong overexpression, we speculate about the activity of each phosphorylatable site (left).

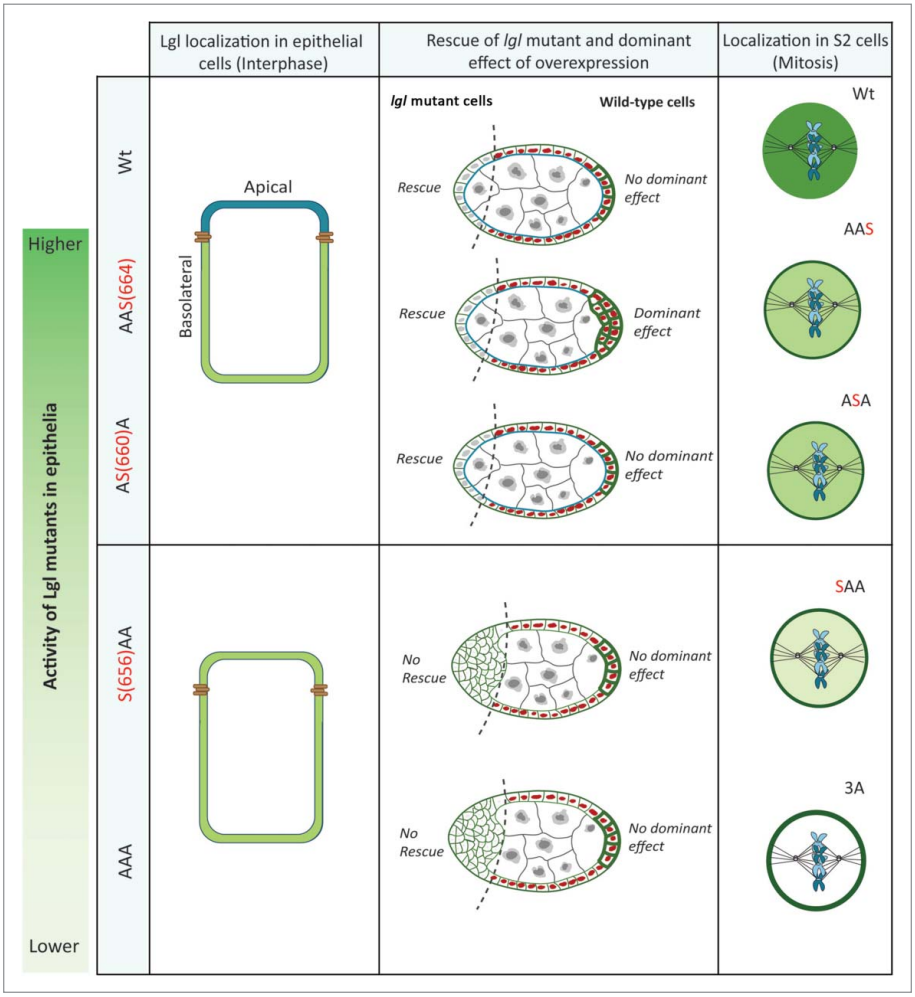

interaction with the plasma membrane provides one possible explanation for the higher activity of Lgl singly phosphorylated on S664.

SIGNIFICANCE OF LGL PHOSPHOREGULATION DURING EPITHELIAL MITOSIS

Lgl cytoplasmic relocalization at mitotic entry raises the possibility of a general function to promote faithful chromosome segregation. This is consistent with an early study performed in mammalian HEK293 cells that described mitotic spindle misorganization and chromosome missegregation upon overexpression of Lgl2 C-terminal domain or upon Lgl1 and Lgl2 knockdown.[41] A similar mitotic role for Lgl has also been documented in the wing imaginal disk epithelium.[10] However, the relevance of Lgl on chromosome segregation seems to be context-specific as we did not detect defects that could be unambiguously linked to chromosome segregation upon loss of

lgl function in syncytial embryos, follicle cells and S2 cells.[11]

Lgl cortical displacement could also be involved in the control of cortical-dependent events during mitosis since, for instance, the reorganization of the actomyosin cortex supports a number of important functions, including mitotic cell rounding, spindle orientation and cytokinesis.[42] Follicle cells expressing the aforementioned Lgl double mutant forms or a membrane-targeted form of Lgl revealed defects in spindle orientation axis.[10,11] So, which cortical mechanisms controlling mitotic spindle orientation could be potentiated by Lgl cortical release? Lgl binding to non-muscle myosin II (NMII) heavy chain has been proposed to inhibit Myosin filament formation *in vitro*.[15,16] Thus, it would be reasonable to consider that Lgl exclusion induces changes in cortical actomyosin contractility and possibly in mitotic cell rounding, which are known to influence planar spindle alignment.[34,43] However, despite the cortical retention of Lgl^{3A} during mitosis, and possible inhibition of actomyosin contractility, Lgl^{3A} expression does not affect mitotic spindle orientation.[11]

The main difference between Lgl^{3A} and the double mutant forms could lie in the ability to bind Dlg's GUK domain.[19] Dlg participates in the planar orientation of cell division in epithelia, acting on the recruitment of the spindle orientation protein Pins (LGN in vertebrates), which mediates the connection of astral microtubules to the lateral cortex.[34,44,45] Pins interaction with Dlg is also controlled by Aurora A phosphorylation.[46] Furthermore, functional and crystallographic studies have shown that phosphorylated Pins and Lgl bind to the same region of Dlg's domain.[19,45,47,48] Thus, maintenance of the Lgl/Dlg complex during mitosis is anticipated to impair Pins ability to bind Dlg, with the consequent spindle orientation defects that are observed upon expression of double mutant forms of Lgl in the follicular and wing disc epithelia.[10,11] Importantly, the Pins pathway is activated during prophase,[46] concurrent with Lgl cortical release.[11] Aurora A may therefore coordinate the dissociation of the Lgl/Dlg complex with the formation of Pins/Dlg complex. However, it is unclear why all Lgl is released from the cortex and the plasma membrane to transiently free Dlg. The finding that membrane-targeted Lgl induces spindle orientation defects[10] favors the importance of decreasing Lgl local concentration, which would compete with phospho-Pins despite the lower affinity of phospho-Lgl to the Dlg's GUK domain.[19,47]

CONCLUSIONS AND PERSPECTIVES

Recent advances highlight the importance of cell cycle dependent kinases for the regulation of polarity proteins to reshape the organization of the cytoskeleton during epithelial mitosis, and for the preservation of tissue architecture during proliferation. Aurora A provides the link between cell cycle regulation and the reorganization of apico-basal polarity complexes,[10,11] whereas another mitotic kinase, Plk1, couples the disassembly of planar cell polarity with mitotic division.[49] Furthermore, delocalization of apical polarity proteins, such as Par-6, aPKC, Baz and Crumbs, also occurs during symmetric cell division in some epithelial cell types.[11,29,30,44] A study in the *Drosophila* notum implicated lateral spreading of the apical proteins Par-6 and aPKC in the assembly of the isotropic actomyosin cortex that controls mitotic cell rounding.[30] Following our observation that Lgl cortical release occurs prior to the lateral spreading of Par-6 and aPKC,[11] it will be interesting to determine whether retaining Lgl at the cortex would also affect the cortical spreading of aPKC/Par-6, and subsequently their ability to drive cortical actin assembly.

The precise nature of Lgl regulation in distinct phosphorylation sites has yet to be elucidated. For instance, how site interdependence influences the importance of each serine along the cell cycle remains to be understood. One important conclusion that can be drawn from the analysis of single phosphorylatable mutants is that Lgl phosphorylation within the BH domain also positively controls Lgl activity in a site-specific manner. Future work will reveal how site specific phosphorylation number and order acts *in vivo* to control binding to the plasma membrane and cortical proteins. Furthermore, two other evolutionarily conserved

serines within Lgl BH motif, and other phosphorylated sites detected by mass spectrometry using *Drosophila* embryos,[50] may provide alternative residues to fine-tune Lgl function. Given the involvement of Lgl in a myriad of cellular processes that control development, homeostasis and disease, understanding the conserved features of its regulation in multiple organisms will have important impact in the future of epithelial biology.

DISCLOSURE OF POTENTIAL CONFLICTS OF INTEREST

No potential conflicts of interest were disclosed.

ACKNOWLEDGMENTS

We thank the other authors of the paper that resulted in this commentary (Claudio Sunkel, Cátia Carvalho and Guilherme Ventura) and Mariana Osswald for valuable comments on this manuscript.

FUNDING

S.M. holds a PhD fellowship from FCT (Fundação para a Ciência e a Tecnologia) SFRH/BD/99898/2014. E.M is currently funded by an Investigator FCT position, and was previously supported by a grant from FCT (PTDC/BIA-BMC/120132/2010).

REFERENCES

1. Rodriguez-Boulan E, Macara IG. Organization and execution of the epithelial polarity programme. Nat Rev Mol Cell Biol 2014; 15:225-42; PMID:24651541; http://dx.doi.org/10.1038/nrm3775
2. Bilder D, Li M, Perrimon N. Cooperative regulation of cell polarity and growth by Drosophila tumor suppressors. Science 2000; 289:113-6; PMID:10884224; http://dx.doi.org/10.1126/science.289.5476.113
3. Bilder D, Schober M, Perrimon N. Integrated activity of PDZ protein complexes regulates epithelial polarity. Nat Cell Biol 2003; 5:53-8; PMID:12510194; http://dx.doi.org/10.1038/ncb897
4. Tanentzapf G, Tepass U. Interactions between the crumbs, lethal giant larvae and bazooka pathways in epithelial polarization. Nat Cell Biol 2003; 5:46-52; PMID:12510193; http://dx.doi.org/10.1038/ncb896
5. Elsum I, Yates L, Humbert PO, Richardson HE. The Scribble-Dlg-Lgl polarity module in development and cancer: from flies to man. Essays Biochem 2012; 53:141-68; PMID:22928514; http://dx.doi.org/10.1042/bse0530141
6. Gateff E. Malignant neoplasms of genetic origin in Drosophila melanogaster. Science 1978; 200:1448-59; PMID:96525; http://dx.doi.org/10.1126/science.96525
7. Kuphal S, Wallner S, Schimanski CC, Bataille F, Hofer P, Strand S, Strand D, Bosserhoff AK. Expression of Hugl-1 is strongly reduced in malignant melanoma. Oncogene 2006; 25:103-10; PMID:16170365; http://dx.doi.org/10.1038/sj.onc.1209508
8. Nam KH, Kim MA, Choe G, Kim WH, Lee HS. Deregulation of the cell polarity protein Lethal giant larvae 2 (Lgl2) correlates with gastric cancer progression. Gastric Cancer 2014; 17:610-20; PMID:24337435; http://dx.doi.org/10.1007/s10120-013-0324-0
9. Betschinger J, Mechtler K, Knoblich JA. The Par complex directs asymmetric cell division by phosphorylating the cytoskeletal protein Lgl. Nature 2003; 422:326-30; PMID:12629552; http://dx.doi.org/10.1038/nature01486
10. Bell GP, Fletcher GC, Brain R, Thompson BJ. Aurora kinases phosphorylate Lgl to induce mitotic spindle orientation in Drosophila epithelia. Curr Biol 2015; 25:61-8; PMID:25484300; http://dx.doi.org/10.1016/j.cub.2014.10.052
11. Carvalho CA, Moreira S, Ventura G, Sunkel CE, Morais-de-Sa E. Aurora A triggers Lgl cortical release during symmetric division to control planar spindle orientation. Curr Biol 2015; 25:53-60; PMID:25484294; http://dx.doi.org/10.1016/j.cub.2014.10.053
12. Strand D, Raska I, Mechler BM. The Drosophila lethal(2)giant larvae tumor suppressor protein is a component of the cytoskeleton. J Cell Biol 1994; 127:1345-60; PMID:7962094; http://dx.doi.org/10.1083/jcb.127.5.1345
13. Strand D, Jakobs R, Merdes G, Neumann B, Kalmes A, Heid HW, Husmann I, Mechler BM. The Drosophila lethal(2)giant larvae tumor suppressor protein forms homo-oligomers and is associated with nonmuscle myosin II heavy chain. J Cell Biol 1994; 127:1361-73; PMID:7962095; http://dx.doi.org/10.1083/jcb.127.5.1361
14. Betschinger J, Eisenhaber F, Knoblich JA. Phosphorylation-induced autoinhibition regulates the cytoskeletal protein Lethal (2) giant larvae. Curr Biol 2005; 15:276-82; PMID:15694314; http://dx.doi.org/10.1016/j.cub.2005.01.012

15. Dahan I, Yearim A, Touboul Y, Ravid S. The tumor suppressor Lgl1 regulates NMII-A cellular distribution and focal adhesion morphology to optimize cell migration. Mol Biol Cell 2012; 23:591-601; PMID:22219375; http://dx.doi.org/10.1091/mbc.E11-01-0015
16. Dahan I, Petrov D, Cohen-Kfir E, Ravid S. The tumor suppressor Lgl1 forms discrete complexes with NMII-A and Par6alpha-aPKCzeta that are affected by Lgl1 phosphorylation. J Cell Sci 2014; 127:295-304; PMID:24213535; http://dx.doi.org/10.1242/jcs.127357
17. Plant PJ, Fawcett JP, Lin DC, Holdorf AD, Binns K, Kulkarni S, Pawson T. A polarity complex of mPar-6 and atypical PKC binds, phosphorylates and regulates mammalian Lgl. Nat Cell Biol 2003; 5:301-8; PMID:12629547; http://dx.doi.org/10.1038/ncb948
18. Yamanaka T, Horikoshi Y, Sugiyama Y, Ishiyama C, Suzuki A, Hirose T, Iwamatsu A, Shinohara A, Ohno S. Mammalian Lgl forms a protein complex with PAR-6 and aPKC independently of PAR-3 to regulate epithelial cell polarity. Curr Biol 2003; 13:734-43; PMID:12725730; http://dx.doi.org/10.1016/S0960-9822(03)00244-6
19. Zhu J, Shang Y, Wan Q, Xia Y, Chen J, Du Q, Zhang M. Phosphorylation-dependent interaction between tumor suppressors Dlg and Lgl. Cell Res 2014; 24:451-63; PMID:24513855; http://dx.doi.org/10.1038/cr.2014.16
20. Kallay LM, McNickle A, Brennwald PJ, Hubbard AL, Braiterman LT. Scribble associates with two polarity proteins, Lgl2 and Vangl2, via distinct molecular domains. J Cell Biochem 2006; 99:647-64; PMID:16791850; http://dx.doi.org/10.1002/jcb.20992
21. Hattendorf DA, Andreeva A, Gangar A, Brennwald PJ, Weis WI. Structure of the yeast polarity protein Sro7 reveals a SNARE regulatory mechanism. Nature 2007; 446:567-71; PMID:17392788; http://dx.doi.org/10.1038/nature05635
22. Dong W, Zhang X, Liu W, Chen YJ, Huang J, Austin E, Celotto AM, Jiang WZ, Palladino MJ, Jiang Y, et al. A conserved polybasic domain mediates plasma membrane targeting of Lgl and its regulation by hypoxia. J Cell Biol 2015; 211:273-86; PMID:26483556; http://dx.doi.org/10.1083/jcb.201503067
23. Bailey MJ, Prehoda KE. Establishment of Par-Polarized Cortical Domains via Phosphoregulated Membrane Motifs. Dev Cell 2015; 35:199-210; PMID:26481050; http://dx.doi.org/10.1016/j.devcel.2015.09.016
24. Hutterer A, Betschinger J, Petronczki M, Knoblich JA. Sequential roles of Cdc42, Par-6, aPKC, and Lgl in the establishment of epithelial polarity during Drosophila embryogenesis. Dev Cell 2004; 6:845-54; PMID:15177032; http://dx.doi.org/10.1016/j.devcel.2004.05.003
25. Wirtz-Peitz F, Nishimura T, Knoblich JA. Linking cell cycle to asymmetric division: Aurora-A phosphorylates the Par complex to regulate Numb localization. Cell 2008; 135:161-73; PMID:18854163; http://dx.doi.org/10.1016/j.cell.2008.07.049
26. Atwood SX, Prehoda KE. aPKC phosphorylates Miranda to polarize fate determinants during neuroblast asymmetric cell division. Curr Biol 2009; 19:723-9; PMID:19375318; http://dx.doi.org/10.1016/j.cub.2009.03.056
27. Besson C, Bernard F, Corson F, Rouault H, Reynaud E, Keder A, Mazouni K, Schweisguth F. Planar cell polarity breaks the symmetry of PAR protein distribution prior to mitosis in Drosophila sensory organ precursor cells. Curr Biol 2015; 25:1104-10; PMID:25843034; http://dx.doi.org/10.1016/j.cub.2015.02.073
28. Macara IG, Guyer R, Richardson G, Huo Y, Ahmed SM. Epithelial homeostasis. Curr Biol 2014; 24:R815-25; PMID:25202877; http://dx.doi.org/10.1016/j.cub.2014.06.068
29. Morais-de-Sa E, Sunkel C. Adherens junctions determine the apical position of the midbody during follicular epithelial cell division. EMBO Rep 2013; 14:696-703; PMID:23774295; http://dx.doi.org/10.1038/embor.2013.85
30. Rosa A, Vlassaks E, Pichaud F, Baum B. Ect2/Pbl acts via Rho and polarity proteins to direct the assembly of an isotropic actomyosin cortex upon mitotic entry. Dev Cell 2015; 32:604-16; PMID:25703349; http://dx.doi.org/10.1016/j.devcel.2015.01.012
31. Guillot C, Lecuit T. Adhesion disengagement uncouples intrinsic and extrinsic forces to drive cytokinesis in epithelial tissues. Dev Cell 2013; 24:227-41; PMID:23410938; http://dx.doi.org/10.1016/j.devcel.2013.01.010
32. Founounou N, Loyer N, Le Borgne R. Septins regulate the contractility of the actomyosin ring to enable adherens junction remodeling during cytokinesis of epithelial cells. Dev Cell 2013; 24:242-55; PMID:23410939; http://dx.doi.org/10.1016/j.devcel.2013.01.008
33. Herszterg S, Leibfried A, Bosveld F, Martin C, Bellaiche Y. Interplay between the dividing cell and its neighbors regulates adherens junction formation during cytokinesis in epithelial tissue. Dev Cell 2013; 24:256-70; PMID:23410940; http://dx.doi.org/10.1016/j.devcel.2012.11.019
34. Nakajima Y, Meyer EJ, Kroesen A, McKinney SA, Gibson MC. Epithelial junctions maintain tissue architecture by directing planar spindle orientation. Nature 2013; 500:359-62; PMID:23873041; http://dx.doi.org/10.1038/nature12335
35. Bergstralh DT, Lovegrove HE, St Johnston D. Lateral adhesion drives reintegration of misplaced cells into epithelial monolayers. Nat Cell Biol 2015; 17:1497-503; PMID:26414404; http://dx.doi.org/10.1038/ncb3248

36. Huang J, Zhou W, Dong W, Watson AM, Hong Y. Directed, efficient, and versatile modifications of the Drosophila genome by genomic engineering. Proc Natl Acad Sci U S A 2009; 106:8284-9; PMID:19429710; http://dx.doi.org/10.1073/pnas.0900641106
37. Musch A, Cohen D, Yeaman C, Nelson WJ, Rodriguez-Boulan E, Brennwald PJ. Mammalian homolog of Drosophila tumor suppressor lethal (2) giant larvae interacts with basolateral exocytic machinery in Madin-Darby canine kidney cells. Mol Biol Cell 2002; 13:158-68; PMID:11809830; http://dx.doi.org/10.1091/mbc.01-10-0496
38. Graybill C, Prehoda KE. Ordered multisite phosphorylation of lethal giant larvae by atypical protein kinase C. Biochemistry 2014; 53:4931-7; PMID:25000553; http://dx.doi.org/10.1021/bi500748w
39. Joberty G, Petersen C, Gao L, Macara IG. The cell-polarity protein Par6 links Par3 and atypical protein kinase C to Cdc42. Nat Cell Biol 2000; 2:531-9; PMID:10934474; http://dx.doi.org/10.1038/35019573
40. Yamanaka T, Horikoshi Y, Suzuki A, Sugiyama Y, Kitamura K, Maniwa R, Nagai Y, Yamashita A, Hirose T, Ishikawa H, et al. PAR-6 regulates aPKC activity in a novel way and mediates cell-cell contact-induced formation of the epithelial junctional complex. Genes Cells 2001; 6:721-31; PMID:11532031; http://dx.doi.org/10.1046/j.1365-2443.2001.00453.x
41. Yasumi M, Sakisaka T, Hoshino T, Kimura T, Sakamoto Y, Yamanaka T, Ohno S, Takai Y. Direct binding of Lgl2 to LGN during mitosis and its requirement for normal cell division. J Biol Chem 2005; 280:6761-5; PMID:15632202; http://dx.doi.org/10.1074/jbc.C400440200
42. Cadart C, Zlotek-Zlotkiewicz E, Le Berre M, Piel M, Matthews HK. Exploring the function of cell shape and size during mitosis. Dev Cell 2014; 29:159-69; PMID:24780736; http://dx.doi.org/10.1016/j.devcel.2014.04.009
43. Luxenburg C, Pasolli HA, Williams SE, Fuchs E. Developmental roles for Srf, cortical cytoskeleton and cell shape in epidermal spindle orientation. Nat Cell Biol 2011; 13:203-14; PMID:21336301; http://dx.doi.org/10.1038/ncb2163
44. Bergstralh DT, Lovegrove HE, St Johnston D. Discs large links spindle orientation to apical-basal polarity in Drosophila epithelia. Curr Biol 2013; 23:1707-12; PMID:23891112; http://dx.doi.org/10.1016/j.cub.2013.07.017
45. Saadaoui M, Machicoane M, di Pietro F, Etoc F, Echard A, Morin X. Dlg1 controls planar spindle orientation in the neuroepithelium through direct interaction with LGN. J Cell Biol 2014; 206:707-17; PMID:25202028; http://dx.doi.org/10.1083/jcb.201405060
46. Johnston CA, Hirono K, Prehoda KE, Doe CQ. Identification of an Aurora-A/PinsLINKER/Dlg spindle orientation pathway using induced cell polarity in S2 cells. Cell 2009; 138:1150-63; PMID:19766567; http://dx.doi.org/10.1016/j.cell.2009.07.041
47. Zhu J, Shang Y, Xia C, Wang W, Wen W, Zhang M. Guanylate kinase domains of the MAGUK family scaffold proteins as specific phospho-protein-binding modules. Embo J 2011; 30:4986-97; PMID:22117215; http://dx.doi.org/10.1038/emboj.2011.428
48. Johnston CA, Doe CQ, Prehoda KE. Structure of an enzyme-derived phosphoprotein recognition domain. PLoS One 2012; 7:e36014; PMID:22545154; http://dx.doi.org/10.1371/journal.pone.0036014
49. Shrestha R, Little KA, Tamayo JV, Li W, Perlman DH, Devenport D. Mitotic Control of planar cell polarity by polo-like kinase 1. Dev Cell 2015; 33:522-34; PMID:26004507; http://dx.doi.org/10.1016/j.devcel.2015.03.024
50. Zhai B, Villen J, Beausoleil SA, Mintseris J, Gygi SP. Phosphoproteome analysis of Drosophila melanogaster embryos. J Proteome Res 2008; 7:1675-82; PMID:18327897; http://dx.doi.org/10.1021/pr700696a